Dynamics of Pleistocene climate change in the South Atlantic Ocean

Reading commettee: prof.dr. H.W. Arz
dr. T.M. Dokken
dr. J.-B.W. Stuut
dr. H.B. Vonhof
dr. M. Ziegler

"Dynamics of Pleistocene climate change in the South Atlantic Ocean"
PhD thesis

"Dynamiek van Pleistocene klimaatveranderingen in de Zuid-Atlantische Oceaan"
Academisch proefschrift

ISBN: 978-90-6464-767-3

Cover image: Mirco Scussolini
Printing: GVO drukkers & vormgevers B. V.
This research received funding by the European Community's Seventh Framework Programme FP7/2007-2013 – Marie-Curie ITN, under grant agreement no.238512, GATEWAYS project.

VRIJE UNIVERSITEIT

Dynamics of Pleistocene climate change in the South Atlantic Ocean

ACADEMISCH PROEFSCHRIFT

ter verkrijging van de graad Doctor aan
de Vrije Universiteit Amsterdam,
op gezag van de rector magnificus
prof.dr. F.A. van der Duyn Schouten,
in het openbaar te verdedigen
ten overstaan van de promotiecommissie
van de Faculteit der Aard- en Levenswetenschappen
op dinsdag 6 mei 2014 om 11.45 uur
in de aula van de universiteit,
De Boelelaan 1105

door

Paolo Scussolini

geboren te Udine, Italië

promotor:	prof.dr. H. Renssen
copromotor:	dr. F.J.C. Peeters

Contents

A preface

How does the surface of the earth work? What is the interplay between water and air, and the continents and the sea floor? Can we understand the laws underlying this cosmos of countless revolving and clashing particles whose result we call climate? The piece in your hands originates from the preoccupation with the intimate functioning of the land and oceans, the places where we spend the vast majority of our time, and from the persuasion that to decrypt the the turbulent phenomena under our eyes the ancient affairs of the matter must lie under the magnifying glass. To glance into the old memories of this evolving planet is no job for the feeble hearted, nor for the exact mind. There is no measuring the height, the weight, the speed, the warmth of things that rest by now only in our imagination. The past is stone dead. Yet, in stone indeed, and in matter creeping towards the stony form, headstrong men have gazed and found the traces of the past, and even earnestly formulated protocols to make sense of them, to even attribute numbers to events long forgotten. These devices from a line of wayward men of knowledge I have learned to handle during three years. I have husbanded the transformation of mute substrate from underneath the sea into inaccurate and imprecise number; and I have accompanied my product to that of my fellows before and beside me, so that the communion of our scanty tiles might form a grater and more discernible image. In a process so patently akin to a legitimate form of magic, I performed the science of the past oceans. Looking now at this manuscript, and behind it at the concatenation of events of which it tells, events amidst the dark and cold sea, where nothing but Atlantic water is for hundreds of meters above and below and left and right, events in the sedimentology lab and down its sinks, events of green beaches swallowed by the relentlessly growing blue waves, events into the slender plasma torch where heat is more intense than on the surface of the sun, and events in front of a gleaming word document late at night, I am stupefied at the prodigy of man's questioning. With the joyous purpose of adding my humble tile to the relentlessly focusing chronicle of all of the above, I assembled the following pages.

I should have been a pair of ragged claws
Scuttling across the floors of silent seas.
T.S. Eliot

Mi raccomando, divertiti.
E. Moras

1

Introduction

This Ph.D. thesis deals with the reconstruction of climatic features from the earth's past. Namely, it aims at understanding aspects of climate in the South Atlantic region during periods of prominent, global climate change of the Pleistocene epoch.
This introductory chapter serves the reader in two ways. It outlines a number of concepts upon which the following research chapters are built: section 1.1 deals with general Pleistocene climatological concepts, section 1.2 with oceanographic and atmospheric ones, and section 1.3 with methodological ones. Once such premises are laid, section 1.4 of the introduction leads the reader more specifically through the scientific framework in which the thesis finds place, and through the research questions therein addressed. Further details of each of the topics treated are then discussed in the specific introductory sections of the respective research chapters.

1.1 Climate change in the Pleistocene

The study of the earth's geological substrates has made clear that climate changed dramatically in the past. The present global warming, and the multitude of associated changes in climate features, are only the latest manifestations of the capacity that our planet's surface has to rearrange the physical and chemical configuration of water and air masses' circulation through time. Climatic reconstructions for the Pleistocene have revealed that the mean temperature and composition, of the atmosphere and of the ocean, varied over time-scales from millennia to millions of years (Emiliani, 1955; Shackleton, 1967; Dansgaard et al., 1993; Lisiecki and Raymo, 2005; Jouzel et al., 2007; Lüthi et al., 2008) primarily responding to two external forcings. The first one is continental drift, which by altering the disposition of continents and water bodies affects the sensitivity of the earth's climate to the second forcing, which is due to variations in the parameters of the earth's orbit around the sun, causing changes in the distribution of solar radiation. The former forcing operates at the so-called tectonic time-scale (10^6 – 10^9 years), and the latter at the orbital time-scale (10^3 – 10^5 years), and is also known as orbital forcing. In the last millions of years, continental drift generated a number of changes in the position of landmasses that drastically impacted the global climate and ocean circulation. Those are: the uplifting of Himalayas (~50-40 10^6 years ago), which had profound bearing on atmospheric circulation of the Asian continent (e.g., Zhisheng et al., 2001); the opening of the Drake passage (~20 10^6 years ago) and consequent formation of the Antarctic Circumpolar Current (Lagabrielle et al., 2009); and the closure of the Panama strait (~4 10^6 years ago), which created a gradient of salinity between the Atlantic and Pacific Oceans with strong implications on the oceans' circulation (Keigwin, 1982).

While the dating of such events is still a matter of investigation, it is important to note that our knowledge of the orbital forcing can already be considered adequate, thanks to the ground-breaking work of Milutin Milanković (1941). This mathematician unravelled the cyclicity of change in the three parameters that characterize the earth's orbit around the sun (Fig. 1.1). These (and their respective main periodicity components [Laskar et al., 2004]) are: 1) eccentricity, or the degree of deviation from a circular orbit (~410, 125 and 95 thousand years, kyr); 2) obliquity, or the tilt of the earth's rotational axis with respect to the orbital plane (~41 kyr); and 3) precession of the equinoxes, or the orientation of the rotational axis with respect to the firmament (~23 and 19 kyr). This work was further developed in more recent times, mainly by André Berger (e.g., Berger, 1978), with refinement of the quantification of the solar radiation that the earth received at the top of the atmosphere. It appears that the climate system is characterized, as any other physical entity, by its own resonance, i.e., it oscillates in response to specific frequencies. For the Pleistocene epoch, which is the interest of this thesis, the most evident result of such combination of orbital frequencies (Fig. 1.1 A-C) is the periodical change of state of the climate system, swaying between glacials and interglacials: the glacial cycles (Hays, 1976a) (Fig. 1.1 D).

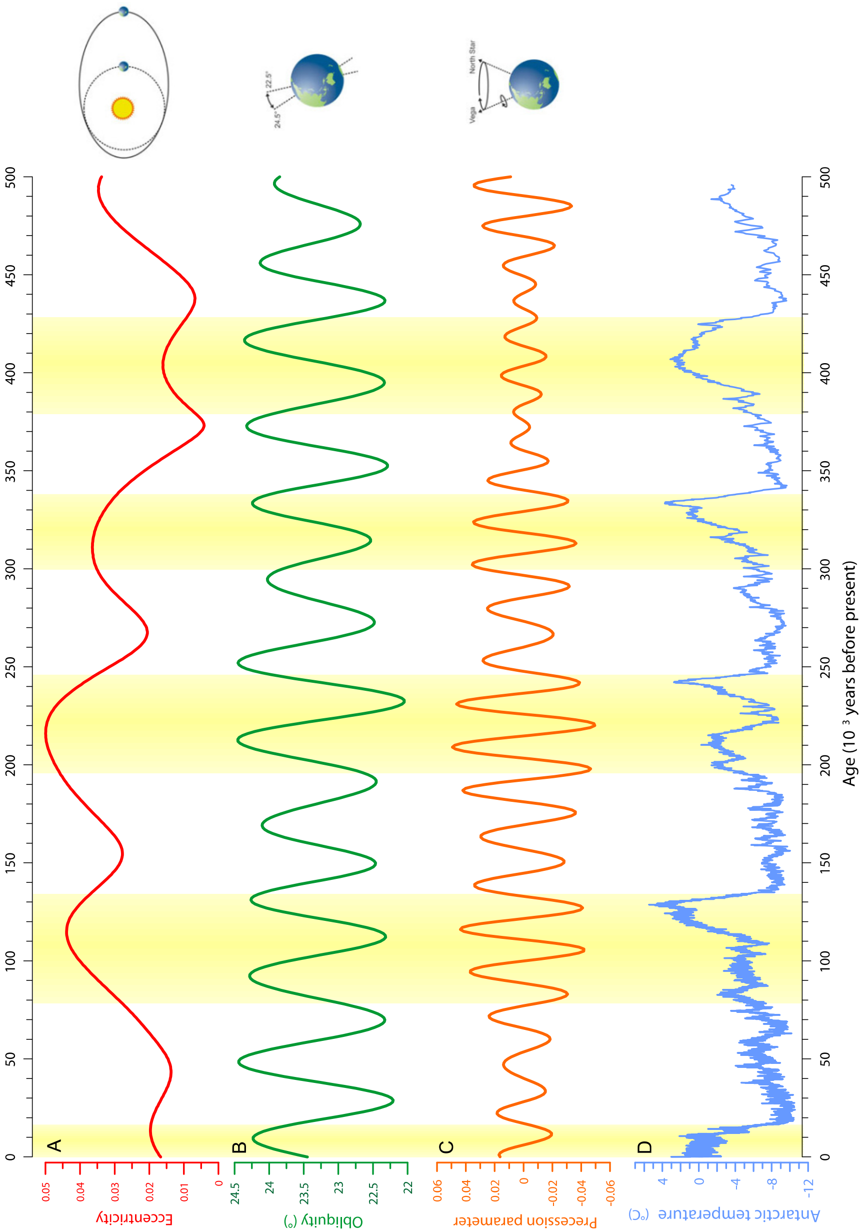

Fig. 1.1. The parameters of the earth's orbit around the sun, depicted in their temporal evolution for the last 500 thousand years, and illustrated in diagrams. A) Eccentricity quantifies the deviation of the orbit from a circle; B) the obliquity angle, reflects the tilt of the earth's rotational axis with respect to the orbital plane; and C) the precession parameter indicates the orientation of the rotational axis with respect to the firmament (data from Laskar et al., 2004). Those orbital parameters appear to influence the earth's climate, resulting in the glacial-interglacial cycles, exemplified by D) the temperature variation reconstructed from Antarctic ice cores (Jouzel et al., 2007).

When looking closer into the geologic record, we note that the sub-orbital time scales ($\leq 10^3$ years) are the typical domain where the so-called internal forcings of the climate system are at play (e.g., Dokken et al., 2013). These consist of feedback mechanisms, i.e., processes between the components of the climate system, which amplify or weaken climate change (e.g., Ruddiman, 2008). Certain climatic feedbacks are relevant for Pleistocene climate change, and have received vast attention. For instance, positive (amplifying) feedbacks of warming climate change are: the retention of atmospheric heat caused by increasing amounts of water vapour (Hall and Manabe, 1999); the reduction in the albedo of the earth's surface, and therefore the earth's capacity to reflect part of the incoming solar radiation back to space, caused by the waning snow cover (Hall, 2004); the decreased capacity of the warming oceans to dissolve, and hence sequester, CO_2 from the atmosphere (Takahashi et al., 1993). In the last decades, the human capability to think of these processes, and of their interrelations, in an integrated manner has received great support from the expanding skills of computers. Climate models of increasing spatial-temporal resolution have been set up, mimicking the dynamic interactions between the various parts of the climate system. In particular, paleoclimate model simulations have greatly advanced the understanding of the role of feedbacks in determining the climatic changes observed in the records (for a comprehensive review see Crucifix [2012]).

1.1.1 Climate change of the glacial cycles

During the Pleistocene, the earth periodically fluctuated between periods of generally colder climate, with the presence of large ice sheets, known as glacials, and periods of warmer average temperatures, with reduced ice cover, i.e., interglacials. Those glacial cycles still constitute a puzzle to the earth sciences, and specifically to paleoclimate research, which investigates the physical mechanisms behind them. Further, the implications of a more complete understanding of the mechanisms behind these prominent transitions between climate states are particularly relevant in the view of the climate change that is presently underway. Advances in the investigation of the geological past are progressively shedding light upon the changes that accompanied the cyclic variations, that unsettled the earth’s surface at least over the last two million years. Developments in the use of climate proxies (see section 1.3) enable us to infer past regional and global climatic states, and the age thereof, with higher precision and accuracy. This allows with diminishing incertitude the understanding of the complex system of feedbacks that composes our climate system. By these means, paleoclimate reconstructions, like those contained in this thesis, aim to improve our knowledge of the sensitivity of the climate system (Jansen et al., 2007; Toggweiler and Lea, 2010). This knowledge, in turn, is a prerequisite for the prediction of how the system will react to the present and forthcoming anthropogenic forcing by greenhouse gases.

1.2 Oceans, atmosphere and climate

1.2.1 The Oceans' role in climate

The oceans act in a variety of ways to influence climate. Those are primarily: the sequestration of atmospheric carbon; the regulatory effect of the water masses on temperatures; the distribution of heat by means of the ocean's circulation. The oceans host large communities of photosynthesizers, that account for about half of the planet's primary production (Denman et al., 2007). By this mechanism carbon (in the form of CO_2) is sequestered from the atmosphere and moved to the deep water layers (mostly in the form of $CaCO_3$; Falkowski et al., 2000). Part of that amount is incorporated in the sediments deposited at the ocean's floor, and part remains available to re-enter the carbon cycle, and the atmospheric circulation, under modified oceanographic circumstances (Anderson and Carr, 2010). Presently, about half of the anthropogenic CO_2 emissions are thus absorbed by the oceans (Sabine et al., 2004). Even more important for climate is the high heat capacity of water, compared to other components of the earth's surface, such as the land and the atmosphere. The oceans can store large amounts of heat with relatively small changes in their temperatures, and are therefore efficient thermal regulators. Further, the high heat capacity makes the overturning of oceanic water masses, either superficial or deep, a global distributor of heat both in a meridional and in a zonal direction (Fig. 1.2) (Broecker, 1991). In particular, the circulation of the Atlantic Ocean, the so-called Atlantic meridional overturning circulation (AMOC), is a sensitive component of the climate system.

1.2.2 The Atlantic Meridional Overturning Circulation

The AMOC presents a three-dimensional pattern of circulation (for a review see Kuhlbrodt et al., 2007) (Fig. 1.2). Water emerges from depth in so-called upwelling areas, which are located mostly around Antarctica, and along the coast of the continents, where the process is largely wind-driven (e.g., Toggweiler and Samuels, 1993), and secondarily in the middle of the oceanic gyres, where upwelling occurs due to vertical mixing. Upwelled waters are then transported latitudinally and longitudinally along the ocean surface and subsurface, and they sink in specific sites where they have the chance to become denser, due to thermohaline processes (Broecker, 1991), thus closing the vertical cycle. The interest of this thesis rests mainly on the upper-branch of the AMOC, i.e., on aspects of its surface, and near-surface, currents. For this reason the upper scheme of circulation is further scrutinized in the following paragraph, drawing mostly from the work of Gordon (1986), Kuhlbrodt et al. (2007), Speich et al. (2007) and Garzoli and Matano (2011).

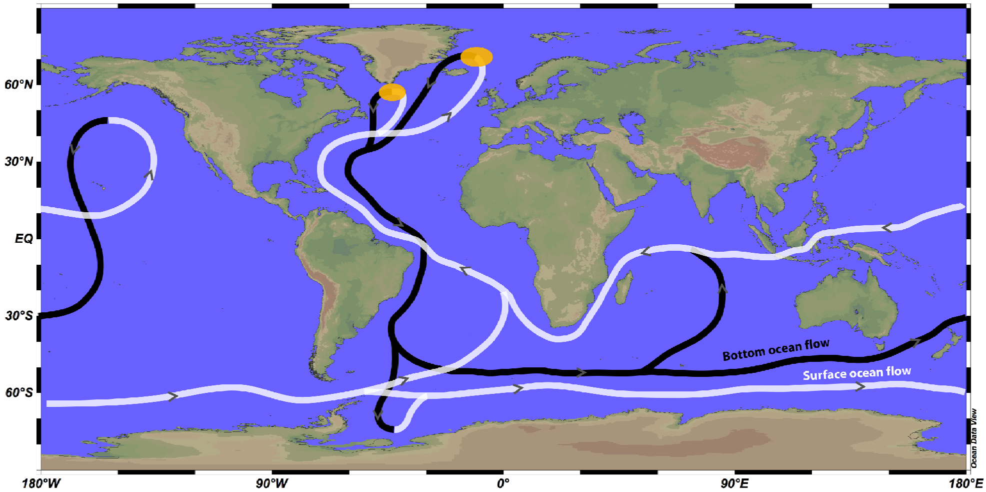

Fig. 1.2. Schematic and simplified global arrangement of oceanic circulation, the "ocean conveyor belt". Surface ocean currents are indicated in white, and bottom currents in black; the areas of formation of North Atlantic deep water are shown in orange (drawn mostly from Broecker [1991] and Rahmstorf [2002]).

Upper level waters of the AMOC enter the Atlantic from the Indian, Pacific and Southern Oceans (for a review of South Atlantic upper circulation, see section 1.2.3). Entering the North Atlantic by the conduit of the North Brazil Current (de Silveira et al., 1994; see section 1.2.3), waters accumulate heat from the tropical regions. They continue the path north-westward within the Guyana Current and then the Caribbean Current, and circulate into the warm pool of the Gulf of Mexico, thereby further building up their heat and salt content. Out of these tropical regions, the main flow continues from Florida north-eastwards across the North Atlantic in the form of the broad western boundary current of the Gulf Stream, transporting large quantities of water (~3.2 Sv (1 Sverdrup = 10^6 m^3 s^{-1}) [Baringer and Larsen, 2001]) and of heat (~1.3 PW [Larsen, 1992]). Additionally, the Gulf Stream is responsible for most of the northward transfer of salt (e.g., Treguier et al., 2012) The Gulf Stream also constitutes the western branch of the North Atlantic gyre, whereas the northern branch is constituted by the North Atlantic Current. While part of these waters recirculate southwards along the Canary Current, and then westward through the North Equatorial Current, another portion of the North Atlantic Current reaches the northernmost regions of the North Atlantic, thereby determining the mild climate of Europe, much convenient for this densely populated continent. Upon arrival in the Nordic, Labrador and Irminger Seas, salt-rich waters of mostly tropical origin cool down. Because water density is inversely related to temperature, and directly related to salinity, the thermo-haline conditions achieved at the aforementioned seas allow upper waters to achieve higher density than the underlying water masses, and trigger the process of deep convection (Marshall and Schott, 1999). Upper waters thus sink to the ocean floor, and form what is known as North Atlantic deep water (NADW) (e.g., Hansen et al., 2004). This mass flows to the south at depths of 2 to 4 km, mostly over the western side of the Atlantic basin (Fig. 1.2); once NADW has reached the tip of South America, it turns east and flows across the southern boundary of the South Atlantic, eventually mixing with deep waters from different sources to form the circumpolar deep water.

The process of NADW formation plays an important role in explaining climate change during the Pleistocene glacial cycles. In particular, during glacial times, large amounts of fresh water from greater continental ice sheets (and secondarily from sea ice) interfered with the formation of NADW in the regions where it is now observed (Duplessy et al., 1988), by preventing upper waters of southern source from acquiring enough density as to allow their convection to deeper ocean layers. This likely had cascading effects on the NADW as well as on the global climate system, like model experiments have shown (e.g., Knutti et al., 2004; Stouffer et al., 2006; Kleinen et al., 2009; Anderson and Carr, 2010; Weijer et al., 2012). It seems, especially, that the AMOC variability over glacial-interglacial cycles was tightly connected to the processes of NADW formation (McManus et al., 1999). Namely, during deglaciations, the enhanced freshwater fluxes from melting continental ice sheets affected NADW to the extent that the AMOC slowed down (Negre et al., 2010) or became more shallow (Lynch-Stieglitz et al., 2007; Thornalley et al., 2013) than at present.

An important outcome of the Atlantic circulation, outlined above, is that owing to the meridional heat transport, from the South Atlantic, and then from the tropics northwards, a net surface transfer of heat from the South to the North Atlantic occurs (the North Atlantic heat piracy) (Wunsch, 1980; Seidov and Maslin, 2001). Even though the task is not a trivial one (e.g., Perez et al., 2011), the meridional heat transport from the South to the North Atlantic by the AMOC is quantified, and has recently been estimated at 0.54 ± 0.14 PW (Garzoli et al., 2013), agreeing with previous calculations of Perez et al. (2011).

1.2.3 Oceanography and paleoceanography of the South Atlantic

The South Atlantic Ocean has received less research attention than the North Atlantic. In particular, paleoclimate reconstructions have traditionally been centred preferentially at the northern end of the Atlantic basin. More recently, the relevance of processes of South Atlantic origin to the equilibrium and variability of the AMOC, and therefore of the whole climate system, has emerged more clearly (e.g., Toggweiler and Samuels, 1995; Knorr and Lohmann, 2003; Biastoch et al., 2008b; Garzoli and Matano, 2011). This motivates research efforts aimed at a better understanding of the South Atlantic history. This is the topic of this thesis.

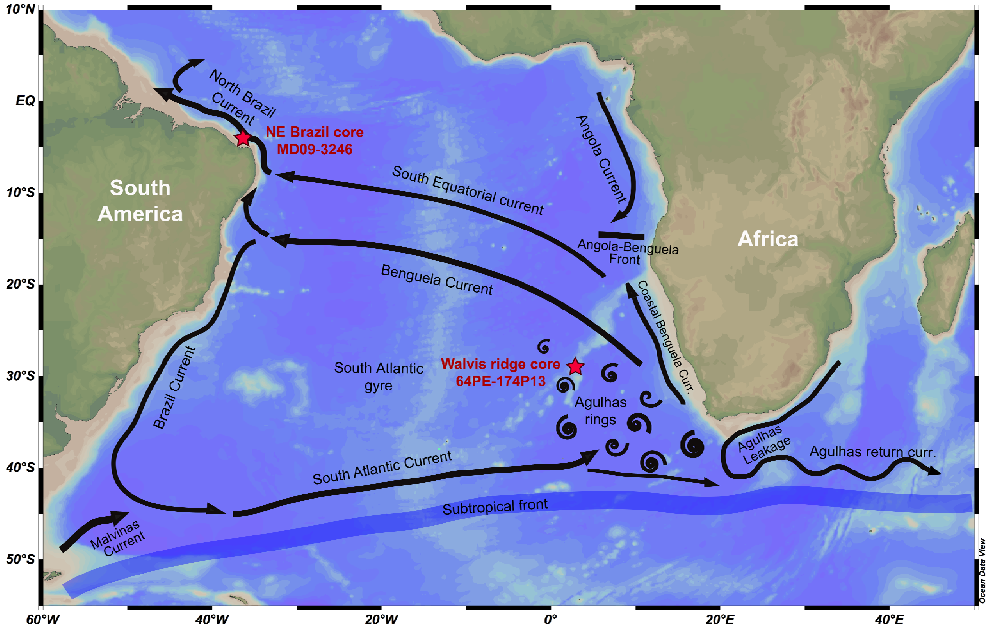

Fig. 1.3. Map of the South and tropical Atlantic Ocean. Indicated are the positions of the two cores studied in this thesis, core 64PE-174P13 from the central Walvis Ridge (2900 m depth) and core MD09-3246 from the northeast Brazilian continental margin (900 m depth), the surface currents (drawn mostly from Stramma and England [1999]), and other oceanographic features treated.

The South Atlantic Ocean has as its northern boundary the North Atlantic at the equator, as its southern boundary the Southern Ocean at 60°S, as its eastern boundary the Indian Ocean at the longitude of Cape Agulhas (20°E), and as its western boundary the Pacific Ocean at the longitude of the Drake Passage (Fig. 1.3). Surface and intermediate waters circulating within this basin proceed from the Indian Ocean, through the Agulhas leakage (Lutjeharms, 2006; see following paragraph), from the Pacific Ocean, through the Drake Passage (Toggweiler and Samuels, 1995), and from the Southern Ocean, incorporated along the pseudo-zonal flow of the South Atlantic Current. The most prominent oceanographic structure of the South Atlantic is the subtropical gyre that takes its name (Stramma and England, 1999). This is an anti-cyclonic flow of waters, composed at its periphery of the following current system: the Benguela Current on the eastern flank (Garzoli and Gordon, 1996), the South Equatorial Current on the north (Stramma and Schott, 1999), the southward-flowing Brazil and the northward Malvinas Currents, separated by the Brazil-Malvinas confluence, on the west (Goni et al., 2011), and the South Atlantic Current on the south. South Atlantic waters are then shed to the North Atlantic mostly by means of the North Brazil Current (de Silveira et al., 1994). As a result of the action of this system of currents, the South Atlantic is characterized by a meridional volume transport of ~18 Sv (Dong et al., 2009; Garzoli et al., 2013), which, in turn, determines a northward heat flux (Dong et al., 2009).

As it constitutes the origin of the upper branch of the AMOC, and as the latter has notably changed its volume transport during the Pleistocene (Broecker et al., 1990; Lynch-Stieglitz et al., 2007; Negre et al., 2010; Hesse et al., 2011), the South Atlantic has supposedly also undergone substantial modification of its current system (Wefer et al., 1996; Clauzet et al., 2007). In particular, during glacial periods, the set of fronts at the south of the basin, i.e. the subtropical and subpolar fronts, are believed to have seized more northerly locations (Hays et al., 1976; Bé and Duplessy, 1976; Bard and Rickaby, 2009). This might have meant restrained Indian to Atlantic passage of the Agulhas leakage (Peeters et al., 2004).

The Agulhas system and the southeast Atlantic

Along the east coast of Africa, from about 27° S southwards, flows the Agulhas Current, the strongest western boundary jet current there is, transporting about 70 Sv at speeds up to 2 m s^{-1} (Lutjeharms, 2006; 2007) (Fig. 1.3). Its path is determined by the profile of the continent's shelf break. Its waters bear two main origins: on the coastal side flow masses from the Indian Ocean, Arabian and Red Seas, while on the offshore side waters derive from the Atlantic and Southern Oceans (Beal et al., 2006). This twofold composition of the Agulhas Current betrays the structure of surface and subsurface water masses of the ocean where it originates, and hints at the fact that the southeast Indian Ocean circulation is characterized by a gyre. In its southern track, the current stands out from the surrounding because of its relatively high surface-to-intermediate water temperature. Its temperature at the surface ranges from 23 to 26° C (Gordon et al., 1987), with a gradient up to 5-6° C from the adjacent waters, a contrast that emerges sharply also from satellite images (Lutjeharms, 2007; Beal et al., 2011). The salinity of the Agulhas Current is on average 35.4 practical salinity units (Gordon et al., 1987).

The angular momentum it has accumulated implies that once the current has approached the tip of southern Africa, it detaches from the continent, following the Agulhas bank, and bends dramatically to the south, forming the most intense current retroflection observed on Earth (Gordon, 2003). Not all of the Agulhas Current retroflects, though: a part of it is shed to the South Atlantic in the form of rings and filaments (Schouten et al., 2000; Lutjeharms and Cooper, 1996): this is named the Agulhas leakage (AL). The bulk of the Agulhas Current, anyway, completes a 180° retroflection and becomes the Agulhas Return Current, which meanders eastwards, circumventing the Agulhas plateau to the north, and roughly parallels the Antarctic Circumpolar Current, and with it defines the subtropical-subpolar front. Eventually, most of the Agulhas Return Current recirculates within the Indian gyre. Since a notable portion of the Agulhas Current (about 15 Sv [Biastoch et al., 2008a; van Sebille et al., 2010]) enters the South Atlantic gyre, and since ultimately the latter waters are partially incorporated in the Agulhas Return Current to the east, researchers have proposed the concept of a "supergyre" (Gordon, 1986; Speich et al., 2007), of which the Agulhas system is the undisputed protagonist.

The processes controlling the Agulhas system are the object of present research (Beal et al., 2011). The system has been monitored over the last two decades, and data analysis suggests that the AL is intensifying under present warming conditions (Rouault et al., 2009), as indicated by the increase in eddy kinetic energy registered in the Agulhas retroflection area (90 $cm^2 s^{-2}$ per decade [Backeberg et al., 2012]). The formation of rings appears ultimately connected to the pace of formation of Natal pulses upstream (van Leeuwen et al., 2000). Natal pulses, in turn, are large cyclonic meanders that form from the Agulhas Current about the Natal Bight area. Downstream, the shedding of rings seems to be mainly controlled by the longitudinal position of the retroflection: the more westward its position, the higher the AL transport (van Sebille et al., 2009a). In turn, the point of retroflection shows large variability, and appears to be determined by the latitudinal position and the intensity of the westerlies band (Biastoch et al., 2009; Durgadoo et al., 2013). The inertia of the current also plays an important role in the amount of AL released (van Sebille et al., 2009b), a circumstance that opens a question, also for the paleoceanographic community: is/was the strength of the AL coupled to the intensity of the Agulhas Current?

In addition, it is important to stress the peculiar location of the Agulhas Current and AL in the global oceanic circulation (Fig. 1.2 and 1.3). The Agulhas Current receives waters that have crossed the Indian Ocean mainly coming from the shallow and articulated region of the Indonesian Throughflow, and to a lesser extent from recirculation within the southwest Indian Ocean sub-gyre (Simon et al., 2013). In turn, water masses in the Indonesian Throughflow proceed from the Pacific Ocean. After spilling into the southeast Atlantic, Agulhas waters join those of Pacific and Southern Ocean origin that constitute the surface and intermediate circulation of the subtropical gyre, and of the southern half of the surface branch of the AMOC. A portion of the waters thus formed is then able to pass to the North Atlantic via the North Brazil Current. Then they gain additional heat and salinity in the Gulf of Mexico and therefore travel north-eastward across the North Atlantic, to reach the areas of formation of NADW, thus starting the southward branch of the AMOC at depth.

Because it occupies such a crucial position in the scheme of oceanic currents, the Agulhas system is simultaneously a sensitive and an influential bottleneck of ocean circulation, which entertains important cause-effect relationships with the other parts of the earth's ocean and climate. In the Pleistocene perspective, it has been hypothesized that intense rearrangements of the mean latitudinal position of atmospheric circulation features, such as occurring during glacial terminations (Cheng et al., 2009; Denton et al., 2010), have changed the gateway to the AL: during glacial times a more northern location of the subtropical and subpolar fronts might have nearly shut the AL down (Franzese et al., 2006), whereas at terminations a southward shift of fronts and attendant wind belts seems to have opened a wider-than-present passage for it to enter the South Atlantic (Peeters et al., 2004; Bard and Rickaby, 2009; Simon et al., 2013). In Chapter 4, I discuss and provide support for this hypothesis.

The western tropical Atlantic and the North Brazil Current

Another portion of the South Atlantic is also the object of the reconstructions reported in this thesis, i.e. the western tropical Atlantic. In that region, the northern branch of the South Atlantic subtropical gyre, constituted by the southern South Equatorial Current, carries waters westwards, approaching the Brazil landmass at ~15° S (Stramma and England, 1999) (Fig. 1.3). There it splits into the south-directed Brazil Current, and the northward North Brazil Current (da Silveira et al., 1994; Schott et al., 1998). The latter is an intense western boundary current with core speeds of up to 100 cm sec^{-1}, at 100-200 m depth; it displays seasonal variability linked to the latitudinal position of the easterlies wind field and of the intertropical convergence zone (ITCZ; see section 1.2.4). The North Brazil Current flows parallel to the continental margin, merges at about 5° S with the northern South Equatorial Current, and subsequently splits. Its eastward retroflection feeds the Equatorial Undercurrent and the rest spills northwestward into the Caribbean in form of eddies (Stramma and Schott, 1999), in a fashion reminiscent of the mechanism oulined for the Agulhas system. Again in analogy to the Agulhas at the interface of the Indian and Atlantic Oceans, the North Brazil Current, retroflection and eddies guard the passage of surface and subsurface waters from the South into the North Atlantic Ocean. Being a bottleneck in the transport of salt from the South Atlantic into the northern AMOC, past changes in the North Brazil Current could have had repercussions on AMOC transport variability. Namely, previous studies have attributed paleo variations in this system to changes either in AMOC, as for the increased temperature of the upper ocean registered for times of reduced AMOC (Arz et al., 1999a), or in the ITCZ position, as for the glacial curtailment of the South-to-North Atlantic transport proposed by Wilson et al. (2011).

1.2.4 The Intertropical convergence zone and the monsoon systems

Another salient feature of the climate and paleoclimate system is the latitudinal distribution of the mean wind fields, and of the boundaries between them, also known as fronts (Fig. 1.4) (for a review see Barry and Chorley [2003]). The wind circulation is connected to the existence of three atmospheric "cells" per hemisphere: the polar, the Ferrel and the Hadley cells. A predominant surface wind field is associated with the lower branch of each cell: easterly trade winds characterize the surface expression of the Hadley cells between the subtropical fronts, while mid-latitude westerlies are found at the surface of the Ferrel cells from the horse latitudes to the polar fronts, and polar easterlies act in correspondence with the Polar cells, beyond the polar fronts.

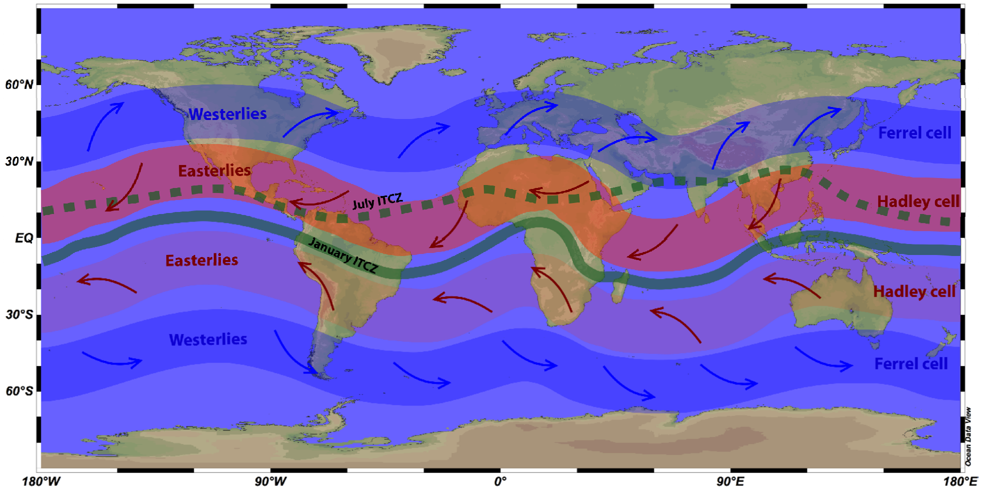

Fig. 1.4. Schematic organization of the dominant surface wind fields. Wind circulation at the tropics forces the position of the intertropical convergence zone (ITCZ), a band of high convection and precipitation. The ITCZ has a more northerly position in boreal summer, and conversely in winter. Depicted is the boreal winter configuration of the Hadley and Ferrel tropospheric cells, which determine the easterly and the westerly wind bands, respectively. The lighter shading of the Hadley cell in the Southern Hemisphere indicates that the Hadley cell is properly defined only in the winter hemisphere, thus the northern one in this case.

The junction between the easterly trade winds belts of each hemisphere is the ITCZ. This is a low-pressure band of westward flowing air masses, and it is found approximately in correspondence of the thermal equator of the earth, the area characterized by the maximum surface temperature, differentiated from the geographic equator because of the uneven distribution of land and ocean masses between the two hemispheres. Due to the convergence of air masses over the warm thermal equator, most of the upward motion of the earth's atmosphere occurs over the ITCZ. This vertical displacement attracts surface water masses from higher latitudes, and those are deviated westwards by the Coriolis effect: the easterly trade winds. The air elevated at the ICTZ is then subdued mostly between the Hadley and the Ferrel cells. Because of the large oceanic evaporative processes that characterize the thermal equator, in correspondence to the ITCZ humid air masses are lifted, and as a consequence the ITCZ generally carries moisture and storms. While its mean position is 5° N (Philander et al., 1996), the ITCZ undergoes meridional (along meridians) seasonal shifts, reaching its northernmost position during boreal summer, and conversely during winter.

Along the ITCZ, the main monsoon systems are found, such as the East Asian, the Indian, the West African, the North and South American monsoons (Trenberth et al., 2000). These are atmospheric circulation patterns that characterize areas where, during the warmer season, a strong gradient in the heating of land and ocean surface occurs. Typically, monsoon systems imply strong seasonal changes in precipitation, with the annual occurrence of one wet and one dry phase (Hastenrath, 1991). These are brought about by complete, or near-complete, reversal in wind circulation. During the wet season, the land warms up more than the sea surface, due to the higher heat capacity of water, and because of convection of water underneath the sea surface. Over the relatively warm continents, air masses rise, creating a low-pressure system at the surface, drawing moist air from over the ocean onto the continent, and causing intense precipitation. Since the ITCZ is defined by the position of the tropical wind belts, and since monsoon systems are determined by wind patterns, the position of the ITCZ has a strong influence on the monsoons (e.g., Yancheva et al. 2007). Also, because thermal mechanisms are at the core of monsoon dynamics, the forcing to which monsoonal systems are most sensitive is insolation, which varies on an annual basis, but also on orbital timescales (see section 1.1). In fact, paleo reconstructions from loess plateaus (e.g., Liu and Ding, 1998), speleothems (Wang et al., 2001), lakes (Ledru et al., 2005; An et al., 2011) and marine sediments (Peterson et al., 2000) have shown that monsoon intensity changed on a wide range of time scales, reflecting both changes in regional insolation (e.g., Cruz et al., 2005) and global climate change (Wang et al., 2004).

1.3 The climate proxies used in this study

Most instrumental climate observations only extend as far back as the 19th century. Therefore, to reconstruct the variables of older climate researchers make use of proxies. Climate proxies are sources of information, found in physical remains (like tree rings, pollen, ice cores, ocean sediments), that reflect past climatic and environmental parameters, such as for example temperature, humidity, chemical composition, salinity. In paleoceanography, shells of foraminifera are the most used carrier of proxies for past ocean conditions, in particular for temperature (Lea, 2003; Feldmeijer et al., 2013). These unicellular organisms are amoeboid protists that secrete their calcite shells in aquatic environments. While most species of foraminifera inhabit the seafloor (forming part of the benthos community, hence called *benthic* foraminifera), about ~50 species (Kucera, 2007) live in the upper water column (forming part of the plankton community, hence *planktic* foraminifera [Emiliani, 1991]) within the photic zone, or closely underneath it, where they can either predate on photosynthetic plankton, or benefit from the photosynthesis of their own symbionts. The oldest used proxies from foraminifera are derived from the species' distribution within their community, which provide information about ocean temperature and ecological conditions (e.g., Phleger, 1939; Rau et al., 2002). Later, the geochemistry of their calcite shells was recognized as a carrier of paleoceanographic proxies. In particular, the stable isotope composition is widely used as a proxy for and water composition and temperature, and the trace element composition (the ratio between Mg and Ca in the calcite) serves as a proxy for ocean temperature (Kucera, 2007; Katz et al., 2010). In this thesis mainly the chemical composition of the shells is used, and therefore in the next section an overview of such proxies is provided. Planktic foraminifera have long been studied in their natural environment, by collecting them with plankton nets, and more recently also in laboratory cultures, since the work of Bé and colleagues (1977): by these means the knowledge about the mechanisms behind the formation of their proxies is implemented. Besides planktic foraminifera, I also used proxies extracted from the bulk sediments, making use of thermo gravimetric analysis (TGA; Coats and Redfern, 1963), and X-ray fluorescence (XRF) scanning (e.g., Jansen et al., 1992), which provide information about the changing origin of the sedimented material, and the proportions thereof. TGA is a method to determine the total abundance of carbonates in dried samples, based on the principle of temperature-dependent incremental degradation of the carbonate fraction of the sediments, which are weighted along the process. The principle behind XRF-scanning consists of irradiating the sediments along a core with X-rays, and in analysing the secondary x-radiation emitted by the sediment. The emission spectra are element-specific, which permits to recognize their abundance in the sediment matrix. This is a relatively expedite and inexpensive manner to obtain a record of sedimentary history with virtually the maximum resolution. This technique provides the basis for the study in Chapter 5, where the ratio between titanium and calcium XRF counts is used as a proxy for terrigenous versus pelagic sediment abundance at the Brazil continental margin. In addition, as presented in Chapter 3 and in the outlook in Chapter 6, I apply XRF scanning also to the Walvis Ridge core.

1.3.1 Oxygen isotopes in foraminifera

A bit of history

In the 1950's, Cesare Emiliani understood that the idea of Urey (1947), of using the isotopic composition of calcite as a thermometer for the waters in which it has calcified, could be applied to organically precipitated material, namely the shells of planktic foraminifera, for reconstructing the temperature of waters of the geological past. In his study of 1955 (Emiliani, 1955) he selected planktic foraminifera from sediment cores in the Pacific and Atlantic Oceans, dissolved their calcite in acid, and measured the isotopic composition of oxygen ($\delta^{18}O$) in the released CO_2. This constituted the first record of water temperatures for the geological past, which matched so well with terrestrial observations and seemed so solid that the author adventured in the prevision of the arrival of another ice age in about 10,000 years. Emiliani, as Epstein before him (Epstein et al., 1951), already noted that his oxygen isotopes did not represent only temperature, but also the composition of the water in which calcification took place. Differences in the composition of oxygen in water masses exist between tropical and polar, surface and bottom waters, but also along geological time. Emiliani argued that during glacial times, the large accumulation of ice, and the relative fractionation processes, must have affected the global composition of oceanic water (by enriching it in ^{18}O), and calculated, by estimating the global ice mass accumulated during the last glacial, a glacial-to-interglacial correction of 0.7 ‰ (permil).

Another landmark in the field must be attributed to Nicholas Shackleton who, in 1967, coupled benthic $\delta^{18}O$ to Emiliani's planktic $\delta^{18}O$ from the same sediments, and recognized that the glacial-to-interglacial differences are largely due to the "extraction of large amounts of water from the oceans during glacial periods and recirculation of this water during periods when glaciers were at their present levels", instead of being a record of oceanographic events (Shackleton, 1967). Paleotemperatures needed then to be re-calculated according to a time-varying correction for ice volume change, accounting for as much as 1.6 ‰ $\delta^{18}O$ variation between glacial and interglacials. This different interpretation of the $\delta^{18}O$ data was welcomed as a new powerful stratigraphic tool, and opened the next phase of studies on the variability of the Pleistocene climate.

More studies on the nature of the glacial cycles were conducted: Broecker and van Donk (1970) generated a now-classic saw-tooth record of planktic foraminifera isotopes that depicted glacial cyclicity over the last million years, and were thus able to analyse in more detail the orbital mechanisms underlying climatic shifts. This line of research led to the generation of the so-called isotopic "stacks", i.e. integrated compilations of foraminiferal $\delta^{18}O$ curves (Imbrie et al., 1984; Martinson et al., 1987; Huybers and Wunsch, 2004; Lisiecki and Raymo, 2005) that served, and still serve, to unravel the timing of glacial cycles, and to assign dates to marine records beyond the age-applicability of radiocarbon dating (about ~40 kyr).

Other studies revealed important details about this revolutionary but complicated proxy. Duplessy et al. (1970) obtained different $\delta^{18}O$ values for different species of benthic foraminifera from the same samples, and thus proposed fractionation processes to be controlled by factors other than mere temperature. Shackleton et al. (1973) were for the first time able to collect enough foraminifera from plankton tows as to allow isotopic measurements on them. Their results questioned Emiliani's assumption, that foraminiferal calcite is deposited in equilibrium conditions. In other words, they proved the existence of the so-called "vital effects", a sort of "black box" of likely metabolic or environmental processes that controls the incorporation of heavy oxygen in the calcite lattice, and that decades later still puzzles biologists. To reassure researchers, Graham et al. (1981) found that departure from isotopic equilibrium is a characteristic of the species, and that it generally remains constant through geological time, i.e. the $\delta^{18}O$ was still fit for paleo temperature application. Later, Duplessy et al. (1981) opened a still-fervent era of research that focuses on understanding the calcification depth of foraminifer species, from their $\delta^{18}O$ composition. Work of that type, largely based on the use of open-close plankton nets, which permit the realization of depth-constrained tows, has produced a wealth of knowledge on the calcification depth range of planktic foraminifera. This enables nowadays paleoceanographers to selectively target paleo water masses at specific depth, as I did for Chapters 2, 3 and 4.

In more recent times, steps have been made towards using foraminiferal $\delta^{18}O$ to reconstruct temperatures. As mentioned, the complication of this parameter is ascribable to its dependency upon three factors (Fig. 1.5): I) the ice volume existing on the planet at a given time, II) the local $\delta^{18}O$ anomaly of seawater, in turn largely dependent on salinity, III) the calcification temperature. To constrain component I, the strategy has often been to use the available reconstructions of relative sea level, and to apply a correction to foraminiferal $\delta^{18}O$ converting the coeval sea level value (e.g., Waelbroeck et al., 2002) into $\delta^{18}O$ units. When the first direct proxies for temperature came into use (i.e. proxies as U^{k}_{37}, from coccolithophors' alkenones [Brassell et al., 1986], as Tex_{86}, from lipids of crenarchaeota [Schouten et al., 2002], and as Mg/Ca ratio on foraminiferal calcite [Nürnberg et al., 1996]), knowing the temperature dependence of $\delta^{18}O$ (e.g., from the culture work of Bemis et al. [1998] or Erez and Luz [1982]), it became possible to constrain also factor III and to extract the local $\delta^{18}O$ anomaly of seawater, which provides a qualitative indication of calcification salinity (for a review, see Rohling, 2007).

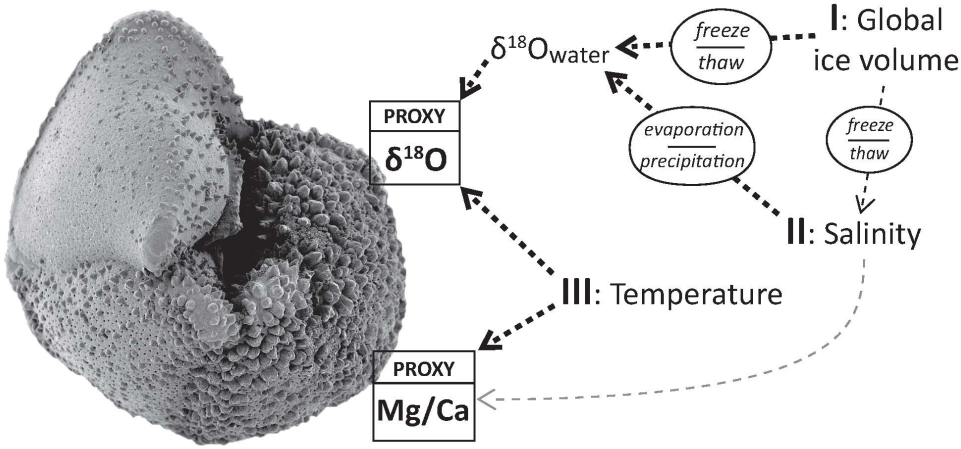

Fig. 1.5. Conceptual illustration of the $\delta^{18}O$ and Mg/Ca proxies from foraminiferal calcite, with the parameters that determine the incorporation of the signal, and the physical processes that govern isotopic fractionation. The electron microscope photograph of *Globorotalia truncatulinoides* was kindly provided by Brett Metcalfe, VU Amsterdam.

Single specimen analysis

Foraminifera are usually analysed in multi-specimen groups, for two main reasons: for better instrumental performance and ease, and because the common scope is to reconstruct average climatic conditions, for which pooling a larger number of specimen is better fit, as it more closely approximates the average composition of the population in the sample. Still, a notable limitation of this approach is that it does not allow addressing questions regarding the variability within the foraminiferal population.

Killingley and colleagues (1981) were the first who ventured to analyse the isotopic composition of individual foraminifer shells. The available instrumentation, though, limited the applicability to the largest specimens, and it was not until much later that the first studies were carried out on individual shells of the size commonly used for paleoceanographic purposes (smaller than ~400 μm, for the need of constraining life-stage related distortions [Duplessy et al., 1981]). This enabled paleoceanographers to include variability in the vocabulary of their research. Oceanographic variability indeed is associated to phenomena as seasonality, which has been investigated applying this approach by Billups and Spero (1996) and Ganssen et al. (2011), and El Niño southern oscillation, whose extremes Koutavas et al. (2006) and Leduc et al. (2009) tried to capture from foraminifera in the Eastern Equatorial Pacific. In Chapter 3, I present a novel application of the individual foraminifera $\delta^{18}O$ approach, that assists the reconstruction of the intensity of specific oceanographic features, across a period of marked climatic change in the Pleistocene.

In perspective, the science of foraminiferal isotope proxies will likely be advanced by the latest developments in high-performance analytical techniques. Whereas in the days of Emiliani hundreds of large foraminifera were necessary to obtain a single $\delta^{18}O$ value, it will probably become routine to assess isotopic composition in micrometer-spots on the cross section of a shell, by means of ion microprobe (Kozdon et al., 2009) and nanoSIMS (secondary ion mass spectrometry) (Vetter et al., 2013).

1.3.2 Magnesium to calcium ratio in foraminifera

Mg^{2+} abundance in foraminiferal calcite, relative to Ca^{2+}, shows a depletion of two orders of magnitude, in comparison with inorganically precipitated calcite (Bentov and Erez, 2006). Even though the application of the Mg/Ca paleo thermometer is relatively recent, the knowledge of this mechanism is much older than for the oxygen isotopes. Already in the early 20th century, Clarke and Wheeler (1922) understood that in calcifying organisms, the abundance of magnesium incorporated in their shell could be related to temperature, since the Mg content of the oceans seems relatively constant. Later, Chave (1954) confirmed the hypothesis that, together with causes related to the mineralogy and species' specificities, temperature plays a role in determining organic Mg inclusion.

The culture experiments of Nürnberg et al. (1996) yielded the first Mg/Ca-to-temperature relationship, which was linear. But since the work of Lea et al. (1999) it has been established that foraminiferal Mg/Ca dependence on temperature is better depicted by an exponential relationship, of the type $Mg/Ca = A\ exp^{BT}$, where T is temperature, and A and B are species-specific constants obtained through regression analysis.

Since then, many efforts have been placed on determining accurate calibrations for use in paleothermometry, with methods comprising live culturing, and comparison of plankton tows, sediment traps and core top samples with measured ocean temperatures (e.g., Mashiotta et al., 1999; Elderfield and Ganssen, 2000; Anand et al., 2003). Figure 1.6 shows a number of species-specific calibration curves proposed in the literature, for some species commonly used in paleoceanography, and employed for temperature reconstruction in Chapter 4.

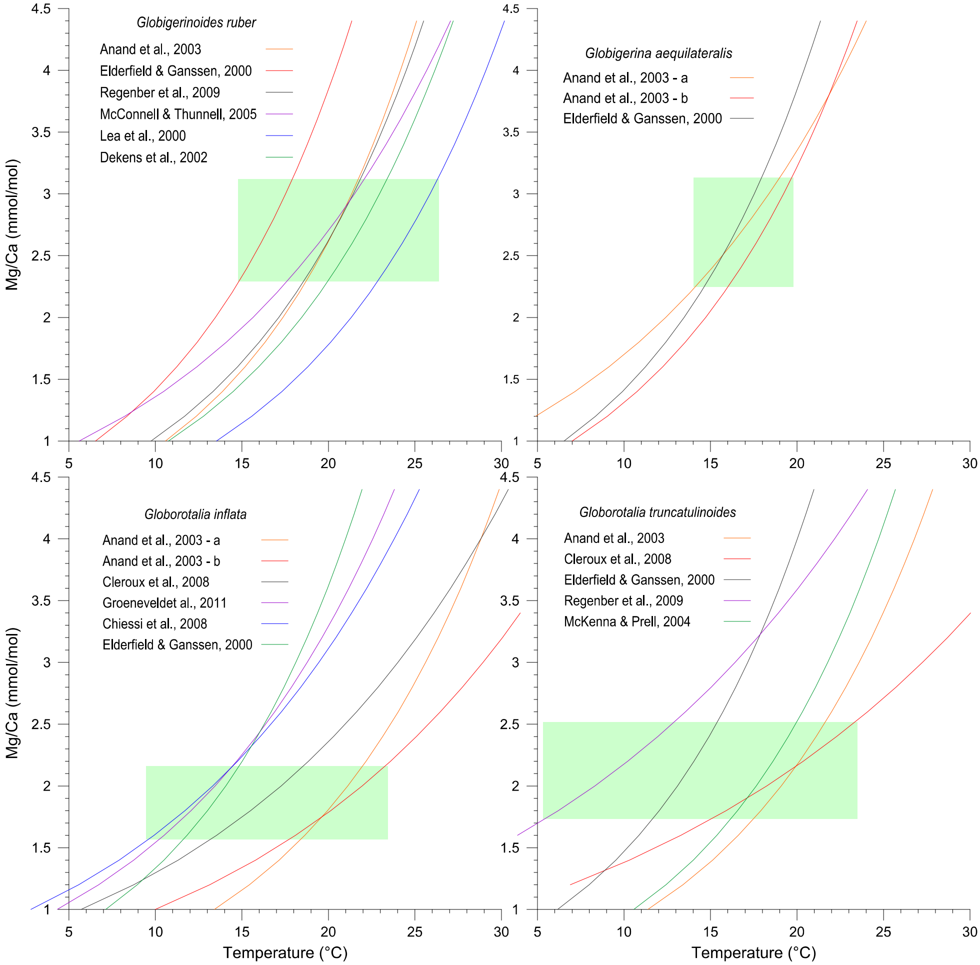

Fig. 1.6. A set of published species-specific calibration curves that convert Mg/Ca ratios from foraminifer shells into calcification temperatures. Curves are presented for the four planktic species treated in Chapter 4. The green areas represent the range of Mg/Ca values obtained from the fossil samples of core 64PE-174P13 (central Walvis Ridge), and the corresponding range of inferred temperatures. Evidently, the choice of the calibration curve determines large differences in absolute values of temperatures, and in some cases also in the range. The choice of calibration curve must therefore be taken carefully, considering the geographical and hydrological features of the site, and the paleontological characteristic of the material.

In recent years, some controversy arose regarding the applicability of the proxy as reliable paleothermometer, due to a larger influence of salinity on the incorporation of Mg (KIsakürek et al., 2008; Arbuszewski et al., 2010) than previously suggested by the pioneering studies of Nürnberg et al. (1996) and Lea et al. (1999). The latest assessments on the matter, though, constrain the Mg/Ca sensitivity in the order of only 4 % per salinity unit change (Hönisch et al., 2013), therefore warranting the continuation of its paleothermometer application.
Expectedly, there is interest in employing the Mg/Ca approach to individual shells (as considered in the former section for $\delta^{18}O$), to directly infer temperature variability.

Decisive strides have been made towards this objective during the last decade. For this scope an alternative, flow-through cleaning technique has been devised, that prevents excessive sample loss during preparation (see following paragraph) and enables the preparation of single shells for measurement (Haley and Klinkhammer, 2002). Morever, high-performance spectroscopy techniques are applied that allow very small quantities of calcite to be analysed, by means of laser ablation (Eggins et al., 2003) or microprobe (Sadekov et al., 2005) systems. The obstacle to a wide application of the latter techniques has to do with the heterogeneous distribution of Mg across the foraminiferal shell, which makes it still arbitrary to extract representative average values from the single specimens.

Installing trace element lab facilities at the VU Amsterdam

A problematic aspect of the use of this Mg/Ca proxy is the existence of contaminant phases that fill, coat and adhere to the calcite shell found in the sediments (Pena et al., 2005). Those substrates, often due to the abundance of clays and to post-depositional interaction of the shell lattice with the sediment matrix, are frequently rich in Mg, and therefore bias paleotemperature reconstructions, typically to the warmer side. For this reason a number of cleaning steps are necessary to prepare samples prior to analysis, and cleaning protocols have been formalized (e.g., Martin and Lea, 2002; Barker et al., 2003). I was interested in applying this Mg/Ca technique to work out upper ocean temperatures for the marine cores studied in this thesis, and I therefore decided to install, at the VU Amsterdam, the laboratory facilities needed to perform the rigorous cleaning outlined in Barker et al. (2003) (for details refer to section 4.2.2), and to develop a protocol for analysis of the cleaned samples using a Varian 720 ES ICP Optical Emission spectroscope. The stability of the measurements is testified by the very good reproducibility of the external calcite standard ECRM 752-1 (Greaves et al., 2005). The results of those analyses are presented in Chapter 4, supported by further methodological details about the cleaning and by specifications about instrumental performance, and in the outlook of Chapter 6.

1.4 Research scopes and outline

In the first three sections of this introduction, I have explained the sensitivity and the relevance of the South Atlantic Ocean with respect to the climate system, and the methodologies that I used for my paleo reconstructions. Now I am able to present the aim of the studies included here, while outlining the structure of the thesis.
The EU project GATEWAYS (www.gateways-itn.eu), which funded the realization of the work here presented, aims at investigating the Agulhas system in its present and past variability, with observational, modelling and proxy approaches. My work is based on the latter approach, using the marine proxies outlined in the previous section to reconstruct past hydrological features. In addition, in Chapter 3, I present an example of how proxy data can be integrated to the output of modern-ocean modelling, to aid the interpretation of the sedimentological evidence, and to validate paleo research hypotheses.

The paleo Agulhas Current has recently been investigated in its northern section by Caley et al. (2011), and in its southern section by Simons et al. (2013). The past hydrological variability of the AL area was the object of the research of recent geochemical studies of Martínez-Méndez et al. (2010), Marino et al. (2013) and Kasper et al. (2014). The quantification of the AL itself has been the focus of Peeters et al. (2004), who defined an "Agulhas leakage fauna" from sampling a modern Agulhas ring, and applied the index to faunal counts down-core, and of the geological study of Franzese et al. (2006). Also, the position of the Agulhas retroflection has been studied through the isotopic composition of the sediment by Franzese et al. (2009).
No proxy study to date has aimed to seize the effect of the AL in the Atlantic. The works presented here focus on the paleoceanographic phenomena that took place downstream the AL in the AMOC, specifically in the southeast Atlantic and in the western tropical Atlantic, to test the hypothesis that the AL might have had a considerable effect upon the AMOC during times of climate change (e.g., Berger and Wefer, 1996; Knorr and Lohmann, 2003). For this, two marine sediment cores were selected, one at a proximal and one at a more distal location with respect to the AL area (Fig. 1.3).

Studying the origin area of the upper AMOC

The proximal core, 64PE-174P13, was extracted from the central Walvis Ridge (at a water depth of 2900 m), a location presently underneath the trajectory of most Agulhas rings (Boebel et al., 2003) (Fig. 1.3). The bathymetry of the central Walvis Ridge seems to function as a channel for the passage of the rings (Dencausse et al., 2010), potentially associated with the return path of NADW (van Sebille et al., 2012). On the other hand, the central Walvis Ridge is situated on the eastern flank of the subtropical gyre. This combination of circumstances makes the setting ideal for our scope of assessing the result of the AL in this region at the origin of the upper branch of the AMOC.

In Chapter 2, I address the following research questions: How did the South Atlantic upper ocean stratification change during Pleistocene climate oscillations? Can we recognize a systematic glacial-interglacial pattern of this region's thermocline? Would that show synchronism with shifts in the amount of Indian Ocean input?
For this scope, I reconstruct the surface and thermocline hydrography for the whole extent of the core, using the oxygen-isotope composition of two planktic foraminifera taxa with distinct depth habitats. This enables the computation of a proxy for upper ocean stratification, whose temporal evolution appears to be strongly paced by the last five glacial-interglacial cycles.

Chapter 3 focuses on an interval of prominent climate change, the penultimate termination (T-II, around 130,000 years before present), and addresses the question as to whether the observed AL peak (Peeters et al., 2004) actually penetrated the subtropical gyre circulation. Besides the paleoceanographic scope, I concentrate on a rather methodological question, i.e. whether it is possible, from foraminiferal proxies, to assess the paleo intensity of hydrographic features such as perturbations from eddy structures.

In Chapter 4 the emphasis remains on termination II. In this study I am interested in connecting changes in the hydrography of this delicate region to prominent variability at the AL area, revealed by published records (Marino et al., 2013). I am interested also in understanding how temperature and salinity changed in the frame of the rearrangements of the AMOC that took place around T-II, to shed light on the role of the South Atlantic during the climatic shift from MIS 6 to 5. Further, I want to clarify the role of this oceanic region in the pattern of two-step deglaciation that is emerging in the literature for T-II (e.g., Cannariato and Kennett, 2005; Landais et al., 2013). This time I investigate temperature and salinity changes at high resolution and at various depths in the water column.

Studying the western tropical Atlantic, underneath the ITCZ

The work on the NE Brazil core, MD09-3246, retrieved close to the continental shelf (at a water depth of 900 m) (Fig. 1.3), is aimed at reconstructing the precipitation regime of the adjacent land region over several glacial cycles, and to connect it to changes in atmospheric circulation. Previous studies, based on marine sediments from the same region, have shown that precipitation over the NE Brazilian continent responded positively to the abrupt cooling events that occurred repeatedly in the North Atlantic during the last glacial period (Arz et al., 1998; 1999b; Behling et al., 2000). Speleothem reconstructions from various areas in Brazil testify the broad synchronicity of the changes in South American summer monsoon recorded in southern Brazil (Cruz et al., 2005; Wang et al., 2006), in western Amazonia (Cheng et al., 2013), and in northeastern Brazil (Wang et al., 2004). A connection has already been hypothesized between the paleo monsoons of the two hemispheres (Wang et al., 2004). A recent research question is whether displacements of the ITCZ were substantially synchronous during climate changes of the Pleistocene; in other words whether it is appropriate to consider a mechanism of Global-Paleo-Monsoon (Wang, 2009; Cheng et al., 2012; Kutzbach et al., 2008; Caley et al., 2011). I address this question in Chapter 5 of this thesis, where a new record of South American summer monsoon variability over the last ~0.4 million years is correlated to the time series of East Asian summer monsoon.

In Chapter 6 I synthesize the results and conclusion that emerged from the various studies contained in the thesis, and examine the responses that this work has been able to provide to the outlined research questions. Further, in an outlook section, I present a number of ideas for future research that originated from the work performed, and from additional paleo questions that took form during the process.

2

A record of the last 460 thousand years of upper ocean stratification from the central Walvis Ridge, South Atlantic

Paolo Scussolini and Frank J. C. Peeters

Earth and Climate Group, Vrije Universiteit, Amsterdam.

Published in *Paleoceanography*, 28(3), 426-439.

Abstract

The upper branch of the Atlantic Meridional Overturning Circulation predominantly enters the Atlantic Ocean through the southeast, where the subtropical gyre is exposed to the influence of the Agulhas leakage (AL). To understand how the transfer of Indian Ocean waters via the AL affected the upper water column of this region, we have generated new proxy records of planktic foraminifer from a core on the central Walvis Ridge, on the eastern flank of the South Atlantic Gyre. We analysed the isotopic composition of sub-surface dweller *Globigerinoides ruber* sensu lato, and thermocline *Globorotalia truncatulinoides* sinistral, spanning the last five Pleistocene glacial-interglacial cycles. The former displays a response to obliquity, suggesting connection with high latitude forcing, and a warming tendency during each glacial termination, in response to the inter-hemispheric seesaw. The $\delta^{18}O$ difference between the two species, interpreted as a proxy for upper ocean stratification, reveals a remarkably regular sawtooth pattern, bound to glacial-interglacial cyclicity. It rises from interglacials until glacial terminations, with fast subsequent decrease, appearing to promptly respond to deglacial peaks of AL. Stratification, however, bears a different structure during the last cycle, being minimal at Last Glacial Maximum, and peaking at Termination I. We suggest this to be the result of the intensified glacial wind field over the South Atlantic gyre and/or of the invasion of the South Atlantic thermocline by Glacial North Atlantic Intermediate Waters. The $\delta^{13}C$ time-series of the two species have a similar glacial-interglacial pattern, whereas their difference is higher during interglacials. We propose that this may be the result of the alternation of intermediate water masses in different circulation modes, and of a regionally more efficient biological pump at times of high pCO_2.

2.1 Introduction

As the understanding of the oceans' circulation evolves, it becomes more apparent that the transfer of Indian Ocean waters into the South Atlantic via the AL (Fig. 2.1) plays a key role in determining the variability of the Atlantic Meridional Overturning Circulation (AMOC) (Venegas et al., 1998; Biastoch et al., 2008; Garzoli and Matano, 2011). It is currently agreed that during the last Pleistocene glaciation the AMOC was more sluggish (Hesse et al., 2011; Negre et al., 2010) or superficial (Lynch-Stieglitz et al., 2007) than at present. Reduction in turnover strength was most severe during the deglaciation (McManus et al., 2004, Gherardi et al., 2005), before punctually recovering its fashion when climate re-emerged to its interglacial mode. It has been suggested that an explanation of this phenomenon, from hampered deglacial to interglacial restored AMOC, involves changes in the AL input: a key point in the upper branch of the global circulation (Knorr and Lohmann, 2003; Peeters et al., 2004; Bard and Rickaby, 2009; Marsh et al., 2007). To test this hypothesis, research has shown how this southern connection was strengthened and weakened through time, with fauna (Peeters et al., 2004) and sediment (Franzese et al., 2006) from the Indian Ocean leaking into the Southern Atlantic in concomitance with Pleistocene deglaciations. To further our understanding of the repercussions of this contribution, it is necessary to shift the focus to the portion of the South Atlantic downstream from the AL. It has been shown in lagrangian models how the heat and salinity of the South Atlantic, that is relevant to the surface branch of the AMOC, is contained at the depths of the thermocline, in the South Atlantic Central Water, of which probably 90% originates from the Indian Ocean via the AL "warm route" (Donners and Drijfhout, 2004), in contrast to the "cold route" from the Pacific Ocean, via the Drake Passage. This explains the necessity of studying the thermocline at the junction between the South Atlantic Gyre (SAG) system and the AL area, and of verifying the effect of the "warm route" on the structure of the South Atlantic upper ocean. In this context the following research questions must be addressed. How did the South Atlantic upper ocean stratification change during Pleistocene climate oscillations? Can we recognize a systematic glacial-interglacial (G-IG) pattern of this region's thermocline? And, would that show synchronism with shifts in the amount of Indian Ocean input?

2.1.1 Foraminifera proxy use

The calcite of planktic foraminifera is commonly used to obtain information about water masses in the geological record. Still, a great limitation of analysing a single species to characterize the past ocean is that the derived picture is necessarily adimensional, i.e., it fails to capture the vertical structure of the upper ocean, and the gradients of physical-chemical properties that drive circulation.

A number of micropaleontological studies have examined the potential of isotopically analysing more than one species along sedimentary records (e.g., Ganssen and Troelstra, 1987; Wefer et al., 1996; Lea et al., 2000; Spero et al., 2003), but only in a few studies were inter-specific signature differences calculated, and utilized as evidence of shifts in upwelling regimes (Whitman and Berger, 1992; Mohtadi et al., 2005) or with the explicit aim of inferring the stratification of ancient oceans (e.g., Douglas and Savin, 1978). The reliability of the latter method has been testified for the Indian (Williams and Healy-Williams, 1980) and for the Atlantic Ocean (Mulitza et al., 1997; Steph et al., 2009; Simstich et al., 2012); the outcome of such approaches confirms that analysis on pairs of planktic species can function as proxies for the stratification of the upper water masses.

2.1.2 Oceanographic setting

In order to address our questions, we opted for a location that is representative of the SAG, and also under the influence of the AL, downstream the "conveyor belt". We selected a setting not affected by the upwelling associated with the southwest African margin, which inevitably entangles the oceanographic record.

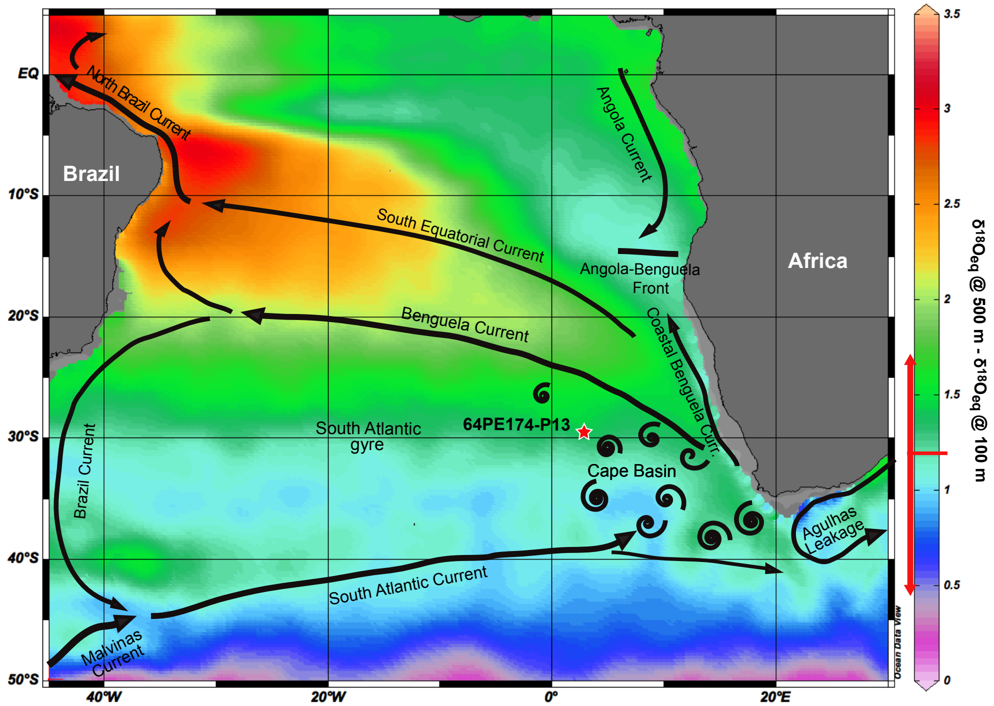

Fig. 2.1. Location of the studied core, and organization of sub-surface, South Atlantic Central Waters currents. Coloured contours denote the $\Delta^{18}O$ between the $\delta^{18}O_{eq}$ at 100 m and 500 m depth, calculated as outlined in Methods. Red lines along the legend indicate core top value and range in the record. Currents are drawn mostly from Stramma and England (1999). Map generated with Ocean Data View (http://odv.awi.de).

The central Walvis Ridge is situated underneath the southeast sector of the SAG, at the interface between the SAG and the turbulent ocean portion that has been referred to as Cape Cauldron (Boebel et al., 2003; Gordon, 2003; Giulivi and Gordon, 2006) (Fig. 2.1). The site is crossed at the surface mostly by SAG waters from the SW, advected by the South Atlantic current, which bear the influence of the Southern Ocean, and flow to NE, therefore feeding what is considered the oceanic branch of the Benguela Current (e.g., Garzoli and Gordon, 1996; Garzoli and Matano, 2011). Circulating within the permanent thermocline are primarily Eastern and Western South Atlantic Central Waters (Poole and Tomczak, 1999); Gordon et al. (1992) have shown that the majority of thermocline waters in the southeast Atlantic is derived from the Indian Ocean. Additionally, an important source of thermocline water at the central Walvis Ridge are the Agulhas rings that, escaping Cape Cauldron, preferentially travel in close proximity to our study site (e.g., Goni et al., 1997; Dencausse et al., 2010; Boebel et al., 2003; van Sebille et al., 2012); at this point rings still contain masses of Indian Ocean origin, characterized by temperature and salinity that exert considerable influence on the mean circulation of the southeast Atlantic (e.g., Matano and Beier, 2003; Garzoli and Matano, 2011). Waters thus formed constitute the early upper branch of the AMOC.

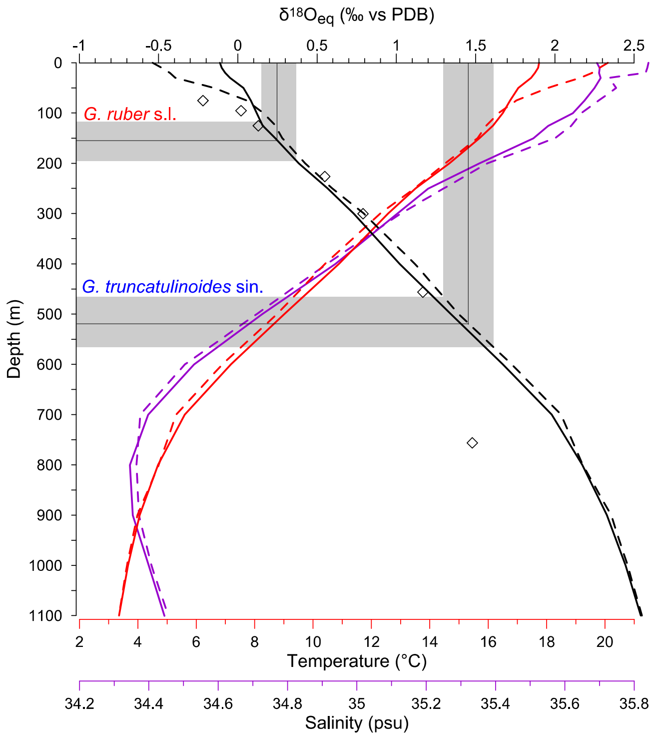

Fig. 2.2. Upper ocean hydrography for the core location, using data from the Word Ocean Atlas 2009 (Locarnini et al., 2010): $\delta^{18}O_{eq}$ (black, see Methods), temperature (red), salinity (purple), and density (brown) profiles for the core location, in October (*G. ruber* s.l. highest abundance, continuous lines), and December (*G. truncatulinoides* sin. highest abundance, dashed

lines). $\delta^{18}O_{eq}$ from Lonçaric et al. (2006) is represented by the open diamonds. Grey bands represent standard deviation (see Methods).

The mixed layer depth varies seasonally, reaching its maximum in (austral) winter (~100 m) and shoaling in summer to a minimum of ~30 m (Fig. 2.2) (World Ocean Atlas 2009 [Locarnini et al., 2010]). The permanent thermocline extends to a depth of ~700 m, and its shape does not undergo relevant seasonal modifications, save for a slight cooling at depths of 100 to 300 m in autumn and winter (Fig. 2.2). The low sedimentation rate that derives from the pelagic setting and the oligotrophic conditions of the SAG, have discouraged the generation of paleoceanographic records with a resolution that permits the observation of sub-orbital scale variability.

With this study we intend to fill a gap, regarding the current understanding of sub-orbital dynamic connections between the AL system and the South Atlantic circulation. We present sub-surface and thermocline paleoceanographic records of foraminiferal stable isotopes, and we deliver the first upper ocean stratification record of the east SAG, for the last five Pleistocene climate cycles. We show that the rhythmicity of this oceanographic series is powerful on the 100 thousand years (kyr) band, and that it reveals a pattern strictly bound to G-IG successions, allowing us to formulate a number of mechanisms that link SAG stratification to the Agulhas leakage and to changes in AMOC.

2.2 Methods

Piston core 64PE-174P13 (hereinafter 174P13) is 760 cm long and was extracted from the central Walvis Ridge (29° 45.71' S, 2° 24.10' E) at a depth of 2912 m (Fig. 2.1), during the MARE III expedition in 2001. Sediments are described as carbonate ooze, reflecting the relatively low pelagic sedimentation regime.

Sampling was conducted at 4 cm intervals (and at 2 cm, dependent upon time resolution). Fossil planktic foraminifera *Globigerinoides ruber* sensu lato (s.l.) and *Globorotalia truncatulinoides* sinistral (sin.) were picked from a narrow size fraction, 250-300 μm, to minimize size-related effects that introduce distortions in the data set. This size fraction is free of pre-adults and, in the case of *G. truncatulinoides* sin., of individuals that have undergone gametogenic calcification (Duplessy et al., 1981), which would confound the interpretation of their isotopic signal. Additionally, due to the large size variability of *G. truncatulinoides* sin. in the record, larger shells of this taxon (350-500 μm) were selected from a small subset of samples ($n = 20$), to evaluate the implications of shell size and gametogenic calcite for the $\delta^{18}O$ signal. These additional analyses yielded values that differ at times notably from the 250-300 μm fraction, generally displaying higher variability (Fig. 2.3), which we attribute to the wider size range of our additional measurements, and to the higher associated variability in the calcification depth. From these results, however, we cannot ascertain a systematic offset between the two size classes (t-value = 0.338, t-probability = 0.739, DF = 19); the null-hypothesis that the composition of large and small sized shells is the same cannot be rejected.

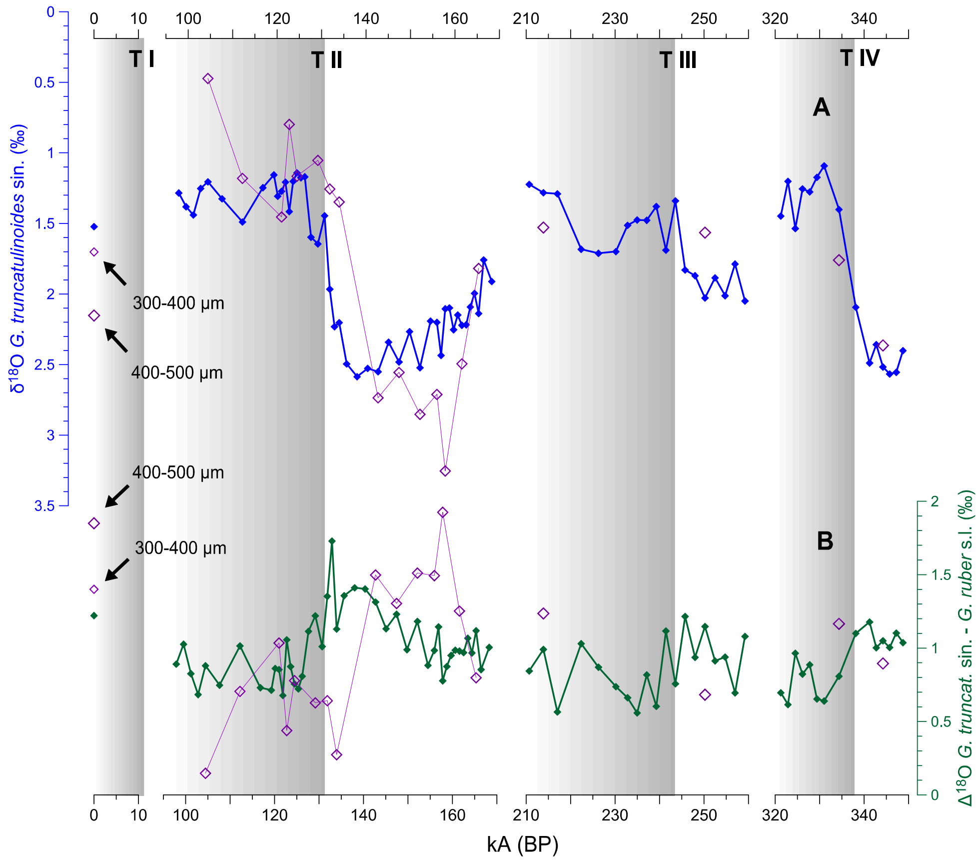

Fig. 2.3. A: *G. truncatulinoides* sin. $\delta^{18}O$, from size fraction 250-300 μm (blue, full diamonds) and 350-500 μm (purple, open diamonds). B: $\Delta^{18}O$ between *G. truncatulinoides* sin. and *G. ruber* s.l., calculated using *G. truncatulinoides* sin. $\delta^{18}O$ from the size fraction 250-300 μm (green, full diamonds), and 350-500 μm (purple, open diamonds).

Between 35 and 55 shells for each species were crushed, and a portion of approximately 150 μg of homogenized calcite fragments was used for stable isotope analysis. This approach was adopted to maximize the number of shells involved, and therefore the analyses' representativeness of the foraminiferal population. Isotopic measurements were conducted in duplicate, using a Thermo Finnigan Delta Plus mass spectrometer equipped with a Gas Bench II preparation device at the Vrije Universiteit, Amsterdam. The instrumental reproducibility was routinely monitored using international calcite standards NBS 19 and IAEA-CO-11 (Ishimura et al., 2008), and yielded an average error of ±0.10 ‰ (1 σ) for both oxygen and carbon. A correction was applied for external standard offset, to improve inter-run comparability.

Due to the inherent variability typical of fossil foraminifera populations (Killingley et al., 1981) some repeats bore anomalously vast discrepancies (> 0.2 ‰); in those cases triplicate measurements were performed. The standard deviation of the duplicates was less than 0.08 ‰ for both species, and for both oxygen and carbon.

From each of the two curves we subtracted the record of the average contribution of the global accumulation of ice to the mean $\delta^{18}O$ of seawater ($\delta^{18}O_{sw}$), also called ice volume effect (IVE). The latter was calculated using the model model of Bintanja and van de Wal (2008), forced to match the LR04 global foraminifer $\delta^{18}O$ stack (Lisiecki and Raymo, 2005). Prior to subtraction, we converted the IVE dataset to the PDB scale. The propagated error is ± 0.12 ‰ for both species. The age-scale coherence of the model with that assigned to core 174P13 prevents excessive artefacts generated by time offsets. The $\delta^{18}O$ curves freed of the IVE (hereinafter $\delta^{18}O$-IVE) therefore represent estimations of local temperature and salinity changes.

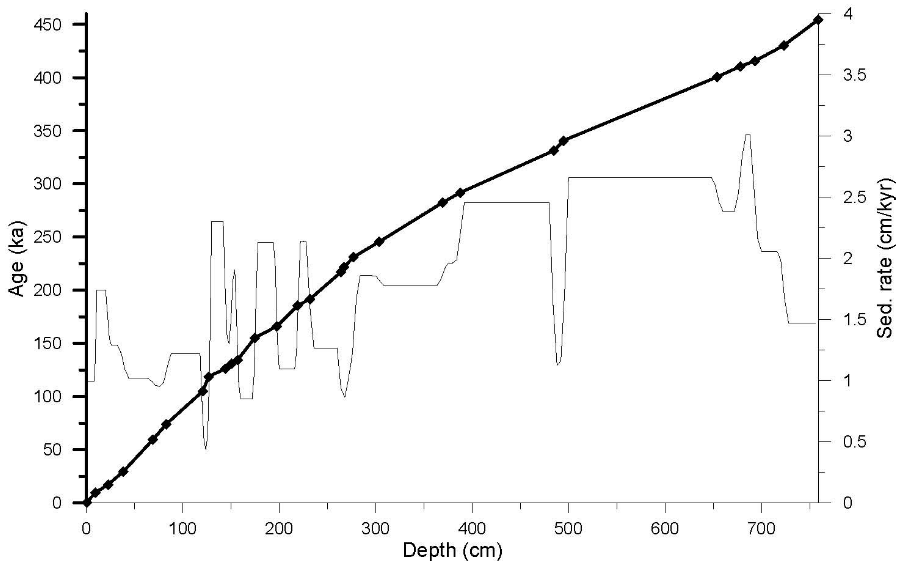

Fig. 2.4. Age-depth plot (bold line) and sedimentation rate (thin line) for core 64PE-174P13.

The stratigraphy for core 174P13 is based on alignment of our *G. truncatulinoides* sin. record to the LR04 $\delta^{18}O$ stack (Lisiecki and Raymo, 2005) (Fig. 2.4 and 2.5 A). This species was chosen for the age control because, calcifying deeper, it is less prone to incorporate in its $\delta^{18}O$ distortions due to the higher temperature and salinity variability of the surface (see rest of Methods), which are not negligible in the sub-tropics.

2.2.1 Calcification depth and $\delta^{18}O$ equilibrium

The choice of the symbiont-bearing *G. ruber* to obtain a sub-surface water signal was motivated by the quantity of studies based on stratified net samples, that confirm its photic zone habitat (Deuser et al., 1981; Lonçaric et al., 2006; Peeters and Brummer, 2002), dictated by the light requirement of its symbionts. Successful use in previous paleoceanographic studies (e.g., Thunell et al., 1999; Dekens et al., 2002; Schmidt et al., 2004), attests ecologic and genetic stability across the Pleistocene, and grants direct comparability of results.

From stratified tows at a location in the proximity of core 174P13, Lonçaric et al., (2006) assigned the base of the productive zone for *G. ruber* at ~125 m, but found highest shell concentrations more shallow, within the seasonal thermocline. Blooms of this species at the central Walvis Ridge occur in (austral) spring and again in winter (Lonçaric et al., 2007).

Modern developments in foraminifera studies render the distinction among sub-species of this taxon obvious and imperative for proxy-based reconstructions, due genetic differences (Aurahs et al., 2011) that are manifest in non-negligible geochemical offsets between morphotypes (Steinke et al., 2005; Kuroyanagi et al., 2008; Numberger et al., 2009). We therefore limited our selection to those *G. ruber* that correspond to the sensu lato morphotype defined by Wang (2000), as it is the most consistently abundant in the core.

For the completion of its reproductive-cycle, the species *G. truncatulinoides* is considered to be dependent on the presence of a deep thermocline (Lohmann and Schweitzer, 1990). Paleoceanographers have often recommended its use to record "deep" upper ocean signals (e.g., Mulitza et al., 1997; LeGrande et al., 2004; Steph et al., 2009; Cleroux et al., 2007; Ufkes and Kroon, 2012). Furthermore, the benefit of using *G. truncatulinoides* for producing a record of thermocline conditions is well supported by observations from core tops extensively covering the Atlantic Ocean, showing how the calcification of this species does not seem to follow isopycnals, nor to depend directly on temperature (LeGrande et al., 2004). We therefore assume that its preferential depth in the record did not depart significantly from today's.

Left and right coiling *G. truncatulinoides* (sinistral and dextral, respectively) correspond to different genotypes (de Vargas et al., 2001; Quillévéré et al., 2011). These have been shown to have distinct ecological preferences, in particular with respect to depth habitat (Lohmann and Schweitzer, 1990; de Vargas et al., 2001), different seasonality (Lonçaric et al., 2007), and are therefore expected to produce discordant geochemical records. We thus decided to select exclusively specimens of the sinistral variety, as it is the deepest calcifying morphotype (Lohmann and Schweitzer, 1990; Ujiiè et al., 2010) and therefore more apt to capture signals at the base of the thermocline. For this species, at the core location, the base of the productive zone has been established at ~400 m (Lonçaric et al., 2006), and its highest seasonal abundance in the early summer (Lonçaric et al., 2007).

To count on a first-hand estimate of the calcification depth of these taxa specifically for the study area, we carried out isotopic measurements on foraminifera from the core top, and compared those to modern local hydrography.

We calculated the isotopic composition of oxygen in sea water ($\delta^{18}O_{sw}$) calibrating in situ measured salinity with $\delta^{18}O$ values determined on water samples from station 154P04 (Lonçaric et al., 2006) ($n=8$; $R^2= 0.96$), adjacent to core 174P13:

$$\delta^{18}O_{sw}\ [PDB] = 0.486\ S - 16.83 - 0.27 \quad (1)$$

where the -0.27 ‰ correction is introduced to convert SMOW scale to PDB (Hut, 1987). We based the calculation of the equilibrium calcification on the empiric relationship of Kim and O'neil (1997) for inorganic calcite precipitation:

$$1000\ \ln(\alpha) = 18.03\ (10^3\ T[K]^{-1}) - 32.42 \quad (2)$$

where α is the fractionation factor between calcite and water, and applied its quadratic approximation of Bemis et al. (1998):

$$T[°C] = 16.1 - 4.64\ (\delta_{eq} - \delta_{sw}) + 0.09\ (\delta_{eq} - \delta_{sw})^2 \quad (3)$$

where δ_{eq} is the isotopic composition of calcite in thermodynamic equilibrium. Solved for δ_{eq}, it yields:

$$\delta_{eq} = \delta_{sw} + 25.778 - 3.333\ (43.706 + T[°C])^{0.5} \quad (4)$$

Interpolating modern water column hydrography we can estimate the apparent calcification depth from the core top $\delta^{18}O$ of the two species. Applying data from World Ocean Atlas 2009 (Locarnini et al., 2010; Antonov et al., 2010) for the month of major occurrence of each species, calcification depth is 150±43 m for *G. ruber* s.l. (October), and 525±50 m for *G. truncatulinoides* sin. (December) (Fig. 2.2). When using to locally measured $\delta^{18}O_{sw}$ (Lonçaric et al., 2006), the depth of *G. ruber* s.l. is 155±26 m, and that of *G. truncatulinoides* sin. is deeper than 750 m. The standard deviation is calculated based on multiple $\delta^{18}O$ measurements in the upper centimeters of the core. Although it is unrealistic to presume that calcite tests are formed at a discrete depth in the ocean, taking into account the vastly incomplete knowledge about the elusive depth at which foraminiferal shells are secreted, we still estimate that our two species record paleoceanographic signals ~350-400 m apart in the water column.

To illustrate the present-day pattern of South Atlantic upper ocean stratification, as close as possible to how it is incorporated in our record, we calculated the difference between the $\delta^{18}O_{eq}$ at 500 m and at 100 m, using temperature and salinity data from the World Ocean Atlas 2009 (Locarnini et al., 2010; Antonov et al., 2010), and applying the aforementioned equilibrium equation, and a South Atlantic salinity-to-$\delta^{18}O$ relationship (slope=0.51, intercept=17.40, n=61, LeGrande and Schmidt, 2006). These values are reported as contoured colors in Fig. 2.1.

2.2.2 Spectral analysis

The time series produced were analysed for their spectral components. To verify in which measure the spectra are influenced by the orbital tuning of our record (the L04 stack is in fact orbitally aligned [Lisiecki and Raymo, 2005]), we also computed them after alignment of our $\delta^{18}O$ to the planktic chronostratigraphy of Huybers (2007) (H07), which does not rely on orbital assumptions. As a further means of control on the robustness of our analysis with respect to the choice of the age model, we calculated spectra also on the time series with age model obtained through tuning of *G. ruber* s.l. $\delta^{18}O$ to the LR04 stack. The spectral results discussed in this work are valid regardless of the age model.

2.3 Results

Core 174P13 spans the past ~460 kyr. The $\delta^{18}O$ curve of both species predominantly displays the imprint of the last five G-IG cycles (Fig. 2.5 A). Spectral analysis of these series reveals identical significant peaks, at 100 and 41 kyr (Fig. 2.7 A). The 100 kyr band of *G. truncatulinoides* sin. is evidently more pronounced than that of *G. ruber* s.l.

2.3.1 *Globigerinoides ruber* s.l. $\delta^{18}O$-IVE

The ice volume effect-free profile of this species presents variability at the sub-G-IG scale in the order of ~0.7 ‰ (Fig. 2.6 B). Underlying this pattern it is visible a long term decrease that continues from MIS 12 to MIS 7. No structure is identifiable that replicates across the five G-IG cycles. Despite that, terminations are characterized by the occurrence of low peaks. Such shifts are very sharp at termination V (T-V) (~1 ‰) and T-I (0.5 ‰). They begin earlier, and have a more gradual development, prior to T-IV, III and II. In the spectrum of *G. ruber* s.l. $\delta^{18}O$-IVE the 41 kyr obliquity band is statistically significant (Fig. 2.7 B).

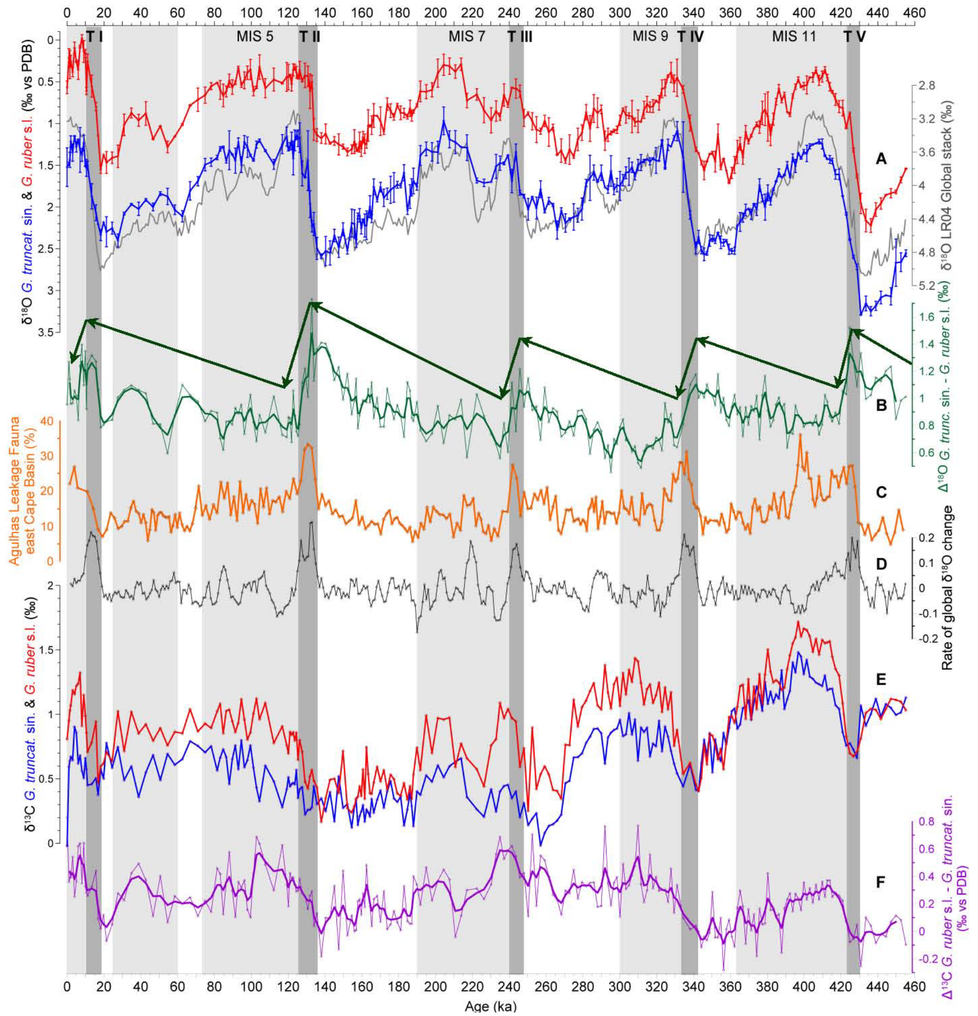

Fig. 2.5. A) δ^{18}O of *G. ruber* s.l. (red, above) and *G. truncatulinoides* sin. (blue, below) (error bars represent inter-measurement standard deviation), and Global δ^{18}O stack of LR04 (grey) (Lisiecki and Raymo, 2005); B) Δ^{18}O between the two species (Gaussian filtered series in bold, arrows emphasize the sawtooth pattern); C) Agulhas Leakage Fauna from east Cape Basin (Peeters et al., 2004); D) Rate of global δ^{18}O change, calculated as the first derivative of the LR04 stack (using the distance between 5 points in the series, to eliminate excessive noise); E) δ^{13}C of *G. ruber* s.l. and *G. truncatulinoides* sin.; F) Δ^{13}C between the two species (Gaussian filtered series in bold).

2.3.2 *Globorotalia truncatulinoides* sin. δ^{18}O-IVE

Maxima of the δ^{18}O-IVE series of this taxon fall at ~440, 360, 270, 145 and 27 thousand years before present (ka), thus not following the G-IG cycles (Fig 2.6 D). They reveal instead a pointed pulse structure that does not normally appear in oceanographic records, and that is considerably similar to the eccentricity parameter

(Fig. 2.6 C-D). The spectrum of the δ18O-IVE series shows significant periodicity at ~100 kyr, typical of the combination of the orbital components of eccentricity (Fig. 2.7 B).

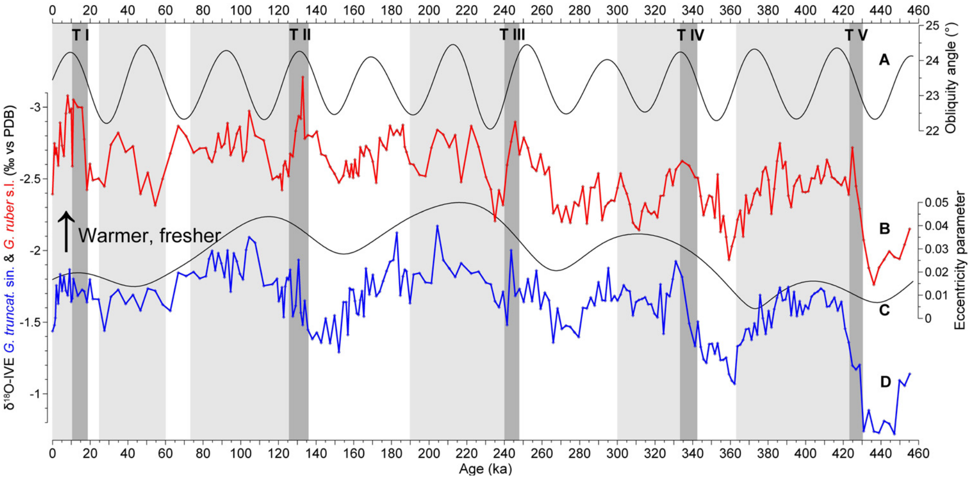

Fig. 2.6. A) Obliquity angle; B) δ18O-IVE of *G. ruber* s.l. (see Methods); C) eccentricity parameter; D) δ18O-IVE of *G. truncatulinoides* sin.

2.3.3 Δ18O difference

The difference in oxygen isotopes composition between the two species (from here Δ18O) is on average 0.91 ‰, and ranges between 0.35 and 1.73 ‰ (Fig. 2.5 B). This composite signal builds up starting from early interglacial stages, reaching maxima precisely at the subsequent glacial terminations, thus diminishing relatively fast, with minima set just upon establishment of full interstadials. For the secondary climatic cycle represented by the evolution from MIS 4 to 2 this is not equally explicit.

The strongest post-deglaciation Δ18O decrease is observed at early MIS 5 (1‰ drop in ~8 kyr), followed by MIS 11 (0.7‰ in 6 kyr), MIS 7 (0.6‰ in 10 kyr), MIS 9 (0.5‰ in 10 kyr) and MIS 1 (0.4% in 5 kyr). After minima, values increase gradually, though superimposed events of sub-orbital scale are visible, during intervals that last from a minimum of ~77 kyr, during MIS 11 to 10, to a maximum of ~108 kyr during MIS 5 to 2. The duration of the Δ18O build-up is consistent across glacial cycles, each regularly constituting ~88-90% of the whole duration of the respective G-IG succession. Along MIS 5 values gently increase as in the precedent cycles, but then drop, rise and fall during MIS 4, MIS 3 and early MIS 2, respectively, steeply increase before T-I, and again decrease along MIS 1.

The spectrum of Δ18O is significant on the period of ~100 kyr, corresponding to the eccentricity main band (Fig. 2.7 C). The alternative age model (based on H07, see Methods) yielded both eccentricity peaks that are more marked, thereby proving that the observed peaks are not artefacts of the orbital tuning of LR04.

2.3.4 $\delta^{13}C$ and $\Delta^{13}C$

The variability in *G. ruber* s.l. $\delta^{13}C$ is larger that that of *G. truncatulinoides* sin. (Fig. 2.5 E), and values of the earlier are almost always higher than the latter's. Besides these differences, the curves of the two species are coupled, and the following considerations hold for both. The heaviest carbon was incorporated in MIS 11 and secondarily in MIS 9. A decreasing trend is indeed visible from MIS 12 to 8 (though *G. truncatulinoides* sin. records a more accentuated decrease). This is followed by a mildly increasing tendency from MIS 6 to 1. To these trends a general G-IG pattern is superimposed, with $\delta^{13}C$ values being heavier during interglacials, and reaching their minima prior to terminations. Exceptionally, from the mid-late MIS 9 to early MIS 8 $\delta^{13}C$ maintains the elevated values it had reached at ~325 ka.

G-IG patterns are less evident for the $\Delta^{13}C$ curve than for $\Delta^{18}O$ (Fig. 2.5 B and F). Still, it is possible to note that the sub-surface-to-thermocline difference is more marked in interglacials, and that there is clear alternation of long-sustained $\Delta^{13}C$ decreases, from each mid-late interglacial until the following late glacial, and successive more rapid increases which, across terminations, develop into full interglacials.

2.5 Discussion

2.5.1 Sub-surface signal

Our analysis confirms observations from the southeast Cape Basin, that the coldest sea surface temperature (SST) over the last 460 kyr were recorded during late MIS 12 (~435 ka), and that the interglacial with longer sustained SST was MIS 11 (Pierre et al., 2001; Dickson et al., 2010) (Fig. 2.6 B).

The shift of ~0.5 ‰ in $\delta^{18}O$-IVE prior to T-I, if interpreted solely in terms of temperature change, is fully compatible with the regional SST warming of 2° C inferred for the last deglaciation from faunal assemblages (Niebler et al., 2003), and from a recent integrated model-data study (Annan and Hargreaves, 2013). The only other relatively fast sub-surface warming/freshening happened before T-V (~1 ‰). The similarity in upper ocean hydrographic changes between these two transitions generally echoes the parallelism previously highlighted between the two following interglacials (MIS 11 and 1, respectively), which bore similar orbital configuration (e.g., Berger and Loutre, 2003; de Abreu et al., 2005). Minima in our record appear aligned to maxima in the tilt of the Earth's axis (obliquity), in particular across terminations (Fig. 2.6 A-B). The spectrum of *G. ruber* s.l. $\delta^{18}O$-IVE corroborates this notation, with the ~41 kyr band emerging as significant (Fig. 2.7 B). Obliquity has recently been suggested as a plausible forcing for T-I and II (Drysdale et al., 2009) and for the entire Pleistocene (Huybers, 2007). It determines the total combined radiation received by the high latitudes of the two hemispheres, and it turned out to be an important component of Antarctic paleo records (Jouzel et al., 2007). This orbital parameter was shown to pace temperature and salinity changes in the Agulhas

Current (Caley et al., 2011), and it is a component of the release of AL in the east Cape Basin (Peeters et al., 2004). We show that it also influences the sub-surface at the central Walvis Ridge, mediated by meridional shifts of the frontal systems at higher latitudes. Such shifts have been postulated for G-IG time scales to result from the intensity of the latitudinal insolation gradient (Hays et al., 1976b; Bard and Rickaby, 2009), in turn paced by obliquity. The contraction and expansion of Antarctic sea ice, associated with such frontal shifts, can regulate the (sub)tropical SST, as modelled by Lee and Poulsen (2006).

The warm/fresh excursions from *G. ruber* s.l. at terminations were also recorded by winter SST maxima from transfer functions in the Namibian upwelling, 10° E of our site (Chen et al., 2002), even though we detect close structural resemblance to their series only for T-V and MIS 3 to 1. Whereas from the record of Chen et al., (2002) it could be incautious to extract SSTs from faunal abundances, due to the implications that the possible transport of *G. ruber* by the AL has on the transfer function, our reconstruction provides a geochemical hint for southeast Atlantic upper ocean warming. Mix et al. (1986) showed how surface warming of the southeast tropical Atlantic corresponded to the last deglacial interval, laying down the first formulation for what became later known as the bipolar seesaw concept (e.g., Broecker, 1998). This is ultimately linked to the strong reduction of the AMOC, brought about by melt water discharge in the North Atlantic (Vellinga and Wood, 2002), as can be seen from the first derivative of the LR04 benthic stack (Fig. 2.5 D), seen primarily as a proxy for the rate of ice volume change. We hence suggest that a response of the southeast Atlantic to this mechanism was a constant mode of G-IG climate change of the last 460 kyr. Further, our sub-surface record also supports the notion of increased efficiency of Indian to Atlantic heat transport at glacial terminations (Knorr and Lohmann, 2003; Peeters et al., 2004).

2.5.2 Thermocline signal

The high δ^{18}O-IVE, likely pointing at remarkably low temperatures at MIS 12, and the sustained climatic optimum of MIS 11 interglacial, from the *G. ruber* s.l. δ^{18}O-IVE and from other studies (Hodell et al., 2000; Dickson et al., 2010), are even more manifest in the *G. truncatulinoides* sin. δ^{18}O-IVE (Fig. 2.6 D), meaning that the intensity of MIS 12 glacial was (regionally) more pronounced in thermocline waters than at the sub-surface. This is in agreement with the lowest values of AL fauna from Peeters et al. (2004), which indicates minimal connection between Indian and South Atlantic Oceans, and thus suggests a potential response of our record to the AL.

The varying position of maxima and minima of the δ^{18}O-IVE of this species, with respect to G-IG cycles, leads us to deduct that Pleistocene climate shifts do not form an exhaustive explanation for variations in the water properties of the east SAG thermocline.

We note that, while tropical intermediate depth warming during likely weakened AMOC (i.e. terminations) was reported for the low-latitude tropics during the last two glacials (Ruhlemann et al., 2004; Lopes dos Santos et al., 2010) and for a more coastal record in the southeast Atlantic during MIS 12 (Dickson et al., 2010), our *G. truncatulinoides* sin. does not clearly reflect this mechanism, and its extension to the southeast Atlantic gyre for the last five deglaciations is not possible. Our findings in this sense seem in line with the temperature insensitivity to changes in the AMOC recently found for the tropical Atlantic thermocline (Huang et al., 2012).

Examining the relationship between thermocline $\delta^{18}O$-IVE signal and eccentricity (Fig. 2.6 C-D), we propose a mechanism of eccentricity-paced regulation of the southeast Atlantic properties of thermocline waters, through changes in the tropical seasonal contrast. As proposed by Berger et al. (2006), there is a strong 100 kyr cycle in the equatorial seasonality that emerges from the difference of the maximum minus minimum insolation record. This modulation of seasonality is noticeable in the tropics and we show how it seems to have a profound impact on thermocline heat content over the last 460 kyr.

2.5.3 Upper ocean stratification

Each species' isotopic composition is a result of the effects of ice volume, temperature, and local seawater anomaly, ultimately attributable to salinity (Emiliani, 1955). Because the IVE is the same in two coeval populations, the magnitude of $\Delta^{18}O$ is governed by the difference between the temperatures recorded by the respective species, plus the difference between the $\delta^{18}O$ of seawater (dependent on salinity).

To interpret the $\Delta^{18}O$, we intend to deal with the complications that commonly affect the use of foraminiferal isotope records. By excluding some of them, we wish to assign a clearer paleoceanographic meaning to the isotopic difference. In the first place, close inspection of assemblages from the 63-125 μm fraction reveals that the shells of delicate juvenile specimens are pristine throughout the core, hence dismissing the possibility that taxon-specific dissolution played a role in scaling the $\Delta^{18}O$ (and the $\Delta^{13}C$), as was to be expected from the results of Howard and Prell (1994), which constrain the glacial Cape Basin lysocline shoaling. Even though the two species have different seasonal occurrence (Lonçaric et al., 2007), a change in the strength of the annual temperature gradient cannot account for a significant portion of the observed changes in $\Delta^{18}O$. In fact, fauna-based reconstructions of Niebler et al. (2003) show that seasonal SST differences in the southeast sector of the South Atlantic remained reasonably stable from the Last Glacial Maximum (LGM) to present. Nevertheless, there is to date no reconstruction of this pattern for older G-IG cycles. Another eventuality that requires attention is that the depths, to which the $\Delta^{18}O$ is referred, might not be stable over the last 0.5 million years. As mentioned before, we are keen on interpreting the record of *G. truncatulinoides* sin. in terms of changes in water mass properties at its presently-observed calcification depths, neglecting distortions to the signal enforced by relevant habitat shift, that probably did not occur (LeGrande et al., 2004). As for the changes in the depth of *G. ruber* s.l., other studies have assessed its habitat stability for the last G-IG cycles (Spero et al., 2003). Moreover, the interpretation of the observed increase in $\Delta^{18}O$ (Fig. 2.5 B) as reflecting habitat migration of *G. ruber* s.l., pursuing warmer conditions in more shallow layers as glacial temperatures deteriorate, does not seem plausible for three reasons. First, it is counter-intuitive that upward migration went as far as to reach levels warmer than at climate optima; second, we examined distribution maps for this species at our location (Arthur et al., manuscript in preparation), and found no significant difference between its present and LGM abundance, meaning that, for either climatic state, *G. ruber* s.l. did not undergo stress levels that warrant meaningful habitat migration; last, because this interpretation does not conciliate with the timing of SST changes recorded elsewhere in the southeast Atlantic (Chen et al., 2002; Peeters et al., 2004).

On another note, to understand the influence of size-related variations in the $\delta^{18}O$ of *G. truncatulinoides* sin. on the $\Delta^{18}O$ (see Methods), we show that the $\Delta^{18}O$ calculated between the larger shells of this species and *G. ruber* s.l. indeed has a less clear pattern (Fig. 2.3). This demonstrates that, by opting for a narrow size fraction of *G. truncatulinoides* sin., we likely targeted a more defined gradient than we would have by picking larger individuals, whose habitat depth is considered less stable, and that have occasionally developed secondary calcite crusts (Mulitza et al., 1997).

Taking into account the aforementioned, we interpret the evolution of the $\Delta^{18}O$ as a proxy for the stratification of the permanent thermocline. Further, being foraminiferal $\delta^{18}O$, as density, directly proportional to salinity and inversely to temperature (Lynch-Stieglitz et al., 1999), we take $\Delta^{18}O$ as a qualitative estimation of density stratification.

Values of $\Delta^{18}O$ are quite low, when compared to what found between surface and thermocline dwellers, in G-IG records from other tropical locations (Wefer et al., 1996; Spero et al., 2003), confirming that along our record the southeast Atlantic maintained a deep thermocline, as it is suggested by the constant presence of *G. truncatulinoides* sin. (Lohmann and Schweitzer, 1990).

Glacial values are statistically different from interglacial ones, with high significance ($p < 0.001$). The sawtooth pattern reveals that stratification was lowest (i.e. deepest thermocline) in interglacials and maximal (thermocline most shallow) at terminations. Note that only the LGM deviates from this scheme, being characterized by a minimum in stratification, and alluding to the exceptional spatial/temporal structure of the last transition. Two different mechanisms must therefore account for changes in the last glacial cycle and in the four preceding ones. We first proceed by proposing a potential explanation for the former.

Several independent proxy (Stuut et al., 2002; Moreno et al., 1999; Lambert et al., 2008; Bard and Rickaby, 2009) and model (Clauzet et al., 2007) reconstructions have pointed out that southern hemisphere easterlies and westerlies blew more intensely during the LGM, as also reflected in stronger upwelling east of our site (Chen et al., 2002). Intensified zonal winds imply enhanced Ekman pumping in the subtropical gyre, at the junction of the two winds systems. This mechanism appears to be reflected in our record, where stratification is minimal at the LGM, when Ekman-induced downwelling was supposedly at its peak, and then swiftly increased before T-I, when winds strength waned.

To assist the interpretation of the older G-IG cycles we recur to comparison with modern observations. As can be seen in the South Atlantic map in Fig. 2.1, between 20°S and 50°S, the present day $\delta^{18}O_{eq}$ difference between 500 and 100 m (see Methods), varies largely with latitude, with values decreasing southwards, while north of 20°S the gradient rather follows the direction of the sub-surface South Equatorial current. In this view, we can infer, for periods of $\Delta^{18}O$ build-up: 1) a south-eastern expansion of the higher stratification zone towards the core site, with subsequent rapid retreat; 2) a gradual rearrangement of the stratification pattern in the South Atlantic basin, with displacement of highly stratified thermocline to the southeast; or a combination of the two. Either of the envisioned scenarios implies substantial alteration of the southern hemisphere AMOC.

Relying on modern ocean observations, the Agulhas Current is clearly identifiable on the basis of its stratification values, markedly lower compared to the surrounding region (Fig. 2.1). This feature is explicit also from observational studies (Lutjeharms, 2006), and is furthermore seen in Agulhas rings entering the South Atlantic (Arhan et al., 2011; Souza et al., 2011), where the anticyclonic rotation depresses the isopycnals. Although the mesoscale processes involved in the encounter of Indian Ocean masses with the South Atlantic are characterized by high complexity (e.g., Biastoch et al., 2008), we formulate a connection of the changes in the stratification of the SAG with the AL. To secure the synchronicity of our record with that of the AL fauna (Peeters et al., 2004), we tuned the $\delta^{18}O$ of the latter to the LR04 stack. We propose a cause-effect relationship between the release of poorly stratified waters from the AL at glacial terminations, and the relatively fast decrease of stratification in our SAG record (Fig. 2.5 B-C). The conceptual succession of events is hypothesized as follows: when the AL "warm route" becomes weaker or, alternatively, loses its characteristic deep thermocline (i.e. it becomes more stratified), stratification at our site progressively builds up, until terminations. At that point the powerful release of AL distributes into the South Atlantic poorly stratified waters characterized by lower thermocline density (Arhan et al., 2011), thereby making our $\Delta^{18}O$ values drop along an interval of 6-10 kyr. In other words, by evaluating the fingerprint of thermocline water masses from modern observations, we are able to propose a mechanism of the effect of the AL in the upper South Atlantic Ocean hydrography.

In turn, the AL fauna appears tightly coupled to the rate of ice volume change (Fig. 2.5 C-D). Remarkably, maxima in the rate of ice volume change, indicating melt water input at terminations, coincide both with SAG stratification drops and with AL peaks. This suggests that fresh water discharge in the North Atlantic caused a southern displacement of southern hemisphere fronts (Timmermann et al., 2007) visible in increased Indian to Atlantic communication south of Africa, coherent with the ideas of, e.g., Hays et al. (1976b) and Bard and Rickaby (2009), thus assigning emphasis to the role of the inter-ocean exchange in the termination of glacial periods.

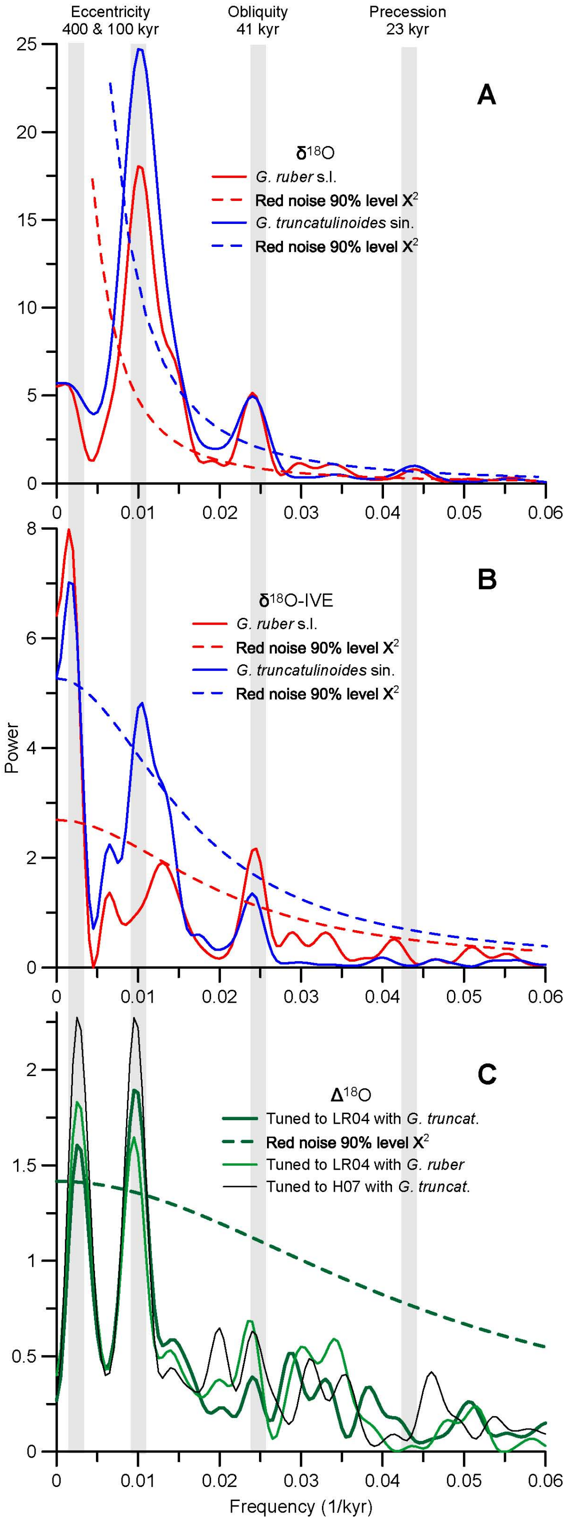

Fig. 2.7. Power spectra, calculated with the AnalySeries software (Paillard et al., 1996) and the Blackman-Tukey method with Welch-type of window. Linear trends were removed. Red noise spectra were estimated to provide significance levels using REDFIT (Schulz and Mudelsee, 2002). A: $\delta^{18}O$ of *G. ruber* s.l. (red) and *G. truncatulinoides* sin. (blue); B: $\delta^{18}O$-IVE of the two species; C: $\Delta^{18}O$ record tuned to LR04 using *G. truncatulinoides* sin. (bold green line) and *G. ruber* s.l. (thin green line), and tuned to H07 using *G. truncatulinoides* sin. (black) (see Methods). Dashed lines indicate the corresponding red noise spectra at the 90% significance level.

2.5.4 Periodicity of stratification

The spectral peak of the $\Delta^{18}O$ at 100 kyr compares with the G-IG cycle, but also with orbital eccentricity (Fig. 2.7 C). It is renown that eccentricity effect on insolation is too mild to noticeably force the paleoclimate record (the "100 kyr problem" [Hays et al., 1976a]). Still it is important to keep in mind that the eccentricity cycle functions as a modulator of precession amplitude.

Special interest in the detection of typical G-IG 100 kyr periodicity in the $\Delta^{18}O$ curve arises from acknowledging that, as we have explained, this signal is per definition independent of IVE, which commonly introduces the G-IG pace into foraminifera $\delta^{18}O$ records. In this light we detect in the $\Delta^{18}O$ climatic evolution evidently tied to G-IG cycles, but that is solely explained by changes in water column structure.

Investigating on which of the individual $\delta^{18}O$ curves that compose the $\Delta^{18}O$ is accountable for this pacing, we underline that neither exhibits univocal connection to G-IG cycles. In *G. ruber* s.l. $\delta^{18}O$-IVE the 100 kyr band is not present at all, while obliquity is significant (Fig. 2.7 B). Even though the spectral analysis of *G. truncatulinoides* sin. $\delta^{18}O$-IVE reveals very strong periodicity at ~100 kyr (even stronger when tuned to the H07 chronostratigraphy), the structure of this series does not coincide with G-IG cycles as defined by the $\delta^{18}O$ stacks (Fig. 2.6 D). Considering the aforementioned, the powerful G-IG periodicity of our $\Delta^{18}O$ record is attributable to the thermocline signal. Further research on thermocline water masses, covering several G-IG cycles, is required to disentangle the forcing of orbital parameters on upper ocean stratification at the subtropical latitudes.

2.5.5 Mechanisms determining the ^{13}C gradient

The higher interglacial $\delta^{13}C$ values, and their low glacial counterparts (Fig. 2.5 E), are consistent in magnitude with the carbonate ion effect described by Spero et al. (1997), and with the 40 μmol/kg G-IG shift in $[CO_3^{2-}]$ suggested by these authors, and with the recent finding that Southern Ocean alkalinity was higher during glacials than interglacials, over the time-span of core 174P13 (Rickaby et al., 2010). The decreasing trend of MIS 12 to 8, also visible in benthic $\delta^{13}C$ from the southeast Cape Basin (Pierre et al., 2001), and in the Pacific Ocean (e.g., Mix et al., 1995), corresponds to the mid-Brunhes climatic event (e.g., Jansen et al., 1986). The heaviest values of both species at MIS 11 are in agreement with planktic records in the Southern Ocean (Hodell et al., 2000). Notably, in late MIS 9 and early MIS 8 $\delta^{13}C$ maintains the high values it had reached at ~325 ka. This plateau is observable also at similar longitude at 42.5° S (Hodell et al., 2000), and therefore probably indicates long sustained productivity at the junction of the Southern and Atlantic Oceans. Further, the absence of resemblance of our $\Delta^{13}C$ curve (Fig. 2.5 F) to that of site 1087 (Pierre et al., 2001) tells that our results are not extendable to the upwelling area further to the east, but seem representative of the low productivity region trapped in the SAG.

Several mechanisms might have concurred to determine the discrepancies in the $\delta^{13}C$ of our two species, and the resulting $\Delta^{13}C$. In the first place, the mentioned carbonate ion dynamics vary with water depth, and their effect on foraminifera $\delta^{13}C$ was shown to be species-specific, likely due mainly to the activity of symbionts (Spero et al., 1997). To our knowledge there is no such published study dealing with *G. truncatulinoides*, and exploration of the differential effect is thus so far precluded.

We therefore discuss two causes that likely had large impact on the $\Delta^{13}C$. It is currently understood that, in the framework of the reorganization of water masses in the glacial Atlantic, Antarctic Intermediate Waters (AAIW) were supplanted, at their present depth, by Glacial North Atlantic Intermediate Waters (GNAIW) (Curry and Oppo, 2005; Lynch-Stieglitz et al., 2007), with heavier $\delta^{13}C$. Evidence of isotopic signature changes at the latitudes and depth of core 174P13 is only available from benthic results in the west of the basin, basically indicating that the GNAIW did not reach 30° S at the Brazil margin (Curry and Oppo, 2005). In the absence of indications for the eastern longitudes, it is difficult to draw the geometry of the southern invasion of GNAIW. Nevertheless, it is plausible to postulate that similar water masses played a role also during older glacials. If indeed such water invested the southeast Atlantic, it would have been sensed by our *G. truncatulinoides* sin. in the low part of its calcification depth range (Mulitza et al., 1998a), thereby recording a signal enriched in ^{13}C relative to the sub-surface. This is sustained by the lowest values of $\Delta^{13}C$ reached during the five glacials embraced by 174P13. In addition, this hypothesis of southern extension of GNAIW seems coherent with a more uniform upper water column, and a minimized density stratification seen in our $\Delta^{18}O$ for the LGM, whereas it does not seem to have prevailed in dictating the $\Delta^{18}O$ stratification in older glacials.

Still, the graduality of the $\Delta^{13}C$ increases across terminations requires another explanation than merely the GNAIW to AAIW shift, which must have occurred faster. The higher variability of *G. ruber* s.l. $\delta^{13}C$ with respect to *G. truncatulinoides* sin. (Fig. 2.5 E), similar to what was reported for the north edge of the SAG (core GeoB 1413 [Wefer et al., 1996]) possibly indicates that this species captures the productivity-induced effects on seawater ^{13}C more efficiently. Likewise, the constantly higher sub-surface values, compared to the thermocline, reflect the production-respiration budget, which differs in the two layers, and the photosynthetic activity of symbionts hosted by *G. ruber* s.l. (Spero, 1998). Generally, heavier $\delta^{13}C$ corresponds to enhanced phytoplankton production. Because of these dynamics, the surface to intermediate ^{13}C gradient seems to function as a proxy for the vertical nutrient gradient in the eastern tropical Atlantic (Mulitza et al., 1998b). Given the decreasing gradient of the ratio between production and respiration, from the photic zone to the less productive thermocline, we see how the $\Delta^{13}C$ might also provide a qualitative measure of the intensity of the "biological pump". It appears therefore that this process worked best during climate optima, generally losing efficiency as glacials progressed into their coldest phase. This allows the hypothesis that at times of higher pCO_2 (Luthi et al., 2008) this region of the ocean functioned more efficiently as atmospheric carbon sink.

Unfortunately, a complete clarification of the predominant causes of the $\Delta^{13}C$ shifts is still impeded by the not yet resolved geometry of the GNADW southward extension, not to mention that of similar north-source water masses in older glacials. Also necessary are more strict constrains on past thermodynamic processes determining the ^{13}C of intermediate waters upon interaction with the atmosphere (Charles et al., 1993).

2.6 Summary and conclusions

We produced O and C isotope records of sub-surface and thermocline dwelling foraminifera, covering the last five G-IG cycles, for a sector of the ocean that links the AL with the AMOC, previously undocumented at these time scales.

1. Sub-surface low $\delta^{18}O$-IVE values indicate warming/freshening, and appear paced by obliquity, suggesting response to high latitude dynamics. Their coincidence with glacial terminations testifies a response of this region to the bipolar seesaw, and is compatible with a SAG warming resulting from increased AL input.
2. In contrast, the SAG thermocline $\delta^{18}O$ does not parallel G-IG successions, whereas it is rather anchored to eccentricity cycles.
3. MIS 12 appears the most extreme glacial of the last five, with exceptionally heavy thermocline $\delta^{18}O$ values. The SAG seems to record the minimal transfer of warm Indian Ocean waters seen from the east Cape Basin.
4. The upper ocean $\Delta^{18}O$ gradient is a proxy for density stratification, revealing a sawtooth pattern that is strictly bound to G-IG cycles, as also evident in the frequency spectrum. From MIS 12 to 5, stratification was minimal during interglacial optima, increased until the following termination, and then dropped relatively fast. We propose that the gradual increase in stratification indicates a progressive loss of Indian Ocean input to the South Atlantic from the AL, and that the quick drop, well synchronized with intense AL release at terminations, depicts a SAG thermocline readily replenished by poorly stratified waters from the Agulhas Current.
5. Exceptionally, stratification was minimal during LGM. Given the availability of paleo records for this period, we are able to provide potential mechanisms for this observation, namely enhanced Ekman downwelling forced by the intensified wind field over the SAG, and/or southward invasion of GNAIW. Both mechanisms imply profoundly altered LGM South Atlantic circulation.
6. The $\Delta^{13}C$ pattern seems to reflect the substitution of GNAIW to AAIW, repeatedly over the last five glacials, and/or a more efficient biological pump at interglacials, lending support to the idea of increased surface productivity at times of high pCO_2.

Our study depicts the southeast Atlantic as a sensitive area for dynamics of G-IG transitions, and provides a mechanism for the connection between SAG and AL. We underline that to reconstruct past inter-basins communication there is critical need for more records that, reaching below the surface ocean, should target thermocline stratification in key areas, such as the oceanographic bottlenecks of the AL, the Drake Passage and the North Brazil Current, and in other sectors of the SAG.

Acknowledgements

The work described in this paper has received funding from the European Community's Seventh Framework Programme FP7/2007-2013 – Marie-Curie ITN, grant agreement n° 238512, GATEWAYS project. We thank Geert-Jan Brummer for making the core available, and Ralph Schneider for his advice on the drilling location.

3

Paleo Agulhas Rings enter the subtropical gyre during the penultimate deglaciation

Paolo Scussolini[1, 2], Erik van Sebille[3], Jonathan V. Durgadoo[4]

[1] Earth and Climate Group, Vrije Universiteit, Amsterdam.
[2] The Bjerknes Centre for Climate Research, Uni Research, Bergen, Norway.
[3] Climate Change Research Centre & ARC Centre of Excellence for Climate System Science, University of New South Wales, Sydney.
[4] GEOMAR Helmholtz Centre for Ocean Research Kiel, Germany.

Published in *Climate of the Past*, 9(6), 2631-2639.

Abstract
A maximum in the strength of Agulhas leakage has been registered at the interface between the Indian and South Atlantic oceans during glacial Termination II (T-II). This presumably transported the salt and heat necessary to maintain the Atlantic circulation at rates similar to the present day. However, it was never shown whether these waters were effectively incorporated into the South Atlantic gyre, or whether they retroflected into the Indian and/or Southern Oceans. To resolve this question, we investigate the presence of paleo Agulhas rings from a sediment core on the central Walvis Ridge, almost 1,800 km farther into the Atlantic basin than previously studied. Analysis of a 60-year dataset from the global-nested INALT01 model allows us to relate density perturbations at the depth of the thermocline to the passage of individual rings over the core site. Using this relation from the numerical model as the basis for a proxy, we generate a time series of variability of individual *Globorotalia truncatulinoides* $\delta^{18}O$. We reveal high levels of pycnocline depth variability at the site, suggesting enhanced numbers of Agulhas rings moving into the South Atlantic gyre around T-II. Our record closely follows the published quantifications of Agulhas leakage from the east of the Cape Basin, and thus shows that Indian Ocean waters entered the South Atlantic circulation. This provides crucial support to the view of a prominent role of the Agulhas leakage in the shift from a glacial to an interglacial mode of the Atlantic circulation.

3.1 Introduction

A transport of upper water masses takes place around the tip of South Africa, where the Agulhas retroflection spills Indian Ocean waters into the South Atlantic (Lutjeharms, 2006; Beal et al., 2011, and references therein) (Fig. 3.1). This Agulhas leakage (hereafter AL) is an important component of the salt and heat transport into the Atlantic Ocean (Gordon et al., 1992; Weijer et al., 2001; Dong et al., 2012). The recipient of this transfer is the Cape Basin, in which a host of complex and turbulent phenomena occur (e.g., Olsen and Evans, 1986; Boebel et al., 2003; Doglioli et al. 2006).
Waters of Indian Ocean origin travel across the Cape Basin in a variety of forms and shapes. These can be broadly characterized as anticyclonic (e.g., Schouten et al., 2000), cyclonic eddies (Hall and Lutjeharms, 2011), and filaments (or streamers, or liners) wound between the spinning eddies (Lutjeharms and Cooper, 1996; Treguier et al., 2003). It is not yet clear how the AL is partitioned between these transport features (e.g., Doglioli et al., 2006; van Sebille et al., 2010a), but a significant part of the AL is in the form of rings (van Sebille et al., 2010a; Dencausse et al., 2010).

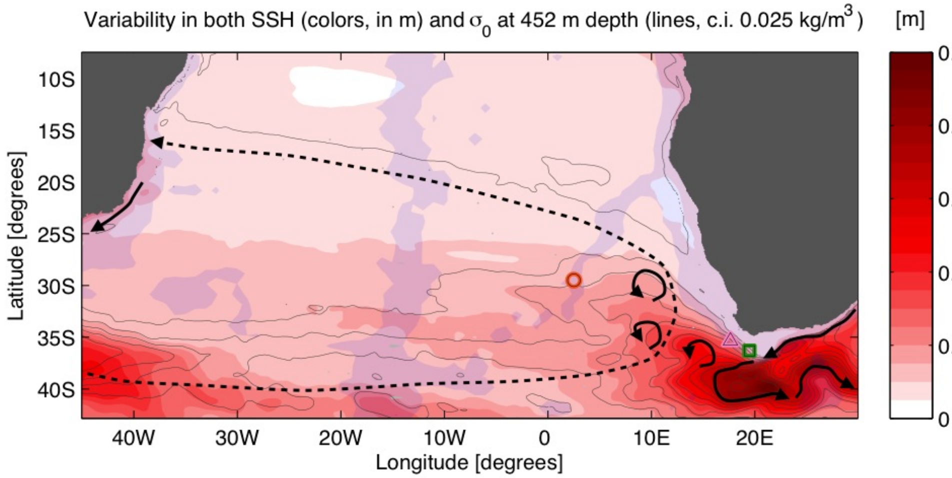

Fig. 3.1. Map of the Southeast Atlantic, with location of the core studied here (orange circle), of the Cape Basin record (pink triangle) of Peeters et al. (2004), and of the Agulhas Bank Splice (green square) of Martínez-Méndez et al. (2010). Also indicated are contoured variabilities of both sea surface height (SSH; colours) and of σ_θ at the 452 m depth model level (lines) over the basin, in the INALT01 model (see Methods). The blue arrows show the schematics of the water currents discussed here: Agulhas current, Agulhas rings and cyclones, and South Atlantic gyre circulation.

3.1.1 Agulhas rings and the thermocline

Agulhas rings have been described as quite regular features of mostly barotropic flow, and as the greatest and most energetic mesoscale eddies in the world (Clement and Gordon, 1995; Olson and Evans, 1986). Approximately 6 rings are spawned per year

and they reach, though then very diminished, as far as 40°W (Byrne et al., 1995). Their most conspicuous characteristic, upon entrance into the Cape Basin, is the dramatic depression they impose on isotherms, isopycnals and isohalines (Arhan et al., 2011; Souza et al., 2011; Giulivi and Gordon, 2006), as they transport water that is much warmer and saltier than the surroundings, from the sub-surface to at least ~1000 m depth (van Aken et al., 2003).
It is understood indeed that the bulk of the AL happens below the surface, at the depths of the thermocline (Donners and Drijfhout, 2004; Doglioli et al., 2006; Van Sebille et al., 2010b). Observations of Gordon et al. (1992) show that across the Cape Basin thermocline, two thirds of the water between the 9°C and 14°C isotherms is of Indian Ocean origin. The observational study of Richardson (2007) reveals that while surface drifters adopt more northerly trajectories closer to the Benguela Current, floats at ~800 m travel right over the central Walvis Ridge. Souza et al. (2011) maintain that the largest heat perturbation introduced by Agulhas rings occurs at depths between 200 and 600 m.

3.1.2 In search of a missing paleo link

In the last decades, researchers have come to consider the AL mechanism to play an important role in the changes of heat and salt transports into the Atlantic Ocean during Pleistocene climate shifts (e.g., Berger and Wefer, 1996). The hypothesis of a reduced Indian to Atlantic transfer during glacial periods is compatible with the northward shift of the oceanographic fronts south of Africa (Hays et al., 1976; Bé and Duplessy, 1976; Bard and Rickaby, 2009).
While paleoceanographic research on marine sediments has made a convincing case that Agulhas Current (Hutson, 1980) and AL (Franzese et al., 2006) were reduced during glacial times, most of the evidence was gathered in the easternmost part of the Cape Basin, depicting intense presence of Indian Ocean waters during glacial terminations (Flores et al., 1999; Peeters et al., 2004; Marino et al., 2013) (Fig. 3.1 and 3.2 B). As modern observations show, a significant fraction of Agulhas rings that reach the Cape Basin successively bend either south, to the Southern Ocean, or re-join the Agulhas retroflection (Dencausse et al., 2010; Arhan et al., 2011). These rings have a much smaller impact on the transport of salt and heat into the Atlantic Ocean than those that cross the Walvis Ridge.
Therefore, a key question still remains: were the observed maxima in AL eventually incorporated into the South Atlantic gyre, thus forming the waters that could subsequently cross the equator through the North Brazil Current? To postulate that enhanced AL did result in an increased salt and heat flux into the Atlantic requires the establishment of this paleo connection between the eastern Cape Basin and the South Atlantic circulation.
Here we test this case for the penultimate deglaciation (T-II). The reason for this choice of interval is the intensity and sharpness of the AL release that characterizes this climatic transition, as attested by distinguished peaks in existing Pleistocene reconstructions (Peeters et al., 2004; Martínez-Méndez et al., 2010) (Fig. 3.2 B). Also, marked changes during T-II were recently revealed in AL temperature and salinity

(Marino et al., 2013) and in Southeast Atlantic stratification (Scussolini and Peeters, 2013; Chapter 2), warranting further investigation.
Our hypothesis is rationalized as follows. Regardless of the form it assumes - either rings or filaments - the AL introduces anomalies in the temperature and salinity fields of the South Atlantic subtropical gyre. It is of high interest to both the paleoclimatology and the modern oceanography communities to know whether such perturbations were present over the central Walvis Ridge, almost 1,800 km further downstream into the Atlantic Ocean, and with which intensity, under different climatic frameworks.

Modern analytic techniques enable us to investigate such anomalies, by means of geochemical analysis of microfossils from marine sediments. By selecting the appropriate species of planktic foraminifer, we aim to target water masses at the depth of the thermocline, where variability due to AL should be maximal (Souza et al., 2011). Recently, paleoceanographic research has started to employ the oxygen isotope composition ($\delta^{18}O$) of individual foraminifera, to address questions related to variability. For instance, Billups and Spero (1996) and Ganssen et al. (2011) used single-shell analyses to unravel the range of hydrographic conditions in the Equatorial Atlantic and in the Arabian Sea, respectively, while Koutavas et al. (2006) and Leduc et al. (2009) applied the approach to capture ENSO extremes in the Eastern Equatorial Pacific. A review of this type of analysis, and a rigorous statistical assessment of its potential to capture paleoceanographic variability originating from ENSO were recently provided by Thirumalai et al. (2013).

3.1.3 Rings path and core selection

The path undertaken by Agulhas rings has been the focus of many studies (e.g., Olson and Evans, 1986; Dencausse et al., 2010; Schouten et al., 2000). The SAVE 4 section in years 1989-1990 encountered two Agulhas rings at the central Walvis Ridge, at about 30° S (Gordon et al., 1992). Satellite data (Gordon and Haxby, 1990; Boebel et al., 2003) make it clear that this location is in the full trajectory of rings. Generally, topography seems to be decisive to the displacement of eddies in the Cape Basin (Matano and Beier, 2003; Boebel et al., 2003), and some of the deep canyons in this ridge possibly steer the passage of rings (Byrne et al., 1995; Dencausse et al., 2010; van Sebille et al., 2012). This body of knowledge led us to choose the central Walvis Ridge as an appropriate setting to test our hypothesis.
In addition, we use a high-resolution global ocean circulation model to illustrate the aptitude of our sediment core, and of our foraminifera taxon, to capture the anomalous density expression that result from the passage of Agulhas rings in the present climate.

3.2 Methods

3.2.1 Isotope analysis

We conducted analysis on core 64PE-174P13, retrieved from the central Walvis Ridge (29° 45.71' S, 2° 24.10' E) at the depth of 2912 m (Fig. 3.1). From it we selected 18 sediment samples that span ~70 thousand years (kyr) between Marine Isotope Stage (MIS) 6 and 5, based on the stratigraphy of Scussolini and Peeters (2013; Chapter 2), which is anchored to the LR04 marine isotope stack (Lisiecki and Raymo, 2005). Additionally, we selected two samples, from the core top and from 2 cm in the sediment, representative of near-modern conditions. For each sample, between 18 and 30 specimens of *Globorotalia truncatulinoides* sinistral (left coiling variety) were picked from the size fraction 250-300 μm, to constrain the depth of calcification. We selected this taxon due to its extensively studied depth habitat (e.g., Lohmann and Schweitzer, 1990; Mulitza et al., 1997; Mortyn and Charles, 2003; LeGrande et al., 2004). Lonçaric et al. (2006) report that the calcification depth of this species in our region extends down to ~400 m; other researchers estimated its depth to reach 600 m (Erez and Honjo, 1981), and beyond (Hemleben et al., 1985). The choice of the sinistral variety was mainly due to its regular availability across the interval, testifying to its endemicity (and necessary to perform a sufficient number of individual measurements), and to its ecological preference for a deep thermocline (Lohmann and Schweitzer, 1990). Scussolini and Peeters (2013; Chapter 2), confronting $\delta^{18}O$ values from specimens at the 64PE-174P13 core top, quantified the habitat depth of the fossil specimens around 500 m. These controls imply that *G. truncatulinoides* sin. befits our objective to target the thermocline. A total of 478 isotopic measurements on individual shells were performed at the Vrije Universiteit, Amsterdam, with methods described in Scussolini and Peeters (2013; Chapter 2). The average reproducibility on external standards was better than 0.10 ‰.

Since we are specifically interested in assessing the variability between measurements within samples, it is essential that the typical inter-run fluctuations in instrumental precision do not bias the estimation. For this reason, we corrected the variance of foraminiferal $\delta^{18}O$ by subtracting that of external calcite standards measured in the same sequence, as recommended by Killingley et al. (1981) (Table 3.1).

3.2.2 Model data set

In order to assess the relevance of our core site in recording density anomalies associated with Agulhas rings, we employed the INALT01 model (Durgadoo et al., 2013). This model configuration, based on the NEMO (v3.1.1, Madec, 2008) code, is a high-resolution model of the greater Agulhas region, nested within a half-degree global ocean model. At a 1/10° horizontal resolution, INALT01's nest domain spans the entire South Atlantic including the tropics, between 70° W –70° E and 50° S – 8° N. In the vertical, INALT01 has 46 z-levels: 10 levels in the top 100 m and a maximum of 250 m resolution at depth. The model has been shown to represent the known variability of the greater Agulhas system, including a realistic reproduction of the pathways of Agulhas rings (Durgadoo et al., 2013). For the analysis, 60 years (1948 – 2007) of data from the hind-cast experiment were used.

3.3 Results

3.3.1 Variability of *G. truncatulinoides* individuals

The individual δ¹⁸O values of *G. truncatulinoides* show inter-sample differences in their distribution (Fig. 3.2 A). Their average for each sample is overall not statistically different from the corresponding values from bulk measurements, i.e, many specimens analysed together, from Scussolini and Peeters (2013; Chapter 2) (Fig. 3.2 A), yielding $p = 0.51$ on the t-test for paired samples.

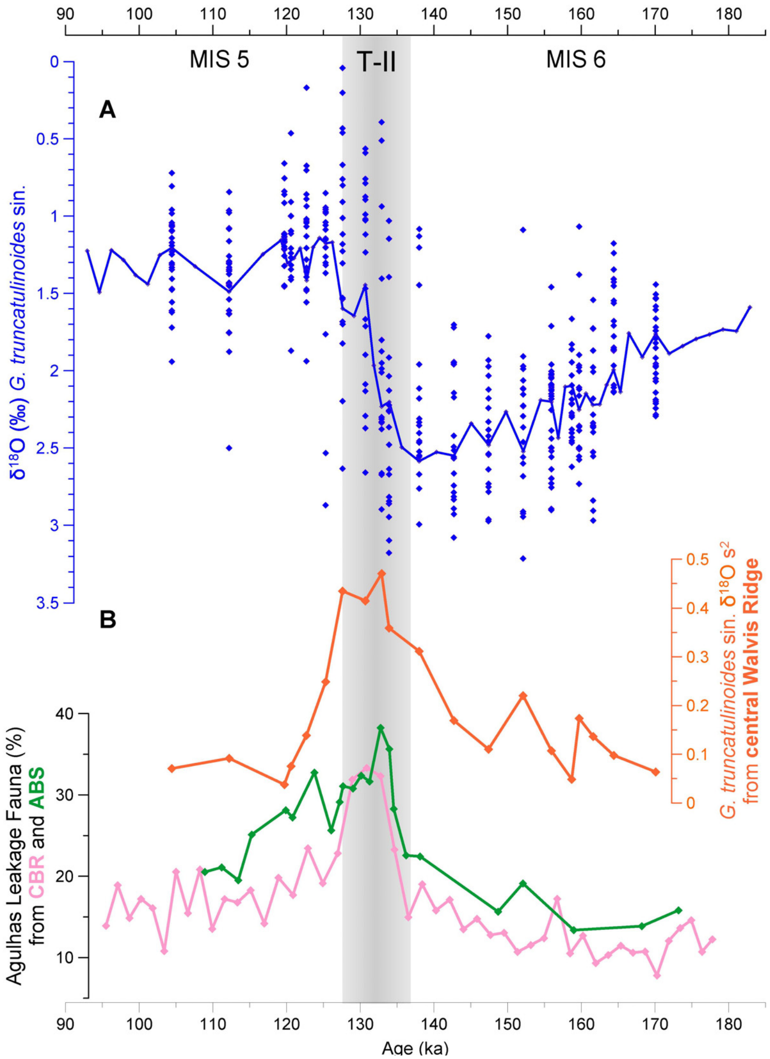

Fig. 3.2 (previous page). A: $\delta^{18}O$ of *G. truncatulinoides* sin. individuals (blue diamonds) and bulk analysis (blue line, Scussolini and Peeters, 2013; Chapter 2). B: Corrected sample $\delta^{18}O$ variance (orange, see Methods); estimation of AL from the Cape Basin record (CBR, Peeters et al., 2004) (pink), and from the Agulhas Bank Splice (ABS, Martínez-Méndez et al., 2010) (green).

The corrected variance of samples changes along the transition from MIS 6 to 5 (Table 3.1; Fig. 3.2 B). It increases from ~145 to ~130 thousand years before present (ka), hence returning more rapidly to levels similar to those of full MIS 6 at ~123 ka, after which it remains stable for at least 20 kyr. Notably, the $\delta^{18}O$ values of the individual foraminifera show a somewhat bimodal distribution in samples at 142.7, 138, 133.9, 132.9 and 130.7 ka. The values of the two near-modern samples are within range of those from early MIS 5 (Table 3.1), with the most recent being lower than that at ~2 ka. This confirms that, as in the penultimate cycle, variability decreases from the beginning of the interglacial.

Sample depth (cm)	Age (ka)	N specimens	Instrument s^2	Sample s^2	**Corrected s^2**
0	~ 0	28	0.025	0.350	**0.325**
2	2.0	18	0.003	0.573	**0.570**
120	104.4	29	0.004	0.074	**0.070**
124	112.2	28	0.015	0.106	**0.091**
129	119.7	19	0.009	0.047	**0.038**
131	120.6	17	0.012	0.087	**0.075**
136	122.7	21	0.003	0.142	**0.139**
142	125.3	20	0.025	0.274	**0.249**
146	127.6	20	0.006	0.440	**0.434**
150	130.7	20	0.006	0.421	**0.415**
154	132.9	19	0.012	0.482	**0.470**
156	133.9	20	0.009	0.368	**0.359**
160	138.0	19	0.009	0.320	**0.311**
164	142.7	20	0.009	0.178	**0.169**
168	147.4	21	0.009	0.119	**0.110**
172	152.1	20	0.006	0.226	**0.220**
176	155.9	30	0.015	0.122	**0.107**
182	158.7	20	0.012	0.061	**0.049**
184	159.7	18	0.009	0.183	**0.174**
188	161.6	19	0.025	0.162	**0.137**
194	164.4	21	0.003	0.101	**0.098**
202	170.1	28	0.004	0.067	**0.063**

Table 3.1. Result of *G. truncatulinoides* sin. individual isotope measurements, and estimation of sample variability, with the respective correction (see Methods).

3.3.2 Effect of Agulhas rings on the central Walvis Ridge water column

Analysis of the INALT01 time series for the South Atlantic basin shows that the variability of sea surface height (SSH), which is a proxy for Agulhas rings (van Sebille et al., 2012), and of potential seawater density (σ_θ) in the thermocline at 452 m depth are strongly related (Fig. 3.1). The highest variabilities at both the sea surface and at 452 m are found south of Africa, in the Agulhas retroflection. From that retroflection area at 20E, high regions of variability extend northwestward into the Cape Basin. Today, the core location is found on the equatorward flank of the ridge of both high sea surface height variability, as well as high variability in density.

The 60-year model data set allows us to describe the temporal variability induced by individual Agulhas ring crossings at our core location (Fig. 3.3 D). In the model layer at 452 m, rings are characterized by peaks of temperature and salinity, and by troughs of density (see for example the ring on the 24th of January 1957 in Fig 3.3 A, and the associated effects on properties in Fig 3.3 D). It is important to note that the effect of temperature overrides that of salinity in determining density within a ring, in agreement with the observations of Giulivi and Gordon (2006) and Arhan et al. (2011).

We can attribute the largest density troughs to Agulhas rings that fully overshadow the core setting (Fig. 3.3 A), and the minor ones to ring flanks moving over it (Fig. 3.3 C). A Fourier analysis of the sea surface height in INALT01 on the site location reveals a clear annual frequency, but also smaller peaks at periods between 150 and 200 days (not shown). It is hence possible to ascertain that out of the roughly six Agulhas rings typically released per year, core 64PE-174P13 presently captures on average one to two full rings, plus a small number of ring flanks.

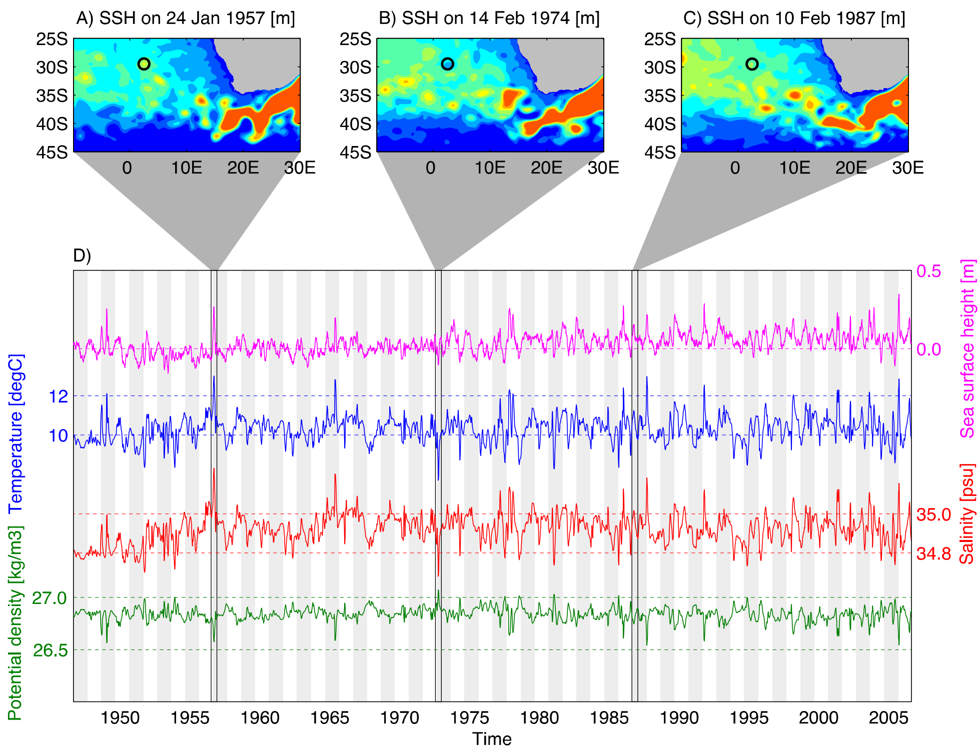

Fig. 3.3. Analysis of model INALT01 output. A, B, and C: SSH maps showing the position of Agulhas Rings with respect to the core location, in three selected situations recurring in the time series (D) of SSH, temperature, salinity and density at 452 m, for the period 1948-2007. A: full overlap with an Agulhas ring (SSH peak); B: overlap with a cyclone (trough); C: partial overlap with an Agulhas ring (small perturbation in the series).

3.4 Discussion

The model data (Figs. 3.1 and 3.3) clearly show that there is a direct relation between the Agulhas rings passing over the core site and variability in density at the depths where *G. truncatulinoides* records its $\delta^{18}O$. However, both the paleo and model records demand some consideration.

Since we have generated a record of foraminifera $\delta^{18}O$ variability across a period of shifting values, it is necessary to examine the role that bioturbation potentially plays in it, since its effect might overlap with that of water column perturbations from the AL. To understand the extent of mixing, we take into consideration other independent sedimentological features of core 64PE-174P13, as obtained from additional analyses.

At T-II, the isotope curve of bulk $\delta^{18}O$ measurements (Scussolini and Peeters, 2013; Chapter 2) (Fig. 3.2 A) exhibits a rather large change in values, of ~1.46 ‰, more than observed in a coeval planktic record from the Southeast Atlantic, whose multi-centennial detail suggests negligible mixing (Marino et al., 2013). Several other sharp shifts are evident in other parts of the curve of *G. truncatulinoides* and in that of *Globigerinoides ruber* (Scussolini and Peeters, 2013; Chapter 2). In particular, the latter species shows an abrupt shift of values at T-II, with 0.57 ‰ change in only 2 cm (154 to 156 cm) (Fig. 3.4 A), and a very constrained spread of measurement repeats ($s < 0.08$ ‰). Furthermore, because we deem *G. ruber* to be less susceptible to the influence of Agulhas rings, due to its more shallow habitat depth, we selected two samples close to this prominent shift, and performed $\delta^{18}O$ measurements on single specimen of this species. We observed that closer to the isotopic shift variability is clearly lower than further from it (Fig. 3.4 B), contrary to what is expected from the effect of bioturbation. Another aspect is the timing of the T-II shift, which differs between *G. truncatulinoides* and *G. ruber*, a phenomenon that is likely better explained through the differential effect of temperature/salinity rather than selective bioturbation (Bard, 2001). The spread of bulk measurement repeats is also a reflection of the variability inherent to a sample and, given pronounced mixing, should be higher at times of $\delta^{18}O$ shift. Variability of repeats over the past 460 kyr (Scussolini and Peeters, 2013, Chapter 2) shows that, while *G. truncatulinoides*' repeats are generally more divergent at terminations, in agreement with our individual analyses, this is not the case for surface-dwelling *G. ruber*. Then, X-ray Fluorescence profiles portray sharp variations in the content of some elements, close to the interval characterized by the variability peak (Fig. 3.4 C). Lastly, the core shows intervals with distinct colour laminations: regardless of the fact these are not visible for the T-II interval, they suggest a setting with relatively undisturbed ocean floor. This is to be expected given the oligotrophic character of the location (Lonçaric et al., 2007), as low food supply anti-correlates with the thickness of sediment mixed layer (Trauth et al., 1997; Smith and Rabouille, 2002).

The ensemble of these properties of the sedimentological material is not reconcilable with prominent mixing, and we regard it as evidence that bioturbative processes alone cannot explain the observed variability peak. Therefore, the phenomenon of increased variability, in such a fully pelagic setting, directly invokes the passage of perturbatory bodies in a field of relatively stable hydrographic conditions.

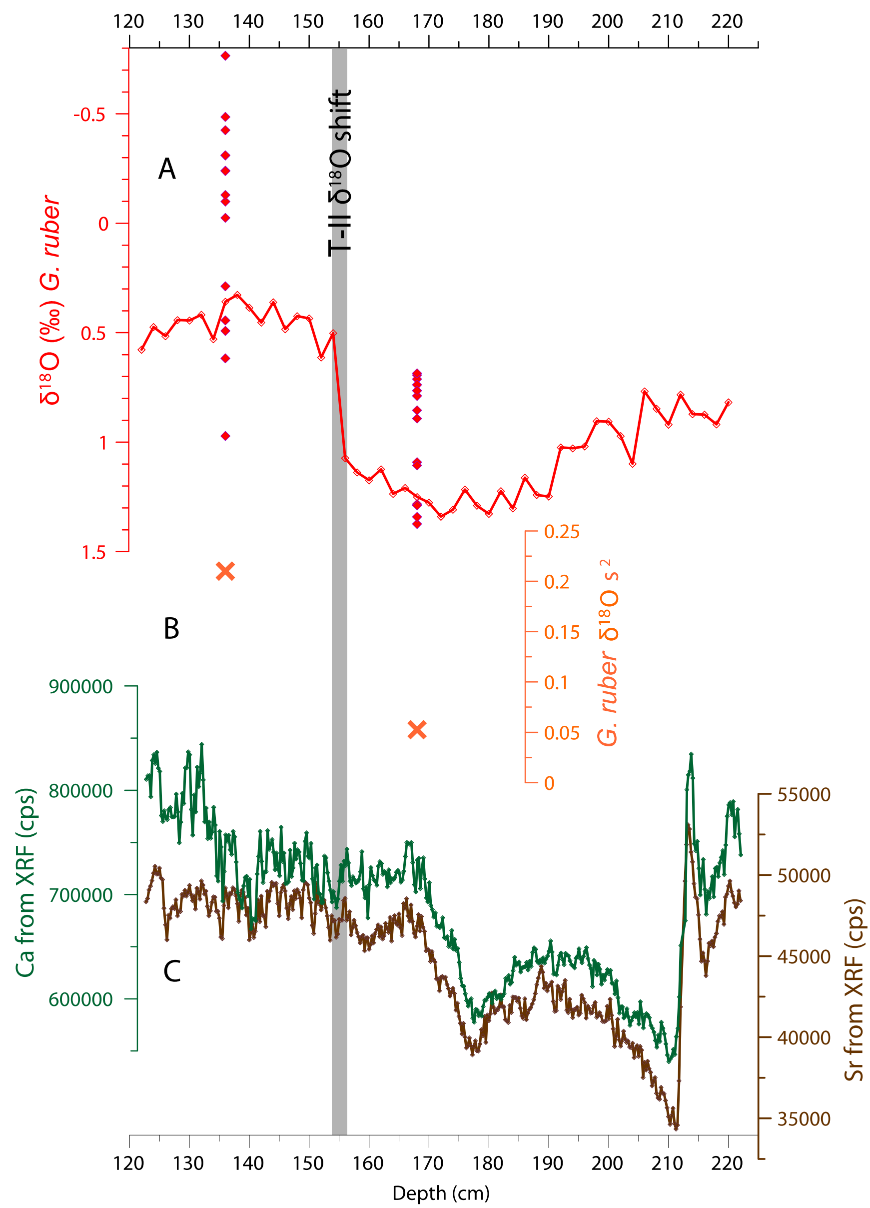

Fig. 3.4. Sedimentological features pointing at a limited role of bioturbation. A: $\delta^{18}O$ of *G. ruber* individuals (purple diamonds) and bulk analysis (red line, Scussolini and Peeters, 2013; Chapter 2). B: Corrected sample $\delta^{18}O$ variance (orange, see Methods). C: Calcium and strontium abundance from X-ray Fluorescence analysis (expressed in counts per second).

Inasmuch as foraminiferal $\delta^{18}O$ is a function of seawater density (e.g., Lynch-Stieglitz et al., 1999), and as in particular *G. truncatulinoides* was found to capture intermediate depth density (LeGrande et al., 2004), we have generated a reconstruction of pycnocline depth variability for the central Walvis Ridge, which we consider to be a paleo proxy for the presence of Agulhas rings / AL.

In this view, more AL reaches the west flank of the Cape Basin as MIS 6 draws to its end, and the influence is maximal right at T-II, likely higher than observed in the modern ocean (Table 3.1, Fig. 3.2 B). The bimodal distribution of samples from ~143 to 130 ka, with clusters of values with low-$\delta^{18}O$, is suggestive of more frequent low-density conditions captured in the foraminiferal geochemistry. This signal can be interpreted as the passage of more Agulhas rings, or of larger and more stable ones, that linger over the core site for longer. Both possibilities point to a stronger AL. Still, the latter seems corroborated by another finding: rings of greater size and stability have been connected to larger variability in the position of Agulhas retroflection (van Sebille et al., 2009). This scenario is particularly plausible at times of climate shift such as T-II, when the system of fronts south of Africa was supposedly more dynamic, likely due to changes in the wind field (Hays et al., 1976; Bé and Duplessy, 1976; Bard and Rickaby, 2009).

We compare the timing of our observations to the published records of Agulhas leakage fauna (a proxy for AL) from the eastern Cape Basin, of Peeters et al. (2004) and Martínez-Méndez et al. (2010) (Fig. 3.2 B). For this purpose, we rendered the age of the records of Peeters et al. (2004) and Martínez-Méndez et al. (2010) compatible with the chronology of our core, by aligning the respective benthic $\delta^{18}O$ curves to the LR04 stack. The remarkable agreement between our variability record and the AL proxies answers the question whether the AL peak at T-II penetrated the South Atlantic circulation. Furthermore, the phenomenon took prominence in our record between ~142 and 138 ka, during maximum glacial conditions. This points to a reaction of the Southern Hemisphere, in terms of thermocline warming and enhanced AL, coherent with the bipolar seesaw mechanism that marked the termination, as recently reformulated by Cheng et al. (2009) and Denton et al. (2010).

While we can assume that the heat and salt associated with AL observed at the central Walvis Ridge have been incorporated into the sub-tropical gyre circulation, it does not directly follow that those waters have made it to the North Brazil Current, and therefore into the North Atlantic. High-resolution ocean models showed that changes in the amount of AL in the Cape Basin do not directly lead to changes in the amount of Indian Ocean water crossing the Equator in the Atlantic (Biastoch et al., 2009; Biastoch and Böning, 2013). Instead, the heat and salt could just have recirculated in the Southern Hemisphere supergyre (e.g., Gordon et al., 1992; Speich et al., 2007).
However, there is modelling evidence that the heat and salt from AL do not have to reach the North Atlantic in order to impact the Atlantic meridional overturning circulation (AMOC) there. In high-resolution ocean models, the salt flux of the North Brazil Current (Biastoch et al., 2008), as well as the intensity of the AMOC (Biastoch and Böning, 2013), seems to be related to AL strength.

Therefore, even if little of the extra AL had made it into the North Atlantic, it could still have imposed an effect on the strength of the AMOC. Authors such as Weijer et al. (2002) have shown that the strength of the AMOC is, to a large extent, determined by the pressure gradient between the southern and northern Atlantic. Increased AL in the South Atlantic, beyond the Cape Basin, could change the meridional density and hence pressure gradients, and thereby the AMOC strength. Furthermore, van Sebille and van Leeuwen (2007) found that Agulhas rings in the South Atlantic Ocean can radiate some of their energy to the North Atlantic, even if no mass is transported across the equator. In that idealized model, that energy might then be used in the North Atlantic to accelerate the AMOC.

In other words, our core on the central Walvis Ridge likely witnessed the AL resumption during T-II, thus lending important support to the idea of its central role in restoring the intensified interglacial mode of the conveyor belt (Gordon et al., 1992; Berger and Wefer, 1996; Weijer et al., 2002; Knorr and Lohmann, 2003). In perspective, we suggest that there is scope for further application of the methodology here presented at this location, in particular to unravel the timing of AL entering the AMOC during the last deglaciation, to address questions as to how the South Atlantic acted during the well-established succession of Older Dryas, Bølling-Allerød and Younger Dryas events that lead to the present warm climate.

3.5 Conclusions

We have presented a novel application for the seldom-utilized analysis of isotopes in individual foraminifera. After preliminary assessment of the extent of sediment mixing processes, the method can conveniently be utilized to unravel paleoceanographic aspects beyond the average state of physicochemical quantities, in particular to test hypotheses relative to mixing of water masses with different characteristics.

In this study, we assessed the paleo-variability in the $\delta^{18}O$ of a thermocline-dwelling taxon, suggesting substantially higher density anomalies into the South Atlantic gyre, around the penultimate termination. Corroborated by a high-resolution assimilative ocean circulation model, we are able to interpret such anomalies as the passage of Agulhas rings, or other leakage features, spawning from the Agulhas Current retroflection. The evidence we present fills a gap between the AL increase recorded around T-II at the interface between the Indian and the Atlantic oceans, and its incorporation downstream into the South Atlantic gyre, and hence also the supergyre. Such a connection is necessary to bolster the current hypothesis of the primary role played by the AL, in the transition from superficial glacial to vigorous interglacial AMOC, either as an active mechanism or rather as a passive feedback trigged by changes in Southern Hemisphere wind fields.

Acknowledgements

P.S. and J.V.D. were funded by the European Community's Seventh Framework Programme FP7/2007-2013 – Marie-Curie ITN, under grant agreement n° 238512, GATEWAYS project. E.v.S. was supported by the Australian Research Council grant number DE130101336. We thank Geert-Jan Brummer for the availability of core 64PE-174P13; Frank Peeters, Gregor Knorr, Conor Purcell and Arne Biastoch for the fruitful discussions and ideas; and Brett Metcalfe for support with the revision of the manuscript. This is publication no. A438 from the Bjerknes Centre for Climate Research.

4

Saline Indian Ocean waters invade the South Atlantic in two steps during glacial termination II

Paolo Scussolini[1,2], Gianluca Marino[3,4], Geert-Jan Brummer[1,5] and Frank J. C. Peeters[1]

[1] Earth and Climate Group, Vrije Universiteit Amsterdam, The Netherlands
[2] Uni Research, Bjerknes Centre for Climate Research, Bergen, Norway.
[3] Institut de Ciència i Tecnologia Ambientals, Univesitat Autònoma de Barcelona, Spain.
[4] Research School of Earth Sciences, The Australian National University, Canberra, Australia.
[5] Marine Geology and Chemical Oceanography, Netherlands Institute for Sea Research, Den Burg, The Netherlands.

Abstract

The Agulhas leakage (AL) supplies heat and salt to the upper branch of the Atlantic meridional overturning circulation (AMOC). Previous studies, based on model simulations and paleoceanographic data, collectively point to the AL as an important modulator of the AMOC, notably during glacial terminations. Yet, our knowledge of the hydrographic impact(s) of past AL variability beyond the southern tip of Africa remains sparse. Here we present time-series of paired Mg/Ca-$\delta^{18}O$ measurements on four different planktic foraminifer species from the central Walvis Ridge, downstream the AL, reconstructing in millennial-scale detail the upper ocean hydrography during glacial termination II (T-II). We find that during T-II: A) The heat content of the upper ocean at the Walvis Ridge increased and subsequently maximized in synchrony with the marine isotopic stage (MIS) 5e (Eemian) warm interval in the Northern Hemisphere. B) The upper ocean $\delta^{18}O_{sw\text{-}ivc}$ profiles allude to higher salt content in the region that closely correlates with the previously reported salinification of the AL area. C) The transfer of salt from the AL to the South Atlantic appears to be transmitted more effectively at thermocline depths, as indicated by the larger $\delta^{18}O_{sw\text{-}ivc}$ anomaly at the thermocline than at the surface. D) Surface temperature and salinity at the Walvis Ridge and in the AL area show a distinct two-step structure, with a reversal amidst the temperature and salinity increases that characterize T-II in the region. This is likely synchronous to a wet interlude that punctuates the weak East

Asian monsoon interval, in turn previously ascribed to the meltwater-forced AMOC slowdown of Heinrich stadial 11. This evidence suggests that the AL and the associated transport of heat and salt to the South Atlantic may have weakened in response to a transient recovery of the AMOC, similar to (but plausibly smaller in magnitude than) the Antarctic Cold Reversal of the last termination.

4.1 Introduction

The subtropical gyre in the South Atlantic Ocean plays an important role in the global ocean circulation, being the main conduit for the warm and saline upper waters that flow northward across the equator, and on to reach the North Atlantic centers of deep convection (e.g., Gordon, 1986; Peterson and Stramma, 1991; Garzoli and Matano, 2011). South Atlantic subtropical gyre waters are sourced from: 1) the Pacific Ocean, connected to the South Atlantic through the Drake Passage (Toggweiler and Samuels, 1995); 2) the Indian Ocean, that spills its subtropical waters at the southern tip of Africa, via the so-called Agulhas leakage (AL) (de Ruijter et al., 1999; Lutjeharms, 2006; Beal et al., 2011); and 3) to a lesser extent the Southern Ocean, whose waters mix along the South Atlantic Current (Stramma and England, 1999).

Focusing on the transport of relatively warm and salty waters from the Indian Ocean via the AL, numerical models simulate a correlation between its intensity and the salt content of the South (Biastoch et al., 2009) and North Atlantic Ocean (Biastoch and Böning, 2013). From the point of view of the geological record, it is particularly interesting that the AL emerges in models as a key component of the transition from glacial to interglacial conditions associated with weak and more vigorous AMOC, respectively (Weijer et al., 2002; Knorr and Lohmann, 2003; 2007). These studies were supported by recent paleoceanographic observations of AL variability on millennial to orbital timescales, with AL maxima occurring in step with glacial terminations (Peeters et al., 2004; Franzese et al., 2006; Martínez-Méndez et al., 2009; Scussolini et al., 2013) and with other abrupt climate shifts (Marino et al., 2013).

4.1.1 Meridional shifts of fronts and the Agulhas leakage during terminations

During glacial terminations, marked rearrangements in atmospheric circulation occurred which were probably global in their extent (Toggweiler and Lea, 2010). For example, a link was found between rising Northern Hemisphere summer insolation, meltwater pulses in the North Atlantic, and weak monsoon intervals (WMIs) in East Asia (Wang et al., 2001; Cheng et al., 2009). Explanations for these links propose that during terminations, catastrophic North Atlantic ice rafting and attendant cooling (McManus et al., 1999) forced a southward displacement of the thermal equator (e.g., Toggweiler et al., 2006; Denton et al., 2010). The circulation of the Ferrel and Hadley cells also took place in a more southern position, and the associated easterly and westerly surface wind fields shifted accordingly. Those conditions are documented in tropical precipitation series from speleothems in the Northern (Wang et al., 2001;

Kelly et al., 2006; Wang et al., 2008; Cheng et al., 2009) as well as in the Southern Hemisphere (SH) (Wang et al., 2004). These changes impacted the atmospheric circulation at tropical latitudes and in the Southern Hemisphere, promoting a southward shift in the position of the SH westerlies, which has recently been identified as an important driver (Toggweiler et al., 2006; Anderson et al., 2009; Toggweiler and Lea, 2010; Lee et al., 2011) of the rises in atmospheric CO_2 concentration associated with the Pleistocene deglaciations (Lüthi et al., 2008). In fact, a number of records spanning the transition from the last glacial maximum to the Holocene document meridional movements of the SH westerly wind belt (Bé and Duplessy, 1976; Prell et al., 1980; Ledru et al., 2005; Lamy et al., 2007; Sikes et al., 2009; De Deckker et al., 2012; Simon et al., 2013). This view is corroborated by models indicating that southerly shifts in the SH westerlies' wind strengthen the AL (de Ruijter and Boudra, 1985; Sijp and England, 2009; Biastoch et al., 2009; Biastoch and Böning, 2013), and conversely for their northward shift (Sijp and England, 2008). We note, anyhow, that the physics of the relationship between SH westerlies and oceanic fronts (Graham et al., 2012) and between westerlies and AL (Durgadoo et al., 2013) are complex, and still the object of present investigation. On the other hand, paleoceanographic evidence suggests that these changes in the Southern Hemisphere atmospheric circulation impacted the oceanic frontal systems, with implications for the transport of warm and saline waters between the Indian and the Atlantic Ocean via the AL (Peeters et al., 2004; Bard and Rickaby, 2009; Marino et al., 2013).

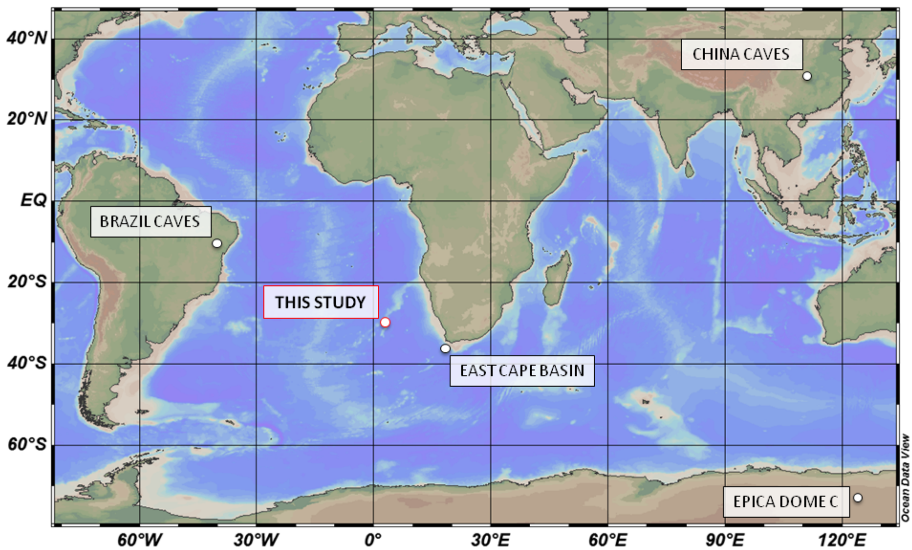

Fig. 4.1. A) Location of the core analyzed and of other records examined in this study. This study is core 64PE-174P13 from the central Walvis Ridge; East Cape Basin records are GeoB-3603-2 and MD96-2081 (Peeters et al., 2004), MD96-2080 (Martínez-Méndez et al., 2010; Marino et al., 2013); China caves records are composed of Sanbao speleothems (Wang et al., 2008; Cheng et al., 2009; Kelly et al., 2006); Brazil caves are Lapa dos Brejões and Toca da Barriguda (Wang et al., 2004); EPICA Dome C ice core record (Jouzel et al., 2007).

These findings collectively make the glacial terminations an ideal target to elucidate the interplay between Indian-to-Atlantic heat and salt transport and the South Atlantic circulation. An increase in the advection of warm and saline waters from around the southern tip of Africa would result in warming and salinification of the upper layers of the South Atlantic gyre. Such changes would result in opposing effects on the calcite $\delta^{18}O$ of planktic foraminifera, thereby making it necessary to isolate the two different signals, temperature and salinity, by means of paired $\delta^{18}O$-Mg/Ca measurements. Further, because the AL introduces heat and salt anomalies from the surface to intermediate water depths (Scussolini et al., 2013, Chapter 3, and references therein), it is important to target those different water masses, i.e. by means of analysis on multiple species of foraminifera. This study presents reconstructions of temperature and seawater $\delta^{18}O$ ($\delta^{18}O_{sw}$, a proxy for seawater salinity changes) from the upper ocean over the central Walvis Ridge, in the east side of the South Atlantic gyre (Fig. 4.1), based on multispecies application of paired $\delta^{18}O$-Mg/Ca proxies.

We place the emphasis on glacial termination II (T-II), treating the interval between MIS 6 and MIS 5 (90 to 180 thousand years before present, ka), for two main reasons: 1) T-II featured an AL release that was likely more prominent and rapid than at T-I (Peeters et al., 2004); 2) recently, a high-resolution record of surface temperature and salinity has become available from the AL region (Marino et al., 2013), which constitutes an ideal comparison to test the effect of the AL waters downstream the AMOC. Further considerations increase the interest in the T-II climatic shift: 3) It featured a deglacial warming in the wider Antarctic-Subantarctic region (Jouzel et al., 2007; Martínez-Garcia et al., 2009) and in deep-ocean temperatures (Elderfield et al., 2012); 4) Dating methods with time-applicability beyond ^{14}C, such as U/Th- and ^{230}Th, have been perfected, and their application to speleothems (Frumkin et al. 2000; Waelbroeck et al., 2008; Cheng et al., 2009; Drysdale et al., 2009; Shakun et al., 2011; Grant et al., 2012), marine cores (Henderson and Slowey, 2000), and corals (Gallups et al., 2002) is allowing to resolve the timing of events around T-II; 5) The notion of a two-step structure for T-II, echoing that of T-I, is acquiring solidity from the replication of the pattern in a number of records (Cannariato and Kennett, 2005; and references therein), not least in the heat and salt pulses from the AL area (Marino et al., 2013).

Here we intend to clarify: the effect of the marked heat and salt transport through the AL upon the upper ocean of the South Atlantic; whether, likewise T-I, there is evidence for a two-step structure of T-II in the South Atlantic; whether this climatic transition implied a change in the total heat content and in the thermocline structure of the upper ocean. We will illustrate that: A) the southeast Atlantic upper hydrography is largely controlled by variability from the AL; B) surface temperature and salinity "reversed" around 133-134 ka, likely responding to a mid-T-II AMOC recovery connected to a Northern hemisphere interstadial; C) across the transition from MIS 6 to 5 the upper ocean increased its heat content, reaching a maximum during the Northern Hemisphere MIS 5e climatic optimum.

4.2 Methods

Planktic foraminiferal stable isotopes and trace elements were analyzed in samples of core 64PE-174P13, from the central Walvis Ridge (29°46'S, 2°24'E, 2912 m water depth), about 1800 km northwest from the AL area (Fig. 4.1). This location is apt to assess the effect of the AL in the subtropical gyre, since it is in the path of present and likely past Agulhas rings shed into the South Atlantic (Scussolini et al., 2013, Chapter 3; and references therein). We sampled the core in the interval from 112 to 212 cm, at 2 cm resolution, and at 1 cm to increase the resolution during the termination, based on the stratigraphy of Scussolini and Peeters (2013, Chapter 2), to cover most of MIS 6 and 5. Samples were washed and foraminifera were picked from the 250-300 μm fraction. Per sample, we selected on average 53 specimens of *Globorotalia truncatulinoides* sinistral (sin.), 56 of *Globigerinoides ruber* sensu lato (s.l.), 45 of *Globorotalia inflata*, 40 of *Globigerina aequilateralis*. Foraminifera were gently crushed, and aliquots of the homogenized calcite fragments were destined to stable isotope and to trace element analyses. The $\delta^{18}O$ was determined as described in Scussolini and Peeters (2013, Chapter 2), on repeated analyses, when the quantity of material allowed.

4.2.1 Age model

The chronology for core 64PE-174P13 that we use in this study is based on three iterative steps. The "ice-core" timescale for the Agulhas Bank core MD96-2080 of Marino et al. (2013) was converted to a radiometric, and therefore "absolute" chronology, using the approach described in Barker et al. (2011). This consisted in applying to the ice core chronology a correction for the offset it manifests with respect to the chronology of radiogenically-dated speleothems. In the next step, we transferred the absolute chronology to the Walvis Ridge core 64PE-174P13 by graphically correlating its $\delta^{18}O$ *G. ruber* profile to the counterpart in core MD96-2080 (Fig. 4.2; Table 4.1), which was obtained from the same foraminifer species and morphotype. Finally, we estimated and propagated the different sources of uncertainty (at the 68%, 1 standard error confidence level) associated with the construction of the chronology for core 64PE-174P13. This error propagation exercise ($\sigma_{chronology}$; Eq. 1) accounts for: (σ_{i}) the uncertainties of the MD96-2080 chronology used by Marino et al. (2013); (σ_{ii}) the uncertainties estimated for the conversion of the ice core to the radiometric ages, discussed in Barker et al. (2011); and (σ_{iii}) the temporal resolution (i.e., sample spacing) of the $\delta^{18}O_{G.\ ruber}$ profiles from 64PE-174P13 and MD96-2080:

(Eq. 1) $$\sigma_{chronology} = \sqrt{(\sigma_{i}^2 + \sigma_{ii}^2 + \sigma_{iii}^2)}$$

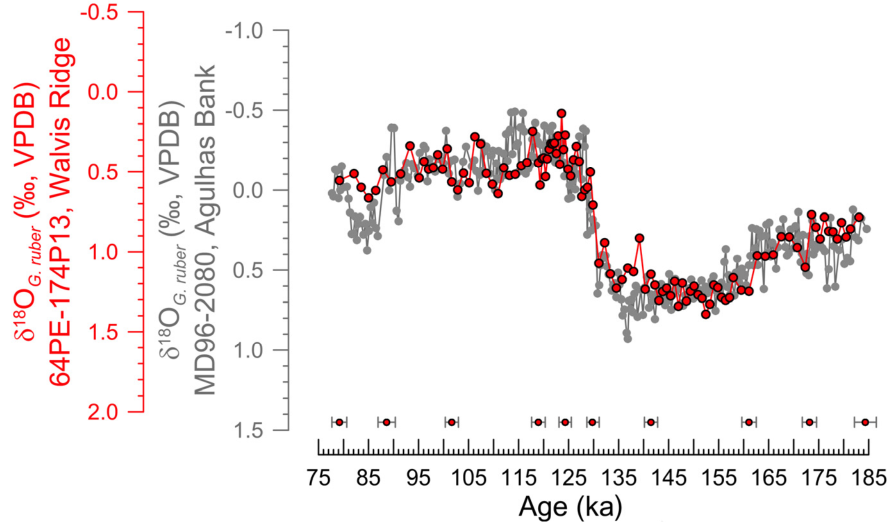

Fig. 4.2. Chronology of core 64PE-174P13. *G. ruber* $\delta^{18}O$ profile from Walvis Ridge core 64PE-174P13 (red) overlain onto the *G. ruber* $\delta^{18}O$ from Agulhas Bank core MD96-2080. The latter had been previously transferred from an ice core (Marino et al., 2013) to an absolute chronology, following Barker et al. (2011). The horizontal error bars are the propagated uncertainties at the 68% confidence level (1 σ) associated with the 64PE-174P13 chronology used in this study (see also Table 4.1).

Depth 64PE-174P13 (cm)	MD96-2080 age (ka)	Mid-point 64PE-174P13 depth (cm)	Mid-point MD96-2080 age (ka)	±1 σ Uncertainty (kyr)
84	77.69	88.0	79.2	1.49
92	80.66			
96	84.72	101.0	88.6	1.73
106	92.54			
114	102.53	115.0	101.7	1.32
116	102.80			
129	118.30	130.0	119.0	1.36
131	119.64			
143	123.65	145.0	124.3	1.23
147	124.98			
151	128.73	155.0	132.8	1.23
159	136.85			
163	140.67	165.0	141.5	1.32
167	142.29			
188	160.49	190.0	161.1	1.44
192	161.67			
204	172.55	205.0	173.2	1.43
206	173.75			
222	180.17	231.0	184.3	2.18
240	188.50			

Table 4.1. Age control points for the synchronization of core 64PE-174P13 (central Walvis Ridge, this study) to core MD96-2080 (Agulhas Bank, Marino et al., 2013).

4.2.2 Mg/Ca analyses and temperature reconstructions

Mg/Ca ratios were analysed with a Varian 720 ES ICP Optical Emission spectroscope, after the foraminiferal calcite was cleaned following the procedure outlined in Barker et al. (2003). Briefly, cleaning comprised sonication and rinsing in ultrapure water and in methanol, oxidation in hydrogen peroxide, and weak acid leaching. After comparison of the concentration of the remaining potentially contaminant elements on the calcite after cleaning with and without a reductive step, the introduction of such additional reductive step was deemed not necessary. External reproducibility was routinely monitored using standard ECRM 752-1, as recommended by Greaves et al. (2005). The average offset of our measurements on such standard was 0.05 mmol/mol Mg/Ca, from a reported nominal value 3.76 mmol/mol (Greaves et al., 2005), which we corrected for in each run. Intra-run precision was on average ± 0.03 mmol/mol (1 σ), corresponding to 0.7%.

Mg/Ca in planktic foraminifera provide an estimation of seawater temperature. We converted Mg/Ca values into calcification temperatures using published species-specific calibrations (Table 4.2). A number of Mg/Ca-to-temperature equations are available from the literature, which differ from one another for causes mostly imputable to the methodology used to derive the calibration itself (sediment trap, core top, culture) and/or the oceanographic setting. The difficulty of assigning coherent calibrations to a data set of Mg/Ca values from different fossil planktic foraminifer species has been faced in previous studies (e.g., Sagawa et al., 2011). For the four species, inhabiting different depths in the ocean (Hecht and Savin, 1972; Savin and Douglas, 1973; Bé, 1977), we selected a set of the calibrations such that, in the resulting dataset, the more shallow species were assigned a warmer temperature, and conversely for the deeper species.

T = ln (Mg/Ca / A) / B			
	A	B	
G. ruber	0.34	0.102	Anand et al. (2003)
G. truncatulinoides sin.	1.32	0.05	Regenberg et al. (2009)
G. aequilateralis	0.86	0.068	Anand et al. (2003)
G. inflata	0.72	0.076	Groeneveld and Chiessi (2011)

Table 4.2. Calibration equations used to obtain temperatures from the Mg/Ca of foraminiferal calcite. Mg/Ca values are expressed in mmol/mol, and T in °C.

4.2.3 Seawater $\delta^{18}O$ anomaly reconstruction

We use paired Mg/Ca-$\delta^{18}O$ time series, in conjunction with contemporaneous records of ice volume changes, to derive local, ice-volume corrected seawater $\delta^{18}O$ anomalies ($\delta^{18}O_{sw\text{-}ivc}$) for each depth at which our foraminifera species dwell. First, we correct the $\delta^{18}O$ measured in the foraminiferal calcite ($\delta^{18}O_{foram}$) for the effect of temperature variations. The effect of temperature is estimated from the Mg/Ca composition, using the relationship of Bemis et al. (1998):

(Eq. 2) $$\delta^{18}O_{seawater} = \delta^{18}O_{foram} - 25.778 + 3.333 \sqrt{(T_{Mg/Ca} + 43.706)}$$

For *G. ruber* we applied a conservative correction of + 0.2 ‰ to its $\delta^{18}O$ values, to account for a "vital effect" assessed in situ (Lonçaric et al., 2006). For the other species we considered the vital effect as negligible (Fairbanks et al., 1980; Loncaric et al., 2006). Subsequently, after converting the VPDB notation to VSMOW, we estimated the $\delta^{18}O_{sw\text{-}ivc}$ by subtracting from the $\delta^{18}O_{seawater}$ the component attributable to variations in mean global seawater $\delta^{18}O$ due to ice-volume variations. For this, we used the recent sea level reconstructions of Grant et al. (2012) for the last 150 kyr, and the one of Rohling et al. (2009) for the period 150-183 ka. We converted sea level into mean ocean $\delta^{18}O_{sw}$ using the relationship of Schrag et al. (2002), namely 0.008 ‰ m^{-1}. In the modern ocean, the $\delta^{18}O_{sw}$ is linearly related to regional seawater salinity changes (e.g., LeGrande and Schmidt, 2006); for this reason we use it, which supports our approach of using $\delta^{18}O_{sw\text{-}ivc}$ as a qualitative indicator of paleo-salinity changes.

4.2.4 Planktic foraminifera calcification depth

Each planktic foraminifer species calcifies along a continuous depth interval (Hemleben et al., 1989). Nevertheless, for convenience of proxy use, a discrete depth is taken to be representative of the average depth of calcification, generally coherent with the geochemical values of the shells collected in the modern water column.

We assessed apparent calcification depths of foraminifera species by comparing core top $\delta^{18}O$ to modern ocean $\delta^{18}O$ of seawater (cfr., Scussolini and Peeters, 2013, Chapter 2). The estimations for *G ruber* and *G. truncatulinoides* (sin.) are outlined in Scussolini and Peeters (2013, Chapter 2). *G. inflata* and *G. aequilateralis* are compared to the modern hydrography of their month of main occurrence (October) (Lonçaric et al., 2007), and reflect an apparent calcification depth of ~500 and 390 m, respectively. In this estimation, vital effects were not considered. Literature on foraminiferal habitat preferences normally assigns shallower depths to the species we treat here. We account such discrepancy largely to the exceptionally deep mixed layer and thermocline of this region (Lonçaric et al., 2006). For this study, we considered that *G. ruber* represents the (sub)surface, and calcifies at ~100 m, *G. aequilateralis* is intermediate (~200 m), *G. inflata* and *G. truncatulinoides* sin. inhabit the thermocline, between ~400 and 500 m.

4.3 Results

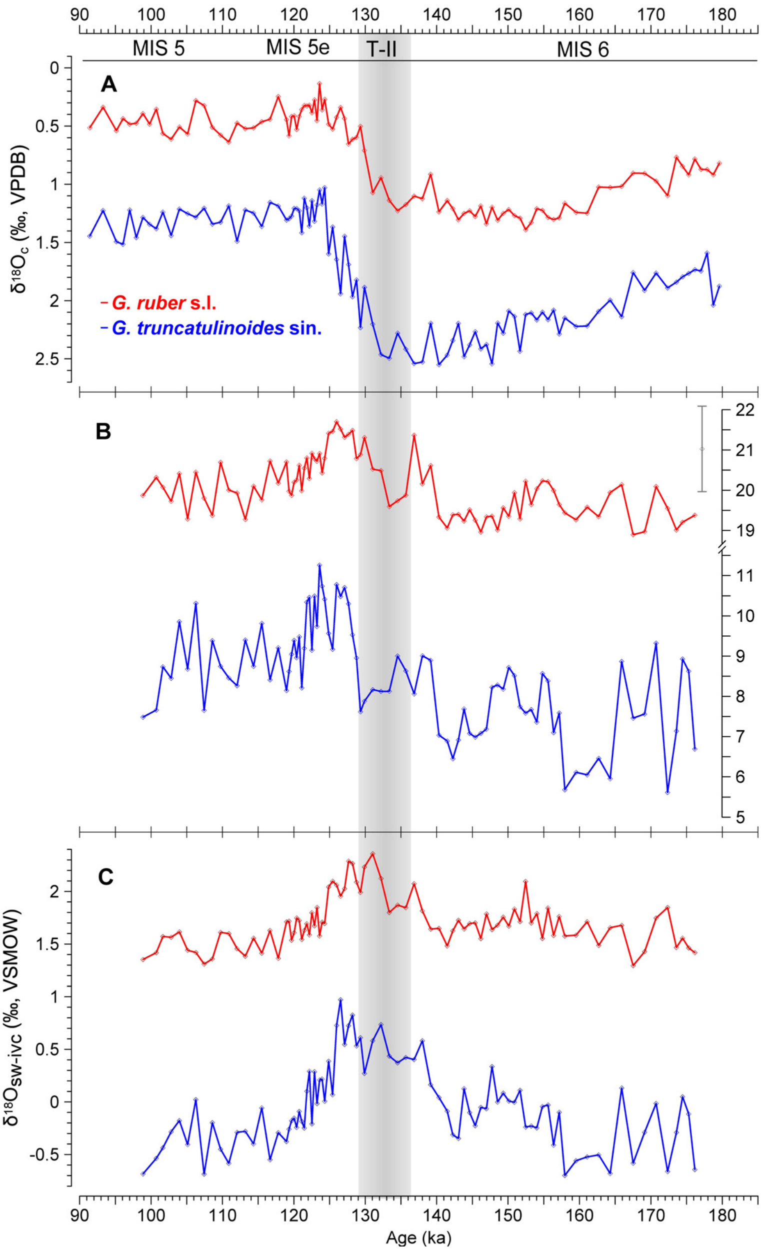

Fig. 4.3. Geochemical results. For surface species *G. ruber*, sub-surface *G. aequilateralis*, and deep-dwelling *G. inflata* and *G. truncatulinoides* sin. we show: A) $\delta^{18}O$; B) Mg/Ca-derived temperatures (grey line indicates the 1 σ error estimated from the pooled standard deviation of repeated measurements); C) $\delta^{18}O_{sw\text{-}ivc}$ anomalies (calculated as in Methods). The grey bar indicates the T-II, as defined by the duration of the Asian weak monsoon interval-II.

4.3.1 $\delta^{18}O$

The $\delta^{18}O$ profiles of the four planktic foraminifera species analyzed for this study present a clear glacial-interglacial modulation of the signal with approximately synchronous $\delta^{18}O$ shifts from heavier glacial MIS 6 to lighter interglacial MIS 5 values (Fig. 4.3 A). Notably, the deglacial $\delta^{18}O$ shift differs in magnitude between the different species; it is largest in *G. truncatulinoides* sin. (1.5 ‰) and minimal in *G. ruber* (~1.1 ‰). Values for all species remained quite stable throughout MIS 5.

4.3.2 Mg/Ca-derived temperatures

For each species, the Mg/Ca temperatures show millennial-scale variations (Fig. 4.3 B), superimposed upon a long-term warming from the colder glacial conditions of MIS 6 to the warmer ones at the beginning of MIS 5. Surface dwelling *G. ruber* displays sub-orbital oscillations during MIS 6. There are two temperature increases prior to and across T-II, while the major warming took place at ~133-128 ka. MIS 5e values were higher than during MIS 6, and subsequently gently decreased after 125 ka. The intermediate species *G. aequilateralis* shows higher temperature variability across MIS 6. The pattern of temperature increase along T-II corresponds largely to that of *G. ruber* (high significance of the t-test on Pearson's correlation between the series; $p < 0.001$). Notably, at 125 ka temperatures of *G. aequilateralis* decreased more sharply than *G. ruber*'s. Deep-dwelling *G. truncatulinoides* sin. temperature fluctuated during MIS 6, then showing prominent warming at ~140 and 129 ka. Temperatures were highest during MIS 5e, and gradually decreased afterwards. The other deep species *G. inflata* manifests more stable values, with a long trend of gradual temperature increase, from 160 ka until the end of T-II.

4.3.3 $\delta^{18}O$ of sea water anomalies – proxy for salinity

The $\delta^{18}O_{sw\text{-}ivc}$ profiles (Fig. 4.3 C) increased for the four species at ~142 ka. A second, sharp increase is visible for the shallower species *G. ruber* and *G. aequilateralis* about halfway into the termination, at ~132 ka. Values for the three species decreased gradually during early MIS 5, from 125 ka, and remain at levels lower than, or similar to, MIS 6 until 100 ka. *G. truncatulinoides* sin. and *G. ruber* (and secondarily *G. inflata*) display especially high values of $\delta^{18}O_{sw\text{-}ivc}$ from ~142 to 125 ka. Notably, the magnitude of the shift to heavier $\delta^{18}O_{sw\text{-}ivc}$ at mid-T-II is double for the deep-dwelling *G. truncatulinoides* than for the shallower *G. ruber*. In the interval between 145-120 ka, the signal from *G. truncatulinoides* sin. leads on that from *G. ruber* by one sample-step (about 0.7 kyr on average). The curve of *G. inflata* generally supports the results of *G. truncatulinoides* sin., but shows milder variations, similarly to the more shallow species.

4.4 Discussion

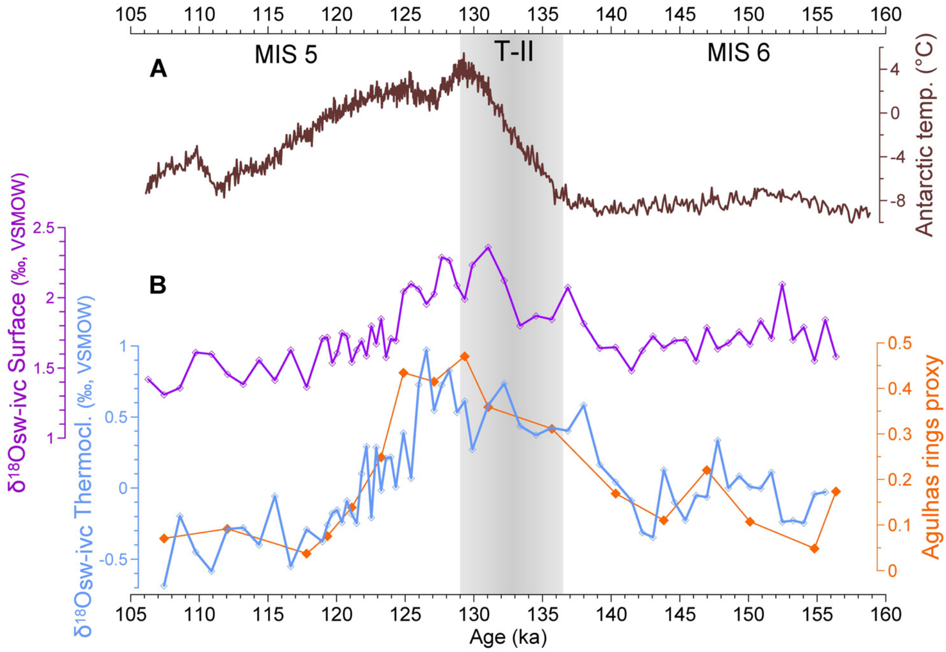

Fig. 4.4. Comparison between proxies of core 64PE-174P13. A) Antarctic temperature from EPICA Dome C (Jouzel et al., 2007) is plotted for stratigraphic reference. The age model EDC3 (Parrenin et al., 2007) is corrected for the offset with respect to the speleothem chronology following Barker et al. (2011). B) $\delta^{18}O_{sw-ivc}$ from surface *G. ruber* and thermocline *G. truncatulinoides* sin. are compared to the proxy for Agulhas rings in the same core (Scussolini et al., 2013, Chapter 3).

The new paleoceanographic proxy records from Walvis Ridge core 64PE-174P13 reveal distinct multi-millennial, positive temperature and $\delta^{18}O_{sw-ivc}$ anomalies at both surface and thermocline depths, starting about ~142 ka (see reconstructions derived from *G. ruber* and *G. truncatulinoides* sin.; Fig. 4.3 B and C). The onset of the temperature and salinity increases led by up to 6 kyr the T-II warming in EPICA Dome C (Jouzel et al., 2007) (Fig. 4.4). In particular, salinity maximized during (at the Walvis Ridge surface) or slightly after (at the thermocline) the attainment of full interglacial conditions in Antarctica (Figure 4.4). In this section we will first utilize our new datasets to attempt a depth-integrated reconstruction of the upper ocean heat content and stratification at the Walvis Ridge between MIS 6 and MIS 5. Then we will discuss the potential climatic controls on the observed changes in upper ocean temperature and salinity in the context of previously published records from AL area and elsewhere.

4.4.1 Increase in upper ocean heat content and changes in stratification

Using the Mg/Ca-derived temperature profiles of the four planktic species, *G. ruber*, *G. aequilateralis*, *G. inflata* and *G. truncatulinoides* sin., each representative of a distinct depth range in the upper water column, we are able to depict the overall thermal evolution of the upper ocean in the southeast Atlantic between 175 and 105 ka (Fig. 4.5 A). It appears that the southeast Atlantic accommodated larger quantities of heat in its upper layers during the last interglacial (MIS 5) compared to the preceding glacial (MIS 6). This is shown by a gradual upper ocean warming between ~141 and 127 ka, which paused between ~136 and 132 ka. This maximum in heat content during MIS5e might be indicative of a more vigorous upper branch of the AMOC, leading to the enhanced export of heat to the North Atlantic during the Eemian thermal optimum (Sánchez Goñi et al., 2012). Further, combining the four temperature datasets, we reconstruct the thermal stratification of the upper ocean (Fig. 4.5 B). Our reconstructed upper ocean thermal stratification is higher during glacial MIS 6 and decreases after T-II, echoing what previously suggested, from the $\delta^{18}O$-based density stratification changes from the same core (Scussolini and Peeters, 2013; Chapter 2). Fig 4.5 B can also be seen as a reconstruction of thermocline depth: following, for example, the 10 or 12° C isotherms, it emerges that the thermocline was more shallow during MIS 6, and deepened during T-II, reaching its deepest levels at MIS 5e.

Fig. 4.5 (next page). Reconstructions of upper-ocean temperature distribution and stratification. A) $\delta^{18}O$ of *G. ruber,* plotted for stratigraphic reference (red), and integrated temperature of the upper 500 m, calculated as the average of multispecies Mg/Ca-derived temperatures (thick line is the 1-kyr low-pass Gaussian filtered dataset). B) Contoured temperatures from the Mg/Ca-based reconstructions from *G. ruber*, *G. aequilateralis*, *G. inflata* and *G. truncatulinoides* sin. The contouring enables integrating datasets with different temporal resolution. Because this is a conceptual illustration, and to improve the readability, we assigned fixed depths in the water column to each foraminifera temperature series, based on the available literature and on our own estimations (see Methods): *G. ruber* at 50 m, *G. aequilateralis* at 150 m, *G. inflata* at 400 m, *G. truncatulinoides* sin. at 500 m. C) $STRA_{trop}$ indexes (Steph et al., 2009) using different combinations of species from our dataset. We used *G. ruber* as a shallow-dweller, *G. truncatulinoides* sin. as a deep-dweller. As intermediate-dwellers, we used *G. inflata* (purple) and *G. aequilateralis* (orange). Thick lines are 1-kyr low-pass Gaussian filtered data. D) Conceptual diagrams are added to aid the interpretation of the $STRA_{trop}$ indexes.

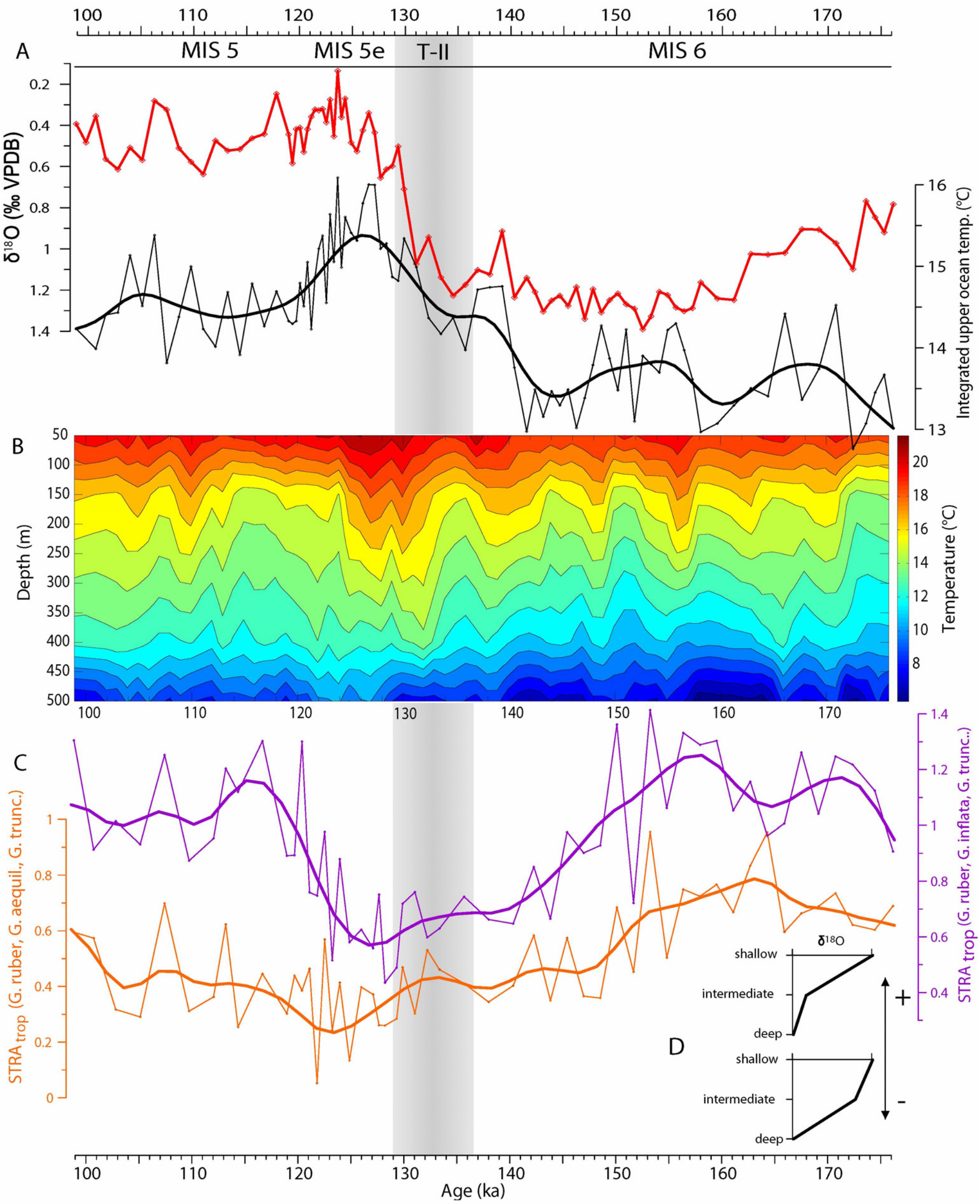

To shed further light onto the patterns of stratification, we attempt to increase the vertical resolution of the reconstruction of thermocline-to-surface density stratification presented in Scussolini and Peeters (2013, Chapter 2). For this we use the multispecies $\delta^{18}O$ dataset, and apply the "$STRA_{trop}$" index, proposed for the tropical Atlantic by Steph et al. (2009) (Fig. 4.5 C), which requires a shallow, an intermediate, and a deep foraminifer species:

(Eq. 3) $$STRA_{trop} = (\delta^{18}O_{intermediate} - \delta^{18}O_{shallow}) / (\delta^{18}O_{deep} - \delta^{18}O_{shallow})$$

We use *G. ruber* for the shallow layer, and *G. truncatulinoides* sin. for the deep one. For the intermediate layer, we use both *G. aequilateralis* and *G. inflata* to obtain two different estimates of the index. Even though we estimated the depth of *G. inflata* in our region to be not much more shallow than *G. truncatulinoides* sin., for this exercise we treated it as "intermediate" dweller mostly on the grounds that in the literature it is commonly assigned a more shallow habitat than *G. truncatulinoides* (e.g., Fairbanks et al., 1980; Loncaric et al., 2006). To higher $STRA_{trop}$ values corresponds a density stratification that is more conspicuous above the depth of the intermediate dwelling species, and thus a likely shallower pycnocline position (see diagram in Fig. 4.5 D). Conversely, a low $STRA_{trop}$ indicates deeper pycnocline. Therefore, regardless of the intermediate dweller chosen, the pycnocline was most shallow around 165-160 ka, ~20 kyr before T-II, and then it became deeper, reaching its maximum depth at about ~128 ka, just after the deglaciation was complete. Subsequently, stratification values gradually return to near-MIS 6 levels after ~15 kyr. This reveals that the transition between MIS 6 and 5 implied a change in the trends of stratification.

Unitedly, the temperature- and the density-integrated reconstructions of upper ocean stratification from core 64PE-174P13 document a southeast Atlantic upper ocean with a more shallow thermo- and pycnocline position during glacial MIS 6, and a relatively low integrated heat content. The climatic transition around T-II implied a deepening of both thermocline and pycnocline, and a clear increase in the heat stored in the upper ocean layers of this region. Our upper-ocean reconstructions of heat content and stratification constitute an ideal term of comparison for paleoclimate model simulations, in transient or in equilibrium form, that aimed at studying how changes in the AMOC might have enforced variations in upper-ocean structure of the South Atlantic Ocean during this climatic transition. This would shed light into the dynamics of heat transport by the Atlantic upper-ocean conveyor.

In the following sections we will focus on the surface and thermocline components of the temperature changes revealed in this integrated analysis. Further, by examining the salinity and temperature changes combined, we will discuss the wider implications of our observations.

4.4.2 Control of the Agulhas leakage on the upper ocean hydrography of the Walvis Ridge

r and p values	64PE-174P13 Surface $\delta^{18}O_{sw-ivc}$	64PE-174P13 Thermocl. $\delta^{18}O_{sw-ivc}$	64PE-174P13 Surface Temp.	64PE-174P13 Thermocl Temp.
64PE-174P13 Agulhas rings proxy [1]	**0.79 (p <0.001)**	**0.84 (p <<0.001)**		
MD96-2080 $\delta^{18}O_{sw-ivc}$ [2]	**0.83 (p <<0.001)**	**0.76 (p <<0.001)**		
MD96-2080 Temp. [2]			**0.55 (p <<0.001)**	0.28 (p < 0.05)

[1] Scussolini et al. (2013, Chapter 3)
[2] Marino et al. (2013)

Table 4.3. Correlation statistics between proxy series of core 64PE-174P13 (central Walvis Ridge) and core MD96-2080 (Agulhas Bank). Values from core MD96-2080 have been resampled at the time step of core 64PE-174P13. Pearson's r correlation coefficients (r) and p significance values are shown. Highly significant correlations are reported in bold.

Our thermocline $\delta^{18}O_{sw-ivc}$ profile suggests that salinity at the Walvis Ridge core site started to increase at 142 ka (Fig. 4.4 B). Since high salinity at thermocline depths is a characteristic of modern waters from the AL, and of those contained in Agulhas anticyclones ("rings"; e.g., van Aken et al., 2003), we compare our thermocline salinity series to a proxy for the Agulhas rings, which was previously presented for the same core 64PE-174P13 (Scussolini et al., 2013, Chapter 3) (Fig. 4.4 B). Briefly, this proxy is based on the variability, within each sediment sample, of $\delta^{18}O$ measurements of *G. truncatulinoides* sin. individual specimens. This is the same signal carrier we use for our thermocline salinity reconstruction, which implies that the two proxies are indicative of the same water mass. For the comparison, we used for the Agulhas rings proxy record presented previously (Scussolini et al., 2013, Chapter 3) the new chronology of this study. Although the resolution is substantially different, the two time series strongly covary (Table 4.3). This suggests that the high salinities documented at the Walvis Ridge around T-II originated in the AL.

To further explore the provenance of water masses feeding the thermocline at the Walvis Ridge, we utilize the $\delta^{13}C$ in *G. truncatulinoides* sin. We note that this profile lacks the "carbon isotope minimum", which is a typical fingerprint of deglacial Subantarctic Mode Waters during deglaciations (Spero and Lea, 2002; Ziegler et al., 2013) (Fig. 4.6). This is contrasted with a $\delta^{13}C$ record based on the same species and morphotype from the Agulhas Plateau (Ziegler et al., 2013), which shows a marked (-0.7‰) $\delta^{13}C$ excursion. It is therefore unlikely that the advection of Subantarctic Mode Waters from the Southern Ocean dominated the thermocline circulation at the Walvis Ridge across T-II. Taken together, these observations argue in favour of a strong control exerted by the inter-ocean transport via the AL on the salt content of the thermocline in the central Walvis Ridge.

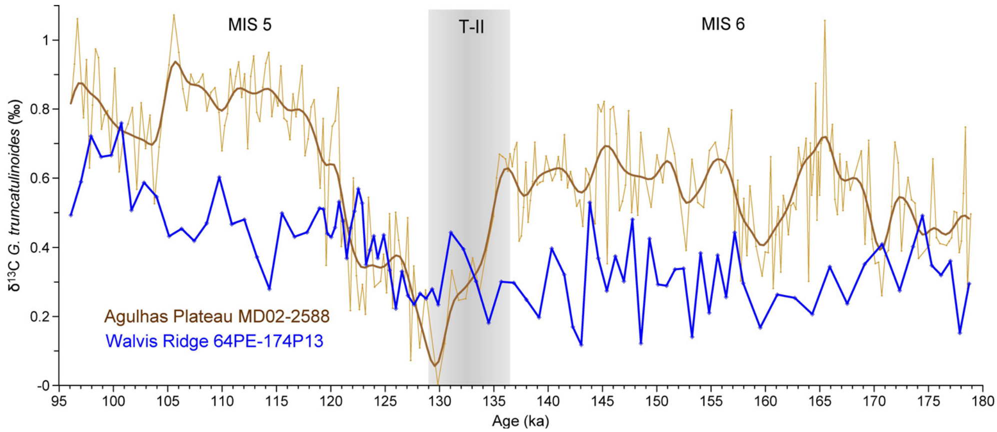

Fig. 4.6. Comparison of thermocline δ^{13}C curves. We compare the δ^{13}C of *G. truncatulinoides* sin. from Walvis Ridge core 64PE-174-13 and to its counterpart from the Agulhas Plateau core MD02-2855 (Ziegler et al., 2013; thick line is the result of a 1-kyr low-pass Gaussian filter).

Warm thermocline waters are also typical of modern AL and rings (Arhan et al., 2011). Still, thermocline δ^{18}O$_{sw\text{-}ivc}$ from *G. truncatuilinoides* sin. mirrors the Agulhas rings proxy closer than Mg/Ca-derived temperatures from the same species (Fig. 4.3 B and 4.4 B), suggesting that salinity is a more conservative property of the AL waters at the thermocline, whereas temperature anomalies might dissipate faster (Beal et al., 2011).

The surface δ^{18}O$_{sw\text{-}ivc}$ trends are similar to those observed at the thermocline, and the correlation to the Agulhas rings proxy is high (Fig. 4.4; Table 4.3). However, the ~0.7 kyr lag of the surface with respect to the deeper series, in combination with the smaller amplitude of the signal, are interesting hints that salinity of AL origin might influence the South Atlantic more promptly at the thermocline levels, while at the surface the signal is also transmitted, but apparently dampened.

We investigate the effects of the variable transport of heat and salt via the AL on the hydrography of the southeast Atlantic upper water column by comparing the new Walvis Ridge records with previously published reconstructions from the Agulhas Bank, i.e., where the AL waters enter the South Atlantic. Both surface δ^{18}O$_{sw\text{-}ivc}$ and temperature profiles from the Walvis Ridge show highly significant correlation to their counterparts from the Agulhas Bank (Marino et al., 2013) (Table 4.3) (Fig. 4.7 A and B). The surface δ^{18}O$_{sw\text{-}ivc}$ records from these two locations are virtually coupled between 145-137 ka (MIS 6), and again from 128 to 112 ka (MIS 5) (as illustrated by the stable offset in Fig. 4.8 B). During T-II, the two δ^{18}O$_{sw\text{-}ivc}$ peaks at the Agulhas Bank (~136 and 131 ka, respectively) coincide, within chronological uncertainty, with δ^{18}O$_{sw\text{-}ivc}$ maxima at the Walvis Ridge. This agrees with the notion that an AL increase promotes salinification of the upper water column in the South Atlantic (Biastoch et al., 2009). The structure of the surface ocean temperature profile from the Agulhas Bank from ~140 to 129 ka (Fig. 4.7 B) resembles the temperatures reconstructed from alkenones of the Cape Basin record of Peeters et al. (2004), which we synchronized to our chronology by aligning the major shifts in Agulhas leakage fauna from adjacent cores GeoB3603-2 (Peeters et al., 2004) and MD96-2080 (Martínez-Méndez et al., 2010) (Fig. 4.7 C). Such increase is also seen in our surface temperature reconstruction, but the connection is less tight than between the $\delta^{18}O_{sw\text{-}ivc}$ records (Table 4.3), and indeed the AL temperature maxima around 135 and 132 ka are not distinguished in the Walvis Ridge record (see offset between the Walvis Ridge and Agulhas bank surface temperatures in Fig. 4.8 A). An explanation for this differential transmission of warm and salt anomalies from the Agulhas is provided by the observation that, at present, the temperature fingerprint from the AL is dissipated relatively fast in the Cape Basin, due to air-sea interactions, while salinity represents a more conservative feature of the AL rings/filaments along their downstream trajectory (Beal et al., 2011; Arhan et al., 2011).

Fig. 4.7 (next page). Comparison of our results with regional and distal records. A) Surface and thermocline $\delta^{18}O_{sw\text{-}ivc}$ from Walvis Ridge core 64PE-174P13, and surface $\delta^{18}O_{sw\text{-}ivc}$ from Agulhas Bank core MD96-2080 (Marino et al., 2013), to which we applied a with 1 kyr low-pass Gaussian filter. Note that the latter curve is replicated for comparison with Walvis Ridge thermocline $\delta^{18}O_{sw\text{-}ivc}$. B) Surface temperatures from the Walvis Ridge, from the Agulhas Bank (Marino et al., 2013; a 1-kyr low-pass Gaussian filter was applied), and from the east Cape Basin core GeoB3603-2 (Peeters et al., 2004). C) AL intensity from faunal counts in cores MD96-2080 (Martínez-Méndez et al., 2010) and GeoB3603-2 (Peeters et al., 2004). The age of core GeoB3603-2 has been adapted to the speleothem chronology by aligning its AL peak to that from core MD96-2080. D) Chinese speleothems from the Sanbao cave (SB23, Wang et al., 2008; SB11 and SB25, Cheng et al., 2009) and Dongge cave (D3 and D4, Kelly et al., 2006) are plotted to show consistency in the reconstruction of the WMI-II, and in the interstadial around ~134 ka, that we interpret as the ACR-II. Growth phases from brazil speleothems (Wang et al., 2004) are plotted to show the consistency of the T-II pattern as emerging from records of tropical climate. E) Greenland computed climate record (Barker et al., 2011), plotted in its GL_T_syn_hi form, which emphasizes millennial scale variability.

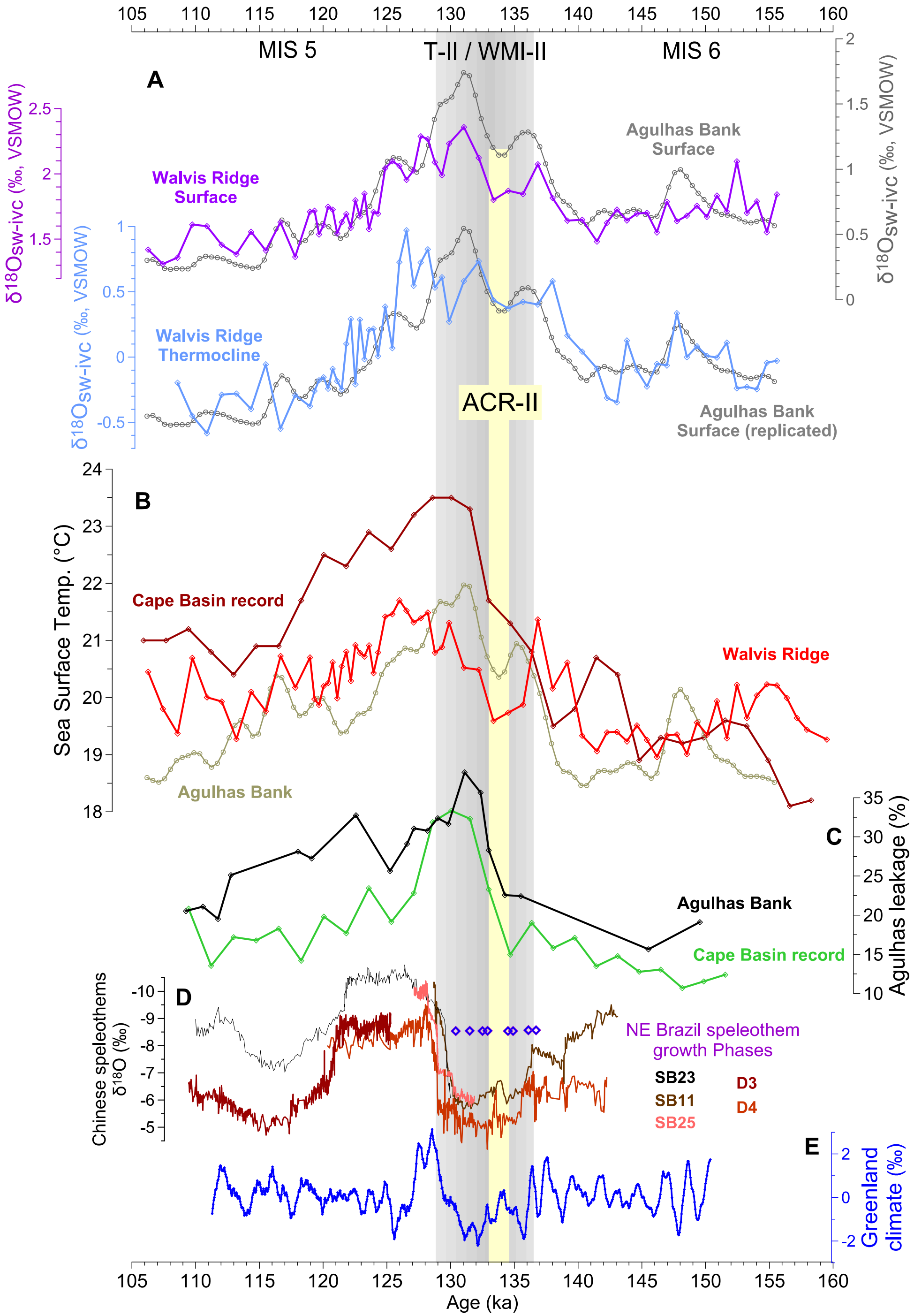

MIS 5
T-II / WMI-II
MIS 6
A
Walvis Ridge Surface
Agulhas Bank Surface
Walvis Ridge Thermocline
ACR-II
Agulhas Bank Surface (replicated)
δ18Osw-ivc (‰, VSMOW)
B
Sea Surface Temp. (°C)
Cape Basin record
Walvis Ridge
Agulhas Bank
C
Agulhas leakage (%)
Agulhas Bank
Cape Basin record
D
Chinese speleothems δ18O (‰)
NE Brazil speleothem growth Phases
SB23
SB11
SB25
D3
D4
E
Greenland climate (‰)
Age (ka)

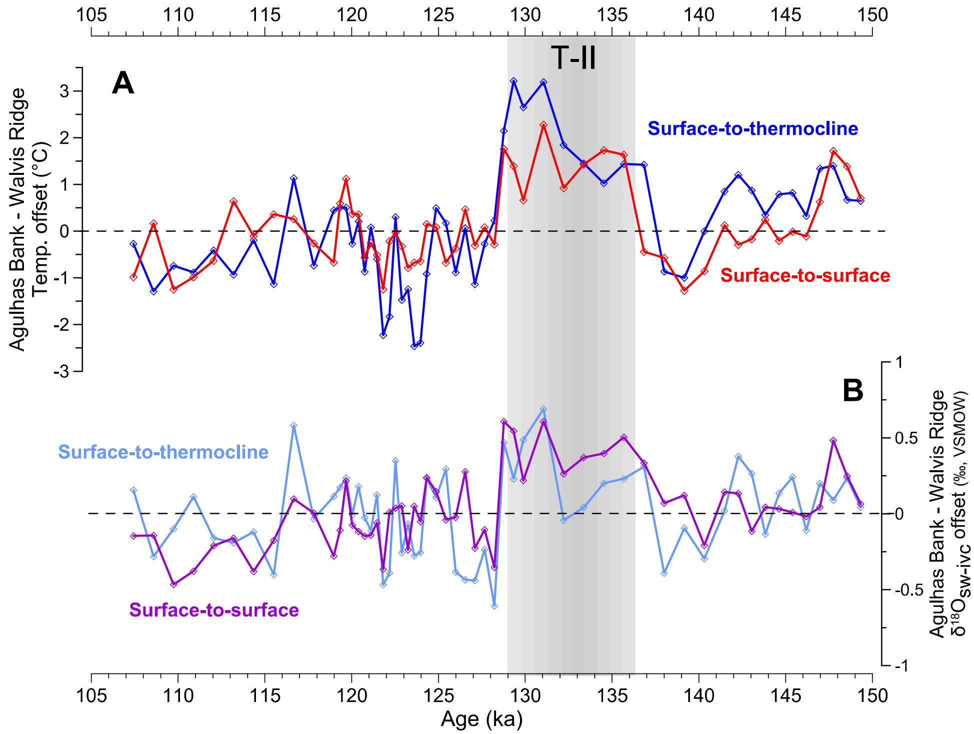

Fig. 4.8. Offsets between geochemical records from the Walvis Ridge and from the Agulhas Bank. We show the offsets of A) temperature and B) $\delta^{18}O_{sw\text{-}ivc}$ between surface and thermocline records from Walvis Ridge core 64PE-174P13 and the surface records from Agulhas Bank core MD96-2080 (Marino et al., 2013). Records are considered as deviations from the mean, to account for differences in the absolute values.

The Walvis Ridge thermocline $\delta^{18}O_{sw\text{-}ivc}$ profile appears as well to be highly correlated to the surface counterpart from the Agulhas Bank (Table 4.3; Fig. 4.7 A and 4.8 B). Also this evidence argues in favor of an AL influence on the hydrography of Walvis Ridge, in line with the notion that such perturbations commonly invest depths from the surface down to the thermocline (Arhan et al., 2011; Scussolini et al., 2013, Chapter 3). Notably, the amplitude of the salinity anomaly at the Walvis Ridge thermocline is higher than at the surface (Fig. 4.7 A). Because waters from the AL contain a low-density anomaly that reaches intermediate ocean depths (Scussolini et al., 2013, Chapter 3), their positive buoyancy, largely due to their relative high temperature, should make them shoal as they travel into the South Atlantic. Still, it is possible to speculate that the density of Agulhas waters might progressively increase further into the south Atlantic, due to the dissipation of their thermal anomaly to the surrounding waters, as they transmit heat northwestwards (Souza et al., 2011). This would contrast the initial shoaling behavior. Our Walvis Ridge thermocline results, where the salt effect persists at a distance more than the temperature one, and where the AL salt anomaly seems to be more visible at the thermocline, allude to this second possibility, of a negative buoyancy of AL waters into the South Atlantic.

In this perspective, reconstruction of thermocline water properties in the AL would be important to clarify those aspects. Also, numerical simulations could help shed light on the vertical propagation of the AL waters and water properties within the South Atlantic. Our results indicate anyway that surface salinity variability from the Agulhas is clearly visible ~1800 km downstream in the South Atlantic, though with different intensities at surface and thermocline depths.

4.4.3 South Atlantic evidence for a two-step T-II

Termination I in the wider North Atlantic region was characterized by a cold phase during Heinrich stadial 1 (HS1), followed by abrupt warming into the Bølling-Allerød (B-A), and by a return to cold conditions during the Younger Dryas (YD) (e.g., Denton et al., 2010). Plausibly, those events were modulated by a sequence of collapse-resumption-reduction of the AMOC (McManus et al., 2004) and of the associated transport of oceanic heat to the high latitude North Atlantic (Broecker, 1991). The cold phases (HS1, YD) in the North Atlantic coincided with distinct WMIs in East Asia (Wang et al., 2001) and with rapid southward shifts (anti-phase response) of the Subtropical Front in the South Atlantic (Barker et al., 2009), with potential implications for the AL system (Biastoch et al., 2009; Beal et al., 2011). The B-A warm interval in the North Atlantic and wet phase in the Asian Monsoon, as well as the coeval cold phase in the SH, known as Antarctic Cold Reversal (ACR) (Jouzel et al., 2007; Barker et al., 2009), reflect the abrupt recovery (Fiedel, 2011) or even overshoot (Liu et al., 2009; Barker et al., 2010) of the AMOC, that lead to the enhanced heat piracy of the North Atlantic.

We use our surface records from the South Atlantic to investigate whether similar interhemispheric climate developments occurred during the penultimate termination. Across T-II, the surface temperature and $\delta^{18}O_{sw\text{-}ivc}$ profiles from core 64PE-174P13 document a brief return to low values (Fig. 4.7 A and B), superimposed upon the long-term warming and salinification discussed above. The colder and fresher conditions at the Walvis Ridge around 135-134 ka correspond, within synchronization uncertainties (Table 4.1), to analog temperature and $\delta^{18}O_{sw\text{-}ivc}$ drops in the records from the AL area (Marino et al., 2013), for which the higher temporal resolution allows to pinpoint the timing and duration of this event more precisely at 134 ± 1.2 ka (Fig. 4.7 A). We interpret these "reversals" at both sites as the hydrographic response of the southeast Atlantic surface ocean to a short-lived reduction of the Indian-to-Atlantic heat and salt transport that punctuated the AL maximum of T-II (Peeters et al., 2004; Martínez -Méndez et al., 2010; Marino et al., 2013). Interestingly, the timing of these hydrographic reversals in the South Atlantic is contemporaneous, within dating uncertainty, with the brief wet interruption of the WMI-II in East Asia (133 ± 1.0 ka in speleothem D4 [Kelly et al., 2006]; 134 ± 1.0 ka in speleothems MSP and MSX [Cheng et al., 2006]; 134 ± 1.5 ka in speleothem SB11 [Wang et al., 2008]) (Fig. 4.7 D). The synthetic Greenland $\delta^{18}O$ record (Barker et al., 2011), on its chronology tuned to the East Asia speleothems, suggests this coincided with a warm phase in the wider North Atlantic region (Fig. 4.7 E). This raises the possibility that the heat and salt transport, from the Indian Ocean, through the AL, to the Walvis Ridge, transiently weakened during this interval, in step with a short-lived resumption of the AMOC. This brief weakening of the AL may be ascribed to the northward shift of the intertropical convergence zone, likely in response to a reactivation of the AMOC (Toggweiler, 2009; Frierson et al., 2013), which also strengthened the boreal monsoon (Cheng et al., 2009).

Therefore, we outline the potential causal mechanism underlying the ~134 ka climatic interval amidst T-II, which, in analogy with the ACR during T-I, we call ACR-II. The combination of the external (insolation) and internal (greenhouse gases, meltwater discharge, bipolar seesaw) forcings acting during deglacial transitions (Liu et al., 2009; Ganopolski and Roche, 2009; Barker et al., 2010) likely caused a transient mid-T-II recovery of the AMOC. This could have been coeval with a possible halting/reduction of freshwater discharge in the northern North Atlantic, reflected in a "pause" in the lightening of North Atlantic benthic isotope records of Lototskaya and Ganssen (1999), Gouzy et al. (2004), Drysdale et al. (2009) (only for the latter a speleothem chronology is available, and locates the event at 136-134 ± 2.5 ka, thus compatible with the ACR-II timing). At this point upper South Atlantic waters were exported to the North Atlantic, thereby abating the excess salinity that accumulated in the southeast Atlantic during T-II, when the AL peaked (Peeters et al., 2004; Marino et al., 2013). Concomitantly, and according to the mechanism proposed by Crowley (1992), the restored southward flow of North Atlantic Deep Water would have subtracted heat from the upper layers of the South Atlantic, leading to cooling (Vellinga and Wood, 2002; Knutti et al., 2004). This could explain the temperature reversal observed at the Walvis Ridge and Agulhas Bank core sites, and the coeval moderate warming at the Iberian Margin (135 ± 2.5 ka; Drysdale et al., 2009) and Greenland (Barker et al., 2011).

4.4.4 Thermocline heat increase at the end of T-II

Having assessed that the bipolar seesaw mechanism governed the surface distribution of heat across the Atlantic basin during T-II, we examine the evolution of the South Atlantic thermocline in relation with other available T-II climatic records, using our Mg/Ca-derived temperature record from *G. truncatulinoides*.

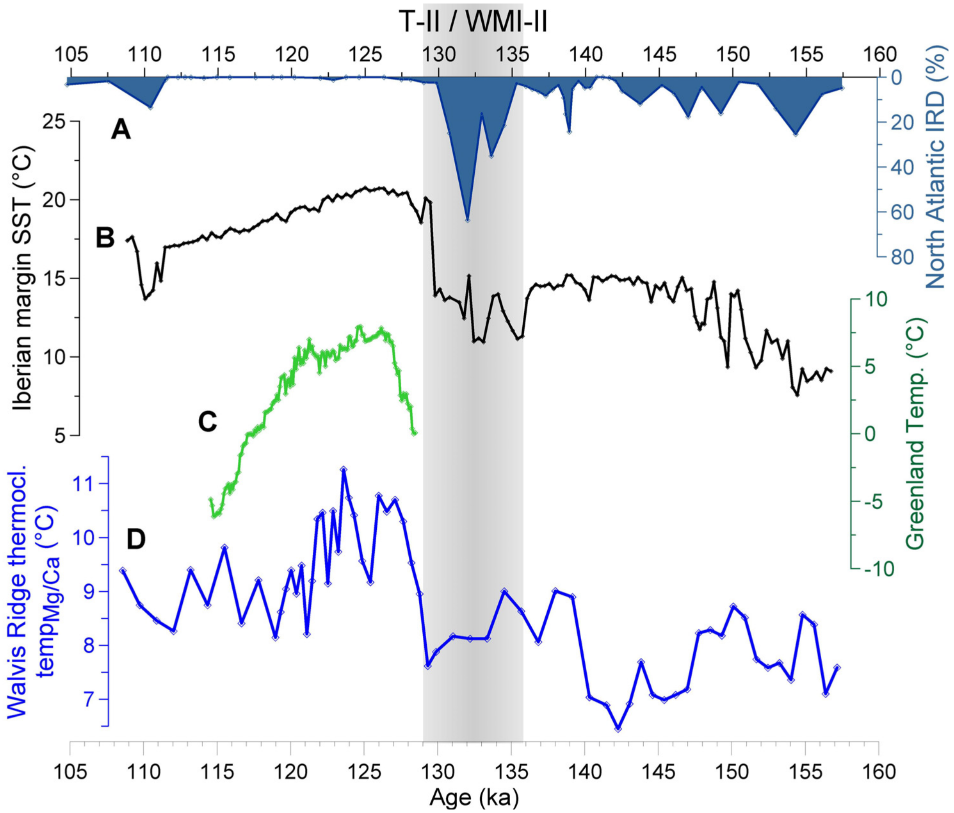

Fig. 4.9. Comparison of the thermocline temperature record from the Walvis Ridge with climate records from the Northern Hemisphere. A) North Atlantic Ice-rafted debris from core ODP 980 (McManus et al., 1999). B) Iberian Margin sea surface temperatures (Martrat et al., 2007). C) Northern Greenland temperatures (NEEM, 2013). D) Thermocline temperature record from Walvis Ridge core 64PE-174P13. Records from core ODP 980 and from the Iberian Margin are harmonized to the Speleo chronology after Barker et al. (2011).

The relatively fast increase in thermocline temperatures at the Walvis Ridge occurs (within dating error) right at the end of T-II (Fig. 4.9 D), absolutely dated at the end of WMI-II (Cheng et al., 2009) (see also Fig. 4.7 D). The conclusion of T-II was likely characterized by rather abrupt changes in Northern Hemisphere climate. After the cold Heinrich stadial 11 (testified by the interval of intense ice rafting in McManus at al. [1999]; Fig. 4.9 A), a sudden increase of temperatures took place, reconstructed for the North Atlantic surface (Martrat et al., 2007; Sánchez Goñi et al., 2012) (Fig. 4.9 B) and from a recent speleothem in France (Wainer et al., 2011), in the changes of vegetation cover from European records at the onset of the warm Eemian interglacial (Sánchez Goñi et al., 1999; Tzedakis et al., 2003), and in the switch to more intense monsoonal activity at the end of the WMI-II in East Asia (Cheng et al., 2009) (Fig. 4.7 D). Recently, the beginning of the Eemian has emerged as a pronounced warming in the wider North Atlantic region, as exemplified by considerable surface melting in North Greenland (NEEM, 2013) (Fig. 4.9 C). It seems thus as though the heat increase at thermocline depths in the southeast Atlantic paralleled the Northern

Hemisphere climatic switch to a warmer state, and the northward shift of the intertropical convergence zone, and attendant atmospheric circulation. Significantly, also thermocline salinity shows maximal values during the onset of the Eemian, when $\delta^{18}O_{sw\text{-}ivc}$ from *G. truncatulinoides* sin. is high between 128 and 125 ka (Fig. 4.7 A). A mechanistic elucidation of this link seems elusive, but our results indicate that inter-hemispheric seesaw distribution of heat cannot account for the temperature changes at our site's thermocline and in the North Atlantic.

4.5 Conclusions

For the penultimate glacial-interglacial cycle, we reconstructed the evolution of temperature and $\delta^{18}O_{sw\text{-}ivc}$ (as proxy for salinity) at multiple upper ocean layers, from the central Walvis Ridge, a location presently downstream the Agulhas leakage.

- We depict the evolution of the vertical thermal structure of the upper ocean, showing that T-II was a turning point for the stratification pattern, which reached its lowest at the end of the deglaciation. The heat contained in the upper-ocean layers increased from MIS 6 until MIS 5e. In particular temperature at the southeast Atlantic thermocline rapidly increased at the end of T-II, paralleling the establishment of warm climatic conditions in the wider North Atlantic during the Eemian period. This could be informative for climate models aiming at simulating the dynamics of upper Atlantic heat transport during this climatic transition.
- Through comparison with published reconstructions of the passage of Agulhas rings over the Walvis Ridge, and of hydrographic variability at the AL area, we ascertained that upper ocean conditions at the Walvis Ridge were strongly influenced by the release of warm saltwater from the AL. Surface and thermocline salt content at the Walvis Ridge tightly reflected salinity rises at the AL area. Two aspects withhold further interest: i) the salt anomaly from the AL seems to have been transmitted more efficiently at the thermocline level; ii) the thermal connection between the AL area and the Walvis Ridge appears weaker than the salinity one. These findings suggest that during T-II AL waters might have dissipated their heat across the Cape Basin, and that this might have affected their density and negatively influenced their buoyancy.
- Our surface temperature and salinity reconstructions at the Walvis Ridge complete the AL area counterparts in depicting a two-step structure of the oceanographic changes over T-II, with a short-lived interval of lower temperature and salinity at ~133-134 ka, likely synchronous with an interruption of the WMI-II. We suggest that this results from the inter-hemispheric seesaw effect of a mid-termination resumption of the AMOC during T-II. This mechanism subtracted heat and salt from the South Atlantic to carry it northwards, in analogy to events around T-I, when the Antarctic Cold Reversal in the Southern Hemisphere corresponded to the Bølling-Allerød interval. While the dynamics behind the B-A / YD succession and the ACR still are debated (Fiedel, 2011), the discovery of a ACR-II type of event in an older deglaciation,

as we now report from the South Atlantic at T-II, can provide indications for model simulations aimed at proposing quantitative mechanisms for this phenomenon. In particular, the different orbital characterization of T-II allows the testing of hypotheses as to an insulation-trigger for B-A / ACR type of events (e.g., Cannariato and Kenneth, 2005).

Acknowledgements

The work described in this paper has received funding from the European Community's Seventh Framework Programme FP7/2007-2013 – Marie-Curie ITN, grant agreement n° 238512, GATEWAYS project. We are grateful to Sanne Vogels and Laura Rodríguez-Sanz for support with the Mg/Ca cleaning, and to John Visser for assistance with the ICP-OES system at the VU Amsterdam.

5

Anti-phasing of Northern and Southern Hemisphere monsoons during the past 420,000 years. Support for a global-paleo-monsoon

Based on: Paolo Scussolini, Frank J. C. Peeters, Helge W. Arz, Jerome Kaiser, Trond M. Dokken, Claire Waelbroeck, and Hans Renssen, manuscript in preparation.

Abstract

Monsoon systems are being recognized as regional manifestations of the globally coordinated, seasonal shifts of the intertropical convergence zone (ITCZ). A number of studies have shown that paleo monsoon intensity was systematically linked to high latitude Northern Hemisphere climate variability, on millennial timescales. In addition, tropical records of precipitation have highlighted an anti-phasing between monsoons in the two hemispheres over the last glacial cycle. To test the persistence of this pattern in the Pleistocene, we studied a marine core from the northeast Brazilian margin, an area sensitive to meridional movements of the ITCZ. We use the Ti/Ca composition of the sediment as a proxy for continental riverine runoff, and we present a 420,000-year long, detailed history of precipitation in the area, which in turn is linked to South American monsoon intensity. On orbital time scales, precipitation shows a positive response to seasonal insolation at its 5° S latitude. We demonstrate that periods of strong South American monsoon corresponded to Northern Hemisphere cold intervals, and to intervals of weak East Asian monsoon, most prominently during the last four glacial terminations, and during the preceding glacials. Our reconstruction indicates that this presently arid region regularly underwent humid spells during the last ~420,000 years, with important implications for the connectivity between Amazon and Atlantic rainforests, and for their paleoecology. Further, the interhemispheric anti-phasing of monsoon records, illustrated for the past four glacial-interglacial cycles, suggests that the response to Northern Hemisphere forcing, superimposed on a latitude-dependent control by seasonal insolation, is a consistent feature of the global monsoon system in the Pleistocene.

5.1 Introduction

The tropics host 40% of the human population and 80% of the planet's biodiversity. The susceptibility of the tropical ecosystems to drought stress raises concerns as to their future preservation. In particular the Amazon rainforest is expected to undergo dryer conditions, in the context of anthropogenic climate change (Phillips et al., 2009; Cheng et al., 2012a). Moreover, changes in the tropics entail feedbacks on the global climate system (Phillips et al., 2009; Cox et al., 2004; da Costa et al., 2010). Changes in the tropical hydrological cycle, have the potential to alter the Earth's climate, through variations in the atmospheric moisture content (Avissar and Werth, 2005), and greenhouse gases levels (Ivanochko et al., 2005), and through changing the upper ocean salinity, which in turn has repercussions on the oceans' meridional overturning circulation (Carlson et al., 2008). Hence there is need, also in the view of the on-going change, to understand the sensitivity of tropical hydroclimate to past climate forcing.

One strategy is to study the Pleistocene epoch, replete with events of climate change on a range of time-scales (e.g., Barker et al., 2011; White et al., 2013). Paleo records of tropical Atlantic hydroclimate encompassing the last glacial cycles commonly show a response of monsoons to insolation, mainly in the precession band (Wang et al., 2004; Baker et al., 2004; Cruz et al., 2005), which is likely due to dependence of regional atmospheric circulation patterns upon variations in the surface heating. This response is confirmed by coupled climate models (Kutzbach et al., 2008; Li et al., 2013). Moreover, distinguished swings in precipitation were registered in shorter times series, across the past glacial cycle (Pokras and Mix, 1987; Absy et al., 1991; Peterson et al., 2000; Ledru et al., 2005) and the Holocene (Hughen et al., 1996; Haug et al., 2001; van Breukelen et al., 2008). Evidence of large shifts in the precipitation regime for older parts of the Pleistocene are available from long time series from North Africa (Rossignol-Strick, 1983), east equatorial Atlantic (Pokras and Mix, 1987), east Asia (Wang et al., 2008; Cheng et al., 2009), and western (Tachikawa et al., 2011; Meckler et al., 2012) and eastern (Rincón-Martínez et al., 2010) equatorial Pacific. For South America, records are typically interrupted around marine isotopic stage (MIS) 4 or 5.

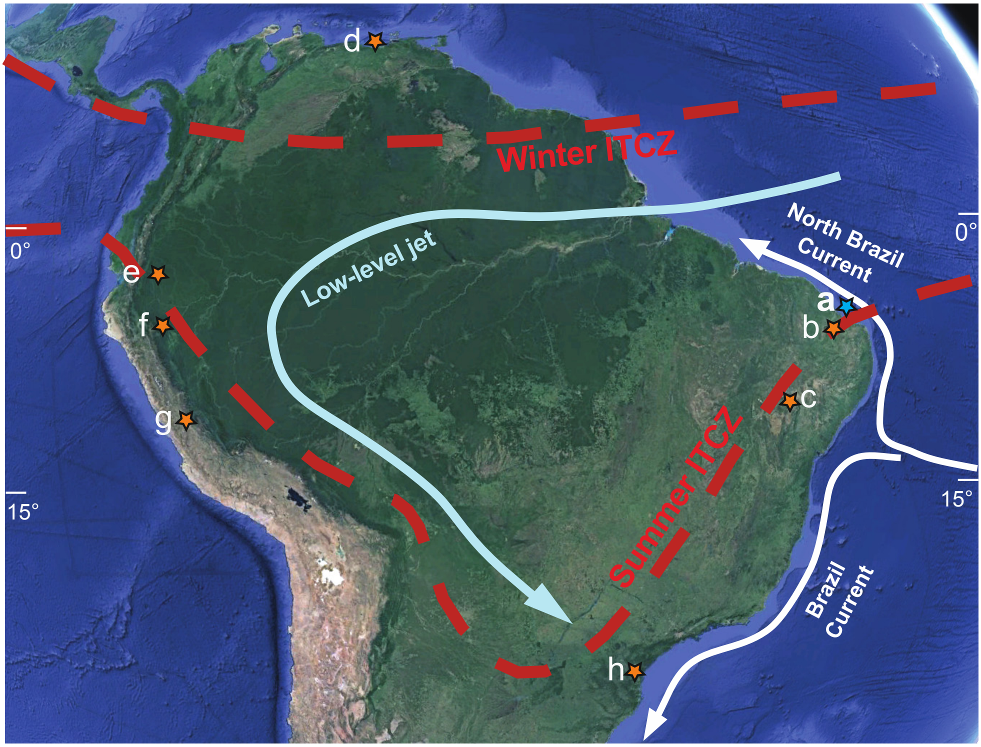

Fig. 5.1. **Map of the northern South American continent**, indicating the intertropical convergence zone in (Southern Hemisphere) winter and summer, and the South Atlantic currents that influence the hydrography at the site of core MD09-3246 (a). Location of other records discussed: b) Rio Grande do Norte caves (Cruz et al., 2009a); c) Lapa dos Brejoes and Toca da Barriguda caves (Wang et al., 2004); d) ODP site 1002 (Peterson et al., 2000); e) Santiago cave (Mosblech et al., 2012); f) Cueva del Diamante and El Condor caves (Cheng et al., 2013); g) Pacupahuain cave (Kanner et al., 2012); h) Botiverà cave (Cruz et al., 2005; 2007; Wang et al., 2006; 2007).

Specifically, for the region of northeastern Brazil, the Nordeste, the general paucity of speleothems is due to the relative aridity. Exceptions to this are the speleothem and travertine growth phases of Wang et al. (2004), who assigned absolute dates to intervals of enhanced precipitation of the last 210 thousand years (kyr) (Fig. 5.1). Another exception is the last deglaciation record of Cruz et al. (2009a). For the adjacent marine realm, the account of western tropical Atlantic hydroclimate is so far limited to the last glacial-interglacial cycle (e.g., Arz et al., 1998; 1999; Jaeschke et al., 2007) (Fig. 5.4). In this study, we present a new time-series of western tropical Atlantic / Nordeste precipitation over the past 420,000 years, from a marine core in the northeast Brazilian margin.

The Nordeste is characterized by a strong seasonal precipitation pattern, with an intense rainfall peak between February and May (Hastenrath, 1991). During these months, the intertropical convergence zone (ITCZ) is displaced southwards, over the region (Hastenrath and Greischar, 1993) (Fig. 5.1), so that northeast trade winds convey evaporative moisture from the Atlantic Ocean (Behling et al., 2000), and the South American summer monsoon (SAM) releases abundant rainfall over the continent. This seasonal relationship between austral insolation and SAM has been reproduced also in the Pleistocene simulation of a coupled ocean-atmosphere global model (Kutzbach et al., 2008), providing an explanation for Pleistocene observations (Wang et al., 2004; Cruz et al., 2005; Wang et al., 2007).

The glacial and deglacial climate of the Nordeste has been studied using pollen (Absy et al., 1991; Behling et al., 2000; Jennerjahn et al., 2004), marine sediments (Arz et al., 1998; 1999) and speleothems (Cruz et al., 2009a) (for a review, see Cruz et al. [2009b]). Together with reconstructions from southern Brazil (Cruz et al., 2005; 2007; Ledru et al., 2005; Wang et al., 2006; 2007) this body of knowledge unravels the history of changes in the SAM (Fig. 5.1).
A merit of those studies is to have drawn the connection between periods of high Nordeste precipitation and North Atlantic Heinrich stadials. The latter are cold intervals, associated with reductions in the rate of Atlantic meridional overturning circulation (AMOC) (Álvarez-Solas et al., 2011; Thornalley et al., 2013), a considerable source of heat advection to the Northern Hemisphere (NH), or with altered intrusion of the AMOC in the northern North Atlantic water column (Dokken et al., 2013). NH cooling likely results in attenuation of the AMOC (e.g., Skinnner et al., 2010), and of the relative northward transport of heat from the South to the North Atlantic. Because of this, heat accumulates in the South Atlantic, making the ocean surface south of the equator relatively warm, in turn causing a southward shift in the ITCZ (Stouffer et al., 2006). Such connection of high-latitude and tropical climate is sustained by models (Chiang et al., 2003; Chiang and Bitz, 2005; Jaeschke et al., 2007), and also explains the North Atlantic forcing of the East Asian Monsoon (EAM) (Cheng et al., 2009). The effect of NH cold phases, however, has an inverse sign on the EAM and the SAM, since southward displacements of the ITCZ subtract moisture (of Pacific and Indian Oceans origin) from the EAM, while conveying it (from the Atlantic) to the SAM. According to recent developments in the understanding of monsoon systems, these seemingly synchronous changes in the two hemispheres are a manifestation of the global monsoon, which responds to the seasonal meridional shifts of the ITCZ (Trenberth et al., 2000; Wang and Ding, 2008). North Atlantic cooling therefore corresponds to wet phases in the Nordeste. This is verified in the paleo record, by Wang et al. (2004; 2006; 2007) and Cruz et al. (2009a), who showed wet phases in Brazil during dry, weak EAM in Heinrich stadials. In addition, Kanner et al. (2012) showed that this interhemispheric antiphasing also holds on a shorter time scale, i.e., during Dansgaard/Oeschger cycles.

With this study we pursue two main goals. 1) We extend the existing record of the SAM further back in time. 2) By comparing this new SAM time series with published reconstructions of the EAM, we assess the synchronicity of past changes in these two components of the global monsoon (Trenberth et al., 2000; Wang and Ding, 2008), and to explore the persistence of this anti-phased teleconnection, mediated by NH forcing. With this, we intend to test the recently proposed concept of "global paleo-monsoon" (Wang, 2009; Cheng et al., 2012b) for rapid climate change of the last four glacial cycles.

Our strategy is to produce a new record of terrigenous runoff from the northeast Brazilian margin, and use it to qualitatively reconstruct the history of precipitation from the Nordeste region. By connecting the events emerging from our record to a previously published, radiocarbon-dated, core from the same region, we show that peaks in precipitation correspond to Heinrich stadials, and to NH cold spells for the last ~120 kyr. This link, in addition to a chronological structure for the remaining part of the record based on a foraminiferal $\delta^{18}O$ stratigraphy, provides the basis for the comparison of our record to Chinese speleothems, reflective of the EAM. The strong correspondence of intervals of high precipitation from our record with those of weak EAM emerges clearly for the last four glacial terminations, for the preceding glacials, and secondarily for the interglacials. We therefore demonstrate that meridional displacement of the ITCZ and attendant rain belt was substantially a global phenomenon, during times of climate change over the past 420 kyr.

5.2 Methods

5.2.1 Core location and sedimentology

Core MD09-3246 (4° 14' S, 37° 6' W) (~34 m length), was retrieved with a Calypso coring system at the northeast Brazil margin, from a depth of 890 m (Fig. 5.1) in the framework of the 'RETRO-project'. This region has a wide continental shelf (~50 km), and the core site is situated only a few km offshore from it. The sedimentology of the region is characterized by an alternation of carbonate-rich intervals of mainly pelagic sediments, and darker intervals with high content of clay, washed by the region's rivulets (Arz et al., 1998).

An approach to study the sedimentological history of core MD09-3246, i.e., the evolution of the proportion of pelagic versus terrestrial sediment, is the determination of the elemental content of Ti versus Ca. Ti is often used as an indicator of the terrigenous component of the sediment (e.g., Jansen et al., 1992), while Ca is a main constituent of biogenic calcite and aragonite, and therefore represents marine sedimentation. The Ti/Ca ratio was already shown to represent the terrigenous, clay-rich component from a core in this area (GeoB 3104-1 [Arz et al., 1998]), on the grounds that marine productivity of the western equatorial Atlantic, and therefore Ca sedimentation, remained nearly constant across glacial-interglacial cycles (Rühlemann et al., 1996). Further, Arz et al., (1998; 1999b) have correlated high terrigenous content in the marine sediment to riverine runoff from the adjacent Nordeste region. Runoff, in turn, reflects the balance between the processes of precipitation and evaporation, being directly proportional to the former, and inversely to the latter. For this region it was suggested that, due to relatively limited catchment area of water bodies in the area, precipitation strongly influences the runoff of terrigenous material (Arz et al., 1998; 1999b). Additionally, palynological studies have confirmed that, over the last glacial cycle, intervals of high runoff, documented in the higher Ti/Ca of the sediment, were characterized by higher humidity and therefore precipitation (Behling et al., 2000), also revealing the timing of the regional ecosystem response to changes in the hydrological cycle (Jennerjahn et al., 2004). On the basis of those works, we interpret runoff, indicated by the Ti/Ca ratio, as a valid, though qualitative, indicator of continental precipitation.

We therefore analysed core MD09-3246 for its elemental composition by means of X-Ray Fluorescence, on a Itrax core scanner equipped with a Cr tube, at the IOW, Rostock-Warnemünde, Germany. The resolution was set to 1 mm, and the exposure time to 15 seconds; the voltage used was 30 kV, and the current 30 mA. Thermo-gravimetric analyses, to measure the relative $CaCO_3$ abundance, have been carried out using a Leco TGA-601 instrument at the VU University, Amsterdam, on ~1 cm^3 of bulk dry sediment.

5.2.2 Foraminiferal stable isotopes

We produced a planktic foraminifer oxygen isotope stratigraphy for core MD09-3246, using surface-dwelling species *Globigerinoides ruber*, variety white sensu stricto. Additionally, we measured the isotope composition of the pink variety of *G. ruber*, to assess which taxon incorporated its oceanographic signal closer to the sea surface. For each variety, we picked about forty specimens per sample, from the size fraction 250-300 μm. A narrow size fraction was chosen to minimize size-related isotope variability. We subsequently crushed the specimens between glass slides, and analysed a portion of the mixed fragments, equivalent to ~60-100 μg, to optimize sample representativeness. The $\delta^{18}O$ value of the calcite was determined on a Thermo Finnigan Delta Plus mass spectrometer equipped with Gas Bench II preparation device at the VU University, Amsterdam, and a Finnigan 252 mass spectrometer with a Kiel carbonate preparation device at the NIOZ, Texel, The Netherlands. By performing cross analyses of the same standard and foraminiferal material, we assessed that there is no offset between the results obtained on the two instruments. Details on instrumental performance are found in Scussolini and Peeters (2013).
For the chronology of the core we utilized both the log(Ti/Ca) and the $\delta^{18}O$ datasets, and the reader is referred to section 5.4.

5.3 Results

5.3.1 Sedimentology results

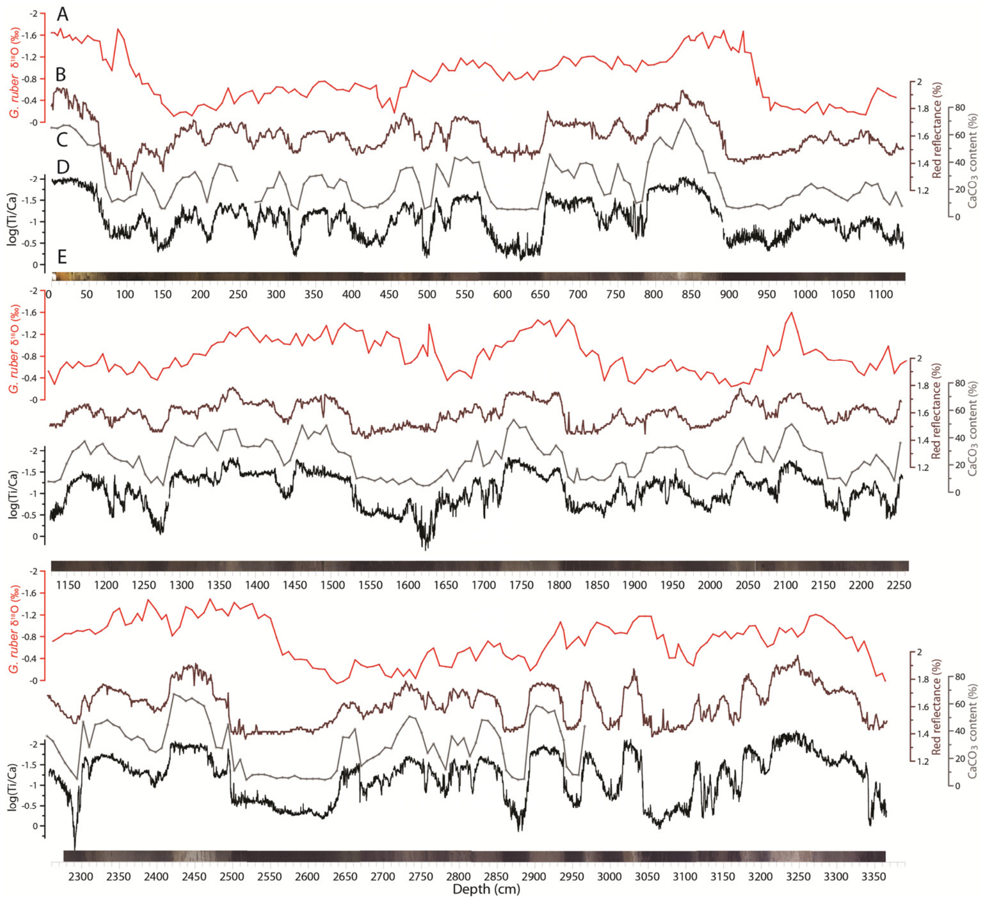

Fig. 5.2. **Results for core MD09-3246**. A) $\delta^{18}O$ of surface foraminifer species *G. ruber*; B) Red reflectance; C) Total carbonate ($CaCO_3$) content; D) log(Ti/Ca) from XRF scanning; and D) images of the core.

Profiles of elemental ratios Ti/Ca, Fe/Ca, Ti/K, and Fe/K show very similar patterns along core MD09-3246. Ti and Fe have both already shown to mirror the terrigenous component of the sediment at this location (Arz et al., 1998). Here we used the ratio of Ti over Ca as a parameter representative of the sedimentation regime because it yields the highest signal to noise ratio. To emphasize variability at low values we plot our results in the log(Ti/Ca) form (Fig. 5.2). Measurements of $CaCO_3$ content (from TGA analysis), of log(Ti/Ca) (from XRF scanning) and of red reflectance (from colour scanning) all correlate well to one another (Fig. 5.2 and 5.3). In particular correlation between $CaCO_3$ content and log(Ti/Ca) is the highest, proving that the Ti/Ca ratio adequately reflects changes in the clays/carbonates ratio, and hence mirrors the pronounced changes in input of terrigenous matter. Such high degree of comparability attests the essential interchangeability of these three methods to obtain a record of the marine versus terrestrial fractions of the sediment, in the depositional regime of the Brazilian continental margin. We therefore used the log(Ti/Ca) from XRF analysis, because of the higher resolution of this dataset. As explained in the Methods (section 5.2), we use it as a proxy for continental runoff and therefore precipitation.

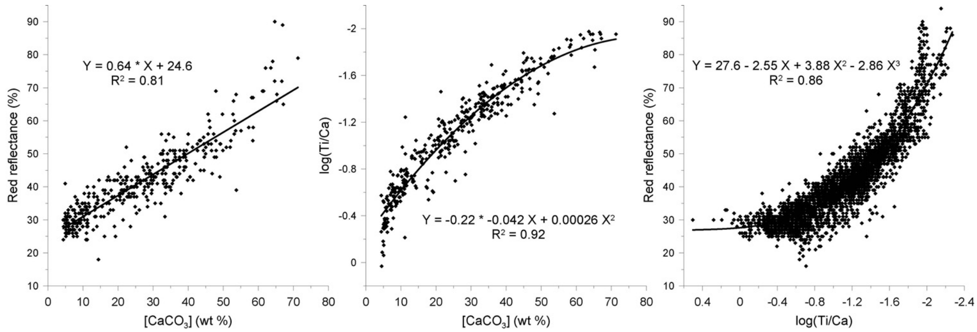

Fig. 5.3. **Bivariate scatter plots of proxy time series data**, showing the correlation between $CaCO_3$ content, log(Ti/Ca), and red reflectance.

5.3.2 Foraminiferal $\delta^{18}O$ results

Variations in the isotopic composition of *G. ruber* white sensu stricto and *G. ruber* pink largely reflect the well-known pattern of Pleistocene glacial-interglacial waxing and waning of continental ice sheets (Fig. 5.6). The shifts to heavier values during deglaciations are: ~1.6 ‰ at T-I, 1.55 ‰ at T-II, 1.2 ‰ at T-III, 1.5 ‰ at T-IV. For T-V we cannot assess it, because of the uncertainty in the age determination of the lower part of the core (see following section 5.4). Coeval $\delta^{18}O$ values of the white and pink varieties differ slightly. The mean offset is only 0.07 ‰, but proves significant ($p<0.01$, $n=88$), thus *G. ruber* pink is systematically heavier.

5.4 Chronologies for core MD09-3246

To determine the chronology of core MD09-3246, we proceeded in an iterative manner. We evaluated a number of strategies and generated four different age models, each of them based on different tuning targets and different underlying assumptions. Based on this process, we are able to motivate the application of a chronology tuned to absolutely dated speleothems. This allows thus to discuss features emerging from our climate record in comparison with previously published ones.

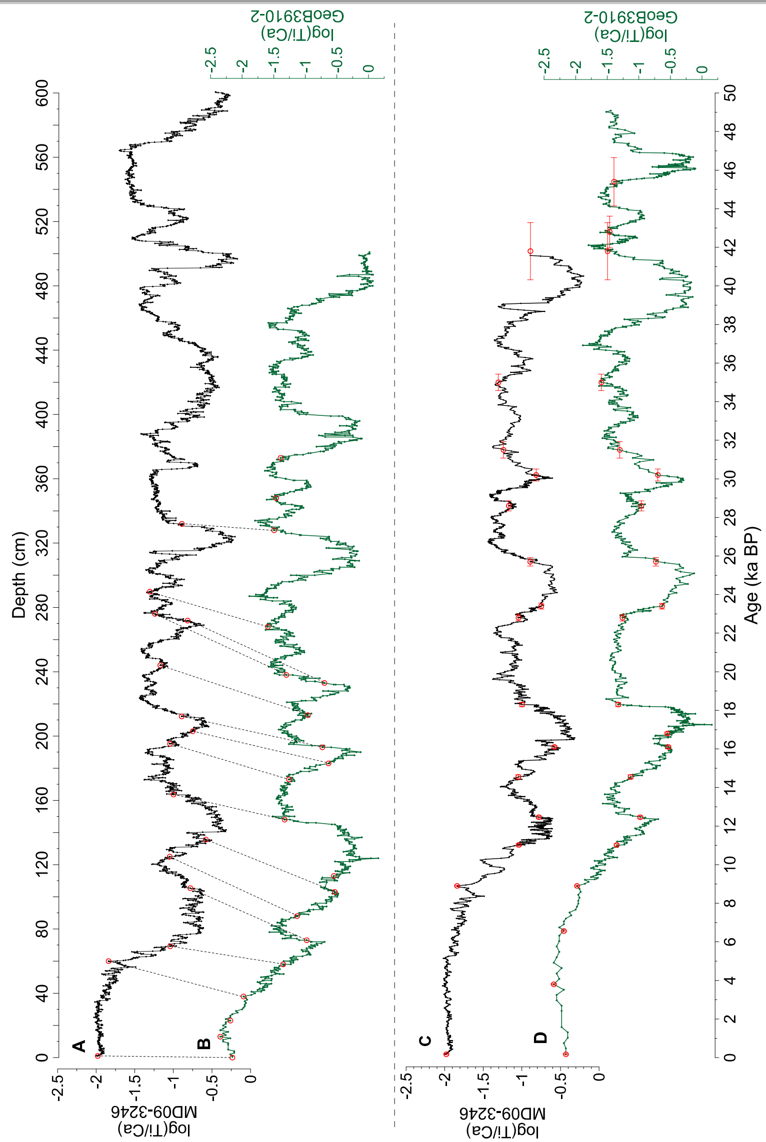

Fig. 5.4. **^{14}C-tuned chronology**. Log(Ti/Ca) profiles of cores MD09-3246 (black) and GeoB3910-2 (green, Jaeschke et al., 2007) A) on their depth scale, and B) after tuning MD09-3246 to the radiocarbon age of GeoB3910-2. Red circles show the ^{14}C dates of core GeoB3910-2, and the ACPs we selected in MD09-3246 for the tuning (see Table 5.1).

5.4.1 ^{14}C-tuned chronology

For the upper part of the core, we provided a chronology based on the resemblance of our log(Ti/Ca) record to an analog adjacent record, reflecting similar depositional circumstances, whose age model is based on radiocarbon dates. This nearby core is GeoB3910-2, retrieved ~80 km east of MD09-3246. The age model of that core was constructed using twenty AMS radiocarbon (^{14}C) dates (Jaeschke et al., 2007). The log(Ti/Ca) in MD09-3246 resembles the radiocarbon-dated counterpart in core GeoB3910-2, and peaks can be satisfactorily correlated for the last ~ 42 kyr (Fig. 5.4). Therefore 15 out of 20 ^{14}C dates can be transposed onto the MD09-3246 record and used as age control points (ACPs) (Table 5.1). Before 42 thousand years before present (ka) the error associated with the age of core GeoB3910-2 becomes larger, and the matching of peaks is very uncertain. We therefore did not use the two oldest ^{14}C dates. Three other dates (3.8, 6.6 and 16.8 ka) were not used because not associated with events in the records of either GeoB3910-2 nor MD09-3246.

MD09-3246 depth (cm)	Age of ACP ± σ (ka)
1.0	0.165 ± 0.03
60.0	8.9 ± 0.04
69.2	11.02 ± 0.06
105.4	12.46 ± 0.07
125.0	14.55 ± 0.11
135.6	16.1 ± 0.07
163.6	18.3 ± 0.11
195.2	22.8 ± 0.17
203.0	23.4 ± 0.15
212.2	25.7 ± 0.22
244.0	28.6 ± 0.26
271.8	30.2 ± 0.31
276.0	31.5 ± 0.43
289.8	35 ± 0.43
332.0	41.8 ± 1.48

Table 5.1. **^{14}C-tuned chronology**: radiocarbon AMS dates from the record of core GeoB3910-2 (Jaeschke et al., 2007) transferred to core MD09-3246.

5.4.2 Greenland chronology

To provide a chronology for the deeper part of the core, we used the connection between the precipitation shifts in our record and climate shifts from Greenland ice cores. Arz et al. (1998) and Jaeschke et al. (2007) showed correspondence between high terrigenous input to the sediment of the Nordeste margin and the Heinrich stadials in Greenland. By comparing the ^{14}C-tuned section of our record to the $\delta^{18}O$ of the North GRIP ice record (NGRIP, 2004), we verify that this generally applies in the case of core MD09-3246 as well (Fig. 5.5 A-B). Based on this link we proceeded to use cold phases from Greenland to align the high log(Ti/Ca) intervals of MD09-3246 (Fig. 5.5 C-E), and thus obtain a longer chronology for our core. We utilized 15 ACPs from the updated Greenland Ice Core Chronology 2005 (GICC05) of NGRIP (compiled by Svensson et al., 2008), available for the last 60 kyr, and 11 ACPs from the original NGRIP chronology (NGRIP, 2004) for the part 60-123 ka (Table 5.2). Since the timing of the peaks of the cool Greenland intervals is uncertain, we utilized instead the shifts indicating the start and the end of each cold interval, and matched these to sedimentary shifts in our log(Ti/Ca) record. Additionally, we used one ACP from the temperature record from the folded ice core of the North Greenland Eemian Ice Drilling project (NEEM, 2013), to date the log(Ti/Ca) shift around 128 ka.

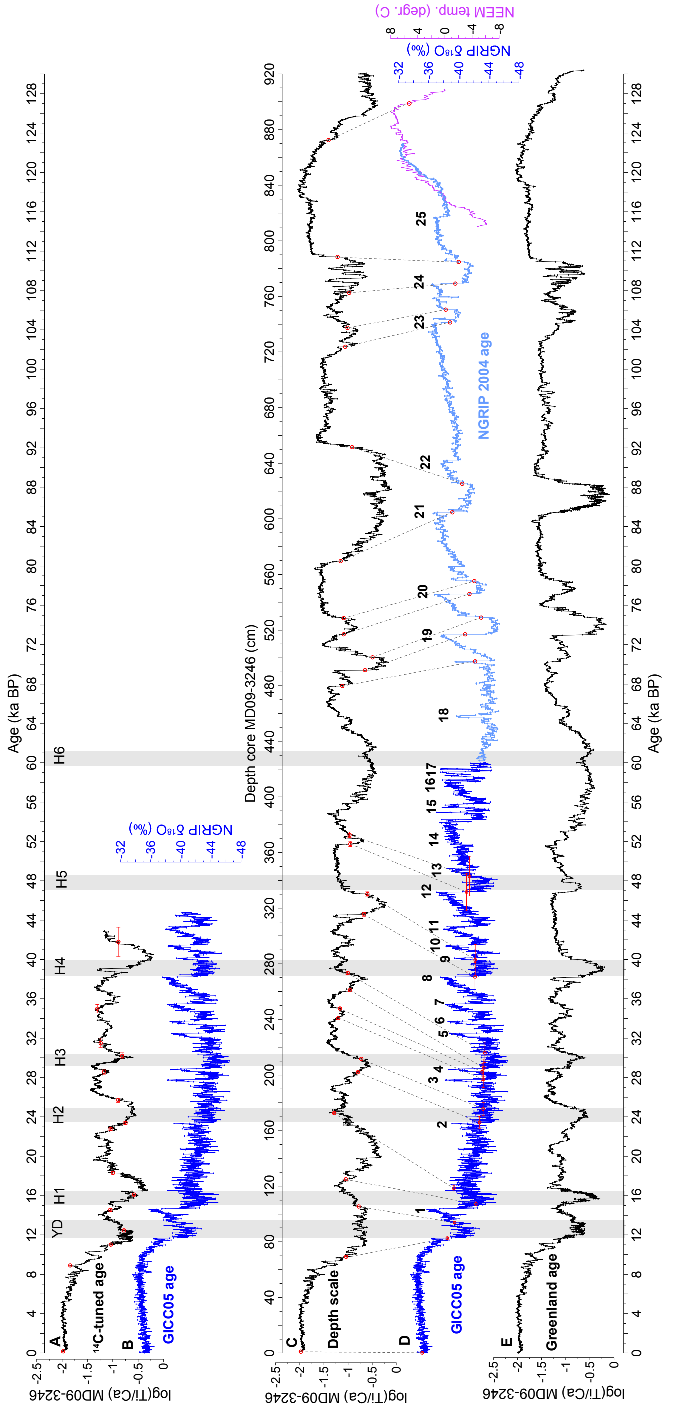

Fig. 5.5. **Greenland chronology**. A) The log(Ti/Ca) of core MD09-3246, on its ^{14}C chronology (with red dots indicating the radiocarbon ACPs), is compared to B) the NGRIP (2004) record on its GICC05 chronology (Svensson et al., 2008). C) log(Ti/Ca) of core MD09-3246 on its depth scale is compared to D) the Greenland record, composed of the NGRIP in its GICC05 and original chronologies, and in the bottom part by the temperature record of NEEM (2013). Red dots indicate the ACPs that we used to obtain the E) Greenland chronology for core MD09-3246 (see Table 5.2).

MD09-3246 depth (cm)	Age of ACP ± σ (ka)	Remark	Reference
1.0	0.02 ± 0.001	Top	Svensson et al. (2008)
69.2	11.68 ± 0.10	End of T-I	Svensson et al. (2008)
105.4	13.26 ± 0.14	Beginning of YD	Svensson et al. (2008)
125.0	15.16 ± 0.19	End of H1	Svensson et al. (2008)
172.6	16.74 ± 0.28	Beginning of H1	Svensson et al. (2008)
202.0	23.44 ± 0.60	Shift	Svensson et al. (2008)
211.6	24.8 ± 0.68	Shift	Svensson et al. (2008)
240.8	27.82 ± 0.84	Shift	Svensson et al. (2008)
247.8	28.58 ± 0.89	Shift	Svensson et al. (2008)
261.0	28.98 ± 0.90	Shift	Svensson et al. (2008)
273.2	30.52 ± 1.00	Shift	Svensson et al. (2008)
315.6	38.24 ± 1.45	Shift	Svensson et al. (2008)
330.2	39.96 ± 1.57	Shift	Svensson et al. (2008)
366.2	46.86 ± 1.91	Shift	Svensson et al. (2008)
372.8	48.44 ± 1.99	Shift	Svensson et al. (2008)
479.8	70.30	Shift	NGRIP (2004)
491.2	73.00	Shift	NGRIP (2004)
500.4	74.75	Shift	NGRIP (2004)
517.0	77.15	Shift	NGRIP (2004)
528.6	78.45	Shift	NGRIP (2004)
569.6	85.45	Shift	NGRIP (2004)
651.6	88.35	Shift	NGRIP (2004)
723.8	104.70	Shift	NGRIP (2004)
737.4	106.05	Shift	NGRIP (2004)
762.6	108.70	Shift	NGRIP (2004)
788.4	110.90	Shift	NGRIP (2004)
872.4	127.00	End of T-II	NEEM (2013)

Table 5.2. **Greenland chronology**: age control points between MD09-3246 log(Ti/Ca) and the Greenland $\delta^{18}O$ (Svensson et al., 2008; NGRIP, 2004) and temperature (NEEM, 2013) records.

5.4.3 LR04 chronology

To obtain a general stratigraphic framework for the part of MD09-3246 older than ~128 ka, we applied a technique frequently used for marine sediment records: we aligned shifts in our foraminiferal $\delta^{18}O$ curve from *G. ruber* to the benthic global LR04 stack of Lisiecki and Raymo (2005). For this we identified and used nineteen ACPs (Fig. 5.6; Table 5.3). This LR04 stratigraphy grants age control over the entire depth of the core, on the orbital-scale, especially at times of prominent $\delta^{18}O$ shift, like glacial terminations.

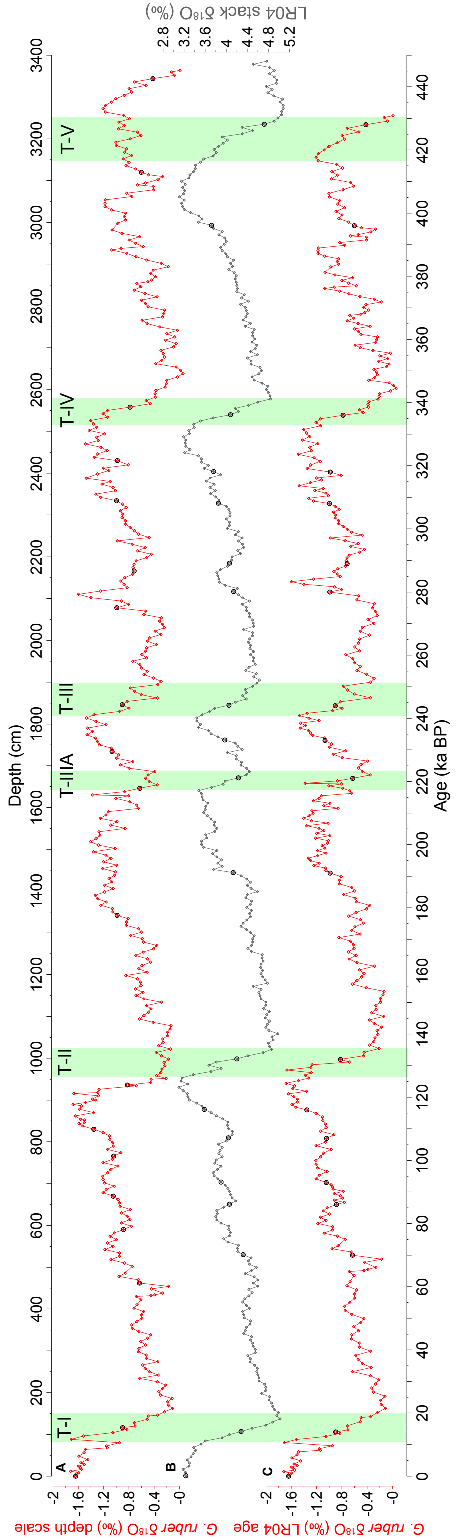

Fig. 5.6. **LR04 chronology**. A) $\delta^{18}O$ of *G. ruber* w. from core MD09-3246 in its depth scale. B) the LR04 $\delta^{18}O$ stack (Lisiecki and Raymo, 2005). C) $\delta^{18}O$ of *G. ruber* w. in its LR04 chronology. Red and grey dots indicate the selected ACPs (see Table 5.3).

MD09-3246 depth (cm)	Age of ACP (ka)	Remarks
0.0	0	Top
116.0	14	T-I
462.0	70	Shift
590.0	86	Shift
670.0	93	Shift
766.0	107	Shift
830.0	116	Shift
936.0	132	T-II
1342.0	191	Shift
1646.0	221	T-IIIA
1734.0	233	Shift
1846.0	244	T-III
2078.0	280	Shift
2166.0	289	Shift
2334.0	308	Shift
2430.0	318	Shift
2558.0	336	T-IV
3120.0	396	Shift
3344.0	428	T-V (uncertain)

Table 5.3. **LR04 chronology**: age control points between MD09-3246 *G. ruber* $\delta^{18}O$ and LR04 stacked $\delta^{18}O$ (Lisiecki and Raymo, 2005).

5.4.4 Speleo chronology

Using the chronologies outlined above, we compare the MD09-3246 record to speleothem climate series of China. By this, we test the persistence of the anti-phasing between the SAM and the EAM, and thus we address one of our research questions. Our approach is based on the outlined assumption, that high northern latitude cool spells imply a southward shift of the ITCZ (Chiang et al., 2003; Chiang and Bitz, 2005, Jaeschke et al., 2007; Toggweiler, 2009), thereby affecting both the EAM and SAM systems (Wang, 2009; Cheng et al., 2012b), and used the record of EAM to provide an absolute chronology for core MD09-3246. In order to do this, we compiled published datasets of speleothem $\delta^{18}O$, from the Sanbao (Wang et al., 2008; Cheng et al., 2009; Cheng et al., 2012c), Hulu (Cheng et al., 2006; Wang et al., 2008), Linzhu (Cheng et al., 2009), and Kesang (Cheng et al., 2012c) caves to obtain a 500 kyr-long continuous record of EAM with the highest possible resolution (Fig. 5.7).

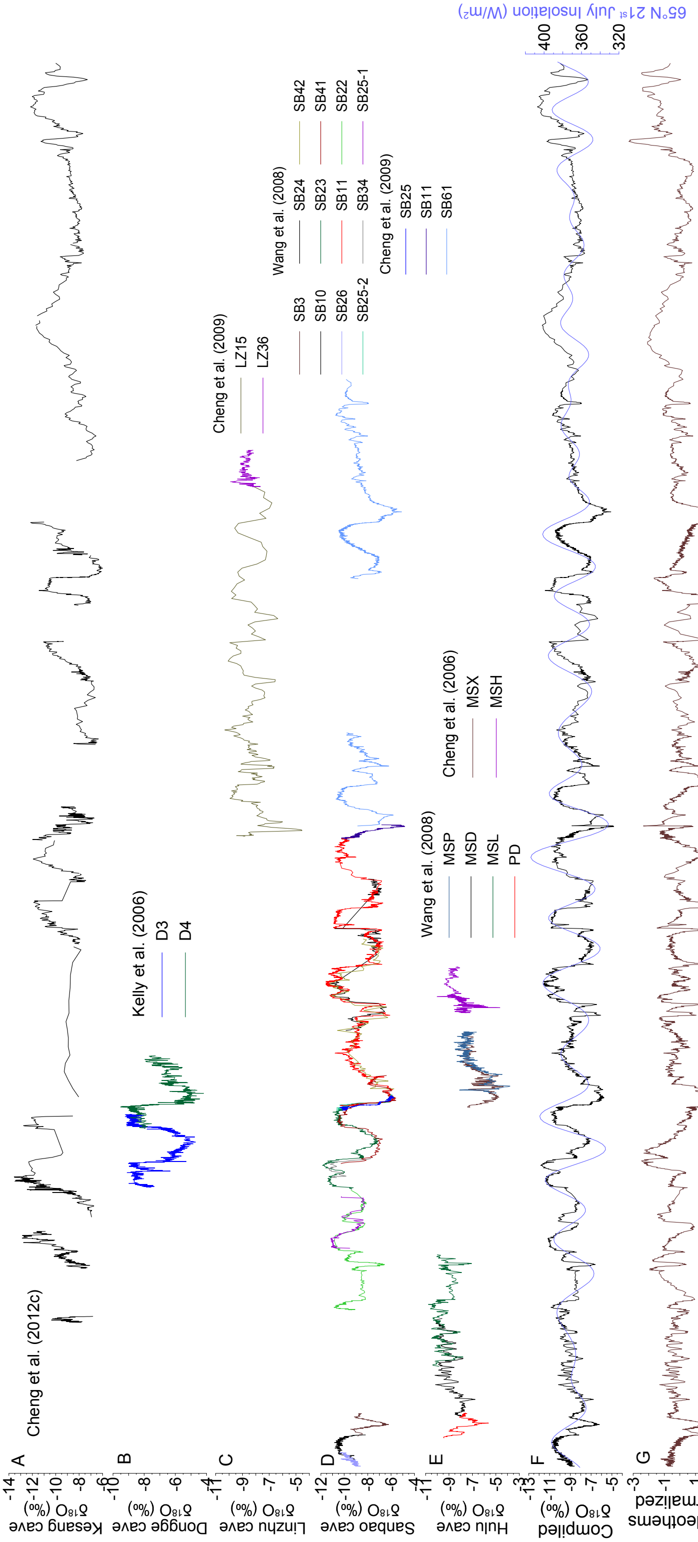

A
B
C
D
E
F
G
Cheng et al. (2012c)
Kelly et al. (2006)
D3
D4
Cheng et al. (2009)
LZ15
LZ36
Wang et al. (2008)
SB3
SB10
SB26
SB25-2
SB24
SB23
SB11
SB34
SB42
SB41
SB22
SB25-1
Cheng et al. (2009)
SB25
SB11
SB61
Wang et al. (2008)
MSP
MSD
MSL
PD
Cheng et al. (2006)
MSX
MSH
Kesang cave δ18O (‰)
Dongge cave δ18O (‰)
Linzhu cave δ18O (‰)
Sanbao cave δ18O (‰)
Hulu cave δ18O (‰)
Compiled δ18O (‰)
Speleothems Normalized
65°N 21st July Insolation (W/m²)
Age (ka BP)

Fig. 5.7 (previous page). **Compilation of Chinese speleothems**. A) to E) Published series of speleothem oxygen isotopes are shown, from different caves in the region of EAM (references are reported in the figure). F) Our continuous 500-kyr compilation of the records with highest available resolution, along with summer insolation at 65° N (Laskar et al., 2004). G) The EAM series normalized for the insolation component (see section 5.4.4).

Because we intended to locate the timing of events when the EAM responded to high latitude NH cold phases, we need to highlight the variability of the EAM record attributable to this type of forcing, as opposed to the variability ascribable to orbital forcing (Wang et al., 2008). For this, we ridded the EAM record of its strong insolation component, i.e. 21st of July at 65° N, a procedure previously proposed by Barker et al. (2011). A further reason for normalizing the EAM with respect to insolation is that it contains an insolation component of substantially different latitude from the record of SAM that we present from core MD09-3246, which would thus confound the comparison. More in detail, whereas paleo records of SAM appear sensitive to Southern Hemisphere insolation at their specific latitude (e.g., Wang et al., 2004; Cruz et al., 2005) (Fig. 5.13 G), those of EAM represent the composite effects of precipitation sources that vary with NH summer insolation (see the conceptual model of Ziegler et al. [2010b]), apparently with a time lag (e.g., Clemens et al., 2010; Cheng et al., 2012b).

For both the speleothem $\delta^{18}O$ and the insolation series, we subtracted from each datum the mean value of the series, and divided it by the series' standard deviation. We then subtracted the normalized values of insolation from the coeval speleothem counterpart (Fig. 5.7). By plotting our log(Ti/Ca) record on its Greenland chronology along with the normalized EAM speleothem series (Fig. 5.8 B-C), we compare peaks in terrigenous sediment with peaks of speleothem $\delta^{18}O$, which are indicative of weak EAM intensity. Out of the 20 weak EAM events that we recognize in the EAM series during the last 130 kyr, 17 are mirrored in our record. In particular, the six Heinrich stadials of the last glacial correspond to weak EAM (Wang et al., 2001), and to strong SAM from our record. For the older part of MD09-3246, based on the general stratigraphic structure provided by the LR04 chronology (Fig. 5.9), we are able to relate the periods of most pronounced terrigenous input off NE Brazil with the weak Asian monsoon intervals (WMI) that characterize terminations (Cheng et al., 2009). Moreover, a connection is apparent at the millennial scale during the four preceding glacial and interglacial periods. This comparison strongly suggests that, throughout the examined interval, the two records were in anti-phase.

Based on this finding, we construct a chronology for core MD09-3246 tuned to the speleothem climate series of China. This will allow for independent comparison with insolation, and with other absolutely-dated speleothems records of precipitations in the South America continent.
We therefore selected a total of 51 ACPs by identifying the major shifts and peaks in both our log(Ti/Ca) record and in the speleothem one (Fig. 5.9 and 5.14 D; Table 5.4). Since the speleothem series does not display a clear isotopic enrichment for T-V, as for the younger terminations, we decided to recur to the synthetic reconstruction

of Greenland climate (Barker et al., 2011) to anchor the bottom part of our record. We therefore assigned the last ACP to a shift to lower log(Ti/Ca) values that we deem coeval with the end of T-V (Fig. 5.14 B and D). We underline anyway that the uncertainty connected with this last ACP is large.

The solidity of the Speleo chronology for MD09-3246 is corroborated by the notation that periods of high Ti input correspond to the highest sedimentation rate, as expected given increased terrigenous loading.

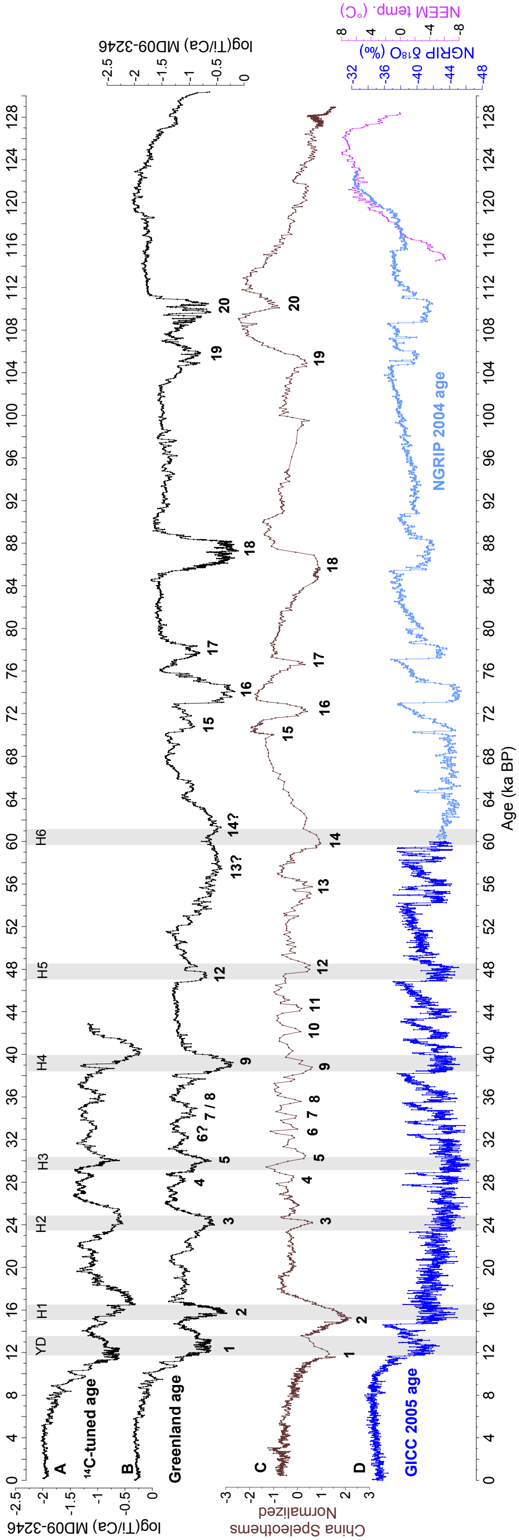

Fig. 5.8. **Construction of the Speleo chronology (upper part of the core).** Comparison of the log(Ti/Ca) of MD09-3246 on its A) ^{14}C and B) Greenland chronologies with C) the normalized records of Chinese speleothems. D) Records of Greenland climate are also shown to locate the Heinrich stadials (NGRIP, 2004; Svensson et al., 2008; NEEM, 2013). Numbers indicate the correspondence of wet events in core MD09-3246 with dry ones in the Chinese speleothems.

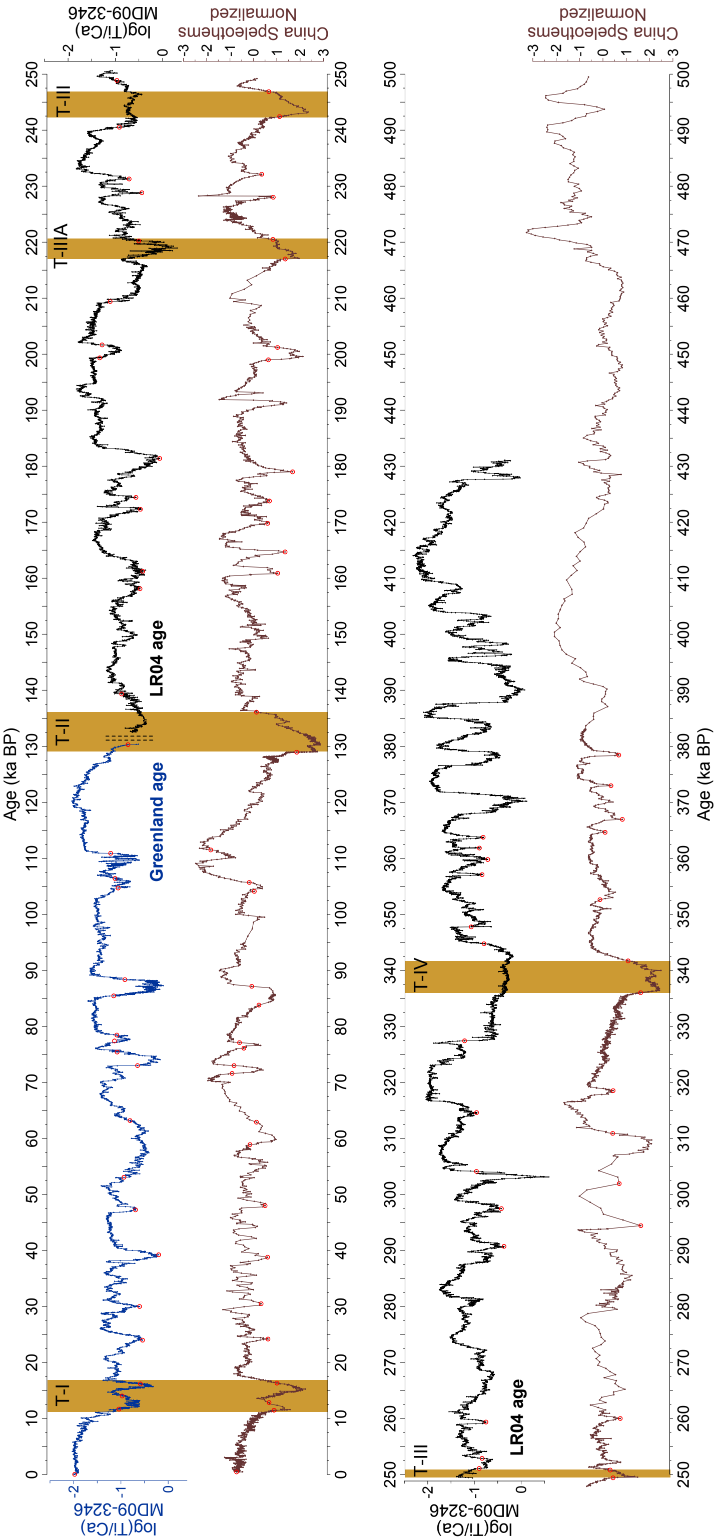
Age (ka BP)
log(Ti/Ca) MD09-3246
China Speleothems Normalized
Greenland age
LR04 age
T-I
T-II
T-IIIA
T-III
T-IV

Fig. 5.9 (previous page). **Construction of the Speleothem chronology (lower part of the core)**. Comparison of the log(Ti/Ca) of MD09-3246 on its Greenland (blue) and LR04 (black) chronologies, to the normalized records of Chinese speleothems (brown). Red dots indicate the ACPs selected for the tuning (see Table 5.4).

MD09-3246 depth (cm)	Age of ACP (ka)	Remarks	Speleothem and reference
1.0	0.46	Top	SB26 Wang et al. (2008)
69.2	11.5	End of Younger Dryas	SB10 Wang et al. (2008)
113.2	12.9	Beginning Younger Dryas	SB3 Wang et al. (2008)
155.6	16.3	Beginning Older Dryas	SB3 Wang et al. (2008)
205.8	24.2	Peak	MSD Wang et al. (2008)
269.0	30.5	Peak	MSD Wang et al. (2008)
324.0	38.8	Peak	MSD Wang et al. (2008)
367.8	48.0	Peak	MSD Wang et al. (2008)
395.4	58.9	Shift	SB22 Wang et al. (2008)
445.0	62.9	Shift	SB22 Wang et al. (2008)
491.2	71.6	Shift	SB22 Wang et al. (2008)
505.0	73.0	Shift	SB22 Wang et al. (2008)
519.2	76.1	Shift	SB22 Wang et al. (2008)
528.6	77.1	Shift	SB22 Wang et al. (2008)
569.6	83.8	Shift	SB25-1 Wang et al. (2008)
651.6	87.2	Shift	SB22 Wang et al. (2008)
723.8	104.1	Shift (uncertain)	SB23 Wang et al. (2008)
740.8	105.7	Shift (uncertain)	SB23 Wang et al. (2008)
788.4	111.5	Shift	SB23 Wang et al. (2008)
889.6	129.0	End of T-II	SB25 Cheng et al. (2009)
977.8	136.1	Beginning of T-II	SB11 Wang et al. (2008)
1110.2	160.9	Shift	SB11 Wang et al. (2008)
1132.2	164.7	Shift	SB11 Wang et al. (2008)
1210.2	169.8	Shift	SB11 Wang et al. (2008)
1225.2	173.8	Shift	SB11 Wang et al. (2008)
1274.2	179.0	Shift	SB11 Wang et al. (2008)
1426.6	199.0	Shift (uncertain)	SB11 Wang et al. (2008)
1450.0	201.2	Shift (uncertain)	SB11 Wang et al. (2008)
1528.4	217.0	End of T-IIIA	SB11 Wang et al. (2008)
1637.8	220.6	Beginning of T-IIIA	SB11 Wang et al. (2008)

1703.4	228.0	Shift	SB11 Cheng et al. (2009)
1728.2	232.3	Shift	SB61 Cheng et al. (2009)
1810.6	242.3	End of second part of T-III	SB61 Cheng et al. (2009)
1877.4	246.9	Beginning of second part of T-III	SB61 Cheng et al. (2009)
1891.6	249.4	End of first part of T-III	SB61 Cheng et al. (2009)
1903.2	250.8	Beginning of first part of T-III	SB61 Cheng et al. (2009)
1942.8	259.7	Shift	SB61 Cheng et al. (2009)
1947.8	260.4	Shift	SB61 Cheng et al. (2009)
2078.6	278.7	Shift	LZ15 Cheng et al. (2009)
2092.4	281.0	Shift	LZ15 Cheng et al. (2009)
2240.8	294.4	Peak	LZ15 Cheng et al. (2009)
2290.8	301.9	Peak	LZ15 Cheng et al. (2009)
2391.2	317.8	Shift	SB61 Cheng et al. (2009)
2411.8	318.9	Shift	SB61 Cheng et al. (2009)
2497.0	336.0	End T-IV	SB61 Cheng et al. (2009)
2640.0	341.7	Beginning T-IV	SB61 Cheng et al. (2009)
2668.2	352.4	Shift (uncertain)	SB61 Cheng et al. (2009)
2755.6	364.6	Peak (uncertain)	SB61 Cheng et al. (2009)
2780.8	367.0	Peak (uncertain)	SB61 Cheng et al. (2009)
2800.0	373.0	Peak (uncertain)	SB61 Cheng et al. (2009)
2818.0	378.4	Peak (uncertain)	SB61 Cheng et al. (2009)
3341.6	424.9	End of T-V (uncertain)	Greenland synth. Barker et al. (2011)

Table 5.4. **Speleo chronology**: age control points between MD09-3246 log(Ti/Ca) and the compiled Chinese speleothems, normalized for their insolation component (see section 5.4.4).

5.4.5 Comparisons and considerations on the proposed chronologies

The ^{14}C-tuned chronology provides an independent basis from which to compare the changes in the terrigenous input to core MD09-3246. Comparison with Greenland climate (Fig. 5.5 A-B) shows general agreement between peaks of high precipitation at the Brazilian margin and Greenland cold phases. Some discrepancies are nevertheless evident, namely for H1 and H4, which we believe are attributable to the limited number of ^{14}C dates available from core GeoB3910-2. Based on the existing connection between Greenland and Nordeste paleoclimates (Arz et al., 1998; Jaeschke et al., 2007) we aligned high log(Ti/Ca) in MD09-3246 with Greenland cold spells (Fig. 5.5 C-E). All Heinrich stadials appear to clearly have a counterpart in our record. Uncertainty, however, persists regarding H6, which might correspond to the high log(Ti/Ca) interval between 400 and 440 cm in MD09-3246. The variability contained in the NGRIP record before 60 ka (NGRIP, 2004) is substantially different from the later (glacial) period: the rapid succession of the Dansgaard-Oeschger cycles is replaced by a lower frequency of changes in the older part of the record (Fig. 5.5 D). Such older cool intervals appear nevertheless to be captured by the Brazil climate record from MD09-3246. Lastly, the oldest part of the Greenland chronology, even though the assignment of the ACP from the record of NEEM (2013) is somewhat ambiguous, shows that the marked temperature increase at the beginning of the Eemian period of North Atlantic climate emerges from the Brazil record as a shift to lower terrigenous input.

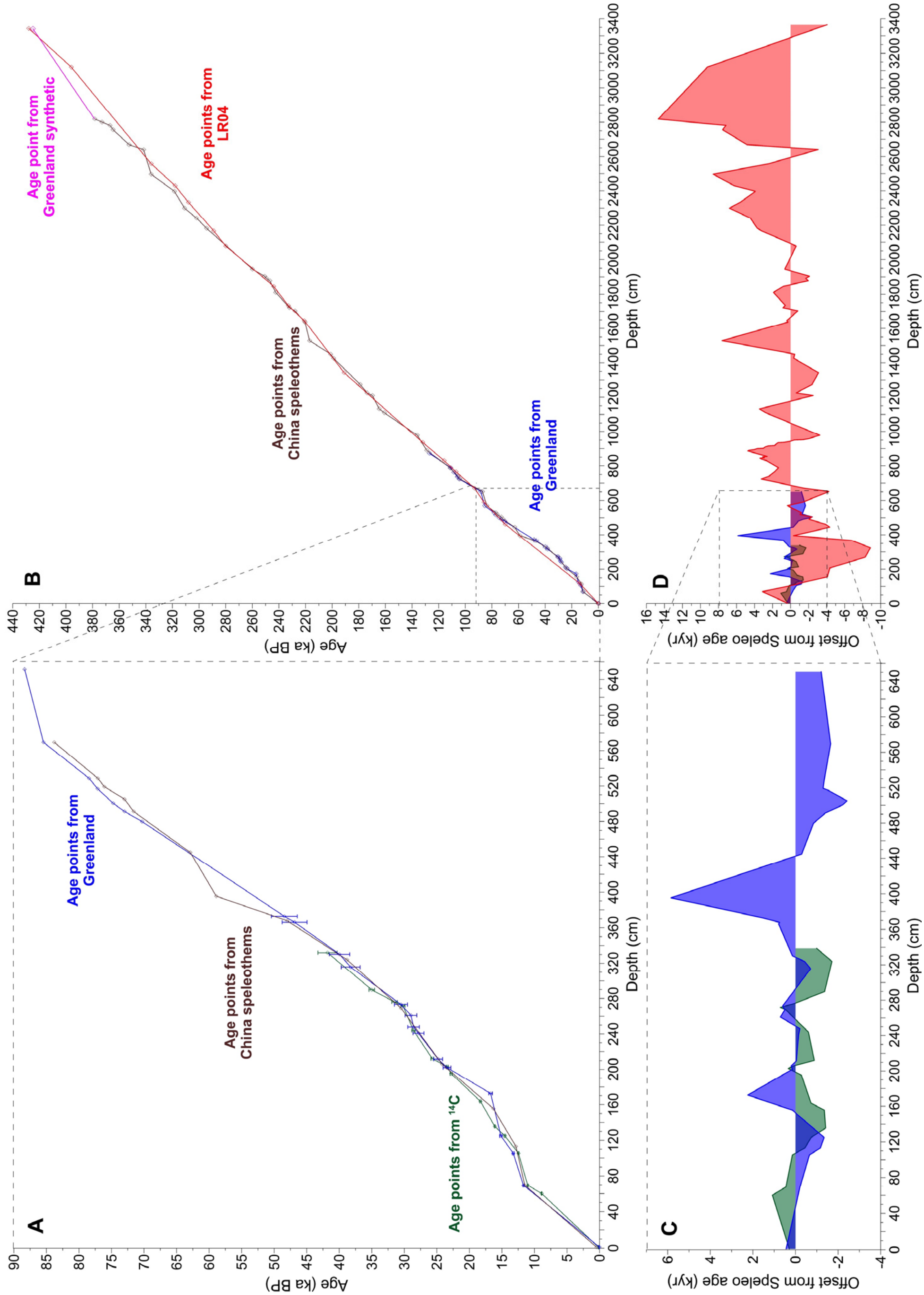

Fig. 5.10. **Comparison of chronologies for core MD09-3246**. ACPs for the four chronologies are reported in depth-age plots (Fig. 11A-B), along with the offsets of the ^{14}C-tuned, the Greenland and the LR04 chronologies with respect to the Speleo one, that we chose to adopt for the Discussion part (Fig. 11C-D).

To examine the differences between the proposed chronologies, we report the ACPs in depth-age plots (Fig. 5.10 A-B), along with the offsets of each chronology with respect to the Speleo one (Fig. 5.10 C-D). The maximum offset between the ^{14}C-tuned and the Speleo chronologies reaches ~1.5 kyr, when the ^{14}C-tuned chronology does not seem to assign a reliable age to the high log(Ti/Ca) that likely corresponds to H1. Comparing the Greenland and Speleo chronologies, a notable discrepancy emerges around 60 ka. At that point, the resemblance of a peak in our record to a δ^{18}O enrichment in the EAM allowed us to assign two ACPs on the Speleo chonology for the interval corresponding to H6 (Fig. 5.8 B-C). This was not possible for the Greenland chronology (Fig. 5.5 C-D). Finally, the largest disagreements are observed when comparing the Speleo and the LR04 chronologies (Fig. 5.10 B and D). Down to a depth of 6 m the Speleo chronology results in younger ages compared to the LR04, which is mostly attributable to the smaller number of shifts available in the curves to be used as ACPs for the LR04 chronology (Fig. 5.6). We will examine some implications of these differences in the section 5.5.5.

Our exploration of the possibilities regarding the chronology of core MD09-3246 suggests that at the orbital time scale all strategies agree on the age assignment, and that at the millennial scale the connection to the Chinese speleothems seems solid. Therefore, for the Discussion we will adopt the Speleo chronology, for three reasons: I) it assigns ages to the whole core; II) it grants independence and compatibility of approach in the comparison with other speleothem records of SAM from the continent; III) we deem the composite record of EAM the most accurately dated climatic record available at these time scales, because of the tight constrains of its ^{230}Th dates (e.g., Wang et al., 2008; Cheng et al., 2009).

5.5 Discussion

5.5.1 Similarity of surface records of *Globigerinoides ruber* white and pink

A difference in the habitat and temperature preference for these two morphotypes has been repeatedly assessed (Williams et al., 1981; Rohling et al., 2004; Numberger et al., 2009). The offset extracted from core MD09-3246 (Fig. 5.16), though a modest one, can be a result of morphotype-specific "vital effects" (e.g., Rohling et al., 2004), or of a difference in the season of growth of the two morphotypes. Alternatively, it may suggest that *G. ruber* pink must have calcified in slightly colder waters, which would challenge the consolidated notion that it dwells in waters shallower and/or warmer than the white variety (Williams et al., 1981; Rohling et al., 2004; Numberger et al., 2009).

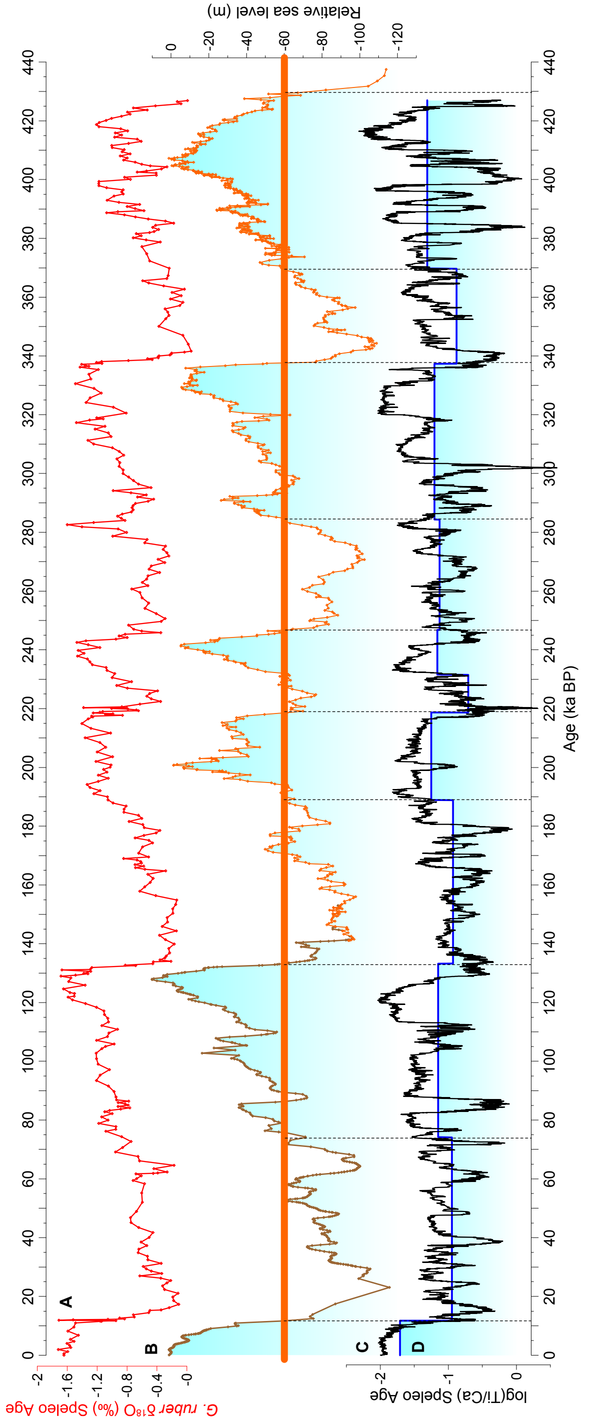

Fig. 5.11. **Evaluation of the effect of sea level fluctuations on the log(Ti/Ca) of core MD09-3246**. A) The $\delta^{18}O$ of *G. ruber* w. is plotted for stratigraphic reference. B) Relative sea level reconstructions (orange: Rohling et al., 2009; brown: Grant et al., 2012). The orange line indicates the relative sea level at which the continental shelf was flooded and exposed when sea level rose and fell, respectively. C) log(Ti/Ca) profile. D) Averaged log(Ti/Ca) values for the segments of the MD09-3246 record defined by shifts between flooded and exposed continental shelf.

5.5.2 Impact of sea level on the terrigenous input off the continental shelf

Sea level fluctuations, and the consequent marked variations in the distance between the core and the shoreline, constitute a potential source for the variability in the Ti/Ca record (Arz et al., 1999b), that we intend to use here as a proxy for terrestrial runoff / precipitation.
The edge of the continental shelf of this region is approximately 50 km wide, and about ~60 m deep (Ponte and Asmus, 1978), and core MD09-3246 is retrieved only about 20 km offshore from it. One can therefore hypothesize that relatively small changes in the proximity of the coast, and of the source of terrigenous input, play an important role for the sedimentological record of our core. Glacial-interglacial sea level variations indeed change the proximity of the coast relative to the core site, and thus have the potential to affect the run-off proxy. Specifically, in episodes in which sea level lowers to the point of exposing the shelf, larger amounts of sediment are more readily available to the core site. To test this hypothesis, we plotted the most recent sea level reconstructions (Rohling et al., 2009; Grant et al., 2012) along our sedimentation series (Fig. 5.11). By doing so, we can subdivide the record in intervals of high-sea-level-stand (when sea level was higher than 60 m below present) and low-sea-level-stand (lower than 60 m below present), corresponding to situations when the location was farther and closer to the shoreline, respectively. The average log(Ti/Ca) values (Fig. 5.11 D) suggest that indeed terrigenous input is higher during low sea level stand. This is opposite to what is observed on the other side of the continent, off Ecuador, where Rincón-Martínez et al. (2010) found higher sedimentation during interglacials. This is due to the fact that their record is of a more pelagic nature, and therefore less susceptible to glacial-interglacial variations in sea level, and to its location at the northern side of the ITCZ, thus receiving more humidity from the continent at times when core MD09-3246 registers a drier Nordeste, corresponding to a more northerly position of the rain belt. The latter mechanism likely explains the anti-phasing with another pelagic site, at the Ceara Rise, ~1000 km northeast from our core, where Rühlemann et al. (2001) showed that the northern part of Brazil was more arid during glacial times. Another study from the Ceará Rise (Rühlemann et al., 1996) reports higher productivity during warm substages. Higher interglacial marine productivity would counteract the effect of sea level changes in our log(Ti/Ca) signal: more carbonate-rich pelagic precipitation, during high-stand/warm phases, and conversely during low-stand/cold phases. We conclude that variations in productivity as those observed by Rühlemann et al. (1996) are either not valid for our record, or are masked by the stronger effect of varying terrigenous input.

Even though sea level seems to have an influence on log(Ti/Ca) absolute values, we have ascertained, on the basis of sea level change reconstructions, that it does not noticeably alter the timing and structure of the prominent shifts in our record. We thus interpret such shifts as reflecting mostly the variations in the precipitation regime on the adjacent NE Brazil continent, as was suggested by Arz et al. (1999b).

5.5.3 Millennial scale variability and continental comparison

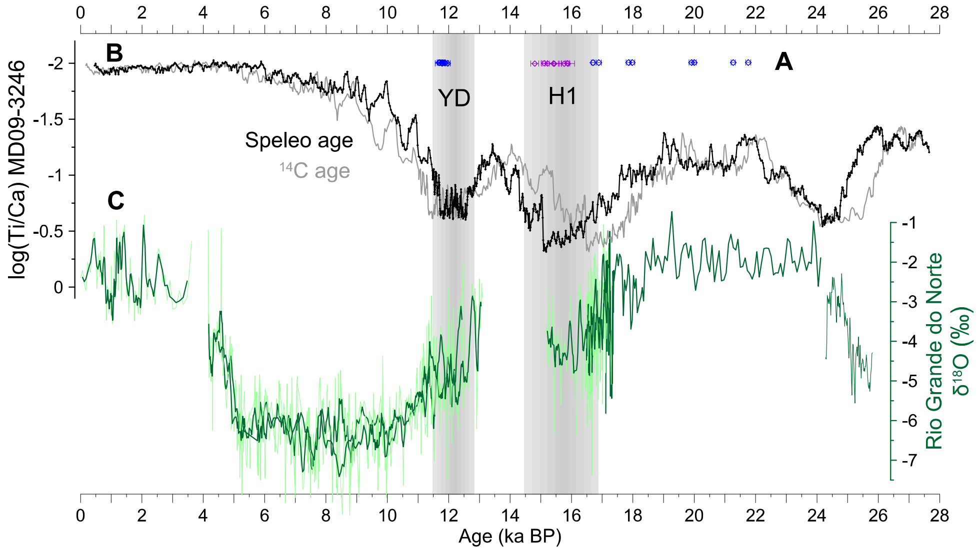

Fig. 5.12. **Regional comparison for the last climatic transition**. A) Speleothem and travertine growth periods from the Nordeste caves Lapa dos Brejoes and Toca da Barriguda (10° 10' S, 40° 50' W) (Wang et al., 2004); B) MD09-3246 log(Ti/Ca); C) Speleothem record from Rio Grande do Norte region (5° 36' S, 37° 44' W) (Cruz et al., 2009a).

The MD09-3246 continental precipitation series generally matches other proximal marine-based reconstructions of the last glacial to interglacial transition (Arz et al., 1998; Behling et al., 2000; Jaeschke et al., 2007). With respect to the regional terrestrial domain, we compare our precipitation record with the absolutely dated speleothems in the adjacent Rio Grande do Norte region, spanning the past ~25 kyr (Cruz et al., 2009a) (Fig. 5.1 and 5.12). After an interval of dissimilar trends around 26-23 ka, patterns become coherent during 22-15 ka: around the last glacial maximum values were stable for both series; then, entering the H1 interval, our terrigenous sediment loading increased, corresponding to a decrease in the speleothems $\delta^{18}O$, both pointing at increased precipitation. We underline that the resemblance is stronger for our record in its Speleo chronology than in the ^{14}C one, suggesting that in this period the former chronology could be more accurate. An almost-inverse pattern emerged during the Holocene, after 11 ka, when light speleothem $\delta^{18}O$ indicated wetter conditions until about 5 ka, whereas our log(Ti/Ca) decreased, pointing at aridification of the Nordeste. Given the close proximity of the two records, an explanation to reconcile the marked difference in Holocene precipitation regime is not straightforward. A qualitative record of rainfall intensity is available from the northern Bahia region (Wang et al., 2004), ~5° south of the Rio Grande do Norte speleothems (Fig. 5.12 A). The growth phases of speleothems and travertines from that record around 15-16 and ~12 ka, indicating more precipitation, seem to match with the peaks in terrigenous sediment from our marine record, and with low $\delta^{18}O$ from the Rio Grande do Norte. On the other hand, the absence of speleothem deposition in northern Bahia during the Holocene, and the low terrigenous input to marine cores nearby MD09-3246 (Arz et al., 1998; Jaeschke et al., 2007) are in contraddiction, as our record, with the highest precipitation recorded at Rio Grande do Norte from 11 to 5 ka. Further, speleothem (van Breukelen et al., 2008) and modeling (Aerts et al., 2006) studies have suggested lower precipitation in the Amazon basin for the early and middle Holocene, consistently with the pattern emerging from our record.

The Speleo chronology of MD09-3246 does not allow the discussion of phasing with changes in other SAM records, because it is not independent from the assumption of inter-hemispheric connection of monsoon systems, due to common forcing by NH cold climate (see section 5.4.4). Nonetheless, we are able to examine the presence/absence and intensity of the response to such forcing in the frame of existing records from of SAM.

Fig. 5.13 (next page). **Comparison of MD09-3246 log(Ti/Ca) with regional and distal records for the last 100 kyr**. A) Isotopic record from NGRIP (2004) ice core, reflecting Greenland climate. B) Record of precipitation from the Cariaco Basin core ODP 1002 (Peterson et al., 2000). C) log(Ti/Ca) from our core MD09-3246. Records of South American summer monsoon, from north to south: D) Santiago cave (3° 1' S, 78° 8' W) (Mosblech et al., 2012); E) Diamante and El Condor caves (~5° 50' S, 77° 25' W) (Cheng et al., 2013); F) Pacupahuain cave (11° 15' S, 75° 48' S) (Kanner et al., 2012); G) Botuverà cave (27° 13' S, 49° 9' W) (Cruz et al., 2005). H) Compilation of Chinese speleothem records, normalized, indicating East Asian monsoon intensity (see section 5.4.4 and Fig. 5.7 for details and references). Arrows indicate for each record the direction of increased precipitation. Blue bars are Heinrich stadials, as defined by the GICC2005 chronology of NGRIP, and grey bars indicate additional intervals of weak EAM (H). All such intervals have a cold counterpart in the Greenland (B), though with evident mismatches in the older part, and most of them are variably reflected in records of SAM (B to G).

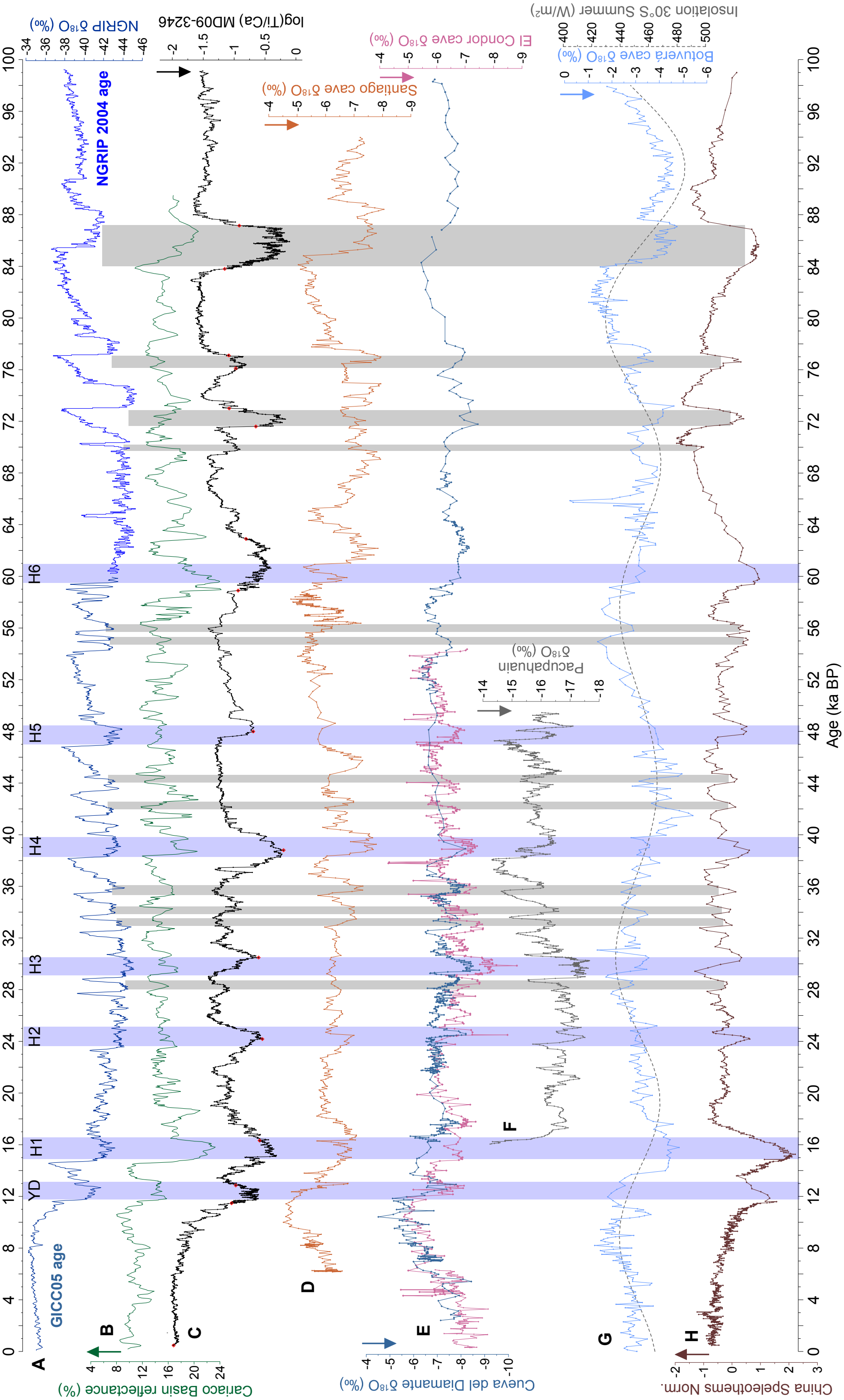

NGRIP δ18O (‰)
NGRIP 2004 age
GICC05 age
log(Ti/Ca) MD09-3246
Santiago cave δ18O (‰)
El Condor cave δ18O (‰)
Botuverá cave δ18O (‰)
Insolation 30°S Summer (W/m²)
Pacupahuain δ18O (‰)
Cariaco Basin reflectance (%)
Cueva del Diamante δ18O (‰)
China Speleothems Norm.
Age (ka BP)
A
B
C
D
E
F
G
H
YD
H1
H2
H3
H4
H5
H6

Heinrich stadials, and shorter NH cold phases, were shown to be strictly coupled with weak EAM conditions (e.g., Wang et al., 2001) (Fig. 5.13 A and H). They are also reflected in South American precipitation records (Fig. 5.13 B to G). They dictate dry climate on the north side of the ITCZ, as evident from the record of the Cariaco Basin (Peterson et al., 2000). Also, they imply wetter conditions upon the southern side of the ITCZ: in western Amazonia (Mosblech et al., 2012; Cheng et al., 2013), the Peruvian Andes (Kanner et al., 2012), and the Nordeste (our record), although with different intensity. Such divergence in monsoon intensity emerging from records at similar latitude is likely the result of changes in the Walker circulation (Cheng et al., 2012b), which are superimposed on meridional movements of the Hadley circulation and the ITCZ. We speculate that the Walker circulation might have been affected by alterations in conditions peripheral to the SAM, i.e., by changes in the AMOC, and attendant interhemispheric redistribution of heat, or in El Niño activity, or in insolation. In other words, the position of the ITCZ, at the millennial time scale, might have varied not only meridionally, but also zonally (Vizy et al., 2007; Cruz et al., 2009a; Cheng et al., 2013).

On the other hand, precipitation records from southern Brazil appear to clearly follow local (30° S) summer insolation changes (Cruz et al., 2005; Wang et al., 2006; Cruz et al., 2007; Wang et al., 2007) (e.g., Fig. 5.13 G), only minorly reflecting NH variability (Wang et al., 2006). Our record, and partially those from Rio Grande do Norte (Cruz et al., 2009a), Santiago (Mosblech et al., 2012) and Pacupahuan (Kanner et al., 2012), indicate that the response of the Nordeste to NH cold phases was more accentuated, as compared to that of southern Brazil. The explanation behind these differential expressions of the SAM likely resides in the trajectory of the low-level jet over the continent (Fig. 5.1). When cold NH climate resulted in a southern shift of the ITCZ, a mechanism applied likely similar to what occurs during Austral summer. Humidity, advected from the tropical Atlantic westwards over Brazil, was deflected by Andean orography to the southeast and to the Atlantic forest (e.g., Cheng et al., 2012b): fractionation of oxygen isotopes, intercurring between oceanic evaporation and rainfall over southern Brazil caves probably resulted in a local dilution of the isotopic signature characteristic of periods of strong NH-forced SAM.

5.5.4 Orbital scale variability: Interhemispheric connection of monsoon shifts during the last four glacial cycles

The continental precipitation series contained in core MD09-3246 displays a direct relationship to Southern Hemisphere autumn insolation at 5° S (Fig. 5.14). A response to insolation at the respective latitude is evident in most records of the SAM (Wang et al., 2004; Cruz et al., 2005; Wang et al., 2007; Mosblech et al., 2012) and is explored and validated by transient model simulations (Kutzbach et al., 2008; Li et al., 2013). Higher insolation entails increased land warming, and therefore higher thermal contrast with the adjacent ocean. As it was hypothesized by Wang et al., (2004), when insolation is maximal at the latitudes of the Nordeste, stronger lows would persist over the northern Brazil continent, implying a southern shift of the ITCZ, and more

Atlantic moisture to be drawn to the continent. The connection with regional insolation holds throughout the record, but is less clear during the last glacial period, and beyond ~355 ka. We propose that this diminished forcing by insolation in our record is due to the lower amplitude of precessional cycles in those intervals (Berger, 1978). We also suggest that a variable response to insolation across glacial-interglacial cycles can in general be expected, since recent transient modelling shows that monsoon systems, while primarily responding to insolation, also display sensibility to the amount of ice sheets and of greenhouse gases (Weber and Tuenter, 2011).

Superimposed on the insolation cycles are the marked wet conditions over the Nordeste during each of the represented glacial terminations (Fig. 5.14). As mentioned, these coincide with weak EAM intervals. The current understanding is that during deglaciations, when large discharge of icebergs in the North Atlantic took place (testified by the ice rafted debris record of McManus et al. [1999]), the AMOC weakened or even collapsed (McManus et al., 2004; Denton et al., 2010). Those changes reverberated to the tropical latitudes, transmitted by rearrangements of atmospheric circulation (Chiang et al., 2003; Chiang and Bitz, 2005; Cheng et al., 2009; Toggweiler, 2009). Both the Hadley cells and the ITCZ shifted southwards, and as a consequence, the distribution of rainfall over tropical latitudes was altered. This emerges from the records of EAM for the last four terminations, and from the severe droughts in northern Borneo speleothems during T-V, T-IV, T-III, T-IIIA and T-I (Meckler et al., 2012). Wang et al. (2004) qualitatively indicated increased rainfall over the Nordeste region of Brazil for T-II and T-I, when a more southern position of the ITCZ carried Atlantic humidity more effectively over the Nordeste. Our new record supports these results, and presents evidence of strong precipitation also for T-IV and T-III, arguing for the validity of the mechanism for the four last terminations.

Further, we show that this pattern is well defined also for the climate shift from MIS 7d to 7c (T-IIIA), when SAM intensification seems greater than for T-III. This agrees with the records of EAM from China and from Borneo, in which T-IIIA emerges as a prominent dry period, similar to any termination strictly defined (Cheng et al., 2009; Meckler et al., 2012). This sustains the climatic relevance that some authors have recently recognized to what can be regarded as the second part of T-III (e.g., Huybers, 2011). Besides, the large amplitude of the obliquity cycle that accompanies the T-IIIA transition highlights the importance of this orbital forcing component for the climatic record (e.g., Huybers and Wunsch, 2005; Huybers, 2007; Drysdale et al., 2009). Notably, the pulse of ice-rafted debris that settled on the North Atlantic sea floor is only minor during this pseudo-termination (McManus et al., 1999) (Fig. 5.14 A). A reason for that could be that the NH ice sheets were likely less developed during MIS 7d, compared to the glacial periods. Nevertheless, the clear cold spell revealed by Martrat et al. (2007) from the Iberian Margin sea surface suggests that it was indeed a forcing from the NH that determined a T-IIIA shift in the ITCZ over the tropics, as emerging from our record, and from that of EAM (Cheng et al., 2009).

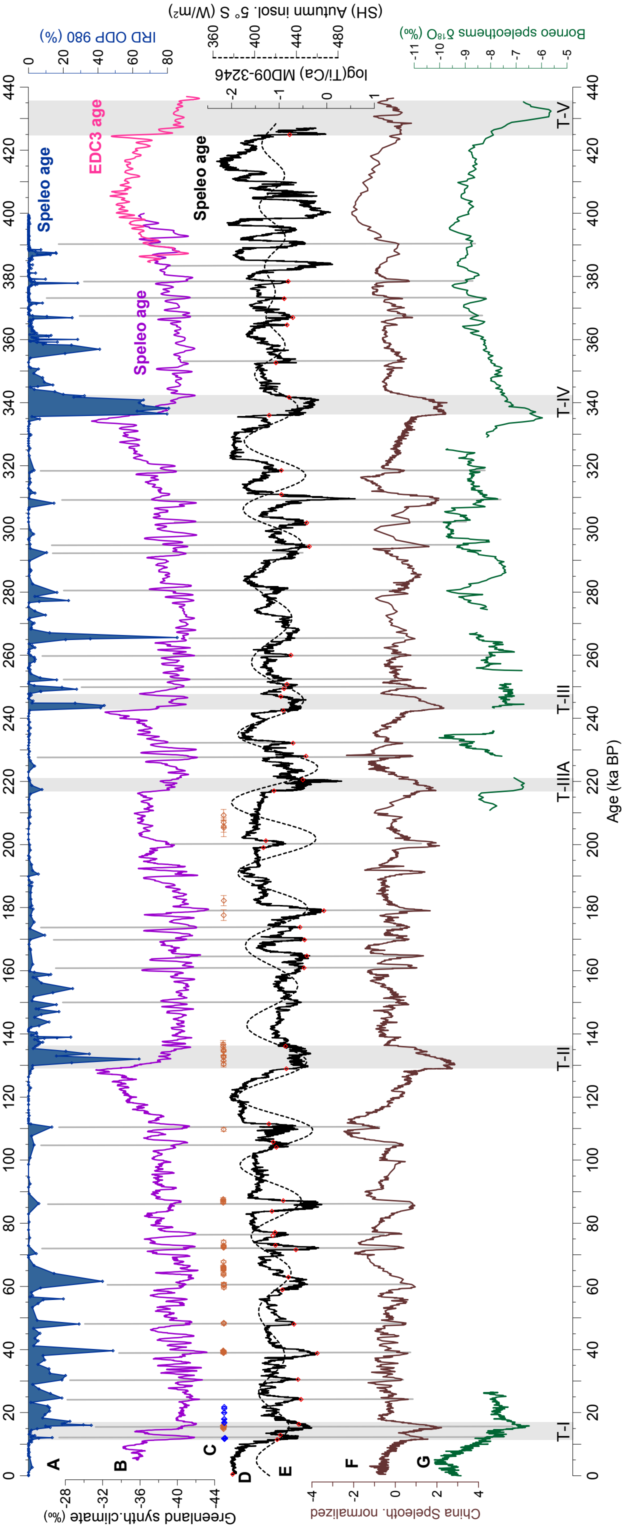
IRD ODP 980 (%)
Greenland synth.climate (‰)
China Speleoth. normalized
log(Ti/Ca) MD09-3246
(SH) Autumn insol. 5° S (W/m²)
Borneo speleothems δ18O (‰)
Age (ka BP)
Speleo age
EDC3 age
Speleo age
Speleo age
A
B
C
D
E
F
G
T-I
T-II
T-IIIA
T-III
T-IV
T-V

Fig. 5.14 (previous page). **Comparison of MD09-3246 log(Ti/Ca) with regional and distal records for the last 420 kyr**. A) Ice rafted debris record from North Atlantic core ODP 980 (McManus et al., 1999). B) Greenland synthetic climate record (Barker et al., 2011). C) Speleothem and travertine growth periods from the Nordeste caves (Wang et al., 2004). D) log(Ti/Ca) from our core MD09-3246. E) Autumn insolation (21st March till 21st of June) at 5° S (Laskar et al., 2004). F) Compilation of Chinese speleothems, normalized (see section 5.4.4 and Fig. 5.7 for details and references). G) Speleothems from northern Borneo (Meckler et al., 2012). Grey bars indicate glacial terminations. Grey lines emphasize evens that are present in both our SAM (core MD09-3246) and in the EAM record from Chinese speleothems, showing wet and dry conditions, respectively. Those are mostly connected to cold stadials in the Greenland synthetic and in the North Atlantic IRD records, to speleothem and travertine growth in the Nordeste, and in some cases to events the Borneo speleothems.

NH climate appeared to force the SAM and EAM also on the millennial time-scale; mostly during the last four glacial periods, and to a minor extent during the interglacials. The grey lines in Figure 5.14 emphasize the connection of NH cold spells, higher precipitation from our SAM record, and weak EAM. A small number of these events seem to find a counterpart also in the recent Australian – Asian monsoon record (Meckler et al., 2012), though large uncertainties in the dating of the latter impede unambiguous matching.

From a paleoecological perspective, the intermittent occurrence of wet periods in the Nordeste throughout the past ~420 kyr was probably paralleled by extension of forest cover replacing the caatinga vegetation characteristic for the area (Behling et al., 2000; Jennerjahn et al., 2004). This in turn could have been crucial for the connection of the Amazon and the Atlantic rainforests. In fact, the development of gallery forest over this presently arid area, could have constituted a corridor between the two rainforests, and allowed genetic exchanges that might have played an important role in establishing their rich biodiversity (Behling et al., 2000; Costa, 2003).

5.5.5 Comparing the Speleo chronology to the marine stacks

Transferring the Speleo chronology of core MD09-3246 to the record of *G. ruber* $\delta^{18}O$ enables an evaluation of the discrepancies between a ^{230}Th-derived chronology and several isotopic stacks that have come of vast use as tuning targets of marine records (Fig. 5.15). Recently, efforts have been made in order to derive a common chronological timeframe for marine isotope records and absolutely dated speleothems (Drysdale et al., 2009; Caballero-Gill et al., 2012), to tackle long-standing climatic questions, such as the timing of the climatic responses to Milanković parameters (Toggweiler and Lea, 2010; Berger, 2013). Whereas the structure and absolute values of our surface $\delta^{18}O$ represent regional conditions, it is reasonable to assume that the timing of the major glacial-interglacial shifts reflects that of ice volume changes, within ± 5-6 kyr (Waelbroeck et al., 2008). Our Speleo chronology is clearly out of phase from the H07 stack of Huybers (2007). It shows notable discrepancies with the SPECMAP stack of Martinson et al. (1987), particularly at the end of T-II and T-I, and at the onset of T-IIIA. But it sustains the general validity of the LR04 stack

(Lisiecki and Raymo, 2005). More in detail, we ascertain that at T-II and T-IV, the LR04 stack, while capturing the beginning of the deglaciations with the same timing in our record, ascribes a shorter duration to them. Regarding transitions to glacials, we note general good agreement between the timing of shifts, but our age control for those intervals is less certain. Caballero-Gill et al. (2012), recently endeavoured, with an approach based on temperature correspondence, to transfer the EAM chronology to marine benthic and planktic records from the South China Sea. A comparison of our *G. ruber* $\delta^{18}O$ with their planktic curve reveals some notable timing disagreements: at T-IV, at T-IIIA and at the end of T-II. During those intervals, the timing agreement is higher between our planktic record and the benthic South China Sea series.

Fig. 5.15 (next page). **Comparison of marine isotope chronologies**. A) *G. ruber* $\delta^{18}O$ record from MD09-3246 on the Speleo chronology, ultimately based on absolutely dated speleothems. B) Benthic and planktic $\delta^{18}O$ records from the South China Sea, also on a speleothem-derived chronology (Caballero-Gill et a., 2012). C) Depth-derived H07 planktic stack of Huybers (2007). Orbitally-tuned benthic stacks: D) LR04 (Lisiecki and Raymo, 2005) and E) SPECMAP (Martinson et al., 1987). Red bars indicate terminations, and green bars interglacial-to-glacial transitions.

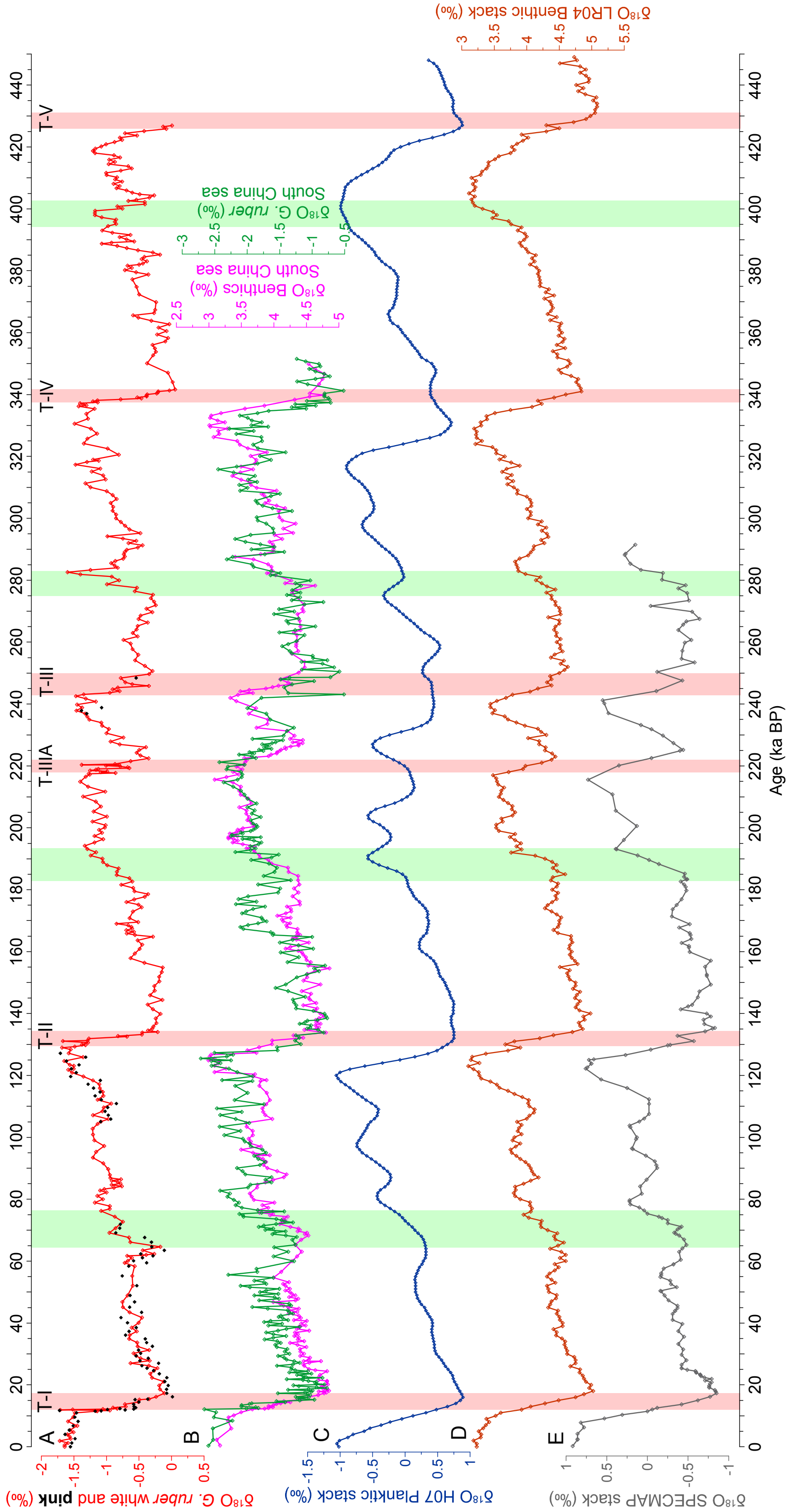
δ18O G. ruber white and pink (‰)
δ18O H07 Planktic stack (‰)
δ18O SPECMAP stack (‰)
δ18O LR04 Benthic stack (‰)
δ18O Benthics (‰)
South China sea
δ18O G. ruber (‰)
South China sea
Age (ka BP)
T-I
T-II
T-IIIA
T-III
T-IV
T-V
A
B
C
D
E

To conclude, the results of this comparative exercise highlight that: I) Orbitally-tuned marine stacks appear to present discrepancies in the timing of the last four terminations when compared to the absolute/radiogenic chronology. Thus, when comparing climate series care should be taken with respect to such inconsistencies. II) There is disagreement between our planktic $\delta^{18}O$ record and the only other long such series that, to our knowledge, has been satisfactorily harmonized to the absolute speleothem chronology (Caballero-Gill et al., 2012). We suggest that the temperature and salinity effects on the foraminiferal $\delta^{18}O$ signal are unlikely to account for the observed offsets. We are therefore keen on attributing those differences to the limitations of either of the two different strategies underlying the transferring of the speleothem chronology to the $\delta^{18}O$ curve.

In perspective, for intervals where our Speleo chronology is most solid, i.e., glacial terminations (see section 5.4.4), further geochemical analysis on foraminiferal from core MD09-3246 withholds potential for insights into the magnitude and timing of tropical hydrographic changes during glacial-interglacial transitions, and therefore into the role of the tropics in shifts of the AMOC.

5.6 Conclusions

Marine core MD09-3246 from the Northeast Brazilian margin presents a Ti/Ca-based record of changes in the continental runoff, that spans the last ~420 kyr. This constitutes a unique and detailed time series of changes in the hydroclimate of the Nordeste, reflecting the intensity of the South American summer monsoon.

The intensity of the SAM appears to have been sensitive to the forcing from Northern Hemispheric cold intervals, such as Heinrich stadials. Previous observations and model studies have indicated that cold NH climate entails atmospheric circulation changes at tropical latitudes, with southern displacement of the intertropical convergence zone that seems to affect both the East Asian and the South American monsoon systems. By adopting a number of independent chronologies for core MD09-3246, based on ^{14}C-tuning, Greenland ice cores chronologies, and the marine isotopic stack LR04, we are able to assess that wet intervals in the Nordeste corresponded to weak EAM. This synchronicity likely held for sub-orbital Heinrich-type of events, and appears most explicit for cold NH phases during deglaciations. We therefore conclude that the SAM and EAM systems were anti-phased during the last four glacial terminations, and the preceding glacials. This provides the conceptual basis to construct a speleothem-based chronology for the record of core MD09-3246. In turn, such chronology enables independent comparison with orbital forcing and with other SAM records from the continent.
We report that, in addition to the outlined NH climate forcing, the amount of local seasonal insolation was a key driver of precipitation in the Nordeste, confirming what was previously observed in shorter (Wang et al., 2006) and non-continuous (Wang et al., 2004) records of SAM.

Globally, paleo monsoons contained a response to insolation, which in turn depended on the latitude and seasonality of the system (Clemens et al., 2010; Cheng et al., 2012b). As a consequence, the insolation component is responsible for the different signatures of the various monsoon records. Nevertheless, a communal response, of the EAM in the Northern and of the SAM in the Southern Hemisphere, to NH cold episodes appears as a consistent feature of the last ~420 kyr. In the framework of the recent discourse regarding the existence of a "global-paleo-monsoon" (Wang, 2009; Caley et al., 2011; Cheng et al., 2012), we suggest that a "global-paleo-monsoon response" to NH forcing was a persistent climatic feature of the last four glacial cycles.

Acknowledgements

Collection of core MD09-3246 took place in the framework of the ESF-EUROMARC initiated 'RETRO' project, co-sponsored by the Research Council of Norway (grant to T.D.), the Nederlandse Organisatie voor Wetenschappelijk Onderzoek (grant.nr. 855.01121 to F.P.), the Centre National de la Recherche scientifique (grant to C.W.) and the Deutsche Forschungsgemeinschaft (grant to H.A.). We wish to thank captain and crew of the R/V G.O. SARS on cruise GS07-150 and captain and crew of the R/V Marion Dufresne on cruise MD173. Furthermore, F.P. and P.S. acknowledge funding from the European Community's Seventh Framework Program FP7/2007-2013 – Marie-Curie ITN, grant agreement 238512, GATEWAYS project, and thank Rainer Zahn, the GATEWAYS community, and Maarten Prins for fruitful discussions. We are grateful to Stefan Mulitza for managing access and equipment for the sampling of core MD09-3246 at MARUM, Bremen. We wish to thank Geert-Jan Brummer for providing access to measurement facilities and Michiel Kienhuis for mass-spectrometer assistance at the NIOZ, Texel, The Netherlands.

6

Synthesis and outlook

6.1 A synthesis

This thesis provides reconstructions of paleoclimatic conditions at two locations in key points of the Atlantic meridional overturning circulation and of the climate system, namely the southeast Atlantic Ocean and the western tropical Atlantic Ocean. In this closing synthesis, I will re-examine the research questions formulated in the introductory Chapter 1, which motivated the studies contained in Chapters 2, 3, 4 and 5. In the light of the results, I will provide an overview of the contribution of the present work to the advance of our understanding in Pleistocene paleoclimatology.

6.1.1 Outcome of the studies on southeast Atlantic paleoceanography

Chapter 1 explained that the southeast Atlantic region has emerged in the literature as a very sensitive and influential area for the circulation in the Atlantic Ocean (e.g., Biastoch et al., 2008b). In particular, it has been repeatedly suggested that the input of relatively warm and saline waters form the Indian Ocean, via the Agulhas leakage might have played a pivotal role in Pleistocene glacial-to-interglacial shifts, by potentially altering the heat and salinity balance of the upper Atlantic waters (Weijer et al., 2002; Knorr and Lohman, 2003). From the field of paleoceanographic observations, the main evidence to sustain this role is the intensification of the inter-ocean transfer of heat and salt through the AL during the last glacial terminations, reconstructed at the interface between the Indian and the Atlantic Oceans (Peeters et al., 2004; Franzese et al., 2006). However, to date no study has expressly aimed at assessing how those Pleistocene variations in AL have influenced the upper waters of the neighbouring southeast Atlantic region, which is the part of the upper branch of the AMOC downstream the AL.

This is precisely the knowledge gap that the studies reported in Chapters 2, 3 and 4 of this thesis intended to fill, and the main reason for studying a new marine sediment core (64PE-174P13) from the central Walvis Ridge, a site situated ~1,800 km downstream the AL area. Each of these studies aimed at solving specific aspects related to the main research question:

How was the South Atlantic circulation affected by changes in the AL, and how do these changes relate to other climatic variations during the last glacial-interglacial cycles?

In the following points, I will discuss how the new findings presented in this thesis have provided answers to the original research questions expressed in Chapter 1.

In **Chapter 2** these questions were addressed: How did the South Atlantic upper ocean stratification change during Pleistocene climate oscillations? Can a systematic glacial-interglacial (G-IG) pattern of this region's thermocline be recognized, and if so how did this pattern relate to variability in the amount of Indian Ocean input from the AL?
The results show that **the upper ocean $\Delta^{18}O$ gradient between shallow and deep dwelling planktic foraminiera, used as a proxy for upper ocean density stratification, reveals a sawtooth pattern strictly connected to G-IG cycles** from MIS 12 to 5. Stratification was minimal during interglacials, increased until the following termination and then dropped relatively fast. **Previously observed variations of AL (Peeters et al., 2004) are a likely cause of the pattern observed in the southeast Atlantic**. I propose that the gradual increase in stratification during glacials indicates a progressive loss of Indian Ocean input from the AL, and that the subsequent quick break-up of stratification, well synchronized with intense AL release at terminations, signaled a southeast Atlantic thermocline readily replenished by poorly stratified (Arhan et al., 2011) waters from the AL. Further, the curve of (sub)surface $\delta^{18}O$-IVE (the foraminiferal $\delta^{18}O$ signal corrected for the ice-volume effect) manifests peaks coinciding with terminations, which also suggests warming compatible with AL rises.

The study presented in **Chapter 3** focuses on the penultimate glacial termination (T-II, ~130,000 years ago). During this prominent climate shift, I intended to understand whether the conspicuous release of AL previously reported from the AL area, at the east of the Cape Basin (Peeters et al., 2004; Martínez-Méndez et al., 2010), actually penetrated the South Atlantic upper ocean circulation.
The outcome gives a positive answer to the research question. Making use of the oceanographic time series generated with a high-resolution ocean circulation model, it is revealed that high density variability at thermocline depth over the Walvis Ridge is related to the passage of Agulhas rings. Based on this observation, a new proxy is devised that, using the geochemical variability associated with populations of thermocline-dwelling planktic foraminifera, infers **higher presence of paleo Agulhas rings over the core site during T-II**. The MIS 6 to 5 development of this proxy reveals close coupling to the published AL reconstructions, and provides necessary grounding to the hypothesis of an effective role in the AMOC played by the AL during deglaciations (Gordon et al., 1992; Knorr and Lohmann, 2003).

In **Chapter 4**, several more questions were addressed regarding events around T-II, the most important being: 1) Did the high salinity and temperature anomalies introduced by the AL at T-II, as reconstructed from the AL area (at the east of the Cape Basin [Marino et al., 2013]), affect the heat and salt budget of the upper South Atlantic Ocean? 2) Did this region's upper ocean participate in the mid-T-II climatic short-lived event that has recently emerged from several records of the Northern Hemisphere (e.g., Wang et al., 2008)?
To address these questions, temperature and (qualitative) salinity proxies were reconstructed for different depths in the upper water column. Results show a high correlation of salinity with the Agulhas rings proxy unraveled from the same core in Chapter 3, and a high degree of connectivity between temperature and salinity at the Walvis Ridge and at the AL area surface (Marino et al., 2013). These correlations strongly suggest that **the southeast Atlantic lay directly under the influence of the AL**. Additionally, the results suggest that high salinity might have been a more conservative property of paleo AL waters downstream the AMOC than heat. Further, the South Atlantic was seemingly more sensitive to AL salinity anomalies at the thermocline than near the sea surface, pointing at a **negative buoyancy of the AL downstream**, potentially due to dissipation of its heat anomaly across the Cape Basin. Another important outcome of this study is that the reconstructed surface temperature and salinity show reversal of their high T-II values at ~133-134 ka, coinciding with their high counterparts from the AL area (Marino et al., 2013). These South Atlantic reversals appear synchronous with climatic events from Northern Hemisphere records (i.e.: with an interruption of the Asian WMI-II [Kelly et al., 2006; Wang et al., 2008], with a warm stadial in Greenland [Barker et al., 2011], and with a "pause" in the lightening of North Atlantic benthic isotopes [Drysdale et al., 2009]). The hypothesis is therefore put forward that **the South Atlantic reacted to the inter-hemispheric seesaw effect of a mid-termination resumption of the AMOC during T-II**. In analogy with the events of T-I (e.g., Barker et al., 2009; 2010), I name the interval emerging from the South Atlantic records "Antarctic Cold Reversal-II" (**ACR-II**).

In conclusion, these studies have contributed to the advance of our understanding through two principal findings:

1) **The Agulhas leakage covered a primary role in determining the South Atlantic hydrography, during Pleistocene glacial terminations**. During the penultimate glacial termination, water masses from the AL seem to have effectively penetrated the South Atlantic gyre (Chapter 3), and to have governed the thermocline (and secondarily, surface) salinity at the central Walvis Ridge (Chapter 4). Moreover, the AL seems to have had a pivotal role during terminations II to V, as its input of poorly stratified waters plausibly determined the stratification changes downstream the AMOC, in the South Atlantic gyre (Chapter 2). This confirms the AL mechanism as a key player in the thermo-haline equilibria of the upper South Atlantic AMOC during prominent climate shifts of the Pleistocene.

2) **The South Atlantic paleoceanographic record reveals a termination II constisting of two steps, interrupted by a climatic event characterized by Atlantic inter-hemisperic seesaw dynamics**. This finding provides an important integration of the paleo evidence from Northern Hemisphere archives, to suggest that AMOC dynamics determined the sequence of events during this strong climatic transition. The presence of an "ACR-type" of event during T-II in turn calls for the investigation (e.g., by means of numerical models) of the forcings at the basis of this brief interruption in the climate trends of the deglaciation.

6.1.2 Outcome of the study of the western tropical Atlantic

Contemporary understanding of monsoon systems portrays them as regional manifestations of the globally coordinated, seasonal shifts of the intertropical convergence zone (Trenberth et al., 2000). The hydroclimate of the Brazilian Nordeste is sensitive to seasonal displacements of the ITCZ, which in turn control the amount of Atlantic moisture received by the continent: this determines the South American summer monsoon (Hastenrath and Greischar, 1993). To improve our understanding of the sensitivity of this system to climatic forcing, it is necessary to extend our knowledge of the history of the SAM in the context of global climate changes of the Pleistocene.

From previous studies it is known that the SAM responded to two types of forcing: 1) high-latitude Northern Hemisphere cooling (e.g., Arz et al., 1998; Chiang and Bitz, 2005); 2) insolation (Wang et al., 2004; Cruz et al., 2005). Further, anti-phasing of the monsoon systems of the Northern and the Southern Hemispheres has been hypothesized (Wang et al., 2004), mediated by the climatic forcing exerted by high-latitude NH cooling (Wang et al., 2006).
In **Chapter 5** I aimed to respond to the following research question:
Was the anti-phased teleconnection, between Boreal and Austral monsoons a systematic pattern for the last Pleistocene glacial cycles?

To address this it was necessary to generate a suitably long, continuous hydroclimate record. For this scope marine sediment core MD09-3246, from the northeast Brazilian margin, was studied. The depositional regime of this area has already been shown to promptly respond to meridional displacements of the ITCZ (Arz et al., 1998), and the core is therefore well suited to investigate the history of the western tropical Atlantic ITCZ.
The study's outcome is a high-resolution record of continental runoff, and therefore of the intensity of the SAM, which extends previous reconstructions from speleothems (Cruz et al., 2009) and sediment (Arz et al., 1998) to about 420 ka. I compared this record to hydroclimate reconstructions from other parts of the continent (e.g., Wang et al., 2004; Cruz et al., 2005; Cheng et al., 2013), from Greenland (NGRIP, 2004), and from the NH tropics (speleothem records of East Asia monsoon [e.g., Wang et al., 2008; Cheng et al., 2009]). It is concluded that

during the last 420 kyr the SAM reflected both the effect of regional insolation and, more prominently, that of forcing by high-latitude NH cold phases. An important implication of the results, which responds to the main research question, is that **the SAM seems to be coupled, and anti-phased, with the EAM during the Pleistocene.** Stepping into the recent debate regarding the existence of a "global-paleo-monsoon" (Wang, 2009; Caley et al., 2011; Cheng et al., 2012), the contribution of Chapter 5 is that both the Austral (South America) and the Boreal (East Asia) monsoon systems responded to climate forcing by high-latitude NH cold phases during the last four glacial cycles. **This points to the Pleistocene persistence of a "global-paleo-monsoon response" to NH forcing**.

6.2 An outlook to future research

The studies presented in this thesis form the basis upon which future paleoclimate research may be carried out. In the next paragraphs I will highlight some aspects of the treated topics that I find to deserve further attention.

6.2.1 Changes in the wind fields over the southeast Atlantic

Core 64PE-174P13 (central Walvis Ridge) was scanned for its XRF elemental profile, at high-resolution (every 0.25 cm) (Fig. 6.1 C-D-E). The abundance of elements that commonly characterize input from terrestrial dust sources, such as iron, silicon and aluminum, normalized to calcium, in turn representing the marine component, show a clear resemblance to the marine record of aeolian dust advection off Namibia (core MD962094 from the northern Walvis Ridge [Stuut et al., 2002]) (Fig. 6.1 F). That record reported that southeastern African climate during the last three glacial periods was characterized by increased winter precipitation (and therefore stronger / northward shifted westerlies wind field), and increased offshore dust advection (and therefore stronger easterlies).

The comparison of the elemental profiles at the two locations suggests that the central Walvis Ridge sediment record, situated much further from the continent, and about 10° more to the south, responded to a similar source of variability. It appears therefore that the central Walvis Ridge record could serve the purpose of extending the available aridity and wind intensity time series by about 150 kyr.

Further, the varying degree of connectivity between the more proximal-northermost (MD962094) and the more distal-southernmost (64PE-174P13) records of Namibian dust might provide information as to the extent of the dust plume arising from southwestern Africa, both in a zonal and in a latitudinal sense. This in turn could add more precise constrains on the intensity of the easterlies, and on their latitudinal position.

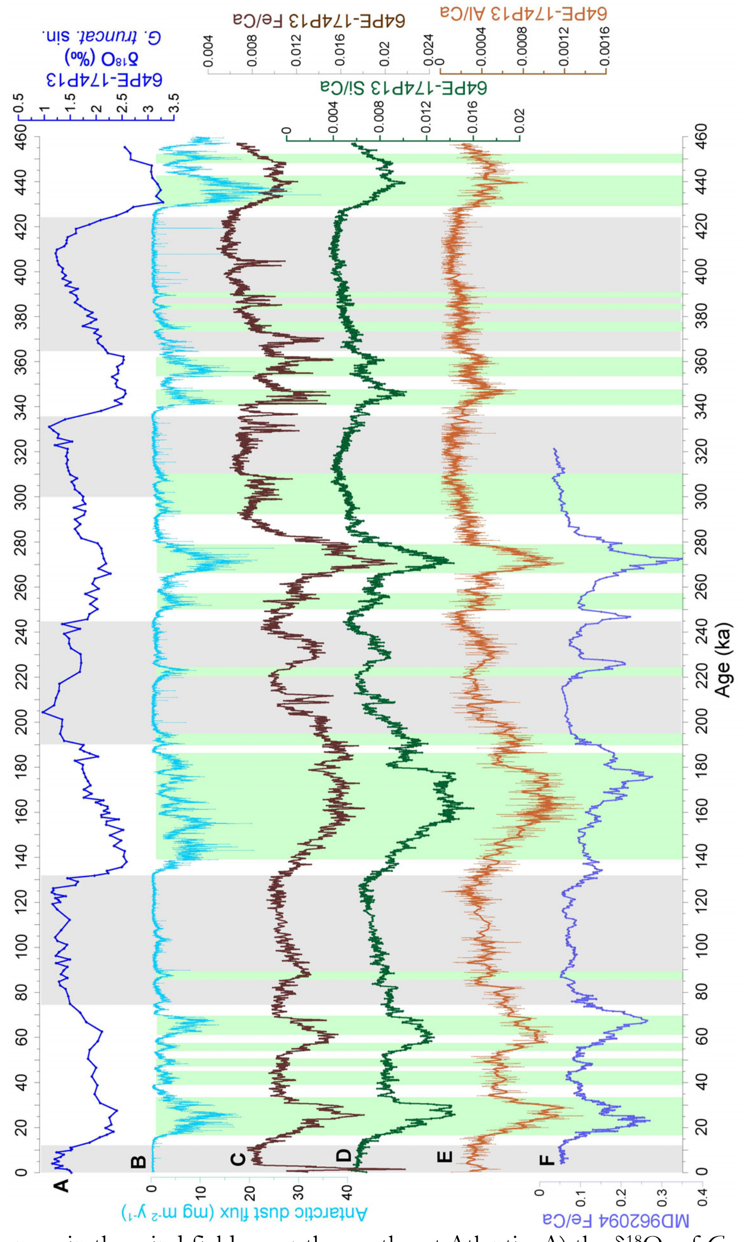

Fig. 6.1. Changes in the wind fields over the southeast Atlantic. A) the $\delta^{18}O$ of *G. truncatulinoides* of core 64PE-174P13 is plotted for stratigraphic reference (Scussolini and Peeters, 2013; Chapter 2). B) Antarctic dust flux from Epica Dome C (Lambert et al., 2012). C-D-E) Elemental ratios from Walvis Ridge core 64PE-174P13, representing likely aeolian advection from terrestrial sources. F) Fe/Ca abundance from northern Walvis Ridge core MD96094 (Stuut et al., 2002), representing advection from southwestern Africa. Green bands indicate dust peaks from Antarctica that are mirrored in either the 64PE-174P13 or the MD962094 XRF records.

Additionally, it is interesting to note that both of these Walvis Ridge elemental records, show strong resemblance to the record of Antarctic dust flux (Lambert et al., 2012) (Fig. 6.1 B). Dust in Antarctic ice has its origin mostly in Patagonia (Delmonte et al., 2010). A connection between Antarctic climate and southwestern Africa aridity has already been suggested (Stuut et al., 2004). On the other hand, a connection between the dust records, across the frontal systems at the interface between the Southern and Atlantic Oceans, offers the possibility to some speculations: 1) It might reflect glacial intensification of the westerlies wind belt, that influenced both the Walvis Ridge records (by enhancing winter precipitation over southwestern Africa) and the Antarctic one (by advecting more dust from Patagonia). 2) It might reveal a coupling between the glacial intensifications of the easterlies and the westerlies wind fields, such that when westerlies blew larger Patagonian dust plumes towards Antarctica, the the easterlies transported more dust from Namibia over the Walvis Ridge. This last possibility is in agreement with previous research indicating general strenghtening of the glacial SH wind field (Moreno et al., 1999; Stuut et al., 2002; Lambert et al., 2008; Bard and Rickaby, 2009). Integrating the 64PE-174P13 XRF results with an approach based on grain size analysis, as in Stuut et al. (2002), would help disentangle the nature of the aeolian fraction, and therefore the mechanism behind its mobilization, i.e. aridity vs easterlies strenght.

6.2.2 Coiling ratio of *G. truncatulinoides* as a proxy for thermocline depth

The planktic foraminifer samples of core 64PE-174P13 can be used to extract additional paleoclimatic information, in the form of the relative abundance of species in the foraminifer community. In particular, the species *G. truncatulinoides* has long been known to present varieties with different coiling directions, that also manifest different ecological preferences (Bé and Tolderlund, 1971). Recent studies have added additional details on the morphotypical and genotypical distribution of this species in the Atlantic Ocean (De Vargas et al., 2001; Quillévéré et al., 2013). Already Lohmann and Schweitzer (1990) suggested that the coiling ratio in populations of this species could provide information as to the depth of the past thermocline. I estimated the relative abundance of sinistral- versus dextral-coiling morphotypes, on the top 330 cm of core 64PE-174P13, counting ~200 specimens per sample, and covering MIS 7 to 1 (Fig. 6.2 D).

These preliminary results therefore suggest that coiling ratio of this species might be controlled by multiple upper ocean characteristics, likely stratification and thermocline temperature. By disentagling their respective influence on the *G. truncatuliunoides* coiling ratio, the use of this faunal parameter as a proxy for upper ocean stratification, or thermocline depth, could be assessed further. In any case, the discrepancies of the coiling ratio with both the $\Delta^{18}O$ and the temperature proxies need to be examined in closer detail, prior to endorsing a wider application for Atlantic paleoceanography.

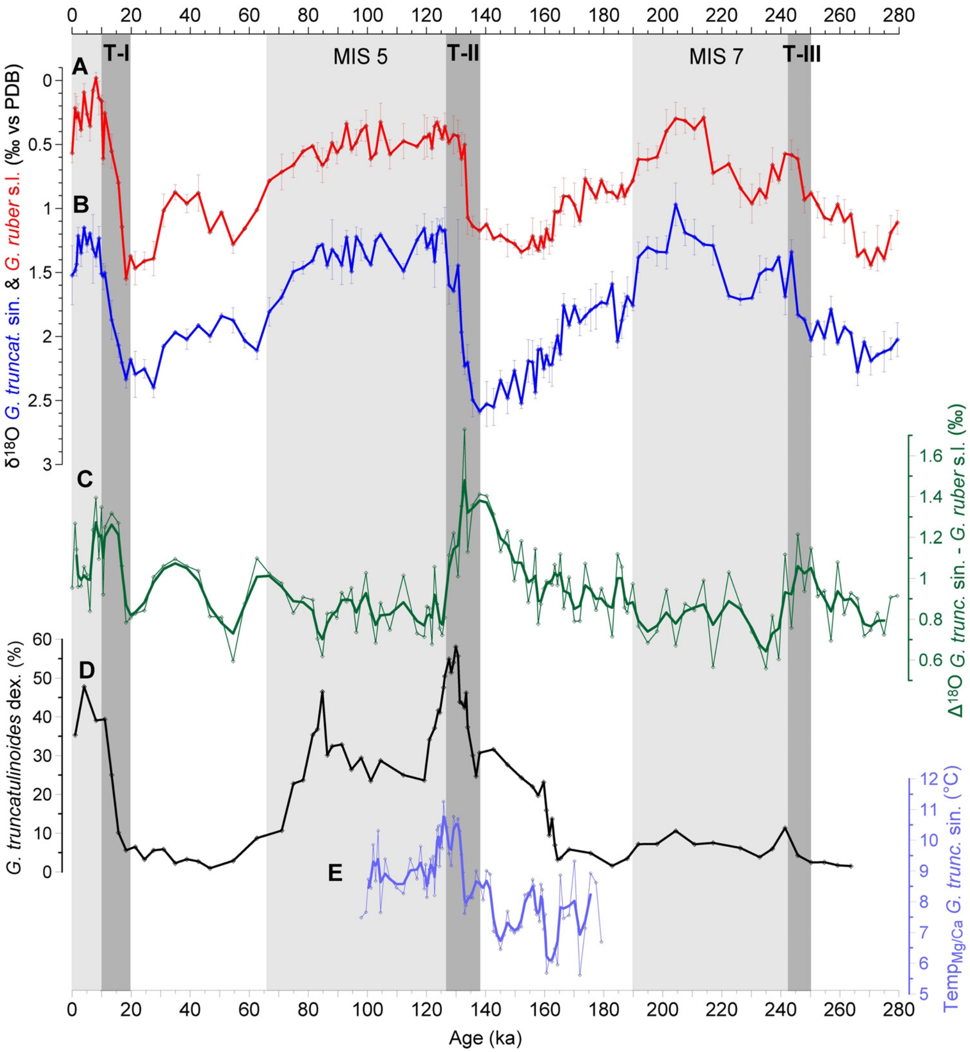

Fig. 6.2. Coiling abundance of *G. truncatulinoides* linked to upper ocean stratification. A-B) $\delta^{18}O$ of surface species *G. ruber* and thermocline *G. truncatulinoides* sin. from Walvis Ridge core 64PE-174P13. C) $\Delta^{18}O$: difference between the $\delta^{18}O$ signals of those two species, used in Scussolini and Peeters (2013; Chapter 2) as a proxy for upper ocean stratification. D) Relative abundance of dextral-coiling morphotype of *G. truncatulinoides*, also a potential proxy for upper ocean stratification. E) Thermocline temperature reconstructed from Mg/Ca of *G. truncatulinoides* sin. (Chapter 4).

6.2.3 Hydrography of the western tropical Atlantic during Termination II

In Chapters 3 and 4, based on the Walvis Ridge core 64PE-174P13, I set the focus on the penultimate glacial termination, motivated by the marked climatic changes that characterize this period, as emerging from previous research (e.g., Peeters et al., 2004;

Jouzel et al., 2007; Martínez-Garcia et al., 2009). Following the same reasoning, it is interesting to look in changes into the western tropical Atlantic upper hydrography, from northeast Brazil core MD09-3246. Whereas the Walvis Ridge region represents the main entrance of waters into the upper AMOC, the location of core MD09-3246 is underneath the bottleneck of northward transfer of upper AMOC waters from the South into the North Atlantic (de Silveira et al., 1994). Therefore a comparison between the two locations could provide information regarding the transmission of the heat and salt anomalies, observed in the southeast Atlantic at T-II, across the South Atlantic. The evidence presented here indicates that rings from the AL entered the subtropical gyre right around the termination (Chapter 3), and that the T-II AL peaks (Marino et al., 2013) warmed up and salinified the thermocline and the surface (Chapter 4).

Interest resides in investigating, from core MD09-3246, whether the observed alterations in the water properties of the southeast Atlantic was reflected further down the conveyor belt, at the North Brazil Current oceanographic bottleneck (de Silveira et al., 1994). This question could be addressed by the reconstruction of surface and sub-surface temperature and salinity, with the multispecies planktic foraminifer δ^{18}O-Mg/Ca paired-proxies approach applied in Chapter 4. Partial results are already available for three species with different depth habitat (Fig. 6.3 B-C) (courtesy of Kirsten Meulenbroek).

The time series of this proxy for thermocline depth bears resemblance to the δ^{18}O-based upper ocean stratification proxy applied in Chapter 2 (Δ^{18}O; Fig. 6.2 C), especially for T-I and T-II. Pre-termination increases of the Δ^{18}O signal seem anyway to lead over the coiling-ratio changes. Interestingly, the Δ^{18}O-based stratification variations around T-III are not reproduced in the coiling ratio of *G. truncatulinoides*. Another potential cause of the observed shift in coiling ratio is the temperature of the thermocline, that was reconstructed for the T-II interval in Chapter 4 (Fig. 6.2 E). In fact, whereas the increase in *G. truncatulinoides* dex. abundance during MIS 6 seems coupled to the Δ^{18}O curve, at T-II it more closely follows the temperature evolution.

G. ruber white (at higher resolution than presented in Chapter 5), *G. aequilateralis* and *G. truncatulinoides* dextral have been analyzed for their δ^{18}O and Mg/Ca composition. Preliminarily results reveal differences in the timing of changes in hydrological properties prior to and around T-II. Further, the absolute Speleo chronology generated for core MD09-3246 and presented in Chapter 5 could enable appropriate phase comparison with the central Walvis Ridge data sets of temperature and salinity presented in Chapter 4, and with the other records therein discussed. This would grant tighter chronostratigraphical control than enabled by tuning to the classic marine stacks.

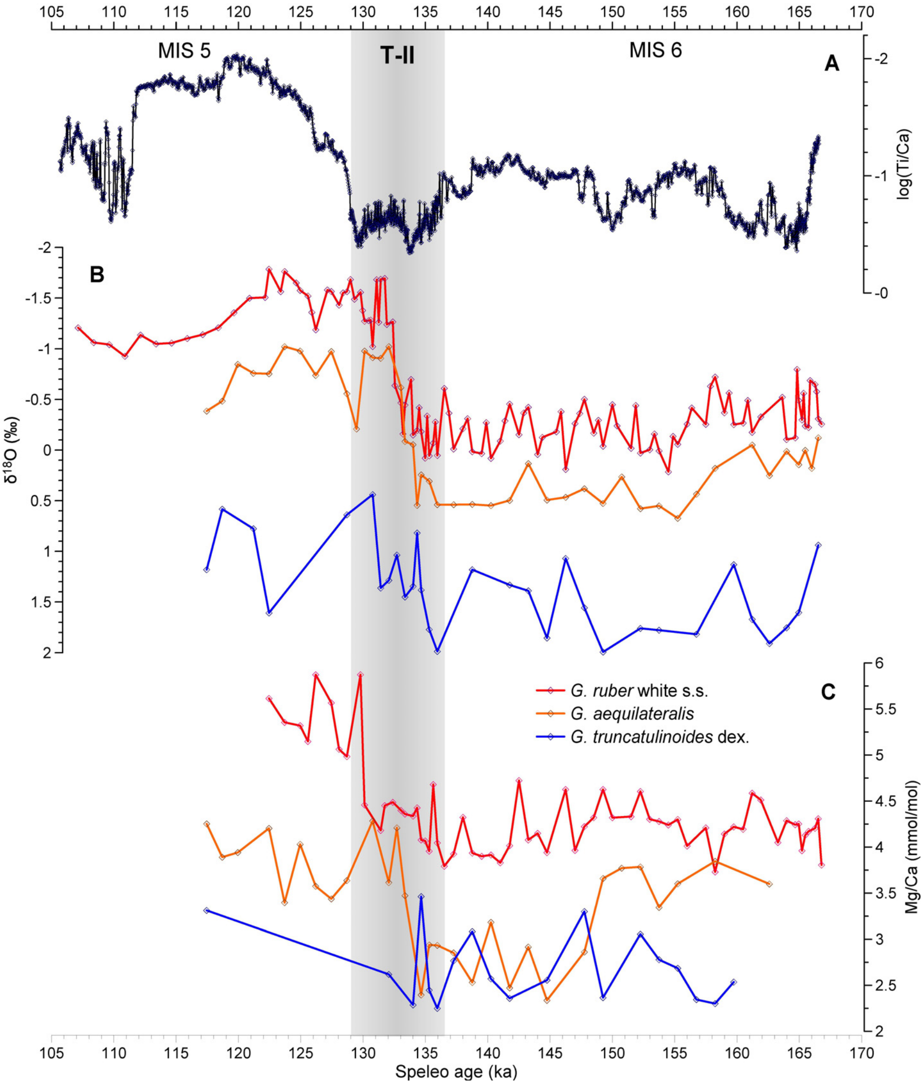

Fig. 6.3. Additional geochemical datasets from planktic foraminifera in northeast Brazilian margin core MD09-3246. A) log(Ti/Ca), a proxy for terrigenous input to the sediment (Chapter 5); B) $\delta^{18}O$ and C) Mg/Ca reconstructions from surface species *G. ruber* sensu stricto, intermediate species *G. aequilateralis*, and deep species *G. truncatulinoides* dextral (courtesy of Kirsten Meulenbroek).

6.2.4 Thermal response of the western tropical Atlantic surface to North Atlantic cooling anomalies over the past four glacial cycles

Thermal variability in response to Pleistocene climate change has been unraveled at high resolution from high latitudes records in the Northern and Southern Hemispere (e.g., NGRIP, 2004; Jouzel et al., 2007). An anti-phased thermal pattern has emerged from the interhemispheric comparison (Blunier et al., 1998), a concept later formalized as the bipolar, or interhemispheric, thermal seesaw (e.g., Stocker and Johnsen, 2003), which appears to have applied also at low latitudes in the Atlantic Ocean (Mix et al., 1986; Barker et al, 2009) during the last glacial cycle.

Paleoceanographic reconstructions from the Iberian Peninsula present a detailed account of rapid changes in surface temperature (e.g., Martrat et al., 2007), which are recurrent at the millennial scale during the past four glacial cycles. Additionally, the synthetic series of Barker et al. (2011), produced on the basis of interhemispheric seesaw assumptions, provides a high-resolution extension of the proxy record (EPICA, 2004; NEEM, 2013) of Greenland temperature variability. The generation of a temperature record from the tropical region of the Atlantic could serve as a low-latitude term of comparison for those accounts of North Atlantic climate variability. Efforts are underway at the IOW, Warnemünde (Germany), to apply the alkenone-based $U^{K'}_{37}$ paleothermometer on the whole extent of core MD09-3246. Preliminary results, in the Speleo chronology of the core (see Chapter 5), suggest phasing of western tropical Atlantic low surface temperatures with cooling in the high-latitude North Atlantic (Jerome Kaiser, IOW, personal communication). This dataset will likely help to shed light on the response of the low latitudes of the Atlantic to the bipolar thermal seesaw (Vellinga and Wood, 2002; Stocker and Johnsen, 2003; Knutti et al., 2004), and to decipher the apparent contrasts emerging from the available proxy evidence (e.g., Arz et al., 1999a; Jaeschke et al., 2007).

6.2.5 Characterization of the western tropical Atlantic hydrography through planktic foraminifera assemblages

Planktic foraminifera from core MD09-3246 contain additional paleoceanographic information that can be used to tackle the questions regarding tropical thermal response to rapid Pleistocene climate change (e.g., Barker et al., 2011) (see above section 6.2.4). One potential research approach is to determine the foraminifera species' distribution within the community (also known as census counts [e.g., Rau et al., 2002]), which enables the reconstruction of ecological conditions and the computation of sea surface temperature through the application of transfer functions (e.g., Chen et al., 2002; Simon et al., 2013). The SST results could be compared to the $U^{K'}_{37}$-derived SST (Section 6.2.4) and to Mg/Ca-derived upper ocean temperatures (Section 6.2.3), and be integrated into a coherent narrative.

6.2.6 Benthic $\delta^{18}O$ record from core MD09-3246

Moreover, it would be interesting to unravel the benthic foraminifer $\delta^{18}O$ stratigraphy of core MD09-3246, to expand on the comparison between the Speleo chronology, generated in Chapter 5, and those based on the classic marine isotope stacks (in particular the widely used benthic $\delta^{18}O$ LR04 curve [Lisiecki and Raymo, 2005]). The difficulty of this approach resides in the scarce abundance of benthic foraminifera amidst a sediment matrix that is heavily loaded with terrigenous particles. Such sedimentary regimes often produce anoxic conditions at the sea floor, which heavily limit the development of the benthos, and therefore the presence of a paleoceanographically viable benthic foraminifer community (e.g., Friedrich, 2010). In fact, inconstant presence of benthic taxa along core MD09-3246 has already been assessed, especially in sections with high Ti/Ca elemental ratio (Pim Kaskes, personal communication). Processing larger quantities of sediment from the core would therefore be a requirement for this study.

List of the abbreviations used

$\delta^{18}O_{sw\text{-}ivc}$: $\delta^{18}O$ of seawater, ice-volume corrected.
$\delta^{18}O$-IVE: $\delta^{18}O$ of foraminifera calcite minus ice-volume effect.
$\Delta^{13}C$: difference between the $\delta^{13}C$ of *G. truncatulinoides* sin. and *G. ruber*.
$\Delta^{18}O$: difference between the $\delta^{18}O$ of *G. truncatulinoides* sin. and *G. ruber*.
AAIW: Antarctic intermediate water.
ACR: Antarctic cold reversal.
AL: Agulhas Leakage.
AMOC: Atlantic meridional overturning circulation.
B-A: Bølling-Allerød.
BP: before present.
EAM: East Asian monsoon.
G-IG: glacial - interglacial.
GNAIW: Glacial North Atlantic intermediate water.
HS: Heinrich stadial.
ka: thousand years before present (age) (from kilo-annum).
kyr: thousand years (duration).
ICTZ: Intertropical convergence zone.
IVE: ice volume effect.
LGM: last glacial maximum.
MIS: marine isotope stage.
NADW: North Atlantic deep water.
NH: Northern Hemisphere.
SAG: South Atlantic gyre.
SAM: South American monsoon.
SH: Southern Hemisphere.
sin.: sinistral.
SSH: sea surface height.
SST: sea surface temperature.
s.l.: sensu lato.
T-I, T-II,… : Termination-I, Termination-II, etc…
WMI: weak monsoon interval.
YD: Younger Dryas.
XRF: X-ray fluorescence.

References

Absy M. L., et al. (1991), Mise en evidence de quatre phases d'ouverture de la foret dense dans le sud-est de l'Amazonie au cours des 60,000 dernieres annees. Premiere comparision avec d'autres regions tropicales. *Comptes Rendues Academie des Sciences Paris*, 312, 673-678.

Aerts, J. C. J. H., H. Renssen, P. J. Ward, H. de Moel, E. Odada, L. M. Bouwer, and H. Goosse (2006), Sensitivity of global river discharges under Holocene and future climate conditions, *Geophysical Research Letters*, 33(19), L19401.

Álvarez-Solas, J., M. Montoya, C. Ritz, G. Ramstein, S. Charbit, C. Dumas, K. Nisancioglu, T. Dokken, and A. Ganopolski (2011), Heinrich event 1: an example of dynamical ice-sheet reaction to oceanic changes, *Clim. Past*, *7*(4), 1297-1306.

An, Z., et al. (2011), Glacial-Interglacial Indian Summer Monsoon Dynamics, *Science*, *333*(6043), 719-723.

Anand, P. H. E., and M. H. Conte (2003), Calibration of Mg/Ca thermometry in planktonic foraminifera from a sediment trap time series, *Paleoceanography*, *18*(2), 1050.

Anderson, R. F., S. Ali, L. I. Bradtmiller, S. H. H. Nielsen, M. Q. Fleisher, B. E. Anderson, and L. H. Burckle (2009), Wind-Driven Upwelling in the Southern Ocean and the Deglacial Rise in Atmospheric CO_2, *Science*, 323(5920), 1443-1448.

Anderson, R. F., and M.-E. Carr (2010), Uncorking the Southern Ocean's Vintage CO_2, *Science*, *328*(5982), 1117-1118.

Annan, J. D., and J. C. Hargreaves (2013), A new global reconstruction of temperature changes at the Last Glacial Maximum, *Clim. Past*, 9(1), 367–376.

Antonov, J. I., D. Seidov, T. P. Boyer, R. A. Locarnini, A. V. Mishonov, H. E. Garcia, O. K. Baranova, M. M. Zweng, and D. R. Johnson (2010), *World Ocean Atlas 2009, Volume 2: Salinity*, 184 pp., U.S. Government Printing Office, Washington, D.C.

Arbuszewski, J., P. deMenocal, A. Kaplan, and E. C. Farmer (2010), On the fidelity of shell-derived d^{18}Oseawater estimates, *Earth and Planetary Science Letters*, *300*(3-4), 185-196.

Arhan, M., S. Speich, C. Messager, G. Dencausse, R. Fine, and M. Boye (2011), Anticyclonic and cyclonic eddies of subtropical origin in the subantarctic zone south of Africa, *J. Geophys. Res.*, *116*(C11), C11004.

Arz, H. W., J. r. Pätzold, and G. Wefer (1998), Correlated Millennial-Scale Changes in Surface Hydrography and Terrigenous Sediment Yield Inferred from Last-Glacial Marine Deposits off Northeastern Brazil, *Quaternary Research*, *50*(2), 157-166.

Arz, H. W., J. r. Pätzold, and G. Wefer (1999a), The deglacial history of the western tropical Atlantic as inferred from high resolution stable isotope records off northeastern Brazil, *Earth and Planetary Science Letters*, *167*, 105-117.

Arz, H. W., J. Pätzold, and G. Wefer (1999b), Climatic changes during the last deglaciation recorded in sediment cores from the northeastern Brazilian Continental Margin, *Geo-Marine Letters*, *19*(3), 209-218.

Aurahs, R., Y. Treis, K. Darling, and M. Kucera (2011), A revised taxonomic and phylogenetic concept for the planktonic foraminifer species Globigerinoides ruber based on molecular and morphometric evidence, *Marine Micropaleontology*, *79*(1-2), 1-14.

Avissar, R., and D. Werth (2005), Global Hydroclimatological Teleconnections Resulting from Tropical

Deforestation, *Journal of Hydrometeorology*, *6*(2), 134-145.

Backeberg, B. C., P. Penven, and M. Rouault (2012), Impact of intensified Indian Ocean winds on mesoscale variability in the Agulhas system, *Nature Clim. Change*, *advance online publication*.

Baehr, J., S. Cunnningham, H. Haak, P. Heimbach, T. Kanzow, and J. Marotzke (2009), Observed and simulated estimates of the meridional overturning circulation at 26.5 degrees N in the Atlantic, *Ocean Sci.*, *5*(4), 575-589.

Baker, P. A., C. A. Rigsby, G. O. Seltzer, S. C. Fritz, T. K. Lowenstein, N. P. Bacher, and C. Veliz (2001), Tropical climate changes at millennial and orbital timescales on the Bolivian Altiplano, *Nature*, 409(6821), 698-701.

Bard, E. (2001), Paleoceanographic implications of the difference in deep-sea sediment mixing between large and fine particles, *Paleoceanography*, *16*(3), 235-239.

Bard, E., and R. E. M. Rickaby (2009), Migration of the subtropical front as a modulator of glacial climate, *Nature*, *460*(7253), 380-383.

Baringer, M. O. N., and J. C. Larsen (2001), Sixteen years of Florida Current Transport at 27° N, *Geophysical Research Letters*, 28(16), 3179-3182.

Barker, S., M. Greaves, and H. Elderfield (2003), A study of cleaning procedures used for foraminiferal Mg/Ca paleothermometry, *Geochem. Geophys. Geosyst.*, *4*(9), 8407.

Barker, S., P. Diz, M. J. Vautravers, J. Pike, G. Knorr, I. R. Hall, and W. S. Broecker (2009), Interhemispheric Atlantic seesaw response during the last deglaciation, *Nature*, *457*(7233), 1097-1102.

Barker, S., G. Knorr, M. J. Vautravers, P. Diz, and L. C. Skinner (2010), Extreme deepening of the Atlantic overturning circulation during deglaciation, *Nature Geosci*, *3*(8), 567-571.

Barker, S., G. Knorr, R. L. Edwards, F. d. r. Parrenin, A. E. Putnam, L. C. Skinner, E. Wolff, and M. Ziegler (2011), 800,000 Years of Abrupt Climate Variability, *Science*, *334*(6054), 347-351.

Barry, R. G., and R. J. Chorley (2003), Atmosphere, weather, and climate, Routledge, London.

Bé, A. W. H. (1977), An ecological, zoogeographic and taxonomic review of recent planktonic foraminifera, *Oceanic Micropaleontology*, *1*, 1-100.

Bé, A. W. H., Tolderlund, D.S., (1971), Distribution and ecology of living planktonic foraminifera in surface waters of the Atlantic and Indian Oceans, in The Micropaleontology of Oceans, edited by B. M. Funnell, Riedel, W.R., pp. 105-149, Cambridge university press, Cambridge.

Bé, A. W., and J. C. Duplessy (1976), Subtropical convergence fluctuations and quaternary climates in the middle latitudes of the Indian ocean, *Science*, *194*(4263), 419-422.

Bé, A. W. H., C. Hemleben, O. R. Anderson, M. Spindler, J. Hacunda, and S. Tuntivate-Choy (1977), Laboratory and field observations of living planktonic foraminifera, *Micropaleontology*, *23*(2), 155-179.

Beal, L. M., T. K. Chereskin, Y. D. Lenn, and S. Elipot (2006), The Sources and Mixing Characteristics of the Agulhas Current, *Journal of Physical Oceanography*, *36*(11), 2060-2074.

Beal, L. M., Wilhelmus P. M. De Ruijter, Arne Biastoch, Rainer Zahn (2011), On the role of the Agulhas system in ocean circulation and climate, *Nature*, *472*, 429-436.

Behling, H., H. W. Arz, J. Pätzold, and G. Wefer (2000), Late Quaternary vegetational and climate dynamics in northeastern Brazil, inferences from marine core GeoB 3104-1, *Quaternary Science Reviews*, *19*(10), 981-994.

Bemis, B. E., H. J. Spero, J. Bijma, and D. W. Lea (1998), Reevaluation of the Oxygen Isotopic Composition of Planktonic Foraminifera: Experimental Results and Revised Paleotemperature Equations, *Paleoceanography*, *13*(2), 150-160.

Berger, A. L. (1978), Long-Term Variations of Daily Insolation and Quaternary Climatic Changes, *Journal* *of the Atmospheric Sciences*, *35*(12), 2362-2367.

Berger, W. H. (2013), On the Milankovitch sensitivity of the Quaternary deep-sea record, *Clim. Past*, *9*(4), 2003-2011.

Berger, W. H., and G. Wefer (1996), Expeditions into the past: Paleoceanographic studies in the South Atlantic, in *The South Atlantic: Present and Past Circulation*, edited by G. Wefer, et al., pp. 363–410, Springer.

Berger, A., and M.-F. Loutre (2003), Climate 400,000 years ago, a key to the future?, in *Earth's Climate and Orbital Eccentricity: The Marine Isotope Stage 11Question, Geophys. Monogr. Ser.*, edited by A. W. Droxler , R. Z. Poore, and L. H. Burckle, pp. 17–26, AGU, Washington, D. C.

Berger, A., M. F. Loutre, and J. L. Mélice (2006), Equatorial insolation: from precession harmonics to eccentricity frequencies, *Clim. Past*, *2*(2), 131-136.

Biastoch, A., and C. W. Böning (2013), Anthropogenic impact on Agulhas leakage, *Geophysical Research Letters*, *40*(6), 1138-1143.

Biastoch, A., J. R. E. Lutjeharms, C. W. Böning, and M. Scheinert (2008a), Mesoscale perturbations control inter-ocean exchange south of Africa, *Geophys. Res. Lett.,* 35(20), L20602.

Biastoch, A., C. W. Boning, and J. R. E. Lutjeharms (2008b), Agulhas leakage dynamics affects decadal variability in Atlantic overturning circulation, *Nature*, *456*(7221), 489-492.

Biastoch, A., C. W. Boning, F. U. Schwarzkopf, and J. R. E. Lutjeharms (2009), Increase in Agulhas leakage due to poleward shift of Southern Hemisphere westerlies, *Nature*, *462*(7272), 495-498.

Billups, K., and H. J. Spero (1995), Relationship between shell size, thickness and stable isotopes in individual planktonic foraminifera from two Equatorial Atlantic cores, *The Journal of Foraminiferal Research*, *25*(1), 24-37.

Bintanja, R., and R. S. W. van de Wal (2008), North American ice-sheet dynamics and the onset of 100,000-year glacial cycles, *Nature*, *454*(7206), 869-872.

Blunier, T., et al. (1998), Asynchrony of Antarctic and Greenland climate change during the last glacial period, *Nature*, 394(6695), 739-743.

Boebel, O., T. Rossby, J. Lutjeharms, W. Zenk, and C. Barron (2003), Path and variability of the Agulhas Return Current, *Deep Sea Research Part II: Topical Studies in Oceanography*, *50*(1), 35-56.

Brassell, S. C., G. Eglinton, I. T. Marlowe, U. Pflaumann, and M. Sarnthein (1986), Molecular stratigraphy: a new tool for climatic assessment, *Nature*, *320*(6058), 129-133.

Broecker, W. S., G. Bond, M. Klas, G. Bonani, and W. Wolfli (1990), A salt oscillator in the glacial Atlantic? 1. The concept, *Paleoceanography*, 5(4), 469-477.

Broecker, W. S. (1991), The great ocean conveyor, *Oceanography*, 4(2), 79-89.

Broecker, W. S. (1998), Paleocean circulation during the last deglaciation: A bipolar seesaw?, *Paleoceanography*, *13*(2), 119-121.

Broecker, W. S., and J. van Donk (1970), Insolation changes, ice volumes, and the O18 record in deep-sea cores, *Rev. Geophys.*, *8*(1), 169-198.

Byrne, D. A., A. L. Gordon, and W. F. Haxby (1995), Agulhas Eddies: A Synoptic View Using Geosat ERM Data, *Journal of Physical Oceanography*, *25*(5), 902-917.

Caballero-Gill, R. P., S. C. Clemens, and W. L. Prell (2012), Direct correlation of Chinese speleothem δ18O and South China Sea planktonic δ18O: Transferring a speleothem chronology to the benthic marine chronology, *Paleoceanography*, *27*(2), PA2203.

Caley, T., et al. (2011), High-latitude obliquity forcing drives the agulhas leakage, *Clim. Past*, *7*(4), 1285-1296.

Caley, T., B. Malaizé, M. Revel, E. Ducassou, K. Wainer, M. Ibrahim, D. Shoeaib, S. Migeon, and V.

Marieu (2011), Orbital timing of the Indian, East Asian and African boreal monsoons and the concept of a 'global monsoon', *Quaternary Science Reviews*, *30*(25–26), 3705-3715.

Cannariato, K. G., and J. P. Kennett (2005), Structure of the penultimate deglaciation along the California margin and implications for Milankovitch theory, *Geology*, *33*(2), 157-160.

Carlson, A. E., D. W. Oppo, R. E. Came, A. N. LeGrande, L. D. Keigwin, and W. B. Curry (2008), Subtropical Atlantic salinity variability and Atlantic meridional circulation during the last deglaciation, *Geology*, *36*(12), 991-994.

Charles, C. D., Wright, James D., Fairbanks, Richard G. (1993), Thermodynamic influences on the marine carbon isotope record, *Paleoceanography*, *8*(6), 691-697.

Chave, K. E. (1954), Aspects of the Biogeochemistry of Magnesium 1. Calcareous Marine Organisms, *The Journal of Geology*, *62*(3), 266-283.

Chen, M.-T., Y.-P. Chang, C.-C. Chang, L.-W. Wang, C.-H. Wang, and E.-F. Yu (2002), Late Quaternary sea-surface temperature variations in the southeast Atlantic: a planktic foraminifer faunal record of the past 600[punctuation space]000 yr (IMAGES II MD962085), *Marine Geology*, *180*(1-4), 163-181.

Cheng, H., R. L. Edwards, Y. Wang, X. Kong, Y. Ming, M. J. Kelly, X. Wang, C. D. Gallup, and W. Liu (2006), A penultimate glacial monsoon record from Hulu Cave and two-phase glacial terminations, *Geology*, *34*(3), 217-220.

Cheng, H., R. L. Edwards, W. S. Broecker, G. H. Denton, X. Kong, Y. Wang, R. Zhang, and X. Wang (2009), Ice Age Terminations, *Science*, *326*(5950), 248-252.

Cheng, H., A. Sinha, and S. M. Colman (2012a), Will summer rain increase or decrease in monsoon regions? (Past), *PAGES News*, *20*(1), 27.

Cheng, H., A. Sinha, X. Wang, F. Cruz, and R. L. Edwards (2012b), The Global Paleomonsoon as seen through speleothem records from Asia and the Americas, *Climate Dynamics*, *39*(5), 1045-1062.

Cheng, H., P. Z. Zhang, C. Spötl, R. L. Edwards, Y. J. Cai, D. Z. Zhang, W. C. Sang, M. Tan, and Z. S. An (2012c), The climatic cyclicity in semiarid-arid central Asia over the past 500,000 years, *Geophysical Research Letters*, *39*(1), L01705.

Cheng, H., A. Sinha, F. W. Cruz, X. Wang, R. L. Edwards, F. M. d'Horta, C. C. Ribas, M. Vuille, L. D. Stott, and A. S. Auler (2013), Climate change patterns in Amazonia and biodiversity, *Nat Commun*, *4*, 1411.

Chiang, J. C. H., and C. M. Bitz (2005), Influence of high latitude ice cover on the marine Intertropical Convergence Zone, *Climate Dynamics*, *25*(5), 477-496.

Chiang, J. C. H., M. Biasutti, and D. S. Battisti (2003), Sensitivity of the Atlantic Intertropical Convergence Zone to Last Glacial Maximum boundary conditions, *Paleoceanography*, *18*(4), 1094.

Chiessi, C. M., S. Mulitza, A. Paul, J. Patzold, J. Groeneveld, and G. Wefer (2008), South Atlantic interocean exchange as the trigger for the Bolling warm event, *Geology*, 36(12), 919-922.

Clarke, F. W., Wheeler, W. C. (1922), The inorganic constituents of marine invertebrates, *USGS Prof. Pap.*, *124*(55).

Clauzet, G., I. Wainer, A. Lazar, E. Brady, and B. Otto-Bliesner (2007), A numerical study of the South Atlantic circulation at the Last Glacial Maximum, *Palaeogeography, Palaeoclimatology, Palaeoecology*, *253*(3-4), 509-528.

Clemens, S. C., W. L. Prell, and Y. Sun (2010), Orbital-scale timing and mechanisms driving Late Pleistocene Indo-Asian summer monsoons: Reinterpreting cave speleothem δ18O, *Paleoceanography*, *25*(4), PA4207.

Clement, A. C., and A. L. Gordon (1995), The absolute velocity field of Agulhas eddies and the Benguela Current, *Journal of Geophysical Research: Oceans*, *100*(C11), 22591-22601.

Cléroux, C., E. Cortijo; J.-C. Duplessy, R. Zahn (2007), Deep-dwelling foraminifera as thermocline temperature recorders, *Geochem. Geophys. Geosyst.*, *8*(4), Q04N11.

Cléroux, C., E. Cortijo, P. Anand, L. Labeyrie, F. Bassinot, N. Caillon, and J.-C. Duplessy (2008), Mg/Ca and Sr/Ca ratios in planktonic foraminifera: Proxies for upper water column temperature reconstruction, *Paleoceanography*, 23(3), PA3214.

Coats, A. W., and J. P. Redfern (1963), Thermogravimetric analysis. A review, *Analyst*, 88(1053), 906-924.

Collins, J. A., et al. (2011), Interhemispheric symmetry of the tropical African rainbelt over the past 23,000 years, *Nature Geosci*, *4*(1), 42-45.

Cortese, G., and A. Abelmann (2002), Radiolarian-based paleotemperatures during the last 160 kyr at ODP Site 1089 (Southern Ocean, Atlantic Sector), *Palaeogeography, Palaeoclimatology, Palaeoecology*, *182*(3-4), 259-286.

Costa, L. P. (2003), The historical bridge between the Amazon and the Atlantic Forest of Brazil: a study of molecular phylogeography with small mammals, *Journal of Biogeography*, *30*(1), 71-86.

Cox, P. M., R. A. Betts, M. Collins, P. P. Harris, C. Huntingford, and C. D. Jones (2004), Amazonian forest dieback under climate-carbon cycle projections for the 21st century, *Theor Appl Climatol*, *78*(1-3), 137-156.

Crowley, T. J. (1992), North Atlantic Deep Water cools the southern hemisphere, *Paleoceanography*, *7*(4), 489-497.

Crucifix, M. (2012), Traditional and novel approaches to palaeoclimate modelling, *Quaternary Science Reviews*, *57*(0), 1-16.

Cruz, F. W., S. J. Burns, I. Karmann, W. D. Sharp, M. Vuille, A. O. Cardoso, J. A. Ferrari, P. L. Silva Dias, and O. Viana (2005), Insolation-driven changes in atmospheric circulation over the past 116,000 years in subtropical Brazil, *Nature*, *434*(7029), 63-66.

Cruz, F. W. J., S. J. Burns, M. Jercinovic, I. Karmann, W. D. Sharp, and M. Vuille (2007), Evidence of rainfall variations in Southern Brazil from trace element ratios (Mg/Ca and Sr/Ca) in a Late Pleistocene stalagmite, *Geochimica et Cosmochimica Acta*, *71*(9), 2250-2263.

Cruz, F. W., M. Vuille, S. J. Burns, X. Wang, H. Cheng, M. Werner, R. Lawrence Edwards, I. Karmann, A. S. Auler, and H. Nguyen (2009a), Orbitally driven east-west antiphasing of South American precipitation, *Nature Geosci*, *2*(3), 210-214.

Cruz, F. W., X. Wang, A. Auler, M. Vuille, S. Burns, L. Edwards, I. Karmann, and H. Cheng (2009b), Orbital and Millennial-Scale Precipitation Changes in Brazil from Speleothem Records, in *Past Climate Variability in South America and Surrounding Regions*, edited by F. Vimeux, F. Sylvestre and M. Khodri, pp. 29-60, Springer Netherlands.

Curry, W. B., and D. W. Oppo (2005), Glacial water mass geometry and the distribution of d13C of ΕCO2 in the western Atlantic Ocean, *Paleoceanography*, *20*(1), PA1017.

da Costa, A. C. L., et al. (2010), Effect of 7 yr of experimental drought on vegetation dynamics and biomass storage of an eastern Amazonian rainforest, *New Phytologist*, *187*(3), 579-591.

da Silveira, I. C. A., L. B. de Miranda, and W. S. Brown (1994), On the origins of the North Brazil Current, *J. Geophys. Res.*, *99*(C11), 22501-22512.

Dansgaard, W., et al. (1993), Evidence for general instability of past climate from a 250-kyr ice-core record, *Nature*, 364(6434), 218-220.

de Abreu, L., F. t. F. Abrantes, N. J. Shackleton, P. C. Tzedakis, J. F. McManus, D. W. Oppo, and M. A. Hall (2005), Ocean climate variability in the eastern North Atlantic during interglacial marine isotope stage 11: A partial analogue to the Holocene?, *Paleoceanography*, *20*(3), PA3009.

De Deckker, P., M. Moros, K. Perner, and E. Jansen (2012), Influence of the tropics and southern westerlies on glacial interhemispheric asymmetry, *Nature Geosci*, *5*(4), 266-269.

de Ruijter, W. P. M., and D. B. Boudra (1985), The wind-driven circulation in the South Atlantic-Indian Ocean-I. Numerical experiments in a one-layer model, *Deep Sea Research Part A. Oceanographic Research Papers*, *32*(5), 557-574.

de Ruijter, W. P. M., A. Biastoch, S. S. Drijfhout, J. R. E. Lutjeharms, R. P. Matano, T. Pichevin, P. J. van Leeuwen, and W. Weijer (1999), Indian-Atlantic interocean exchange: Dynamics, estimation and impact, *J. Geophys. Res.*, *104*(C9), 20885-20910.

de Vargas, C., S. Renaud, H. Hilbrecht, and J. Pawlowski (2001), Pleistocene adaptive radiation in Globorotalia truncatulinoides: genetic, morphologic, and environmental evidence, *Paleobiology*, *27*(1), 104-125.

Dekens, P. S., D. W. Lea, D. K. Pak, and H. J. Spero (2002), Core top calibration of Mg/Ca in tropical foraminifera: Refining paleotemperature estimation, *Geochem. Geophys. Geosyst.*, *3*(4), 1022.

Delmonte, B., P. S. Andersson, H. Schöberg, M. Hansson, J. R. Petit, R. Delmas, D. M. Gaiero, V. Maggi, and M. Frezzotti (2010), Geographic provenance of aeolian dust in East Antarctica during Pleistocene glaciations: preliminary results from Talos Dome and comparison with East Antarctic and new Andean ice core data, *Quaternary Science Reviews*, *29*(1–2), 256-264.

Dencausse, G., M. Arhan, and S. Speich (2010), Routes of Agulhas rings in the southeastern Cape Basin, *Deep Sea Research Part I: Oceanographic Research Papers*, *57*(11), 1406-1421.

Denman, K. L., et al. (2007), Couplings Between Changes in the Climate System and Biogeochemistry, in *Climate Change 2007: The Physical Science Basis. Contribution of Working Group I to the Fourth Assessment Report of the Intergovernmental Panel on Climate Change*, edited by S. Solomon, et al., Cambridge University Press, Cambridge, United Kingdom and New York, NY, USA.

Denton, G. H., R. F. Anderson, J. R. Toggweiler, R. L. Edwards, J. M. Schaefer, and A. E. Putnam (2010), The Last Glacial Termination, *Science*, *328*(5986), 1652-1656.

Deuser, W. G., E. H. Ross, C. Hemleben, and M. Spindler (1981), Seasonal changes in species composition, numbers, mass, size, and isotopic composition of planktonic foraminifera settling into the deep sargasso sea, *Palaeogeography, Palaeoclimatology, Palaeoecology*, *33*(1-3), 103-127.

Dickson, A. J., M. J. Leng, M. A. Maslin, H. J. Sloane, J. Green, J. A. Bendle, E. L. McClymont, and R. D. Pancost (2010), Atlantic overturning circulation and Agulhas leakage influences on southeast Atlantic upper ocean hydrography during marine isotope stage 11, *Paleoceanography*, *25*(3), PA3208.

Doglioli, A. M., M. Veneziani, B. Blanke, S. Speich, and A. Griffa (2006), A Lagrangian analysis of the Indian-Atlantic interocean exchange in a regional model, *Geophysical Research Letters*, *33*(14).

Dokken, T. M., K. H. Nisancioglu, C. Li, D. S. Battisti, and C. Kissel (2013), Dansgaard-Oeschger cycles: Interactions between ocean and sea ice intrinsic to the Nordic seas, *Paleoceanography*, 28(3), 491-502.

Dong, S., S. Garzoli, M. Baringer, C. Meinen, and G. Goni (2009), Interannual variations in the Atlantic meridional overturning circulation and its relationship with the net northward heat transport in the South Atlantic, *Geophysical Research Letters*, 36(20), L20606.

Dong, S., S. Garzoli, and M. Baringer (2011), The Role of Interocean Exchanges on Decadal Variations of the Meridional Heat Transport in the South Atlantic, *Journal of Physical Oceanography*, *41*(8), 1498-1511.

Donners, J., and S. S. Drijfhout (2004), The Lagrangian View of South Atlantic Interocean Exchange in a Global Ocean Model Compared with Inverse Model Results, *Journal of Physical Oceanography*, *34*(5), 1019-1035.

Douglas, R. G., and S. M. Savin (1978), Oxygen isotopic evidence for the depth stratification of tertiary and cretaceous planktic foraminifera, *Marine Micropaleontology*, *3*(2), 175-196.

Drysdale, R. N., J. C. Hellstrom, G. Zanchetta, A. E. Fallick, M. F. Sánchez Goñi, I. Couchoud, J. McDonald, R. Maas, G. Lohmann, and I. Isola (2009), Evidence for Obliquity Forcing of Glacial Termination II, *Science*, *325*(5947), 1527-1531.

Duplessy, J. C., Blanc, P.L., Be¤, A.W.H. (1981), Oxygen-18 enrichment of planktonic foraminifera due to gametogenic calcification below the euphotic zone, *Science*, *213*, 1247-1250.

Duplessy, J. C., N. J. Shackleton, R. G. Fairbanks, L. Labeyrie, D. Oppo, and N. Kallel (1988), Deepwater Source Variations During the Last Climatic Cycle and Their Impact on the Global Deepwater Circulation, Paleoceanography, 3(3), 343-360.

Durgadoo, J. V., B. R. Loveday, C. J. C. Reason, P. Penven, and A. Biastoch (2013), Agulhas Leakage Predominantly Responds to the Southern Hemisphere Westerlies, *Journal of Physical Oceanography*, *43*(10), 2113-2131.

Eggins, S., Patrick De Deckker, John Marshall (2003), Mg/Ca variation in planktonic foraminifera tests: implications for reconstructing palaeo-seawater temperature and habitat migration, *Earth and Planetary Science Letters*, 212(3-4), 291-306.

Elderfield, H., and G. Ganssen (2000), Past temperature and δ18O of surface ocean waters inferred from foraminiferal Mg/Ca ratios, *Nature*, 405 (6785), pp. 442-445.

Elderfield, H., P. Ferretti, M. Greaves, S. Crowhurst, I. N. McCave, D. Hodell, and A. M. Piotrowski (2012), Evolution of Ocean Temperature and Ice Volume Through the Mid-Pleistocene Climate Transition, *Science*, *337*(6095), 704-709.

Emiliani, C. (1955), Pleistocene Temperatures, *Journal of Geology*, *63*, 538-578.

Epstein, S., R. Buchsbaum, H. Lowenstam, and H. C. Urey (1951), Carbonate-water isotopic temperature scale, *Geological Society of America Bulletin*, *62*(4), 417-426.

Erez, J., and S. Honjo (1981), Comparison of isotopic composition of planktonic foraminifera in plankton tows, sediment traps and sediments, *Palaeogeography, Palaeoclimatology, Palaeoecology*, *33*(1-3), 129-156.

Erez, J., & Luz, B. (1982), Temperature control of oxygen-isotope fractionation of cultured planktonic foraminifera, *Nature*, *297*, 220 - 222.

Fairbanks, R. G., P. H. Wiebe, and A. W. H. Bé (1980), Vertical Distribution and Isotopic Composition of Living Planktonic Foraminifera in the Western North Atlantic, *Science*, *207*(4426), 61-63.

Falkowski, P., et al. (2000), The Global Carbon Cycle: A Test of Our Knowledge of Earth as a System, *Science*, 290(5490), 291-296.

Feldmeijer, W., B. Metcalfe, P. Scussolini, and K. Arthur (2013), The effect of chemical pretreatment of sediment upon foraminiferal-based proxies, *Geochemistry, Geophysics, Geosystems*, 14(10), 3996-4014.

Fiedel, S. J. (2011), The mysterious onset of the Younger Dryas, *Quaternary International*, *242*(2), 262-266.

Flores, J.-A., R. Gersonde, and F. J. Sierro (1999), Pleistocene fluctuations in the Agulhas Current Retroflection based on the calcareous plankton record, *Marine Micropaleontology*, *37*, 1-22.

Franzese, A. M., S. R. Hemming, S. L. Goldstein, and R. F. Anderson (2006), Reduced Agulhas Leakage during the Last Glacial Maximum inferred from an integrated provenance and flux study, *Earth and Planetary Science Letters*, *250*(1-2), 72-88.

Franzese, A. M., S. R. Hemming, and S. L. Goldstein (2009), Use of strontium isotopes in detrital sediments to constrain the glacial position of the Agulhas Retroflection, *Paleoceanography*, *24*(2), PA2217.

Friedrich, O. (2010), Benthic foraminifera and their role to decipher paleoenvironment during mid-Cretaceous Oceanic Anoxic Events – the “anoxic benthic foraminifera” paradox, *Revue de Micropaléontologie*, 53(3), 175-192.

Frierson, D. M. W., Y.-T. Hwang, N. S. Fuckar, R. Seager, S. M. Kang, A. Donohoe, E. A. Maroon, X. Liu, and D. S. Battisti (2013), Contribution of ocean overturning circulation to tropical rainfall peak in the Northern Hemisphere, *Nature Geosci*, *6*(11), 940-944.

Frumkin, A., D. C. Ford, and H. P. Schwarcz (2000), Paleoclimate and vegetation of the Last Glacial Cycles in Jerusalem from a Speleothem Record, *Global Biogeochemical Cycles*, *14*(3), 863-870.

Gallup, C. D., H. Cheng, F. W. Taylor, and R. L. Edwards (2002), Direct Determination of the Timing of Sea Level Change During Termination II, *Science*, *295*(5553), 310-313.

Ganopolski, A., and D. M. Roche (2009), On the nature of lead–lag relationships during glacial–interglacial climate transitions, *Quaternary Science Reviews*, *28*(27–28), 3361-3378.

Ganssen, G., and S. R. Troelstra (1987), Paleoenvironmental changes from stable isotopes in planktonic foraminifera from Eastern Mediterranean sapropels, *Marine Geology*, *75*(1-4), 221-230.

Ganssen, G., F. Peeters, B. Metcalfe, P. Anand, S. Jung, D. Kroon, and G.-J. Brummer (2011), Quantifying sea surface temperature ranges of the Arabian Sea for the past 20 000 years, *Clim. Past Discuss.*, *6*, 2795–2814.

Garzoli, S. L., and A. L. Gordon (1996), Origins and variability of the Benguela Current, *J. Geophys. Res.*, *101*(C1), 897-906.

Garzoli, S. L., and R. Matano (2011), The South Atlantic and the Atlantic Meridional Overturning Circulation, *Deep Sea Research Part II: Topical Studies in Oceanography*, *58*(17-18), 1837-1847.

Gherardi, J. M., L. Labeyrie, J. F. McManus, R. Francois, L. C. Skinner, and E. Cortijo (2005), Evidence from the Northeastern Atlantic basin for variability in the rate of the meridional overturning circulation through the last deglaciation, *Earth and Planetary Science Letters*, *240*(3-4), 710-723.

Giulivi, C. F., A.L. Gordon (2006), Isopycnal displacements within the Cape Basin thermocline as revealed by the Hydrographic Data Archive, *Deep-Sea Research Part I-Oceanographic Research Papers*, *53*(8), 1285-1300.

Goni, G. J., S. L. Garzoli, A. J. Roubicek, D. B. Olson, and O. B. Brown (1997), Agulhas ring dynamics from TOPEX/POSEIDON satellite altimeter data, *Journal of Marine Research*, *55*(5), 861-883.

Goni, G. J., F. Bringas, and P. N. DiNezio (2011), Observed low frequency variability of the Brazil Current front, *J. Geophys. Res.*, *116*(C10), C10037.

Gordon, A. L. (1986), Interocean Exchange of Thermocline Water, *J. Geophys. Res.*, *91*(C4), 5037-5046.

Gordon, A. L., and W. F. Haxby (1990), Agulhas Eddies Invade the South Atlantic: Evidence From Geosat Altimeter and Shipboard Conductivity-Temperature-Depth Survey, *J. Geophys. Res.*, *95*(C3), 3117-3125.

Gordon, A. L., J. R. E. Lutjeharms, and M. L. Gründlingh (1987), Stratification and circulation at the Agulhas Retroflection, *Deep Sea Research Part A. Oceanographic Research Papers*, 34(4), 565-599.

Gordon, A. L., R. F. Weiss, W. M. Smethie, Jr., and M. J. Warner (1992), Thermocline and Intermediate Water Communication Between the South Atlantic and Indian Oceans, *J. Geophys. Res.*, *97*(C5), 7223-7240.

Gordon, A. L. (2003), The brawniest retroflection, *Nature*, *421*(6926), 904-905.

Gouzy, A., B. Malaizé, C. Pujol, and K. Charlier (2004), Climatic “pause” during Termination II identified in shallow and intermediate waters off the Iberian margin, *Quaternary Science Reviews*, *23*(14–15), 1523-1528.

Govin, A., C. M. Chiessi, M. Zabel, A. O. Sawakuchi, D. Heslop, T. Hörner, Y. Zhang, and S. Mulitza (2013), Terrigenous input off northern South America driven by changes in Amazonian climate and the North Brazil Current retroflection during the last 250 ka, *Clim. Past Discuss.*, 9(5), 5855-5898.

Graham, R. M., A. M. de Boer, K. J. Heywood, M. R. Chapman, and D. P. Stevens (2012), Southern Ocean fronts: Controlled by wind or topography?, *Journal of Geophysical Research: Oceans*, *117*(C8), C08018.

Grant, K. M., E. J. Rohling, M. Bar-Matthews, A. Ayalon, M. Medina-Elizalde, C. B. Ramsey, C. Satow, and A. P. Roberts (2012), Rapid coupling between ice volume and polar temperature over the past 150,000 years, *Nature*, *491*(7426), 744-747.

Greaves, M., S. Barker, C. Daunt, and H. Elderfield (2005), Accuracy, standardization, and interlaboratory calibration standards for foraminiferal Mg/Ca thermometry, *Geochem. Geophys. Geosyst.*, *6*(2), Q02D13.

Groeneveld, J., and C. M. Chiessi (2011), Mg/Ca of Globorotalia inflata as a recorder of permanent thermocline temperatures in the South Atlantic, *Paleoceanography*, *26*(2), PA2203.

Haley, B. A., and G. P. Klinkhammer (2002), Development of a flow-through system for cleaning and dissolving foraminiferal tests, *Chemical Geology*, 185(1-2), 51-69.

Hall, A., and S. Manabe (1999), The Role of Water Vapor Feedback in Unperturbed Climate Variability and Global Warming, *Journal of Climate*, 12(8), 2327-2346.

Hall, A. (2004), The Role of Surface Albedo Feedback in Climate, *Journal of Climate*, 17(7), 1550-1568.

Hall, C., and J. R. E. Lutjeharms (2011), Cyclonic eddies identified in the Cape Basin of the South Atlantic Ocean, *Journal of Marine Systems*, *85*(1–2), 1-10.

Hansen, B., S. Østerhus, D. Quadfasel, and W. Turrell (2004), Already the Day After Tomorrow?, *Science*, 305(5686), 953-954.

Hastenrath, S. (1991), *Climate dynamics of the tropics*, 488 pp., Kluwer Academic.

Hastenrath, S., and L. Greischar (1993), Circulation mechanisms related to northeast Brazil rainfall anomalies, *Journal of Geophysical Research: Atmospheres*, *98*(D3), 5093-5102.

Haug, G. H., K. A. Hughen, D. M. Sigman, L. C. Peterson, and U. Röhl (2001), Southward Migration of the Intertropical Convergence Zone Through the Holocene, *Science*, *293*(5533), 1304-1308.

Hays, J. D., Imbrie, J., Shackleton, N.J. (1976a), Variations in the Earth's Orbit: Pacemaker of the Ice Ages, *Science*, *194*(4270), 1121-1132.

Hays, J. D., J.A. Lozano, N. Shackleton, G. Irving (1976b), Reconstruction of the Atlantic andWestern Indian Ocean sectors of the 18,000 B.P. Antarctic Ocean, in *Geol. Soc. Amer. Mem*, edited by R. M. Cline, J.D. Hays, pp. 337–372, Geol. Soc. Amer., Boulder.

Hecht, A. D., and S. M. Savin (1972), Phenotypic variation and oxygen isotope ratios in Recent planktonic foraminifera, *The Journal of Foraminiferal Research*, *2*(2), 55-67.

Hemleben, C., et al. (1985), Field and laboratory studies on the ontogeny and ecology of some globorotaliid species from the Sargasso sea off Bermuda, *Journal of Foraminiferal Research*, *15*(4), 254-272.

Hemleben, C., M. Spindler, and O. R. Anderson (1989), *Modern Planktonic Foraminifera*, 363 pp., Springer Verlag, Berlin.

Henderson, G. M., and N. C. Slowey (2000), Evidence from U-Th dating against Northern Hemisphere forcing of the penultimate deglaciation, *Nature*, *404*(6773), 61-66.

Hesse, T., M. Butzin, T. Bickert, and G. Lohmann (2011), A model-data comparison of delta13C in the glacial Atlantic Ocean, *Paleoceanography*, *26*(3), PA3220.

Hodell, D. A., C. D. Charles, and U. S. Ninnemann (2000), Comparison of interglacial stages in the South Atlantic sector of the southern ocean for the past 450 kyr: implifications for Marine Isotope Stage (MIS) 11, *Global and Planetary Change*, *24*(1), 7-26.

Hönisch, B., K. A. Allen, D. W. Lea, H. J. Spero, S. M. Eggins, J. Arbuszewski, P. deMenocal, Y. Rosenthal, A. D. Russell, and H. Elderfield (2013), The influence of salinity on Mg/Ca in planktic foraminifers – Evidence from cultures, core-top sediments and complementary δ18O, *Geochimica et Cosmochimica Acta*, *121*(0), 196-213.

Howard, W. R., and W. L. Prell (1994), Late Quaternary CaCO3 production and preservation in the Southern Ocean: Implications for oceanic and atmospheric carbon cycling, *Paleoceanography*, *9*(3), 453-482.

Huang, E., S. Mulitza, A. Paul, J. Groeneveld, S. Steinke, and M. Schulz (2012), Response of eastern tropical Atlantic central waters to Atlantic meridional overturning circulation changes during the Last Glacial Maximum and Heinrich Stadial 1, *Paleoceanography*, *27*(3), PA3229.

Hughen, K. A., J. T. Overpeck, L. C. Peterson, and S. Trumbore (1996), Rapid climate changes in the tropical Atlantic region during the last deglaciation, *Nature*, *380*(6569), 51-54.

Hut, G. (1987), Consultants' group meeting on stable isotope reference samples for geochemical and hydrological investigations. Report to the Director General*Rep.*, 42 pp, International Atomic Energy Agency, Vienna.

Hutson, W. H. (1980), Bioturbation of deep-sea sediments: Oxygen isotopes and stratigraphic uncertainty, *Geology*, *8*(3), 127-130.

Huybers, P. (2007), Glacial variability over the last two million years: an extended depth-derived agemodel, continuous obliquity pacing, and the Pleistocene progression, *Quaternary Science Reviews*, *26*(1-2), 37-55.

Huybers, P. (2011), Combined obliquity and precession pacing of late Pleistocene deglaciations, *Nature*, *480*(7376), 229-232.

Huybers, P., and C. Wunsch (2004), A depth-derived Pleistocene age model: Uncertainty estimates, sedimentation variability, and nonlinear climate change, *Paleoceanography*, *19*(1), PA1028.

Imbrie, J., J. D. Hays, D. G. Martinson, A. McIntyre, A. C. Mix, J. J. Morley, N. G. Pisias, W. L. Prell, and N. J. Shackleton (1984), The orbital theory of Pleistocene climate: Support from a revised chronology, of the marine $d^{18}O$ record, *In Milankovitch and Climate, part 1. Edited by A. Berger*, 269-305.

Ishimura, T., Tsunogai. U., and Nakagawa, F. (2008), Grain-scale heterogeneities in the stable carbon and oxygen isotopic compositions of the international standard calcite materials (NBS 19, NBS 18, IAEA-CO-1, and IAEA-CO-8), *Rapid Communications in Mass Spectrometry*, *22*, 1925-1932.

Ivanochko, T. S., R. S. Ganeshram, G.-J. A. Brummer, G. Ganssen, S. J. A. Jung, S. G. Moreton, and D. Kroon (2005), Variations in tropical convection as an amplifier of global climate change at the millennial scale, *Earth and Planetary Science Letters*, *235*(1–2), 302-314.

Jaeschke, A., C. Rühlemann, H. Arz, G. Heil, and G. Lohmann (2007), Coupling of millennial-scale changes in sea surface temperature and precipitation off northeastern Brazil with high-latitude climate shifts during the last glacial period, *Paleoceanography*, *22*(4), PA4206.

Jansen, J. H. F., A. Kuijpers, and S. R. Troelstra (1986), A Mid-Brunhes Climatic Event: Long-Term Changes in Global Atmosphere and Ocean Circulation, *Science*, *232*(4750), 619-622.

Jansen, J. H. F., Van der Gast, S. J., Kostner, B., and Vaars, A. (1992), CORTEX, an XRF-scanner for chemical analyses of sediment cores., GEO-MAR Reports, 15.

Jansen, E., et al. (2007), Palaeoclimate, in *Climate Change 2007: The Physical Science Basis. Contribution of Working Group I to the Fourth Assessment Report of the Intergovernmental Panel on Climate Change*, edited by S. Solomon, et al., Cambridge, United Kingdom and New York, NY, USA.

Jennerjahn, T. C., V. Ittekkot, H. W. Arz, H. Behling, J. Pätzold, and G. Wefer (2004), Asynchronous Terrestrial and Marine Signals of Climate Change During Heinrich Events, *Science*, *306*(5705), 2236-2239.

Jouzel, J., et al. (2007), Orbital and Millennial Antarctic Climate Variability over the Past 800,000 Years, *Science*, *317*(5839), 793-796.

Kanner, L. C., S. J. Burns, H. Cheng, and R. L. Edwards (2012), High-Latitude Forcing of the South American Summer Monsoon During the Last Glacial, *Science*, *335*(6068), 570-573.

Kasper, S., M. T. J. van der Meer, A. Mets, R. Zahn, J. S. Sinninghe Damsté, and S. Schouten (2014), Salinity changes in the Agulhas leakage area recorded by stable hydrogen isotopes of C_{37} alkenones during Termination I and II, *Clim. Past*, 10(1), 251-260.

Katz, M. E., B. S. Cramer, A. Franzese, B. Honisch, K. G. Miller, Y. Rosenthal, and J. D. Wright (2010), Traditional and emerging geochemical proxies in foraminifera, *Journal of Foraminiferal Research*, 40(2), 165-192.

Keigwin, L. (1982), Isotopic Paleoceanography of the Caribbean and East Pacific: Role of Panama Uplift in Late Neogene Time, *Science*, 217(4557), 350-353.

Kelly, M. J., R. L. Edwards, H. Cheng, D. Yuan, Y. Cai, M. Zhang, Y. Lin, and Z. An (2006), High resolution characterization of the Asian Monsoon between 146,000 and 99,000 years B.P. from Dongge Cave, China and global correlation of events surrounding Termination II, *Palaeogeography, Palaeoclimatology, Palaeoecology*, *236*(1-2), 20-38.

Killingley, J. S., R. F. Johnson, and W. H. Berger (1981), Oxygen and carbon isotopes of individual shells of planktonic foraminifera from Ontong-Java plateau, equatorial pacific, Palaeogeography, Palaeoclimatology, Palaeoecology, 33(1-3), 193-204.

Kim, S.-T., and J. R. O'Neil (1997), Equilibrium and nonequilibrium oxygen isotope effects in synthetic carbonates, *Geochimica et Cosmochimica Acta*, *61*(16), 3461-3475.

KIsakürek, B., A. Eisenhauer, F. Böhm, D. Garbe-Schönberg, and J. Erez (2008), Controls on shell Mg/Ca and Sr/Ca in cultured planktonic foraminiferan, *Globigerinoides ruber* (white), *Earth and Planetary Science Letters*, *273*(3-4), 260-269.

Kleinen, T., T. Osborn, and K. Briffa (2009), Sensitivity of climate response to variations in freshwater hosing location, *Ocean Dynamics*, 59(3), 509-521.

Knorr, G., and G. Lohmann (2003), Southern Ocean origin for the resumption of Atlantic thermohaline circulation during deglaciation, *Nature*, *424*(6948), 532-536.

Knorr, G., and G. Lohmann (2007), Rapid transitions in the Atlantic thermohaline circulation triggered by global warming and meltwater during the last deglaciation, *Geochemistry, Geophysics, Geosystems*, *8*(12), Q12006.

Knutti, R., J. Fluckiger, T. F. Stocker, and A. Timmermann (2004), Strong hemispheric coupling of glacial climate through freshwater discharge and ocean circulation, *Nature*, *430*(7002), 851-856.

Kohfeld, K. E., R. M. Graham, A. M. de Boer, L. C. Sime, E. W. Wolff, C. Le Quéré, and L. Bopp (2013), Southern Hemisphere westerly wind changes during the Last Glacial Maximum: paleo-data synthesis, *Quaternary Science Reviews*, *68*(0), 76-95.

Koutavas, A., P. B. deMenocal, G. C. Olive, and J. Lynch-Stieglitz (2006), Mid-Holocene El Niño Southern Oscillation (ENSO) attenuation revealed by individual foraminifera in eastern tropical Pacific sediments, *Geology*, *34*(12), 993-996.

Kozdon, R., T. Ushikubo, N. T. Kita, M. Spicuzza, and J. W. Valley (2009), Intratest oxygen isotope variability in the planktonic foraminifer N. pachyderma: Real vs. apparent vital effects by ion microprobe, *Chemical Geology*, *258*(3-4), 327-337.

Kuhlbrodt, T., A. Griesel, M. Montoya, A. Levermann, M. Hofmann, and S. Rahmstorf (2007), On the driving processes of the Atlantic meridional overturning circulation, *Reviews of Geophysics*, 45(2), RG2001.

Kuroyanagi, A., M. Tsuchiya, H. Kawahata, and H. Kitazato (2008), The occurrence of two genotypes of the planktonic foraminifer *Globigerinoides ruber* (white) and paleo-environmental implications, *Marine Micropaleontology*, *68*(3-4), 236-243.

Kutzbach, J. E., W. F. Ruddiman, and W. L. Prell (1997), Possible effects of Cenozoic uplift and CO_2 lowering on global and regional hydrology, in Tectonic Uplift and Climate Change, edited by W. F. Ruddiman, pp. 149-170, Plenum Publishing Corporation, New York.

Kutzbach, J. E., X. Liu, Z. Liu, and G. Chen (2008), Simulation of the evolutionary response of global summer monsoons to orbital forcing over the past 280,000 years, *Climate Dynamics*, *30*(6), 567-579.

Lagabrielle, Y., Y. Goddéris, Y. Donnadieu, J. Malavieille, and M. Suarez (2009), The tectonic history of Drake Passage and its possible impacts on global climate, *Earth and Planetary Science Letters*, 279(3–4), 197-211.

Lambert, F., B. Delmonte, J. R. Petit, M. Bigler, P. R. Kaufmann, M. A. Hutterli, T. F. Stocker, U. Ruth, J. P. Steffensen, and V. Maggi (2008), Dust-climate couplings over the past 800,000[thinsp]years from the EPICA Dome C ice core, *Nature*, *452*(7187), 616-619.

Lambert, F., M. Bigler, J. P. Steffensen, M. Hutterli, and H. Fischer (2012), Centennial mineral dust variability in high-resolution ice core data from Dome C, Antarctica, *Clim. Past*, *8*(2), 609-623.

Lamy, F., J. Kaiser, H. W. Arz, D. Hebbeln, U. Ninnemann, O. Timm, A. Timmermann, and J. R. Toggweiler (2007), Modulation of the bipolar seesaw in the Southeast Pacific during Termination 1, *Earth and Planetary Science Letters*, *259*(3-4), 400-413.

Landais, A., et al. (2013), Two-phase change in CO2, Antarctic temperature and global climate during Termination II, *Nature Geosci*, 6, 1062–1065.

Larsen, J. C. (1992), Transport and Heat Flux of the Florida Current at 27 degrees N Derived from Cross-Stream Voltages and Profiling Data: Theory and Observations, *Philosophical Transactions: Physical Sciences and Engineering*, 338(1650), 169-236.

Laskar, J., P. Robutel, F. Joutel, M. Gastineau, A. C. M. Correia, and B. Levrard (2004), A long-term numerical solution for the insolation quantities of the Earth, *A&A*, 428(1), 261-285.

Lea, D. W. (2003), Elemental and isotopic proxies of marine temperatures, in *The oceans and marine geochemistry*, edited, pp. 365-390, Elsevier, New York.

Lea, D. W., D. K. Pak, and H. J. Spero (2000), Climate Impact of Late Quaternary Equatorial Pacific Sea Surface Temperature Variations, *Science*, *289*(5485), 1719-1724.

Lea, D. W., T. A. Mashiotta, and H. J. Spero (1999), Controls on magnesium and strontium uptake in planktonic foraminifera determined by live culturing, *Geochimica et Cosmochimica Acta*, *63*(16), 2369-2379.

Ledru, M.-P., D.-D. Rousseau, J. Cruz, F.W., C. Riccomini, I. Karmann, and L. Martin (2005), Paleoclimate changes during the last 100,000 yr from a record in the Brazilian Atlantic rainforest region and interhemispheric comparison, *Quaternary Research, 64*(3), 444-450.

Leduc, G., L. Vidal, O. Cartapanis, and E. Bard (2009), Modes of eastern equatorial Pacific thermocline variability: Implications for ENSO dynamics over the last glacial period, *Paleoceanography*, *24*(3), PA3202.

Lee, S.-Y., and C. J. Poulsen (2006), Sea ice control of Plio-Pleistocene tropical Pacific climate evolution, *Earth and Planetary Science Letters*, *248*(1-2), 253-262.

Lee, S.-Y., J. C. H. Chiang, K. Matsumoto, and K. S. Tokos (2011), Southern Ocean wind response to North Atlantic cooling and the rise in atmospheric CO_2: Modeling perspective and paleoceanographic implications, *Paleoceanography*, *26*(PA1214).

LeGrande, A. N., and G. A. Schmidt (2006), Global gridded data set of the oxygen isotopic composition in seawater, *Geophys. Res. Lett.*, *33*(12), L12604.

LeGrande, A. N., J. Lynch-Stieglitz, and E. C. Farmer (2004), Oxygen isotopic composition of Globorotalia truncatulinoides as a proxy for intermediate depth density, *Paleoceanography*, *19*(PA4025).

Li, X., X. Liu, L. Qiu, Z. An, and Z.-Y. Yin (2013), Transient simulation of orbital-scale precipitation variation in monsoonal East Asia and arid central Asia during the last 150 ka, *Journal of Geophysical Research: Atmospheres*, *118*(14).

Lisiecki, L. E., and M. E. Raymo (2005), A Pliocene-Pleistocene stack of 57 globally distributed benthic delta18O records, *Paleoceanography*, *20*(1), PA1003.

Liu, T., and Z. Ding (1998), Chinese leoss and the paleomonsoon, *Annual Review of Earth and Planetary Sciences, 26*(1), 111-145.

Liu, Z., et al. (2009), Transient Simulation of Last Deglaciation with a New Mechanism for Bølling-Allerød Warming, *Science*, *325*(5938), 310-314.

Locarnini, R. A., A. V. Mishonov, J. I. Antonov, T. P. Boyer, H. E. Garcia, O. K. Baranova, M. M. Zweng, and D. R. Johnson, (2010), *World Ocean Atlas 2009, Volume 1: Temperature*, 184 pp., NOAA Atlas NESDIS 68, U.S. Government Printing Office, Washington, D.C.

Lohmann, G. P., and P. N. Schweitzer (1990), *Globorotalia Truncatulinoides*' Growth and Chemistry as Probes of the Past Thermocline: 1. Shell Size, *Paleoceanography*, *5*(1), 55-75.

Lonçaric, N., F. J. C. Peeters, D. Kroon, and G.-J. A. Brummer (2006), Oxygen isotope ecology of recent planktic foraminifera at the central Walvis Ridge (SE Atlantic), *Paleoceanography*, *21*(3), PA3009.

Lonçaric, N., J. van Iperen, D. Kroon, and G.-J. A. Brummer (2007), Seasonal export and sediment preservation of diatomaceous, foraminiferal and organic matter mass fluxes in a trophic gradient across the SE Atlantic, *Progress In Oceanography*, *73*(1), 27-59.

Lopes dos Santos, R. A., M. Prange, I. S. Castaneda, E. Schefuss, S. Mulitza, M. Schulz, E. M. Niedermeyer, J. S. Sinninghe Damste, and S. Schouten (2010), Glacial-Interglacial variability in Atlantic meridional overturning circulation and thermocline adjustments in the tropical North Atlantic, *Earth and Planetary Science Letters*, *300*(3-4), 407-414.

Lototskaya, A., and G. M. Ganssen (1999), The structure of Termination II (penultimate deglaciation and Eemian) in the North Atlantic, *Quaternary Science Reviews*, *18*(14), 1641-1654.

Lüthi, D., et al. (2008), High-resolution carbon dioxide concentration record 650,000-800,000 years before present, *Nature*, 453(7193), 379-382.

Lutjeharms, J. R. E., and J. Cooper (1996), Interbasin leakage through Agulhas current filaments, *Deep Sea Research Part I: Oceanographic Research Papers*, *43*(2), 213-238.

Lutjeharms, J. R. E. (2006), *The Agulhas Current*, Springer, Berlin. Germany.

Lutjeharms, J. R. E. (2007), Three decades of research on the greater Agulhas Current, *Ocean Sci.*, *3*(1), 129-147.

Lynch-Stieglitz, J., W. B. Curry, and N. Slowey (1999), A Geostrophic Transport Estimate for the Florida Current from the Oxygen Isotope Composition of Benthic Foraminifera, *Paleoceanography*, *14*(3), 360-373.

Lynch-Stieglitz, J., et al. (2007), Atlantic Meridional Overturning Circulation During the Last Glacial Maximum, *Science*, *316*(5821), 66-69.

Madec, G. (2008): *NEMO ocean engine*. Note du Pole de modeisation de l'Institut Pierre-Simon Laplace, France, 27, ISSN No 12.

Marchal, O., R. François, T. F. Stocker, and F. Joos (2000), Ocean thermohaline circulation and sedimentary 231Pa/230Th ratio, *Paleoceanography*, 15(6), 625-641.

Marino, G., R. Zahn, M. Ziegler, C. Purcell, G. Knorr, I. R. Hall, P. Ziveri, and H. Elderfield (2013), Agulhas salt-leakage oscillations during abrupt climate changes of the Late Pleistocene, *Paleoceanography*, *28*(3), 599-606.

Marsh, R., W. Hazeleger, A. Yool, and E. J. Rohling (2007), Stability of the thermohaline circulation under millennial CO_2 forcing and two alternative controls on Atlantic salinity, *Geophys. Res. Lett.*, *34*(3), L03605.

Marshall, J., and F. Schott (1999), Open-ocean convection: Observations, theory, and models, *Reviews of Geophysics*, *37*(1), 1-64.

Martin, P. A., and D. W. Lea (2002), A simple evaluation of cleaning procedures on fossil benthic foraminiferal Mg/Ca, *Geochem. Geophys. Geosyst.*, *3*(10), 8401.

Martìnez-Garcia, A., A. Rosell-Melè, W. Geibert, R. Gersonde, P. Masquè, V. Gaspari, and C. Barbante (2009), Links between iron supply, marine productivity, sea surface temperature, and CO_2 over the last 1.1 Ma, *Paleoceanography*, *24*(1), PA1207.

Martínez-Méndez, G., R. Zahn, I. R. Hall, F. J. C. Peeters, L. D. Pena, I. Cacho, and C. Negre (2010), Contrasting multiproxy reconstructions of surface ocean hydrography in the Agulhas Corridor and implications for the Agulhas Leakage during the last 345,000 years, *Paleoceanography*, *25*(4), PA4227.

Martinson, D. G., N. G. Pisias, J. D. Hays, J. Imbrie, T. C. Moore Jr, and N. J. Shackleton (1987), Age dating and the orbital theory of the ice ages: Development of a high-resolution 0 to 300,000-year chronostratigraphy, *Quaternary Research*, *27*(1), 1-29.

Martrat, B., J. O. Grimalt, N. J. Shackleton, L. de Abreu, M. A. Hutterli, and T. F. Stocker (2007), Four

Climate Cycles of Recurring Deep and Surface Water Destabilizations on the Iberian Margin, *Science*, *317*(5837), 502-507.

Mashiotta, T. A., Lea, D.W., Spero, H.J (1999), Glacial-interglacial changes in Subantarctic sea surface temperature and delta18O-water using foraminiferal Mg, *Earth and Planetary Science Letters*, *170*, 417-432.

Matano, R. P., and E. J. Beier (2003), A kinematic analysis of the Indian/Atlantic interocean exchange, *Deep Sea Research Part II: Topical Studies in Oceanography*, *50*(1), 229-249.

McConnell, M. C., and R. C. Thunell (2005), Calibration of the planktonic foraminiferal Mg/Ca paleothermometer: Sediment trap results from the Guaymas Basin, Gulf of California, *Paleoceanography*, *20*(2), PA2016.

McKenna, V. S., and W. L. Prell (2004), Calibration of the Mg/Ca of *Globorotalia truncatulinoides* (R) for the reconstruction of marine temperature gradients, *Paleoceanography*, *19*(2), PA2006.

McManus, J. F., D. W. Oppo, and J. L. Cullen (1999), A 0.5-Million-Year Record of Millennial-Scale Climate Variability in the North Atlantic, *Science*, *283*(5404), 971-975.

McManus, J. F., R. Francois, J.-M. Gherardi, L. D. Keigwin, and S. Brown-Leger (2004), Collapse and rapid resumption of Atlantic meridional circulation linked to deglacial climate changes, *Nature*, *428*(6985), 834-837.

Meckler, A. N., M. O. Clarkson, K. M. Cobb, H. Sodemann, and J. F. Adkins (2012), Interglacial Hydroclimate in the Tropical West Pacific Through the Late Pleistocene, *Science*, *336*(6086), 1301-1304.

Milanković , M. (1941), *Kanon der Erdbestrahlung und seine Andwendung auf das Eiszeitenproblem*, 633 pp., Royal Serbian Academy Special Publication, Belgrade.

Mix, A. C., W. F. Ruddiman, and A. McIntyre (1986), Late Quaternary paleoceanography of the Tropical Atlantic, 1: Spatial variability of annual mean sea-surface temperatures, 0-20,000 years B.P, *Paleoceanography*, *1*(1), 43-66.

Mix, A. C., N.G. Pisias, W. Rugh, J. Wilson, A. Morey, T. Hagelberg (1995), Benthic foraminiferal stable isotope record form Site 849, 0-5 Ma: Local and global climate changes. , in *Proc. ODP, Scientific Results*, edited by P. N.G., L. Mayer, T. Janecek, A. Palmer-Julson, T.H. vanAndel, pp. 371-412, Ocean Drilling Program, College Station, TX.

Mohtadi, M., D. W. Oppo, A. Lückge, R. DePol-Holz, S. Steinke, J. Groeneveld, N. Hemme, and D. Hebbeln (2011), Reconstructing the thermal structure of the upper ocean: Insights from planktic foraminifera shell chemistry and alkenones in modern sediments of the tropical eastern Indian Ocean, *Paleoceanography*, *26*(3), PA3219.

Moreno, P. I., T.V. Lowell, G.H. Denton, G.L. Jacobson, Jr., and B.G. Andersen (1999), Abrupt changes in vegetation and climate during the last glacial maximum and last termination in the Chilean lake district: A case study from Canal de la Puntilla (41ºS). *Geografiska Annaler*, *81*, 285-312.

Mortyn, P. G., and C. D. Charles (2003), Planktonic foraminiferal depth habitat and delta18O calibrations: Plankton tow results from the Atlantic sector of the Southern Ocean, *Paleoceanography*, *18*(2), 1037.

Mosblech, N. A. S., M. B. Bush, W. D. Gosling, D. Hodell, L. Thomas, P. van Calsteren, A. Correa-Metrio, B. G. Valencia, J. Curtis, and R. van Woesik (2012), North Atlantic forcing of Amazonian precipitation during the last ice age, *Nature Geosci*, *5*(11), 817-820.

Mulitza, S., Anke Dürkoop, Walter Hale, Gerold Wefer and Hans Stefan Niebler (1997), Planktonic foraminifera as recorders of past surface-water stratification, *Geology*, *25*, 335-338.

Mulitza, S., C. Rühlemann, T. Bickert, W. Hale, J. Pätzold, and G. Wefer (1998b), Late Quaternary d13C gradients and carbonate accumulation in the western equatorial Atlantic, *Earth and Planetary Science Letters*, *155*, 237-249.

Mulitza, S., T. Wolff, J. Pätzold, W. Hale, and G. Wefer (1998a), Temperature sensitivity of planktic foraminifera and its influence on the oxygen isotope record, *Marine Micropaleontology*, *33*(3-4), 223-240.

Negre, C., R. Zahn, A. L. Thomas, P. Masque, G. M. Henderson, G. Martinez-Mendez, I. R. Hall, and J. L. Mas (2010), Reversed flow of Atlantic deep water during the Last Glacial Maximum, *Nature*, *468*(7320), 84-88.

NEEM, Project Members (2013), Eemian interglacial reconstructed from a Greenland folded ice core, *Nature*, *493*(7433), 489-494.

NGRIP Members (2004), High-resolution record of Northern Hemisphere climate extending into the last interglacial period, *Nature*, *431*(7005), 147-151.

Niebler, H. S., H. W. Arz, B. Donner, S. Mulitza, J. Pätzold, and G. Wefer (2003), Sea surface temperatures in the equatorial and South Atlantic Ocean during the Last Glacial Maximum (23–19 ka), *Paleoceanography*, *18*(3), 1069.

Numberger, L., C. Hemleben, R. Hoffmann, A. Mackensen, H. Schulz, J.-M. Wunderlich, and M. Kucera (2009), Habitats, abundance patterns and isotopic signals of morphotypes of the planktonic foraminifer *Globigerinoides ruber* (d'Orbigny) in the eastern Mediterranean Sea since the Marine Isotopic Stage 12, *Marine Micropaleontology*, *73*(1–2), 90-104.

Nürnberg, D., J. Bijma, and C. Hemleben (1996), Assessing the reliability of magnesium in foraminiferal calcite as a proxy for water mass temperatures, *Geochimica et Cosmochimica Acta*, *60*(5), 803-814.

Olson, D. B., and R. H. Evans (1986), Rings of the Agulhas current, *Deep Sea Research Part A. Oceanographic Research Papers*, *33*(1), 27-42.

Paillard, D., L. Labeyrie, and P. Yiou (1996), Macintosh Program performs time-series analysis, *Eos Trans. AGU*, *77*(39), 379-379.

Parrenin, F., et al. (2007), The EDC3 chronology for the EPICA Dome C ice core, *Clim. Past*, *3*(3), 485-497.

Peeters, F. J. C., and G.-J. A. Brummer (2002), The seasonal and vertical distribution of living planktic foraminifera in the NW Arabian Sea, *Geological Society, London, Special Publications*, *195*(1), 463-497.

Peeters, F. J. C., R. Acheson, G.-J. A. Brummer, W. P. M. de Ruijter, R. R. Schneider, G. M. Ganssen, E. Ufkes, and D. Kroon (2004), Vigorous exchange between the Indian and Atlantic oceans at the end of the past five glacial periods, *Nature*, *430*(7000), 661-665.

Pena, L. D., E. Calvo, I. Cacho, S. Eggins, and C. Pelejero (2005), Identification and removal of Mn-Mg-rich contaminant phases on foraminiferal tests: Implications for Mg/Ca past temperature reconstructions, *Geochem. Geophys. Geosyst.*, *6*(9), Q09P02.

Perez, R. C., S. L. Garzoli, C. S. Meinen, and R. P. Matano (2011), Geostrophic Velocity Measurement Techniques for the Meridional Overturning Circulation and Meridional Heat Transport in the South Atlantic, *Journal of Atmospheric and Oceanic Technology*, 28(11), 1504-1521.

Peterson, R. G., and L. Stramma (1991), Upper-level circulation in the South Atlantic Ocean, *Progress In Oceanography*, *26*(1), 1-73.

Peterson, L. C., G. H. Haug, K. A. Hughen, and U. Röhl (2000), Rapid Changes in the Hydrologic Cycle of the Tropical Atlantic During the Last Glacial, *Science*, *290*(5498), 1947-1951.

Philander, S. G. H., D. Gu, G. Lambert, T. Li, D. Halpern, N. C. Lau, and R. C. Pacanowski (1996), Why the ITCZ Is Mostly North of the Equator, *Journal of Climate*, *9*(12), 2958-2972.

Phillips, O. L., et al. (2009), Drought Sensitivity of the Amazon Rainforest, *Science*, *323*(5919), 1344-1347.

Phleger, F. B. (1939), Foraminifera of a submarine cores from the continental slope, *Geological Society of America Bulletin*, 50, 1395-1422.

Pierre, C., J. F. Saliege, M. J. Urrutiaguer, and J. Giraudeau (2001), Stable isotope record of the last 500 k.y. at Site 1087 (Southern Cape Basin), in *Proc. ODP, Sci. Results*, edited by G. Wefer, Berger, W.H., and Richter, C., pp. 1-22.

Pokras, E. M., and A. C. Mix (1987), Earth's precession cycle and Quaternary climatic change in tropical Africa, *Nature*, *326*(6112), 486-487.

Ponte, F., and H. Asmus (1978), Geological framework of the Brazilian continental margin, *Geologische Rundschau*, *67*(1), 201-235.

Poole, R., and M. Tomczak (1999), Optimum multiparameter analysis of the water mass structure in the Atlantic Ocean thermocline, *Deep Sea Research Part I: Oceanographic Research Papers*, *46*(11), 1895-1921.

Prell, W. L., W. H. Hutson, D. F. Williams, A. W. H. Bé, K. Geitzenauer, and B. Molfino (1980), Surface circulation of the Indian Ocean during the last glacial maximum, approximately 18,000 yr B.P, *Quaternary Research*, *14*(3), 309-336.

Quillévéré, F., R. Morard, G. Escarguel, C. J. Douady, Y. Ujiié, T. de Garidel-Thoron, and C. de Vargas (2013), Global scale same-specimen morpho-genetic analysis of *Truncorotalia truncatulinoides*: A perspective on the morphological species concept in planktonic foraminifera, *Palaeogeography, Palaeoclimatology, Palaeoecology*, *391, Part A*(0), 2-12.

Rahmstorf, S. (2002), Ocean circulation and climate during the past 120,000 years, *Nature*, *419*(6903), 207-214.

Rau, A. J., J. Rogers, J. R. E. Lutjeharms, J. Giraudeau, J. A. Lee-Thorp, M. T. Chen, and C. Waelbroeck (2002), A 450-kyr record of hydrological conditions on the western Agulhas Bank Slope, south of Africa, *Marine Geology*, *180*(1-4), 183-201.

Regenberg, M., S. Steph, D. Nürnberg, R. Tiedemann, and D. Garbe-Schönberg (2009), Calibrating Mg/Ca ratios of multiple planktonic foraminiferal species with [delta]18O-calcification temperatures: Paleothermometry for the upper water column, *Earth and Planetary Science Letters*, *278*(3-4), 324-336.

Rickaby, R. E. M., H. Elderfield, N. Roberts, C. D. Hillenbrand, and A. Mackensen (2010), Evidence for elevated alkalinity in the glacial Southern Ocean, *Paleoceanography*, *25*(1), PA1209.

Rincon-MartÌnez, D., F. Lamy, S. Contreras, G. Leduc, E. Bard, C. Saukel, T. Blanz, A. Mackensen, and R. Tiedemann (2010), More humid interglacials in Ecuador during the past 500 kyr linked to latitudinal shifts of the equatorial front and the Intertropical Convergence Zone in the eastern tropical Pacific, *Paleoceanography*, *25*(2), PA2210.

Rohling, E. J., et al. (2004), Reconstructing past planktic foraminiferal habitats using stable isotope data: a case history for Mediterranean sapropel S5, *Marine Micropaleontology*, *50*(1-2), 89-123.

Rohling, E. J., K. Grant, M. Bolshaw, A. P. Roberts, M. Siddall, C. Hemleben, and M. Kucera (2009), Antarctic temperature and global sea level closely coupled over the past five glacial cycles, *Nature Geosci*, *advanced online publication*.

Richardson, P. L. (2007), Agulhas leakage into the Atlantic estimated with subsurface floats and surface drifters, *Deep Sea Research Part I: Oceanographic Research Papers*, *54*(8), 1361-1389.

Rickaby, R. E. M., H. Elderfield, N. Roberts, C. D. Hillenbrand, and A. Mackensen (2010), Evidence for elevated alkalinity in the glacial Southern Ocean, *Paleoceanography*, *25*(1), PA1209.

Rohling, E. J. (2007), Progress in paleosalinity: Overview and presentation of a new approach, *Paleoceanography*, *22*(3), PA3215.

Rossignol-Strick, M. (1983), African monsoons, an immediate climate response to orbital insolation, *Nature*, *304*(5921), 46-49.

Rouault, M., P. Penven, and B. Pohl (2009), Warming in the Agulhas Current system since the 1980's, *Geophys. Res. Lett.*, *36*(12), L12602.

Ruddiman, W. F. (2008), Earth's Climate, Past and Future (2nd edition), W. H. Freeman.

Rühlemann, C., M. Frank, W. Hale, A. Mangini, S. Mulitza, P. J. Müller, and G. Wefer (1996), Late Quaternary productivity changes in the western equatorial Atlantic: Evidence from 230Th-normalized carbonate and organic carbon accumulation rates, *Marine Geology*, *135*(1-4), 127-152.

Rühlemann, C., B. Dickmann, S. Mulitza, and M. Frank (2001), Late Quaternary Changes of Western Equatorial Atlantic Surface Circulation and Amazon Lowland Climate Recorded in Cear· Rise Deep-Sea Sediments, *Paleoceanography*, *16*(3), 293-305.

Rühlemann, C., S. Mulitza, G. Lohmann, A. Paul, M. Prange, and G. Wefer (2004), Intermediate depth warming in the tropical Atlantic related to weakened thermohaline circulation: Combining paleoclimate data and modeling results for the last deglaciation, *Paleoceanography*, *19*(1), PA1025.

Sadekov, A. Y., S. M. Eggins, and P. De Deckker (2005), Characterization of Mg/Ca distributions in planktonic foraminifera species by electron microprobe mapping, *Geochem. Geophys. Geosyst.*, *6*(12), Q12P06.

Sabine, C. L., et al. (2004), The Oceanic Sink for Anthropogenic CO_2, *Science*, 305(5682), 367-371.

Sagawa, T., Y. Yokoyama, M. Ikehara, and M. Kuwae (2011), Vertical thermal structure history in the western subtropical North Pacific since the Last Glacial Maximum, *Geophys. Res. Lett.*, *38*, L00F02.

Sánchez Goñi, M. F., F. Eynaud, J. L. Turon, and N. J. Shackleton (1999), High resolution palynological record off the Iberian margin: direct land-sea correlation for the Last Interglacial complex, *Earth and Planetary Science Letters*, *171*(1), 123-137.

Sánchez Goñi, M. F., et al. (2012), European climate optimum and enhanced Greenland melt during the Last Interglacial, *Geology*, *40*(7), 627-630.

Savin, S. M., and R. G. Douglas (1973), Stable Isotope and Magnesium Geochemistry of Recent Planktonic Foraminifera from the South Pacific, *Geological Society of America Bulletin*, *84*(7), 2327-2342.

Schott, F. A., J. Fischer, and L. Stramma (1998), Transports and Pathways of the Upper-Layer Circulation in the Western Tropical Atlantic, *Journal of Physical Oceanography, 28*(10), 1904-1928.

Schouten, M. W., W. P. M. de Ruijter, P. J. van Leeuwen, and J. R. E. Lutjeharms (2000), Translation, decay and splitting of Agulhas rings in the southeastern Atlantic Ocean, *J. Geophys. Res.*, *105*(C9), 21913-21925.

Schouten, S., E. C. Hopmans, E. Schefuß, and J. S. Sinninghe Damsté (2002), Distributional variations in marine crenarchaeotal membrane lipids: a new tool for reconstructing ancient sea water temperatures?, *Earth and Planetary Science Letters*, *204*(1–2), 265-274.

Schmidt, M. W., H. J. Spero, and D. W. Lea (2004), Links between salinity variation in the Caribbean and North Atlantic thermohaline circulation, *Nature*, *428*(6979), 160-163.

Schulz, M., and M. Mudelsee (2002), REDFIT: estimating red-noise spectra directly from unevenly spaced paleoclimatic time series, *Computers & Geosciences*, *28*(3), 421-426.

Schrag, D. P., J. F. Adkins, K. McIntyre, J. L. Alexander, D. A. Hodell, C. D. Charles, and J. F. McManus (2002), The oxygen isotopic composition of seawater during the Last Glacial Maximum, *Quaternary Science Reviews*, *21*(1-3), 331-342.

Scussolini, P., and F. J. C. Peeters (2013), A record of the last 460 thousand years of upper ocean stratification from the central Walvis Ridge, South Atlantic, *Paleoceanography*, *28*(3), 426-439.

Scussolini, P., E. van Sebille, and J. V. Durgadoo (2013), Paleo Agulhas rings enter the subtropical gyre during the penultimate deglaciation, *Clim. Past*, *9*(6), 2631-2639.

Seidov, D., and M. Maslin (2001), Atlantic ocean heat piracy and the bipolar climate see-saw during Heinrich and Dansgaard–Oeschger events, *Journal of Quaternary Science*, *16*(4), 321-328.

Shackleton, N. J. (1967), Oxygen isotope analyses and Pleistocene temperatures re-assessed, *Nature, 215*, 15-17.

Shakun, J. D., S. J. Burns, P. U. Clark, H. Cheng, and R. L. Edwards (2011), Milankovitch-paced Termination II in a Nevada speleothem?, *Geophysical Research Letters*, *38*(18), L18701.

Sijp, W. P., and M. H. England (2008), The effect of a northward shift in the southern hemisphere westerlies on the global ocean, *Progress In Oceanography*, *79*(1), 1-19.

Sijp, W. P., and M. H. England (2009), Southern Hemisphere Westerly Wind Control over the Ocean's Thermohaline Circulation, *Journal of Climate*, *22*(5), 1277-1286.

Sikes, E. L., W. R. Howard, C. R. Samson, T. S. Mahan, L. G. Robertson, and J. K. Volkman (2009), Southern Ocean seasonal temperature and Subtropical Front movement on the South Tasman Rise in the late Quaternary, *Paleoceanography*, *24*(2), PA2201.

Simon, M. H., K. L. Arthur, I. R. Hall, F. J. C. Peeters, B. R. Loveday, S. Barker, M. Ziegler, and R. Zahn (2013), Millennial-scale Agulhas Current variability and its implications for salt-leakage through the Indian–Atlantic Ocean Gateway, *Earth and Planetary Science Letters*, *383*(0), 101-112.

Simstich, J., S. J. Lorenz, and H. A. Bauch (2012), Evaluation of past stratification changes in the Nordic Seas by comparing planktonic foraminiferal d18O with a solar-forced model, *Marine Micropaleontology*, *94-95*, 91-96.

Skinner, L. C., S. Fallon, C. Waelbroeck, E. Michel, and S. Barker (2010), Ventilation of the Deep Southern Ocean and Deglacial CO2 Rise, *Science*, 328(5982), 1147-1151.

Smith, C. R., and C. Rabouille (2002), What controls the mixed-layer depth in deep-sea sediments? The importance of POC flux, *Limnol. Oceanogr*, *47*(2), 418-426.

Souza, J. M. A. C., C. de Boyer MontÈgut, C. Cabanes, and P. Klein (2011), Estimation of the Agulhas ring impacts on meridional heat fluxes and transport using ARGO floats and satellite data, *Geophys. Res. Lett.*, *38*(21), L21602.

Speich, S., B. Blanke, and W. Cai (2007), Atlantic meridional overturning circulation and the Southern Hemisphere supergyre, *Geophysical Research Letters*, *34*(23).

Spero, H. J. (1998), Life history and stable isotope geochemistry of planktonic foraminifera, in *Isotope paleobiology and paleoecology*, edited by R. a. C. Norris, RM, pp. 7-36, Paleontological society, Tuscalosa.

Spero, H. J., and D. W. Lea (2002), The Cause of Carbon Isotope Minimum Events on Glacial Terminations, *Science*, *296*(5567), 522-525.

Spero, H. J., J. Bijma, D. W. Lea, and B. E. Bemis (1997), Effect of seawater carbonate concentration on foraminiferal carbon and oxygen isotopes, *Nature*, *390*(6659), 497-500.

Spero, H. J., K. M. Mielke, E. M. Kalve, D. W. Lea, and D. K. Pak (2003), Multispecies approach to reconstructing eastern equatorial Pacific thermocline hydrography during the past 360 kyr, *Paleoceanography*, *18*(1), 1022.

Steinke, S., H.-Y. Chiu, P.-S. Yu, C.-C. Shen, L. Löwemark, H.-S. Mii, and M.-T. Chen (2005), Mg/Ca ratios of two Globigerinoides ruber (white) morphotypes: Implications for reconstructing past tropical/subtropical surface water conditions, *Geochem. Geophys. Geosyst.*, *6*(11), Q11005.

Steph, S., M. Regenberg, R. Tiedemann, S. Mulitza, and D. Nürnberg (2009), Stable isotopes of planktonic foraminifera from tropical Atlantic/Caribbean core-tops: Implications for reconstructing upper ocean stratification, *Marine Micropaleontology*, *71*(1-2), 1-19.

Stocker, T. F., and S. J. Johnsen (2003), A minimum thermodynamic model for the bipolar seesaw, *Paleoceanography*, *18*(4), 1087.

Stouffer, R. J., et al. (2006), Investigating the Causes of the Response of the Thermohaline Circulation to Past and Future Climate Changes, *Journal of Climate*, *19*(8), 1365-1387.

Stramma, L., and M. England (1999), On the water masses and mean circulation of the South Atlantic Ocean, *J. Geophys. Res.*, *104*(C9), 20863-20883.

Stramma, L., and F. Schott (1999), The mean flow field of the tropical Atlantic Ocean, *Deep Sea Research Part II: Topical Studies in Oceanography*, *46*(1-2), 279-303.

Stuut, J.-B. W., M. A. Prins, and J. H. F. Jansen (2002), Fast reconnaissance of carbonate dissolution based on the size distribution of calcareous ooze on Walvis Ridge, SE Atlantic Ocean, *Marine Geology*, *190*(3–4), 581-589.

Stuut, J.-B. W., X. Crosta, K. van der Borg, and R. Schneider (2004), Relationship between Antarctic sea ice and southwest African climate during the late Quaternary, *Geology*, *32*(10), 909-912.

Svensson, A., et al. (2008), A 60 000 year Greenland stratigraphic ice core chronology, *Clim. Past*, *4*(1), 47-57.

Tachikawa, K., O. Cartapanis, L. Vidal, L. Beaufort, T. Barlyaeva, and E. Bard (2011), The precession phase of hydrological variability in the Western Pacific Warm Pool during the past 400 ka, *Quaternary Science Reviews*, *30*(25–26), 3716-3727.

Takahashi, T., J. Olafsson, J. G. Goddard, D. W. Chipman, and S. C. Sutherland (1993), Seasonal variation of CO_2 and nutrients in the high-latitude surface oceans: A comparative study, *Global Biogeochemical Cycles*, *7*(4), 843-878.

Thirumalai, K., J. W. Partin, C. S. Jackson, and T. M. Quinn (2013), Statistical constraints on El Niño Southern Oscillation reconstructions using individual foraminifera: A sensitivity analysis, *Paleoceanography*, *28*(3), 1-12.

Thornalley, D. J. R., S. Barker, J. Becker, I. R. Hall, and G. Knorr (2013), Abrupt changes in deep Atlantic circulation during the transition to full glacial conditions, *Paleoceanography*, 28(2), 253-262.

Thunell, R., E. Tappa, C. Pride, and E. Kincaid (1999), Sea-surface temperature anomalies associated with the 1997-1998 El Nino recorded in the oxygen isotope composition of planktonic foraminifera, *Geology*, *27*(9), 843-846.

Timmermann, A., et al. (2007), The Influence of a Weakening of the Atlantic Meridional Overturning Circulation on ENSO, *Journal of Climate*, *20*(19), 4899-4919.

Toggweiler, J. R. (2009), Shifting Westerlies, *Science*, *323*(5920), 1434-1435.

Toggweiler, J. R., and B. Samuels (1993), New Radiocarbon Constraints on the Upwelling of Abyssal Water to the Ocean's Surface, in *The Global Carbon Cycle*, edited by M. Heimann, pp. 333-366, Springer Berlin Heidelberg.

Toggweiler, J. R., and B. Samuels (1995), Effect of Drake Passage on the global thermohaline circulation, *Deep Sea Research I*, 42(4), 477-500.

Toggweiler, J. R., and D. W. Lea (2010), Temperature differences between the hemispheres and ice age climate variability, *Paleoceanography*, *25*(2), PA2212.

Toggweiler, J. R., J. L. Russell, and S. R. Carson (2006), Midlatitude westerlies, atmospheric CO_2, and climate change during the ice ages, *Paleoceanography*, *21*(2), PA2005.

Trauth, M. H., M. Sarnthein, and M. Arnold (1997), Bioturbational mixing depth and carbon flux at the seafloor, *Paleoceanography*, *12*(3), 517-526.

Treguier, A. M., O. Boebel, B. Barnier, and G. Madec (2003), Agulhas eddy fluxes in a 1/6(degree) Atlantic model, *Deep-Sea Research II*, 50, 251–280.

Treguier, A. M., J. Deshayes, C. Lique, R. Dussin, and J. M. Molines (2012), Eddy contributions to the meridional transport of salt in the North Atlantic, *Journal of Geophysical Research: Oceans*, *117*(C5), C05010.

Trenberth, K. E., D. P. Stepaniak, and J. M. Caron (2000), The Global Monsoon as Seen through the Divergent Atmospheric Circulation, *Journal of Climate*, *13*(22), 3969-3993.

Tzedakis, P. C., J. F. McManus, H. Hooghiemstra, D. W. Oppo, and T. A. Wijmstra (2003), Comparison of changes in vegetation in northeast Greece with records of climate variability on orbital and suborbital frequencies over the last 450 000 years, *Earth and Planetary Science Letters*, *212*(1–2), 197-212.

Ufkes, E. L. S., and D. Kroon (2012), Sensitivity of south-east Atlantic planktonic foraminifera to mid-

Pleistocene climate change, *Palaeontology*, *55*(1), 183-204.

Ujiiè, Y., T. de Garidel-Thoron, S. Watanabe, P. Wiebe, and C. de Vargas (2010), Coiling dimorphism within a genetic type of the planktonic foraminifer Globorotalia truncatulinoides, *Marine Micropaleontology*, *77*(3-4), 145-153.

Urey, H.C., 1947. The thermodynamic properties of isotopic substances. *Journal of the Chemical Society* (Resumed): 562-581.

van Aken, H. M., A. K. van Veldhoven, C. Veth, W. P. M. de Ruijter, P. J. van Leeuwen, S. S. Drijfhout, C. P. Whittle, and M. Rouault (2003), Observations of a young Agulhas ring, Astrid, during MARE in March 2000, *Deep Sea Research Part II: Topical Studies in Oceanography*, *50*(1), 167-195.

van Breukelen, M. R., H. B. Vonhof, J. C. Hellstrom, W. C. G. Wester, and D. Kroon (2008), Fossil dripwater in stalagmites reveals Holocene temperature and rainfall variation in Amazonia, *Earth and Planetary Science Letters*, 275(1–2), 54-60.

van Leeuwen, P. J., W. P. M. de Ruijter, and J. R. E. Lutjeharms (2000), Natal pulses and the formation of Agulhas rings, *J. Geophys. Res.*, *105*(C3), 6425-6436.

van Sebille, E., and P. J. van Leeuwen (2007), Fast Northward Energy Transfer in the Atlantic due to Agulhas Rings, *Journal of Physical Oceanography*, *37*(9), 2305-2315.

van Sebille, E., C. N. Barron, A. Biastoch, P. J. van Leeuwen, F. C. Vossepoel, and W. P. M. de Ruijter (2009a), Relating Agulhas leakage to the Agulhas Current retroflection location, *Ocean Sci.*, *5*(4), 511-521.

van Sebille, E., A. Biastoch, P. J. van Leeuwen, and W. P. M. de Ruijter (2009b), A weaker Agulhas Current leads to more Agulhas leakage, *Geophys. Res. Lett.*, *36*(3), L03601.

van Sebille, E., P. J. van Leeuwen, A. Biastoch, and W. P. M. de Ruijter (2010a), On the fast decay of Agulhas rings, *Journal of Geophysical Research: Oceans*, *115*(C3).

Van Sebille, V. L., Biastoch, and De Ruijter (2010b), Flux comparison of Eulerian and Lagrangian estimates of Agulhas leakage: A case study using a numerical model *Deep Sea Res. I*, *57*, 319-327.

van Sebille, E., W. E. Johns, and L. M. Beal (2012), Does the vorticity flux from Agulhas rings control the zonal pathway of NADW across the South Atlantic?, *J. Geophys. Res.*, *117*(C5), C05037.

Vellinga, M., and R. A. Wood (2002), Global Climatic Impacts of a Collapse of the Atlantic Thermohaline Circulation, *Climatic Change*, *54*(3), 251-267.

Venegas, S. A., L. A. Mysak, and D. N. Straub (1998), An interdecadal climate cycle in the South Atlantic and its links to other ocean basins, *J. Geophys. Res.*, *103*(C11), 24723-24736.

Vizy, E. K., and K. H. Cook (2007), Relationship between Amazon and high Andes rainfall, *Journal of Geophysical Research: Atmospheres*, *112*(D7), D07107.

Vonhof, H. B., and R. J. G. Kaandorp (2009), Climate Variation in Amazonia during the Neogene and the Quaternary, in *Amazonia: Landscape and Species Evolution*, edited, pp. 199-210, Wiley-Blackwell Publishing Ltd.

Waelbroeck, C., N. Frank, J. Jouzel, F. Parrenin, V. Masson-Delmotte, and D. Genty (2008), Transferring radiometric dating of the last interglacial sea level high stand to marine and ice core records, *Earth and Planetary Science Letters*, *265*(1-2), 183-194.

Wainer, K., et al. (2011), Speleothem record of the last 180 ka in Villars cave (SW France): Investigation of a large $\delta^{18}O$ shift between MIS6 and MIS5, *Quaternary Science Reviews*, 30(1–2), 130-146.

Wang, L. (2000), Isotopic signals in two morphotypes of *Globigerinoides ruber* (white) from the South China Sea: implications for monsoon climate change during the last glacial cycle, *Palaeogeography, Palaeoclimatology, Palaeoecology*, *161*(3-4), 381-394.

Wang, P. (2009), Global monsoon in a geological perspective, *Chin. Sci. Bull.*, *54*(7), 1113-1136.

Wang, B. (2012), Will summer rain increase or decrease in monsoon regions? (Present), *PAGES News*, *20*(1), 26.

Wang, B., and Q. Ding (2008), Global monsoon: Dominant mode of annual variation in the tropics, *Dynamics of Atmospheres and Oceans*, 44(3–4), 165-183.

Wang, Y. J., H. Cheng, R. L. Edwards, Z. S. An, J. Y. Wu, C. C. Shen, and J. A. Dorale (2001), A High-Resolution Absolute-Dated Late Pleistocene Monsoon Record from Hulu Cave, China, *Science*, *294*(5550), 2345-2348.

Wang, X., A. S. Auler, R. L. Edwards, H. Cheng, P. S. Cristalli, P. L. Smart, D. A. Richards, and C.-C. Shen (2004), Wet periods in northeastern Brazil over the past 210-kyr linked to distant climate anomalies, *Nature*, *432*(7018), 740-743.

Wang, X., A. S. Auler, R. L. Edwards, H. Cheng, E. Ito, and M. Solheid (2006), Interhemispheric anti-phasing of rainfall during the last glacial period, *Quaternary Science Reviews*, *25*(23-24), 3391-3403.

Wang, X., A. S. Auler, R. L. Edwards, H. Cheng, E. Ito, Y. Wang, X. Kong, and M. Solheid (2007), Millennial-scale precipitation changes in southern Brazil over the past 90,000 years, *Geophysical Research Letters*, *34*(23), L23701.

Wang, Y., H. Cheng, R. L. Edwards, X. Kong, X. Shao, S. Chen, J. Wu, X. Jiang, X. Wang, and Z. An (2008), Millennial- and orbital-scale changes in the East Asian monsoon over the past 224,000-years, *Nature*, *451*(7182), 1090-1093.

Weber, S. L., and E. Tuenter (2011), The impact of varying ice sheets and greenhouse gases on the intensity and timing of boreal summer monsoons, *Quaternary Science Reviews*, *30*(3–4), 469-479.

Wefer, G., et al. (1996), Late Quaternary surface circulation of the South Atlantic: The stable isotope record and implications for heat transport and productivity, in *The South Atlantic: Present and Past Circulation*, edited by G. Wefer, Berger, W.H., Siedler, G., Webb, D.J., pp. 461 – 502, Springer-Verlag, New York.

Wefer, G., Berger, W.H., Siedler, G., Webb, D.J. (Eds.) (1996), *The South Atlantic: Present and Past Circulation*, Springer-Verlag, New York.

Weijer, W., W. P. M. De Ruijter, and H. A. Dijkstra (2001), Stability of the Atlantic Overturning Circulation: Competition between Bering Strait Freshwater Flux and Agulhas Heat and Salt Sources, *Journal of Physical Oceanography*, *31*(8), 2385-2402.

Weijer, W., W. P. M. De Ruijter, A. Sterl, and S. S. Drijfhout (2002), Response of the Atlantic overturning circulation to South Atlantic sources of buoyancy, *Global and Planetary Change*, *34*(3-4), 293-311.

Weijer, W., M. E. Maltrud, M. W. Hecht, H. A. Dijkstra, and M. A. Kliphuis (2012), Response of the Atlantic Ocean circulation to Greenland Ice Sheet melting in a strongly-eddying ocean model, *Geophysical Research Letters*, *39*(9), L09606.

White, S. M., T. M. Hill, J. P. Kennett, R. J. Behl, and C. Nicholson (2013), Millennial-scale variability to 735 ka: High-resolution climate records from Santa Barbara Basin, CA, *Paleoceanography*, *28*(2), 213-226.

Whitman, J. M., and W. H. Berger (1992), Pliocene-Pleistocene oxygen isotope record Site 586, Ontong Java Plateau, *Marine Micropaleontology*, *18*(3), 171-198.

Williams, D. F., and N. Healy-Williams (1980), Oxygen isotopic-hydrographic relationships among recent planktonic Foraminifera from the Indian Ocean, *Nature*, *283*(5750), 848-852.

Williams, D. F., A. W. H. Bé, and R. G. Fairbanks (1981), Seasonal stable isotopic variations in living planktonic foraminifera from bermuda plankton tows, *Palaeogeography, Palaeoclimatology, Palaeoecology*, *33*(1–3), 71-102.

Wilson, K. E., M. A. Maslin, and S. J. Burns (2011), Evidence for a prolonged retroflection of the North Brazil Current during glacial stages, *Palaeogeography, Palaeoclimatology, Palaeoecology*, *301*(1–4), 86-96.

Wunsch, C. (1980), Meridional heat flux of the North Atlantic Ocean, *Proceedings of the National Academy of*

Sciences, *77*(9), 5043–5047.

Yancheva, G., N. R. Nowaczyk, J. Mingram, P. Dulski, G. Schettler, J. F. W. Negendank, J. Liu, D. M. Sigman, L. C. Peterson, and G. H. Haug (2007), Influence of the intertropical convergence zone on the East Asian monsoon, *Nature*, *445*(7123), 74-77.

Zhisheng, A., J. E. Kutzbach, W. L. Prell, and S. C. Porter (2001), Evolution of Asian monsoons and phased uplift of the Himalaya-Tibetan plateau since Late Miocene times, *Nature*, *411*(6833), 62-66.

Ziegler, M., L. J. Lourens, E. Tuenter, F. Hilgen, G.-J. Reichart, and N. Weber (2010a), Precession phasing offset between Indian summer monsoon and Arabian Sea productivity linked to changes in Atlantic overturning circulation, *Paleoceanography*, *25*(3), PA3213.

Ziegler, M., E. Tuenter, and L. J. Lourens (2010b), The precession phase of the boreal summer monsoon as viewed from the eastern Mediterranean (ODP Site 968), *Quaternary Science Reviews*, *29*(11–12), 1481-1490.

Ziegler, M., P. Diz, I. R. Hall, and R. Zahn (2013), Millennial-scale changes in atmospheric CO_2 levels linked to the Southern Ocean carbon isotope gradient and dust flux, *Nature Geosci*, *6*(6), 457-461.

Ziegler, M., M. H. Simon, I. R. Hall, S. Barker, C. Stringer, and R. Zahn (2013b), Development of Middle Stone Age innovation linked to rapid climate change, *Nat Commun*, *4*, 1905.

Dynamiek van Pleistocene klimaatveranderingen in de Zuid-Atlantische Oceaan (Samenvatting in het Nederlands)

Dit proefschrift gaat over de reconstructie van klimatologische kenmerken uit het verleden. Het onderzoek richt zich in het bijzonder op de klimaatgeschiedenis van de Zuid-Atlantische Oceaan gedurende periodes van grootschalige klimatologische verschuivingen tijdens het Pleistoceen. Een goed begrip van deze verschuivingen en de dynamiek erachter is van essentieel belang om de huidige klimaatverandering en de consequenties daarvan te doorgronden.

Uit klimatologische reconstructies voor het Pleistoceen, is gebleken dat de gemiddelde temperatuur en de samenstelling van de atmosfeer en van de oceanen, varieerde op tijdschalen van duizenden tot miljoenen jaren. De belangrijkste oorzaak hiervoor ligt verborgen in twee sturende factoren, ook wel forceringen genoemd, t.w. de verschuiving van continenten en veranderingen in de ruimtelijke verdeling van ontvangen zonnestraling. Deze laatste factor hangt samen met veranderingen in de drie parameters die de aardbaan en stand van de aardas ten opzichte van de zon karakteriseren (de z.g. orbitale parameters): 1) excentriciteit, of de mate van afwijking in de ellipsvormige baan van de aarde om de zon, 2) de scheefstand of de kanteling van rotatie-as van de aarde ten opzichte van het baanvlak, en 3) de precessie van de equinoxen, ofwel de oriëntatie van de rotatie-as ten opzichte van het firmament. De combinatie van de frequenties van verandering in deze drie parameters heeft in het Pleistoceen geleid tot een periodieke verandering van de toestand van het klimaatsysteem, dat daardoor varieerde tussen ijstijden en tussenijstijden: de glaciaal-interglaciaal (G-IG) cycli.

Paleoklimaatonderzoek ontrafelt de fysische mechanismen achter deze cycli en andere variaties in het klimaat. Hierbij wordt gebruik gemaakt van zogeheten proxy data, d.w.z. geologische gegevens waarin informatie over klimaatveranderingen uit het verleden ligt opgeslagen. Recente verbeteringen van deze klimaatproxies stellen ons in staat de geschiedenis van regionale en wereldwijde klimatologische veranderingen en de ouderdom daarvan te reconstrueren met een hogere precisie en nauwkeurigheid. Een achterliggend doel van paleoklimaatreconstructies, zoals gepresenteerd in dit proefschrift, is om onze kennis over het klimaat uit het verleden verbeteren. Deze kennis, op zijn beurt, is een voorwaarde voor een goede voorspelling van de respons van het systeem op de huidige en toekomstige antropogene invloed op het klimaat.

De oceanen zijn een belangrijk onderdeel van het klimaatsysteem. Oceanen beïnvloeden het klimaatsysteem op verschillende manieren. Een zeer belangrijke rol van oceanen is het transport van warmte van de tropen richting beide polen. Dit transport vindt plaats door de oceaancirculatie. De grootschalige circulatie in de Atlantische Oceaan, de zogenaamde Atlantische meridionale omslag (*eng.* 'overturning') circulatie (AMOC), is hierbij met name van belang. Het is gebleken dat de AMOC een zeer gevoelig onderdeel is van het klimaatsysteem.

Een belangrijke eigenschap van de AMOC is dat er netto warmte vanuit de zuidelijke Atlantische Oceaan, en met name de tropen, naar het noorden van de Atlantische Oceaan wordt getransporteerd. Recentelijk is gebleken dat processen in het zuidelijk deel van de Atlantische Oceaan zeer belangrijk zijn voor het evenwicht en de variabiliteit van de AMOC, en dus van het hele klimaatsysteem. Dit onderstreept het belang van wetenschappelijk onderzoek dat gericht is op een beter begrip van de processen in de zuidelijke Atlantische Oceaan in het geologisch verleden. Dit is het onderwerp van dit proefschrift.

Vanuit de Indische Oceaan stroomt regelmatig relatief warm en zout water naar de Zuid Atlantische Oceaan (de z.g. Agulhas “leakage”, oftewel lek, hierna AL genoemd). Dit gebeurt in ringstructuren, de zogeheten Agulhas wervels. Deze Agulhas wervels, ook wel Agulhas ringen genoemd, vormen een belangrijke component van de bovenste tak van de AMOC. Aangezien AL een gevoelige en invloedrijke schakel is in het klimaatsysteem, is het cruciaal om de relaties met de andere onderdelen van het klimaat op aarde goed te begrijpen. Voor de sterkte van de AL is de ligging van de polaire en subpolaire fronten in de zuidelijke Atlantische Oceaan van belang. Tijdens de Pleistocene ijstijden hadden deze fronten een meer noordelijke ligging, wat een verzwakking van de AL zou kunnen hebben betekend. Anderzijds zou tijdens de overgang van glacialen naar interglacialen (de z.g. glaciale terminaties), een zuidwaartse verschuiving van fronten, en de daarmee gepaard gaande windsystemen, een doorgang naar de Zuid-Atlantische Oceaan kunnen hebben geopend die groter is dan tegenwoordig, waardoor de AL sterker kon zijn.

De verschillende delen van het paleo Agulhassysteem zijn recentelijk onderzocht, dat wil zeggen, de noordelijke en zuidelijke Agulhas stroom, de AL, de retroflectie en de Agulhas terug stroming. Tot nu toe heeft weinig onderzoek zich gericht op het effect van de AL in de Atlantische Oceaan. Het onderzoek in dit proefschrift richt zich op de paleoceanografie van het zuidoosten van de Atlantische Oceaan en het westen van de tropische Atlantische Oceaan. Beide locaties bevinden zich ‘stroomafwaarts’ van AL. Mijn onderzoek richt zich met name op de vraagstelling of de AL een meetbaar effect op de AMOC heeft gehad tijdens periodes van klimaatverandering. Hiervoor werden twee mariene sedimentkernen bestudeerd, één proximaal gelegen ten opzichte van het AL-gebied op de Walvis Rug in de Zuid Atlantische Oceaan, en één distaal gelegen, in de tropische Westelijke Atlantische Oceaan.

Teneinde de paleoceanografie te reconstrueren, heb ik gebruik gemaakt van proxies. Door de geochemie te meten van fossiele planktonische foraminiferen, dat zijn microscopisch kleine schelpjes uit mariene sedimenten, heb ik de eigenschappen van de top van de waterkolom van deze twee locaties gereconstrueerd. De **proximale kern 64PE-174P13** is afkomstig van de centrale Walvis Rug, op de oostelijke flank van de grote Zuid Atlantische subtropische wervel; een locatie die op dit moment onder de route van de Agulhas ringen ligt. Dit maakt deze locatie geschikt voor onderzoek naar de gevolgen van de Agulhas water in deze regio. De **distale kern MD09 – 3246** is afkomstig van de westelijke tropische Atlantische Oceaan, verder stroomafwaarts van de AL. Deze kern werd genomen in de buurt van het continentaal plat van noordoost Brazilië, op een waterdiepte van 900 m.

In hoofdstuk 2 richt ik mij op de volgende onderzoeksvragen: 1) Hoe is de stratificatie van de Zuid-Atlantische Oceaan veranderd tijdens Pleistocene klimaatveranderingen? En 2) wat is de relatie in tijd en ruimte van deze veranderingen met de aanvoer van de Indische Oceaan water? Voor dit doel genereerde ik twee zuurstofisotopen proxy tijdseries, voor de hele kern, voor twee soorten planktonische foraminiferen met verschillende calcificatiedieptes. De resultaten tonen aan dat **het verschil tussen de** diep en ondiep levende soorten als maat gebruikt kan worden voor de oceaanstratificatie. **De resulterende curve laat** een zaagtand patroon **zien, die** strikt **samenhangt met** de G-**IG** cycli. Stratificatie was minimaal tijdens interglacialen, nam toe tot de volgende glaciale terminatie en daalde daarna relatief snel. Eerder waargenomen variaties in de AL zijn **de** waarschijnlijke oorzaak van **dit** waargenomen patroon in het zuidoosten van de Atlantische Oceaan.

In hoofdstuk 3 ligt de focus op een interval van prominente klimaatverandering, gedurende de voorlaatste glaciale terminatie (T-II), ongeveer 130.000 jaar geleden. In dit hoofdstuk richt ik mij voornamelijk op de vraag of de eerder waargenomen toename in AL doorgedrongen is tot de subtropische wervel circulatie. De uitkomst **van het onderzoek** bevestigt deze onderzoeksvraag. Gebruikmakend van oceanografische tijdreeksen met een hoog oplossend vermogen die gemaakt zijn met een oceaancirculatiemodel, wordt onthuld dat variabiliteit in hoge dichtheid op thermocliene diepte over de Walvis Rug verband houdt met de passage van Agulhas wervels. Op basis van deze waarneming werd een nieuwe proxy ontwikkeld met behulp van de geochemische variabiliteit van planktonische foraminiferen welke leven in de thermocliene. Dit toont aan dat er meer paleo**-**Agulhas ringen waren op deze **locatie** tijdens T-**II**. Dit bevestigt de hypothese dat de AL een prominente rol heeft gespeeld in de AMOC tijdens deze glaciale terminatie.

In **hoofdstuk 4**, richt ik mij wederom op T - II, maar nu ben ik geïnteresseerd in het verbinden van veranderingen in de temperatuur en het zoutgehalte aan variabiliteit in AL. Mijn interesse gaat hier in het bijzonder uit naar het begrijpen van de rol van temperatuur en het zoutgehalte in de context van oceanografische veranderingen in de Atlantische Oceaan. Om hier meer inzicht in te krijgen zijn proxies voor temperatuur en zoutgehalte ontwikkeld voor verschillende diepten in de waterkolom. De resultaten tonen een hoge correlatie van zoutgehalte met de proxy voor Agulhas ringen uit hoofdstuk 3. Deze correlatie suggereert dat **de zuidoostelijke Atlantische Oceaan sterk onder de invloed lag van oceaanwater dat zijn oorsprong had in de Indische Oceaan**. Bovendien wijzen de resultaten op een negatief drijfvermogen van de AL verder stroomafwaarts, mogelijk als gevolg van de afname van de water temperatuur in het Kaap Bekken (waar het Indische Oceaanwater de Atlantische Oceaan instroomt). Een ander belangrijk resultaat van deze studie is dat de

gereconstrueerde zeeoppervlaktetemperaturen en zoutgehaltes een omslag tonen van hoge naar lage waarden tijdens T-II (~133-134 duizend jaar geleden). Dit omslagpunt blijkt exact samen te vallen met veranderingen in het Kaap Bekken, die eerder werden gedetecteerd in een andere onafhankelijke studie.
Tevens blijkt dat deze Zuid-Atlantische omkeringen synchroon plaatsvinden met klimaatsveranderingen in het noordelijk halfrond.
Daarom wordt de volgende hypothese naar voren gebracht: **de Zuid-Atlantische oceaan reageert op de tegengestelde temperatuurresponse op beide halfronden (opwarming in het noorden, afkoeling in het zuiden, het z.g. "see-saw" effect) dat een gevolg is van de tussentijdse hervatting van de AMOC tijdens T-II**, in navolging van de gebeurtenissen van T-I .

Verder presenteert dit proefschrift het werk dat ik heb gedaan aan een mariene sediment kern uit de westelijke tropische Atlantische Oceaan. Het onderzoek aan kern MD09–3246 richt zich voornamelijk op de sedimentologie van deze kern, en de relatie met veranderingen in atmosferische circulatie. Er is reeds aangetoond dat neerslag in het noordoostelijke deel van het Braziliaanse continent toenam tijdens perioden van abrupte afkoeling in het Noord-Atlantisch gebied gedurende de laatste ijstijd.
Een recente onderzoeksvraag is of verplaatsingen van de inter-tropische neerslag gordel, ook wel inter-tropische convergentie zone (ITCZ) genoemd, synchroon waren met andere tropische klimaatveranderingen tijdens het Pleistoceen. Met andere woorden, ik heb me de vraag gesteld of er sprake zou kunnen zijn van een zogenaamd wereldwijd moesson systeem. Om dit te beantwoorden heb ik in **hoofdstuk 5** een reconstructie gemaakt van de neerslagvariaties over de laatste 420 duizend jaar.

Ik vergeleek deze gegevens met paleohydrologische reconstructies uit Brazilië en andere delen van de wereld, waaronder Azië en Groenland. Ik concludeer dat gedurende de laatste 420 duizend jaar zowel de Zuid-Amerikaanse Moesson als het effect van regionale instraling, maar ook forcering op hoge breedtegraden van invloed zijn geweest op de verplaatsing van de ITCZ. Een belangrijke implicatie van deze resultaten is dat de Zuid-Amerikaanse moesson lijkt te zijn gekoppeld (in anti fase), met de Oost-Aziatische moesson tijdens het laat Pleistoceen. Ingaand op het recente debat over het mogelijke bestaan van een wereldwijd paleomoessonsysteem, laat ik zien dat de paleomoessonsystemen uit Zuid-Amerika en Oost-Azië reageerden op koude fasen op gematigde en hogere breedtegraden van het noordelijk halfrond gedurende de laatste vier glaciale-interglaciale cycli. Dit alles wijst op Pleistocene persistentie van een wereldwijd paleomoessonsysteem dat voornamelijk wordt aangestuurd door klimatologische veranderingen op hogere breedtegraden.

Acknowledgements

I wish to thank a number of persons that contributed to make my way through this work either smooth, pleasant, challenging, fun, realistic, or even simply possible.

To the film expert Anna Dąbrowska, who told me to do a PhD in science. Thank you for believing in me against all odds.
To my former supervisor Teresa Vegas-Vilarrúbia, who lured me into paleoclimate, and prepared me for all this.
To my supervisor Frank Peeters, thank you for bringing me into this project, for providing me with a clear research question from the beginning, and with more research questions all the time. It's been quite a way together, and I really thank you for your generosity, scientific and otherwise.
To my promotor Hans Renssen, many thanks for your contribution and especially for your very important help in the last hectic phases of the thesis.
Thank you Gerald Ganssen and Geert-Jan Brummer for the many ways you've provided advice and precious views. Els Ufkes, thank you very much for the great help since my very first day around, and for the taxonomy training. Special thanks to Gianluca Marino, for the essential and enduring guidance with the trickiest bits of this thesis, through dire straits, 10^4 kilometers, and time zones.

To the scientists in my reading commettee, Helge Arz, Trond Dokken, Jan-Berend Stuut, Hubert Vonhof, Martin Ziegler, who received a thick manuscript as a X-mas present last year, thank you for your careful and rich comments.

To my team of very close fellows in the department: young man Brett Metcalfe, companion in many an adventure, Kristina Arthur, with whom I shared numerous highs and lows, day-in-day-out in the office, Wouter Feldmeijer, pillar of the department and master of laboratories, Sanne Vogels, die met mij Nederlands sprak, Alex Wright, who spoke English with me, in a variety of states. Also thanks to the virtual-reality scientists upstairs, Cedric (missed you around), the ever-joyful Austrians Michael and Marianne, Pepijn, Frazer, Tibaut, Didier. Also hi and thanks to Maarten, Kay and Simon for the interesting discussions, to Kees, Suzanne, Ron, Callum, Kirsten, Esmee, Katrin, Stephi, Frans-Jan, Josepha. Special recognition goes to John Visser for the dedicated support with the ICP-OES, I learned a great deal. Thank you to my new colleagues at IVM for having welcomed me so nicely, Jeroen, Philip, Ralph, Hans, Pieter, Brenden, Peter, Tineke, Toon, Sanne, Laura, Elco, Marieke,... and way too many others to mention!

Acknowledgements go to the (extended) Gateways community, PhDs, postdocs, PIs and project leaders: it's been extremely stimulating to be part of such a world-class scientific group. Thank you for all the good times together.

Thanks also to Erik van Sebille in Sydney, Jerome Kaiser in Warnemünde, Stephan Mulitza and Anne Seidenglanz in Bremen, Claire Waelbroeck in Gif-sur-Yvette, Christian Millo in São Paulo.

I want to mention and thank colleagues and friends at the Bjerknes Centre for Climate Research in Bergen, Norway, for the very interesting scientific interactions and the great human proximity that helped me complete the thesis under very favorable climatic circumstances in the fjords. In particular Jørund, Bjørg, Paul, Kim, Nil, Charla, Øyvind, Kerim, and everyone else. Many thanks to Marit for bearing me and for the very cozy time in Sletten, and to the climbing-partying friends Jenny, Thomas, Anna, Alistair, Ingo, Willem…

I am very grateful to the rest of the Amsterdam bunch, for the Massive role they played, shaking my mind off the Pleistocene during the late nights: Christian, Steffen, Zoltan, Edoardo, Anja, Juliana, and many many more. Without you and without our frolics I'd probably have given this up. Dear thanks to my brother Mirco for the cover work and for the many precious technical directions during these years.

Lastly, I am endlessly grateful to my parents Lucia and Angelo, to my family in Casarsa and Noceto, and to all my people in Italy and in Barcelona, you know who you are.

Bibliography

Scussolini, P., T. Vegas-Vilarrúbia, V. Rull, J. Corella, B. Valero-Garcés, and J. Gomà (2011), Middle and late Holocene climate change and human impact inferred from diatoms, algae and aquatic macrophyte pollen in sediments from Lake Montcortès (NE Iberian Peninsula), Journal of Paleolimnology, 1-17.

Morellón, M., A. Pérez-Sanz, J. P. Corella, U. Buentgen, J. Catalán, P. González-Sampériz, J. J. González-Trueba, J. A. López-Sáez, A. Moreno, S. Pla-Rabes, M. A. Saz-Sánchez, P. Scussolini, E. Serrano, F. Steinhilber, V. Stefanova, T. Vegas-Vilarrúbia and B. Valero-Garcés (2012), A multi-proxy perspective on millennium-long climate variability in the Southern Pyrenees, *Clim. Past*, *8*(2), 683-700.

Scussolini, P., and F. J. C. Peeters (2013), A record of the last 460 thousand years of upper ocean stratification from the central Walvis Ridge, South Atlantic, *Paleoceanography*, *28*(3), 426-439.

Scussolini, P., E. van Sebille, and J. V. Durgadoo (2013), Paleo Agulhas rings enter the subtropical gyre during the penultimate deglaciation, *Clim. Past*, *9*(6), 2631-2639.

Feldmeijer, W., B. Metcalfe, P. Scussolini, and K. Arthur (2013), The effect of chemical pretreatment of sediment upon foraminiferal-based proxies, *Geochemistry, Geophysics, Geosystems*, *14*(10), 3996-4014.

Scussolini, P., G. Marino, G.-J. Brummer, and F. J. C. Peeters, Saline Indian Ocean waters invade the South Atlantic in two steps during glacial termination II, *submitted*.